$^{40}Ar/^{39}Ar$ AND FISSION-TRACK THERMOCHRONOLOGY OF THE CENTRAL TRANS-HUDSON OROGEN, MANITOBA, CANADA

By
Stacey L. Perilli

Submitted in Partial Fulfillment of the Requirements
for the Degree of Master of Science in Geochemistry
December, 2000

Department of Earth and Environmental Science
New Mexico Institute of Mining and Technology
Socorro, New Mexico

ABSTRACT

$^{40}Ar/^{39}Ar$ analysis of hornblende, muscovite, biotite and K-feldspar and apatite fission track thermochronological studies constrain the cooling history of the juvenile terranes of the southern Trans-Hudson Orogen (THO), Canada. The Kisseynew, Flin Flon, Snow Lake and Hanson Lake blocks are four of several lithostratigraphic terranes within the THO that amalgamated during arc-arc and arc-continental collisions between ca. 1.9 to 1.8 Ga. The nature of the boundaries between these terranes is the subject of much discussion and uncertainty and the focus of this study. Thermochronology is used to determine whether the accreted terranes have a common cooling history, or alternately, if each records a separate thermal history. $^{40}Ar/^{39}Ar$ dating of hornblende and micas does not reveal significant age variation across the boundaries of these terranes. However, three distinct age groupings are identified within the study area. Where the Kisseynew, Flin Flon and Hanson Lake blocks intersect, both muscovite and biotite ages are between 1720-1705 Ma, whereas a traverse beginning in north-central Flin Flon and extending into the Kisseynew yields ages that cluster at 1760 Ma, as do those from the Snow Lake region. In contrast, 1800 Ma mica ages are found in the greenschist rocks of the central Flin Flon Belt. Orogen-wide, amphiboles are ~1760 Ma, except in the central Flin Flon where published amphibole ages are 1840-1820 Ma. In the Kisseynew and Snow Lake domains rapid cooling from 500-300°C is suggested by the concordant amphibole and mica ages. The rapid cooling is interpreted to be caused by denudation, however the lack

of any abrupt change in age across terrane boundaries suggest that the denudation occurred after amalgamation of the domains and was not accommodated along mapped domain boundaries. In contrast, the younger 1720-1705 Ma micas occur within the Sturgeon-Weir fault zone and may record uplift along this fault at ca. 1720 Ma. The oldest ages recorded in the low-grade metamorphic rocks of the central Flin Flon indicate that heating caused by overthrusting of the hot Kisseynew rocks at ca. 1.8 Ga did not influence the thermal history of the central Flin Flon domain. Thus, rocks in the central Flin Flon record cooling following 1.84-1.83 Ga metamorphism prior to terminal collapse of the Trans-Hudson Orogen. K-feldspar argon analyses mainly record very slow cooling from ~250 to 150°C between 1600-900 Ma. This protracted cooling suggests that the THO stabilized relatively soon after assembly and that the present erosion surface has not experienced temperature perturbations above ~175°C since ca. 1 Ga. Apatite fission-track thermochronology (~60-100°C), when combined with geological constraints and the low temperature history of the K-feldspars indicated that the THO was exhumed between ca. 800 Ma and the Ordovician. Additionally, fission track length studies, when combined with the constraint imposed by the recorded Ordovician sedimentation, define heating during Paleozoic-Mesozoic burial and post-Cretaceous denudation of ~3.5 km of section. Fission track data do not record any low temperature reactivation of Paleoproterozoic structures.

ACKNOWLEDGEMENTS

I would like to thank Matt Heizler, Shari Kelley, Kent Condie and Laurel Goodwin for serving on my thesis committee. I would especially like to thank Matt for his continued support, guidance, energy, and patience, and Shari and Laurel for their advice and positive encouragement.

Further support came from Pat Bickford and John Lewry, whose knowledge of the thesis area was invaluable. The Manitoba Industry, Trade and Mines, Mineral Division and the Saskatchewan Energy and Mines Division of the Canadian Geological Survey, provided maps and insight as well as assistance in the field. Financial support was provided by the New Mexico Geochronological Research Laboratory and an NSF grant.

A number of others should be thanked as well: Lisa Peters and Rich Esser who have been tremendously helpful over the past two years, Vladimir Ispolatov for having a great sense of humor and acting as my own personal computer consultant, Marta Hemmerich, who is an amazing friend and proofreader, and Shelly Rourke who has become the closest of friends and my biggest supporter. Finally, I would like to thank my mom and dad for their unending love and support.

TABLE OF CONTENTS

LIST OF FIGURES

LIST OF TABLES

LIST OF APPENDICES

INTRODUCTION

Although it is well known that most cratons form through terrane accretion, that they later become tectonically stable and tend to expose mid-crustal rocks (Brown, 1993), the process by which an orogen becomes part of a craton is still not fully understood. In particular, how do each of the accreted terranes internal to the orogen amalgamate during collision? Does each behave as a tectonically independent unit, thereby preserving individual cooling histories, or do they cool as a single unit? In addition, what is the affect of widespread plutonism and metamorphism; will cooling rate vary as a function of the distance from the edge of the craton? Also, how tectonically stable are cratons late in their history? Are ancient structures reactivated? This study is part of a larger thermochronologic study that is addressing these questions across the Trans-Hudson Orogen (THO) of central Canada.

The THO formed about 1.9 –1.8 Ga; it is one of the best preserved and exposed Paleoproterozoic orogens in the world (Lewry and Collerson, 1990). The THO has been the focus of intense mapping and U-Pb geochronology studies and its collisional history is well-constrained (Bickford et al., 1990). The interior of the orogen, the Reindeer Zone, is comprised of a collage of metamorphosed juvenile arc rocks and arc-related sediments that lie between the Archean Superior province and the Archean Rae-Hearne province (Figure 1).

The objective of this study is to document in detail the thermal histories of the terranes of the southern THO that make up the Reindeer Zone. This has been accomplished

Figure 1. a) Locations of the Trans-Hudson Orogen (THO), other Proterozoic orogens (dark grey), orogens younger than 1.8 Ga (light grey), and Archean cratons (Hatch marks). Modified from Lewry et al. 1994. Box shows location of 1(b). b) Location of terranes and sample points for the larger study of the THO. Dashed line encloses thesis study area, within which sample locations are numbered. HLB = Hanson lake block, PW = Pelican Window, SWTZ = Sturgeon-Weir thrust zone, TFZ = Tabbernor Fault Zone, NFSZ = Needle Falls Shear Zone. Red lines indicate location of Lithoprobe seismic lines (numbered).

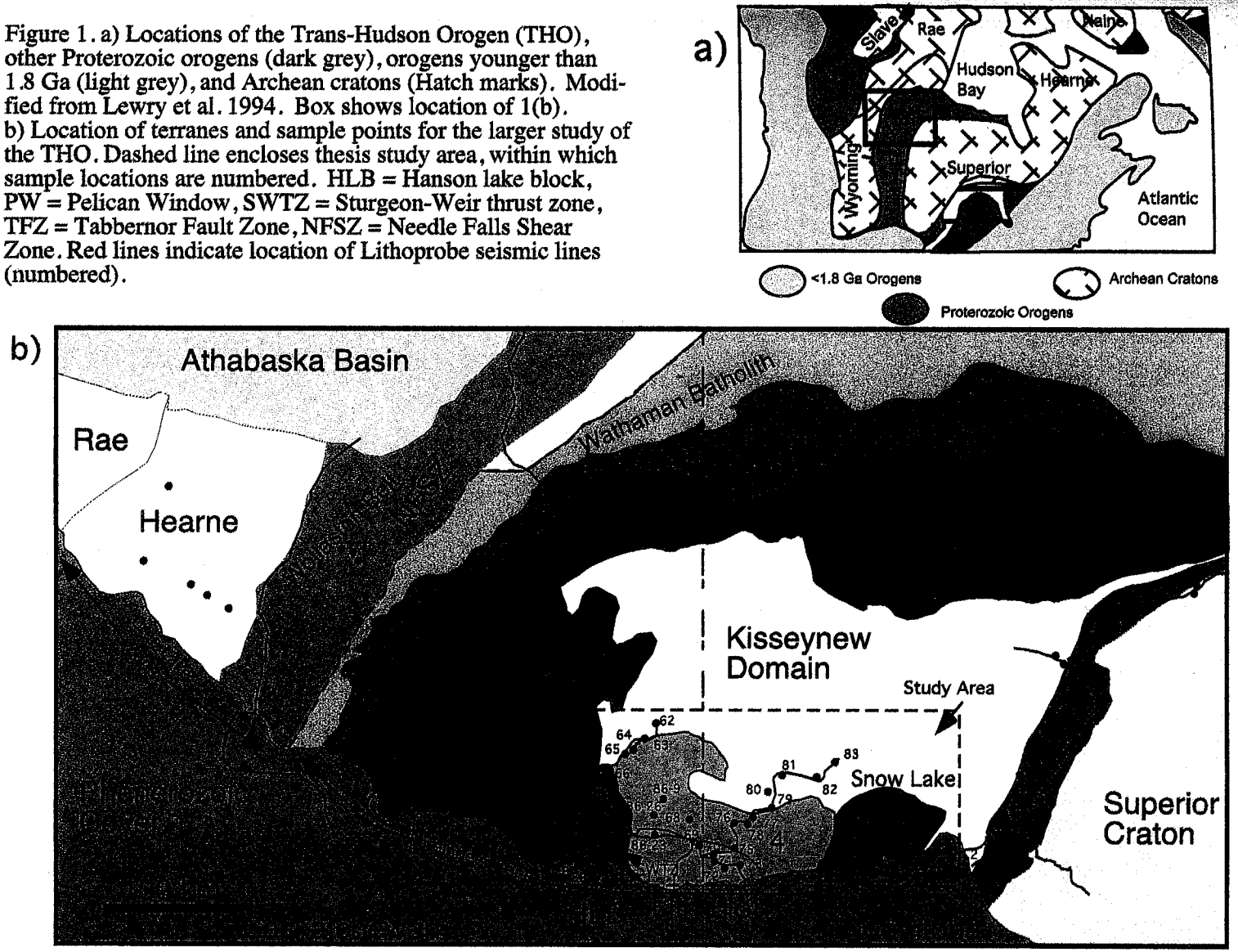

through dating of cogenetic minerals using isotopic systems with a range in closure temperature. Specifically, I have completed $^{40}Ar/^{39}Ar$ dating of coexisting amphiboles (closure temperature of ~500°C; Harrison, 1981), micas (closure temperature of ~300-350°C; Harrison, 1985;), and K-feldspar (~150-300°C; Harrison, 1993) as well as fission track studies in apatite (annealing temperature of ~60 – 120°C; Wagner and Van Den Haute, 1993). These results will be combined with U-Pb accessory mineral (zircon, monazite, and titanite, 800-650 °C) studies performed at Syracuse University in order to provide a thermal history of the interior terranes of the THO extending from ~800 °C through ~100°C. This study describes the thermal history from ~500 to 100°C of four terranes in the central part of the orogen: the Kisseynew, Flin Flon, Hanson Lake and Snow Lake blocks.

GEOLOGIC SETTING

Exposed in Saskatchewan and Manitoba, the Trans-Hudson Orogen (THO) extends from the north-central United States through central Canada into Greenland (Figure 1; Hoffman, 1981; Van Schmus et al., 1987). This orogenic system is essentially a collage of accreted Proterozoic arc-related rocks, reworked Archean basement, and 1.85 – 1.83 Ga metasediments related to the collision between the Rae-Hearne, Wyoming, and Superior Archean provinces as Laurentia formed during the Paleoproterozoic (Lewry and Collerson, 1990). Convergence and arc magmatism began ~1.9 Ga. Juvenile arc volcanism continued between 1.91 and 1.87 Ga. The accretion of the western arcs to the Hearne Province at ~1.855 Ga, and accretion-related intrusions produced the Wathaman-Chipewan Batholith. Intrusive activity continued orogen-wide from 1860 until 1840 Ma in an oceanic - continental collisional environment (Ansdell and Norman, 1995). As collision between the cratons progressed, the island arcs that had formed in the Manikewan Ocean separating the Superior and Hearne provinces were caught up in the collision and now make up the juvenile interior of the orogen. Archean basement (Sask Craton) is exposed in both the Hanson Lake Block and Glennie Domain. Collision of the Hearne and Superior Provinces led to crustal thickening and resultant peak metamorphism at ~1815 Ma (Ansdell and Norman, 1995). Terminal collision and suturing took place in a relatively short period of time between 1.85 and 1.80 Ga (Hoffman, 1988; Lewry et al., 1990).

The THO is divided into four major lithotectonic zones (Figure 1): 1) the Thompson Belt, which forms the eastern boundary with the Superior craton and is largely made up

of metasediments and ultramafic lavas; 2) the Wathaman Batholith, a continental magmatic arc which is analogous to the modern Andes; 3) the Cree Lake Zone (Wollaston Belt), which is comprised mainly of reworked Archean basement, and 4) the Reindeer Zone, a collage of accreted (juvenile) and oceanic terranes (Rottenstone Belt – Kisseynew Domain), underlain by Archean basement (Sask Craton; Lewry and Collerson, 1990; Lewry et al., 1994). Most of the Reindeer Zone evolved in an oceanic – subduction related setting. As the Manikewan ocean closed, the juvenile terranes of the THO collided with the Rae-Hearne provinces. This closure was apparently preceded by the thrusting of arc terranes over the Archean Sask craton along the Sturgeon-Weir fault (Ashton and Lewry, 1994; Lewry et al., 1994). Rocks within the Reindeer Zone have been grouped as follows: 1) Archean basement rocks of the Sask Craton exposed in the Pelican window; 2) 1.92 – 1.83 Ga volcano-plutonic rocks from island arcs, ocean floor and adjacent sedimentary basins, and 1.85-1.83 Ga fluvial sedimentary rocks (Missi Group) and 3) 1.85-1.84 Ga marine sedimentary rocks and volcanics (Burntwood Group; Ansdell et al., 1995; Bickford et al., 1990). The Reindeer Zone is further sub-divided into terranes or domains that are defined by metamorphic grade, lithology, and structural features, including: the Rottenstone Domain, La Ronge Domain, Kisseynew Domain, Glennie Domain, Hanson Lake Block, and Flin Flon Belt. This study will focus on the southernmost part of the orogen, specifically, the Kisseynew Domain, Flin Flon Belt and Hanson Lake Block (Figure 1).

The Hanson Lake Block consists of metavolcanics, volcaniclastics, and granite gneisses. Metavolcanic rocks and metasediments that have been intruded by plutons are known as the Hanson Lake assemblage, which makes up the southern part of this terrane,

the Hanson Lake area. The other major group, the Northern Lights assemblage, is a group of supracrustal rocks including mafic and intermediate metavolcanic rocks (Maxeiner et al., 1999). In the northern part of this terrane, the Archean Sahli and MacMillan Point granite, part of the Sask Craton, are exposed in a window through the overlying gneisses known as the Pelican Window (Van Schmus et al., 1987; Gala et al., 1998). U-Pb dating of zircon from the Sahli granite by Bickford et al. (1986) reveals an age of 1900 Ma. Paleoproterozoic metamorphism can be bracketed between the age of the Sahli granite and the age of the unmetamorphosed cross-cutting intrusives that have been dated to be between 1784±18 and 1759±5 Ma (Gala et al., 1998). Metamorphic grade in the Hanson Lake Block ranges from lower to middle amphibolite facies and generally increases northward (Maxeiner et al., 1999; Zwanzig, 1998). Regional peak metamorphism reached upper amphibolite facies and is thought to have occurred between 1808 and 1804 Ma (Maxeiner et al., 1999). The Hanson Lake Block is bounded on all sides by faults. The Tabbernor fault, a 10 km wide brittle fault zone that extends ~175 km south from the La Ronge – Glennie boundary, defines the western margin of the Hanson Lake Block (Hajnal et al., 1995). Major displacement on the Tabbernor Fault occurred after peak metamorphism and collisional deformation (1.83 –1.80 Ga; Ansdell et al., 1995; Hajnal et al., 1995). Displacement was mostly left lateral strike-slip and the fault zone is thought to have been reactivated intermittently during the Phanerozoic (Hajnal et al., 1995). To the east, the Sturgeon-Weir Thrust defines the boundary between the Hanson Lake Block and the Flin Flon Belt. Here, a block of juvenile arc rocks has been thrust to the SW over the Archean Sask craton along the Pelican and Sturgeon-Weir Thrusts. The hanging wall of the Pelican Thrust is made up of the

southern Hanson Lake, Flin Flon and Attitti blocks (Figures 1 and 2; Gala et al., 1998; Lewry et al., 1990b). The northern boundary with the Kisseynew Domain is defined by the Pelican thrust, where southwest directed thrusting is likely to have occurred between 1830 – 1805 Ma (Gala et al., 1998).

The Kisseynew Domain is made up of deformed amphibolite facies supracrustal gneisses, metagabbros, and metatonalites. The area is host to three distinct assemblages of supracrustal rocks. The first is made up of the schists and migmatites of the Burntwood Suite. The Burntwood Suite is thought to be a deep-water turbidite facies that was deposited on oceanic crust; it is the stratigraphic equivalent of the File Lake Formation in the Flin Flon Belt (Norman et al., 1995). The second assemblage is the quartzofeldspathic gneisses of the Missi Group. The age of the Missi Group can be bracketed between 1835 –1855 Ma; it is correlative to fluvial sedimentary rocks in the Flin Flon Domain. Protoliths include mafic to felsic volcanic, volcaniclastic, and clastic sedimentary rocks (Ansdell et al., 1995). In general, the Missi Group structurally overlies the Burntwood Suite, but complex deformation makes it difficult to determine the original stratigraphic sequence. The third assemblage is the Snow Lake assemblage, consisting of ~1.9 Ga island arc rocks. Along the southern margin of the Kisseynew Domain, high-grade rocks have been thrust southward over the lower-grade rocks of the Flin Flon. Here, sedimentary rocks are folded and intertounged with volcanics. The southern flank of the Kisseynew Domain (SFKD) underwent peak high-temperature, low-pressure metamorphism during compressional deformation, at 1815 Ma. Metamorphic grade is greatest (upper amphibolite to granulite facies) in the central part of the domain, and decreases to greenschist facies toward the south (Gordon et al., 1990).

The Flin Flon Belt consists of subaqueous and subaerial volcanic rocks, associated sedimentary rocks, and a group of intrusives. Volcanic rocks of the Amisk group make up the oldest (1886 Ma) rocks in the Flin Flon Belt (Gordon et al., 1990). These were deposited in a marine environment, although at some localities subaerial environments are recognized. The Amisk Group was intruded by 1.87 –1.86 Ga plutonic rocks, folded, faulted, eroded and later overlain by the Missi Group, consisting of metamorphosed sandstone and polymictic conglomerate (Lucas et al., 1996). The File Lake Formation is the stratigraphic equivalent of the Burntwood Suite, the deep water turbidite facies of the Kisseynew. Metamorphism in the Flin Flon Belt ranges from prehnite-pumpellyite to upper greenschist facies, and generally increases northward toward the Kisseynew. Metamorphism here is thought to be the result of a single thermal event, where greatest metamorphism was reached in the Kisseynew and peak metamorphism occurred at ~1815 Ma (Gordon et al., 1990; Fedorowich, 1995).

The Snow Lake part of the Flin Flon Belt (Figure 1), is comprised of highly deformed and metamorphosed volcanic, sedimentary, and intrusive rocks. Rocks of the Snow Lake area have been grouped into five lithotectonic components: 1) 1.89 Ga metamorphosed basalt, basaltic andesite, dacite, and rhyolite, 2) turbidites of the Burntwood Group, 3) sediments of the Missi Group, 4) successor arc volcanics, and 5) calc-alkaline plutons (David et al., 1996). In general, Snow Lake is dominated by 1.84 – 1.81 Ga fold and thrust structures; this terrane was thrust over the Amisk collage to the west between 1.84 and 1.81 Ga (Bailes and Galley, 1999; Connors, 1996). The entire thrust package has been modified by the intrusion of granitic plutons, folding, and regional metamorphism at 1.82 –1.81 Ga. As in the rest of the Flin Flon Belt,

metamorphic grade increases northward from lower greenschist to upper amphibolite facies (David et al., 1996). Peak metamorphism in the Snow Lake is thought to have occurred at ~5kb and 550°C (Menard and Gordon, 1997)

The boundary between the Kisseynew Domain and the Flin Flon Belt has been the subject of much investigation. The relationship between the high-grade rocks of the Kisseynew Domain, which structurally overlie lower grade rocks of the Flin Flon Belt, is not well understood. Seismic profiles suggest that the present relationship between the two terranes is a low-angle, southward verging thrust that formed during collision with the Superior Craton (Figure 2; Ansdell et al., 1995). The boundary was originally defined by Harrison (1951) as a series of faults he named the Kisseynew lineament. In contrast, Bailes (1980) reported that the lineament does not exist and that the boundary is actually marked by a abrupt increase in metamorphic grade and/or a change in lithology from volcanic to sedimentary rocks. It has also been suggested that the boundary be defined as the sillimanite-biotite-garnet isograd (Gordon et al., 1990). Most recently, Connors (1996) suggested that the most significant difference between the two terranes is in tectono-stratigraphy. Connors (1996) proposed that the boundary between Amisk collage of the Flin Flon Belt and the turbidites of the Kisseynew began as an extensional basin margin. Later, SW-directed thrusting resulted in significant southward translation of the Kisseynew basin over the arc rocks of the Flin Flon Belt. The fault boundary was subsequently folded by NE-SE compression. Pluton emplacement (1.84 – 1.83; Lucas et al., 1996) and peak metamorphic conditions occurred during collision of the juvenile arcs with the Sask Craton and before collision of the eastern THO with the Superior Craton. Therefore, for the purpose of this study, the boundary is defined as the change in rock

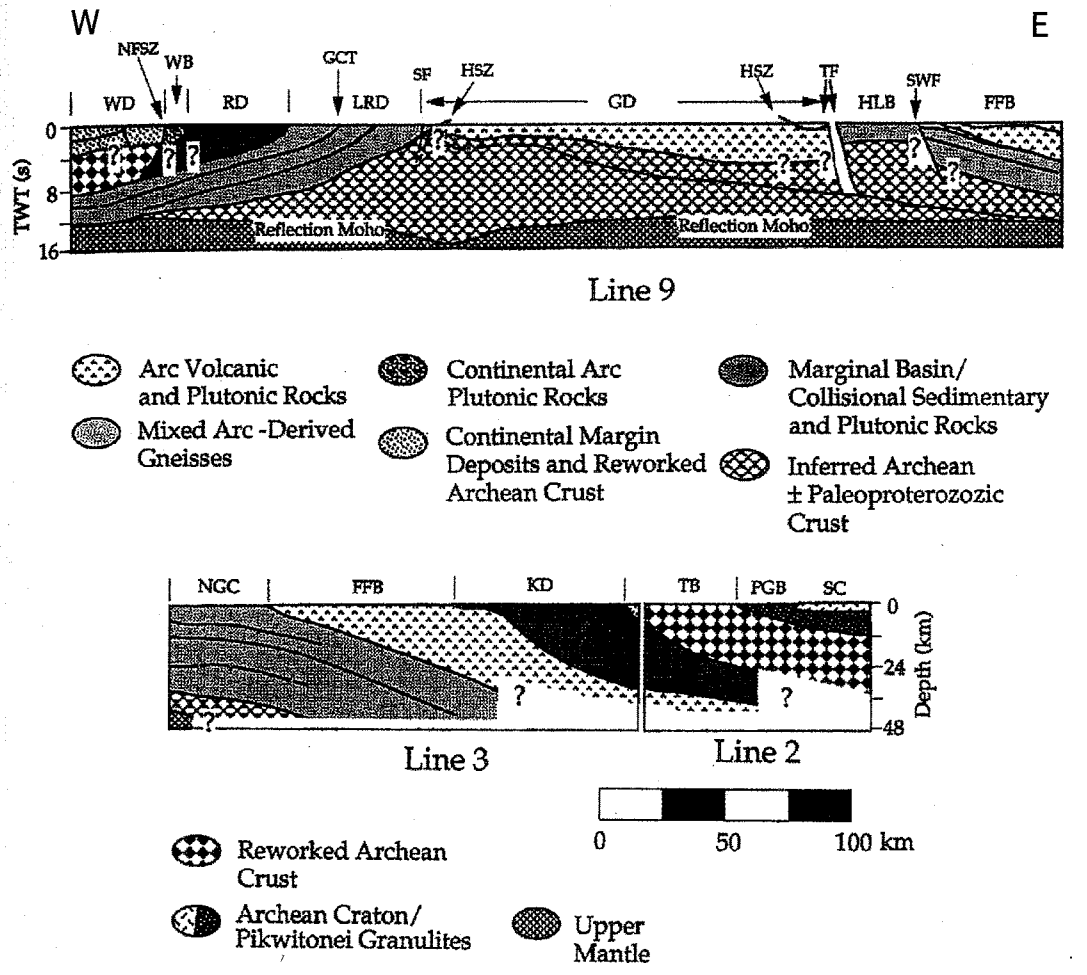

Figure 2. Cross section of the Trans-Hudson Orogen based on Lithoprobe seismic lines. WD= Wollaston Domain, NFSZ = Needle Falls shear zone, WB = Wathaman Batholith, RD = Rottenstone Domain, GCT = Guncoat thrust, LRD = La Ronge Domain, SF = Stanley fault, HSZ = Hartley shear zone, TF = Tabbernor Fault, HLB = Hanson Lake Block, SWF = Sturgeon-Weir fault, FFB = Flin Flon Belt, KD = Kisseynew Domain, TB = Thompson Belt, GD = Glennie Domain, NGC = Namew Gneiss Complex, PGB = Pikwitonei Granulite Domain, SC = Superior Craton. Adapted from Lewry et al., (1994).

type from volcano-plutonic rocks of the Amisk collage in the Flin Flon Belt to turbidites of the Kisseynew Domain that coincides with the Loon Head Lake – Snow Lake fault system in the File Lake area.

ANALYTICAL METHODS

$^{40}Ar/^{39}Ar$

$^{40}Ar/^{39}Ar$ dating was carried out on four hornblende, three muscovite, twenty-four biotite and six K -feldspar samples separated out of rocks of various composition collected throughout the southern THO (Figure 1). The field sampling strategy of the larger study was to sample across the entire orogen, focusing on major fault zones and terrane boundaries. Within the thesis area, two main traverses were taken: a long traverse at a high angle to the Kisseynew/Flin Flon boundary, and a shorter traverse across the Hanson Lake-Kisseynew boundary. Individual minerals were prepared for analysis using standard crushing and sieving techniques. When necessary, samples were run through the Franz magnetic separator and/or heavy liquids. Samples were sized to particle diameters between 0.1 and 1.0mm and ultrasonically cleaned. A binocular microscope was used to hand select the coarsest possible, clean, unaltered hornblende, biotite, muscovite and K-feldspar separates. Fine grained samples (<~60 mesh) were then wrapped in Cu-foil and all samples were placed in 6 or 12-hole machined Al irradiation trays. Packages were irradiated at the University of Michigan Ford reactor for 100 hrs in a known geometry. Neutron flux was monitored using Fish Canyon Tuff sanidine (27.84 Ma) as a standard.

All $^{40}Ar/^{39}Ar$ analysis were completed at the New Mexico Geochronology Research Laboratory (NMGRL) at New Mexico Institute of Mining and Technology. Following irradiation, J-values were determined though CO_2 laser total fusion of Fish Canyon sanidine. Samples were step heated in a double vacuum Mo furnace, during which non-

noble gasses were removed using a GP-50 getter operated at 450°C. Heating was accomplished with a tungsten filament and temperature was monitored with a W-Re thermocouple. Following heating, gas was transferred to the second stage and cleaned using two SAES getters (one at room temperature and one at 450°C) for a total of two minutes. Heating schedules for micas and amphiboles consisted of 12 – 16 heating increments of 8 minutes each. Heating duration for K-feldspars ranged from 10 minutes to 8 hours. Heating schedules consisted of a sequence of duplicate isothermal steps between 450°C and 1100°C, followed by single steps to 1650°C.

Argon isotope abundances were measured using a Mass Analyzer Products (MAP) 215-50 mass spectrometer, and an electron multiplier running at a gain of approximately 2,500 and a sensitivity of 1.0×10^{-15} mol/pA. The mass spectrometer has a resolution of ~450 at mass 40. Typical measured background and blanks are 1.3×10^{-18} mol ^{36}Ar, and 1.0×10^{-16} mol ^{40}Ar for furnace temperatures of 600-1650°C. Due to the age and high radiogenic yield of these samples, blanks were much smaller than the signals and therefore were not a significant source of error in the age calculation. Uncertainties in age are reported at 2σ and include error in the background and isotope measurements, and J-factor.

A single muscovite and biotite, each from sample HUD98-86a, were analyzed using the UV laser at NMGRL. This hand sample contained large mica grains (>5mm) that were easily removed using tweezers. The minerals were irradiated in vacuo and monitored by placing packets of Fish Canyon Tuff Sanidine onto the mica flakes. They were then glued to copper plates and placed in the laser chamber. Laser ablation was accomplished with a quadrupled SL 454 Nd-YAG laser, which produces light at a

wavelength of 266nm. Laser ablation pits were drilled in linear traverses across the grains. Ablation pits are 100x100μm and spaced at 500μm intervals. Laser power was set at 0.5 watts and ablation lasted approximately 5-10 seconds.

In order to investigate the possibility of grain to grain age variation, total fusion experiments were performed on crystal fragments of two micas from the same sample. Gas was extracted using a focused 50-watt CO_2 laser.

For all laser procedures, gas was cleaned of non-noble gasses and isotopes were analyzed using the above-mentioned methods for second stage cleanup. Correction factors were determined though analysis of K-glass and CaF_2 and are given in Table A of Appendix A.

Apatite Fission –Track Analyses

Apatite fission-track analyses were performed on 15 samples from the southern THO. Samples were crushed and apatite was separated using a Franz magnetic separator and heavy liquids. Apatite grains were then mounted on glass slides using epoxy and polished to expose an internal surface. Samples were etched in 5M HNO_3 for 25 seconds in order to reveal the tracks, making them visible with the aid of a microscope. Muscovite detectors were placed adjacent to each slide prior to irradiation, which took place at the Texas A&M reactor. In order to determine the variance in neutron fluence, samples were irradiated along with Corning Glass (CN-6) and Durango apatite standards in a known geometry. Track length measurements were made using a digitizing tablet and petrographic microscope fitted with a drawing table and a 100x dry objective.

Calculation of fission-track ages was accomplished using the external detector method. Induced and spontaneous tracks were counted over a known area with a

minimum of twenty grains per sample to determine the uranium parent-daughter ratio. Durango Apatite (31.4±0.5 Ma) was used for the zeta calculation, a correction factor that incorporates operator observation factors and variance in neutron fluence. Age results for individual grains were run through statistical models including radial plots and the chi squared test to determine the probability of single or multiple populations of tracks. Uncertainties in the fission-track ages reported here include errors in the zeta calibration and decay constant for uranium.

Ages and track length distributions can be entered into a fission-track modeling program based on laboratory annealing experiments and borehole data in order to generate possible thermal histories matching the input data. The AFTSolve modeling program used here, and described in detail in Ketchum et al. (2000), takes into account the known kinetic variability among different apatite chemical compositions. In addition, the AFTSolve model incorporates the orientation of tracks relative to the c-axis and variation in initial track length.

Electron Microprobe Analyses

Major element analysis was done on all mica and amphibole samples. In order to determine whether the apatites separated were flour-apatite or chlor-apatite, four representative apatite samples were analyzed. Mineral separates were ultrasonically cleaned, placed in epoxy in 6 or 9-hole mounts and polished using a series of grinding wheels. Apatite grains previously mounted in epoxy for dating purposes were also used for microprobe analysis. Following polishing, samples were carbon-coated for electrical conductivity. Analysis was done on a Cameca SX-100 electron microprobe using a 10μm beam and a current of 20nA for micas and amphiboles and 15nA for apatite.

RESULTS

$^{40}Ar/^{39}Ar$ Analyses

Detailed geochronology studies were performed on 26 samples from the southern Trans-Hudson Orogen (Figure 1, Table 1, Appendices A and B). For the purpose of this study, a plateau is defined as three contiguous steps that are concordant at 2σ and together comprise at least 50% of the total ^{39}Ar released. A preferred age is the weighted mean age of hand selected steps that generally define the flat portion of an age spectra but fall just outside the plateau criteria. Preferred ages have been assigned by selecting steps that differ by slightly more than 2σ or make up just less than 50% of the ^{39}Ar released but represent the flat portion of the age spectra and are interpreted as the best estimate of the age of each sample. Radiogenic yield for all samples is consistently very high (95-100%), and therefore has been omitted from figures and tables. In addition, UV laser ablation and CO_2 laser fusion were performed on a muscovite – biotite pair from sample HUD98-86A in order to determine intra-grain age gradients or grain to grain age differences. Major element compositions were determined with an electron microprobe for all micas and amphiboles prior to $^{40}Ar/^{39}Ar$ step-heating. For each separate, a number of 10μm points were analyzed. In general, the majority of the sample points were taken on grains of the mineral of interest; the remainder of the analyses are of contaminating or unidentifiable phases within the separate (Appendices C, D). Because the compositions of the mineral separates are intimately linked to the resulting age spectra, microprobe analyses will be discussed in the context of the argon age spectra results.

Table 1) Summary Table of $^{40}Ar/^{39}Ar$ data. Data are reported by sample number, keyed to Figure 1.

				Total Gas		Plateau (Ma)					UTM Coordinates		
Sample	Location	Rock Type	Mineral	Age (Ma)	Error	age	Error	n	%39Ar	MSWD	Zone	Northing	Easting
HUD98-62	Kisseynew	mylonite	biotite	1718.2	2.1	1724.9	1.7	8	91.8	1.51	13U	666878	6155177
HUD98-63	Kisseynew	pelitic schist	biotite	1760.6	2.4	1763.0	3.29	9	99.4	4.1	13U	658127	6144558
HUD98-64	Kisseynew	pegmatite	biotite	1715.2	2.4	1720.7	1.9	8	81.6	0.94	13U	644868	6132374
HUD98-65	Kisseynew	biotite schist	biotite	1704.2	2.4	1706.3	4.21	9	98.8	6.24	13U	"	"
HUD98-66	Kisseynew	biotite schist	biotite	1707.7	2.4	1717.1	4.58	6	73.4	5.29	13U	633217	6120467
HUD98-67	Kisseynew	metatonalite	biotite	1688.6	2.6	1705.7	3.47	8	90.2	4.13	13U	634154	6114443
HUD98-69	Flin Flon	pegmatite	K-feldspar	1361.8	2.3	NA					14U	326696	6076337
HUD98-71	Flin Flon	granodiorite	biottie	1813.6	2.1	1825.9	4.62	8	89.9	7.39	14U	335213	6068181
HUD98-72	Flin Flon	mica granodiorite	biotite	1756.7	2.2	1802.7	8.12	8	77.6	21.75	14U	334934	6069084
HUD98-72	Flin Flon	mica granodiorite	muscovite	1802.1	2.3	1817.6	5.12	7	81.8	7.94			6057007
HUD98-73	Flin Flon	granite	biotite	1764.5	2.1	1805	11	9	93.6	43.59	14U	344410	6053360
HUD98-74	Flin Flon	metasediment	biotite	1700	2.2	1758	14	7	87.7	50.08	13U	689787	6057706
HUD98-75	Flin Flon	quartz diorite	hornblende	1710.7	2.6	1799.9	3.22	3	38.6	2.93	14U	341537	6073751
HUD98-76	Flin Flon	granodiorite	biotite	1754.1	2.2	1767.8	2.48	9	93.7	2.35	14U	342428	6076389
HUD98-77	Flin Flon	quartz diorite	biotite	1761.5	2.5	1777.1	5.36	9	96.3	9.8	14U	355451	6086445
HUD98-78	Flin Flon	granite	biotite	1739.6	2	1760.4	2.12	4	53.2	0.78	14U	no data	
		granite	K-feldspar	1553.7	2.5	NA							
HUD98-79	Kisseynew	biotite schist	biotite	1748.8	2	1755.6	1.66	8	94	2.2	14U	365037	6098646
HUD98-80	Kisseynew	granite gneiss	biotite	1741.4	1.8	1756	5.13	7	89.2	9.69	14U	364869	6106368
		granite gneiss	hornblende	1744.6	2.9	1764.8	3.9	10	91.7	5.27			
		granite gneiss	K-feldspar	1571.3	2.6	NA							
HUD98-81	Kisseynew	biotite garnet schist	biotite	1739.7	2.3	1748.8	2.5	4	54.8	0.74	14U	374700	6117791
HUD98-82	Kisseynew	granodiorite	hornblende	1738.9	3.1	1758.2	2.7	4	89.3	2.44	14U	398249	6116095
HUD98-83	Kisseynew	garnet gneiss	biotite	1707	2.3	1757	16	8	89.6	80.66	14U	402331	6125577
HUD98-83	Kisseynew	garnet gneiss	K-feldspar	1577.8	2.9	NA						no data	
HUD98-84	Snow Lake	granite	biotite	1741	1.8	1763.4	1.94	5	67	2.31	14U		
		granite	K-feldspar	1470.6	2.2	NA							
HUD98-85	Snow Lake	staurolite	biotite	1745	2	1772.4	4.06	6	82.7	4.68	14U	434886	6080590
HUD98-86	Snow Lake	pegmatite	biotite	1570.4	3	NA					14U	450789	6086836
		pegmatite	muscovite	1755.6	2	1758.4	2.49	13	99.1	3.63			
HUD98-87	Snow Lake	calc-silicate inclusion	biotite	1710.4	2.8	1801	16	5	70.8	52.5	14U	446479	6082899
		calc-silicate inclusion	hornblende	1520.3	5.6	1606.3	58.4				14U	446479	6082899
HUD98-88	Snow Lake	staurolite garnet schist	biotite	1734.7	2.5	1756.1	1.6	6	84.4	0.68	14U	446479	6082899
		staurolite garnet schist	muscovite	1684.9	1.9	1734.7	8.57	9	76	33.19	14U	446479	6082899
HUD98-89	Snow Lake	kyanite bearing schist	biotite	1754.5	2.5	1760.9	2.81	8	97.6	2.5	14U	437411	6079536
HUD98-90	Snow Lake	garnet staurolite schist	biotite	1741.2	1.7	1754.6	6.13	9	97.1	17.66	14U	427346	6075590

Of the four hornblende samples, one (HUD98-87, from a calc-silicate incusion in the Snow Lake area) is severely discordant and therefore cannot provide any thermochronologic information (Figure 3). This spectrum shows very young (<1500 Ma) ages over the first 30% of the spectrum, followed by a 1645 Ma step and two more steps younger than 1500 Ma. The last 45% of the gas release is comprised of two heating steps that are concordant and yield an age of 1710 Ma. The total gas age for HUD98-87 is 1520.3 ± 12.2 Ma. The spectrum for HUD98-75, a quartz diorite from the central part of the Flin Flon Belt, yields a severely hump-shaped spectrum (Figure 3). Apparent ages as low as 1600 Ma are observed in the initial steps, and quickly rise to 1805 Ma over a short, flat portion in the intermediate temperature steps, before falling to ~1760 Ma. The spectrum records a total gas age of 1710.7 ± 5.2 Ma. The K/Ca ratio is inversely correlated to the gas release pattern. Probe analysis of the hornblende reveals the presence of both biotite and chlorite. The initial and final heating steps, where K/Ca is high and ages are low may be the result of contaminating biotite degassing whereas the intermediate steps record the degassing of the hornblende. Typical K/Ca ratios for biotite are between 10 and 100, whereas hornblende generally yields K/Ca ratios of less than 1. Microprobe analysis yields an average K/Ca of ~0.07 whereas $^{40}Ar/^{39}Ar$ analysis shows K/Ca no lower than ~0.16, suggesting that even the intermediate steps are a mixture of hornblende and other K-bearing phases. Although a preferred age has been assigned across the three intermediate steps, it seems likely that contamination of the mineral separate is the cause for the shape of the spectrum, and that had a clean hornblende been analyzed (with a K/Ca of 0.068), the spectrum would attain ages older than observed. Therefore, the preferred age of 1800 ± 3 is actually a minimum age.

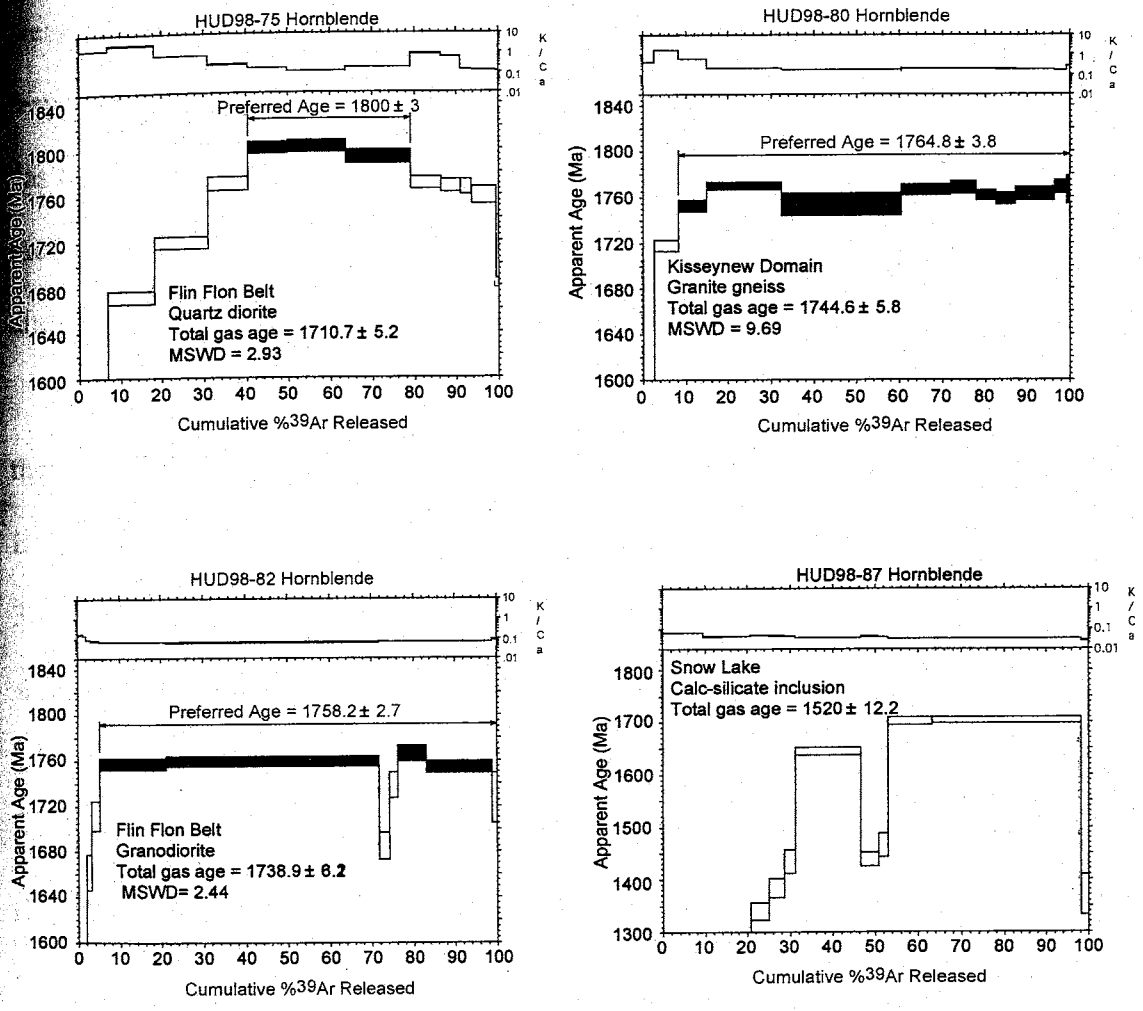

Figure 3. $^{40}Ar/^{39}Ar$ apparent age and apparent K/Ca for hornblende samples. Analytical uncertainty is represented by width of bars. Total gas and and preferred ages are shown on each spectrum. See Figure 1 for sample locations.

Hornblende samples from a granitic gneiss, (HUD98-80) and a granodiorite (HUD98-82), both from the southern flank of the Kisseynew Domain, yield flat age spectra. Nearly 90% of each spectrum yields preferred ages of 1764.8 ± 3.8 and 1758.2 ± 2.7 Ma, respectively. HUD98-82 shows two steps of much lower age and a small fraction of the gas released which correspond to a small increase in K/Ca, probably due to mica inclusions. Microprobe images of these samples show fewer inclusions and less alteration than HUD98-75.

Three muscovite samples from the southern Trans-Hudson Orogen were analyzed; their age and K/Ca spectra are shown in Figure 4. HUD98-86A (a pegmatite within the Burntwood Group) yields a plateau for greater than 90% of the gas released (MSWD = 3.63). The plateau age of 1758.4± 2.5 Ma is nearly identical to the total gas age, 1755.6 ± 9.2 Ma. HUD98-88, a staurolite garnet schist of the Burntwood Group, and HUD98-72, a granodiorite from the Lynx Lake Pluton, have more complex spectra that show a distinctive dip in the central portion of each spectrum, and an overall undulatory pattern (Figure 4). Back-scatter electron images of HUD98-72 reveal inclusions of quartz and K-feldspar as well as chlorite alteration and zoning. The images of HUD98-88 show significant alteration, especially around grain edges, as well as biotite and plagioclase inclusions. Total gas ages are 1684 and 1802 Ma, respectively. The K/Ca ratio mirrors the behavior of gas release throughout all heating steps. In-situ laser analysis of muscovite has revealed significant age gradients within individual crystals in the southwestern United States (Hodges et al., 1994). It is therefore possible that intra-grain age gradients are responsible for the undulatory pattern seen in these spectra.

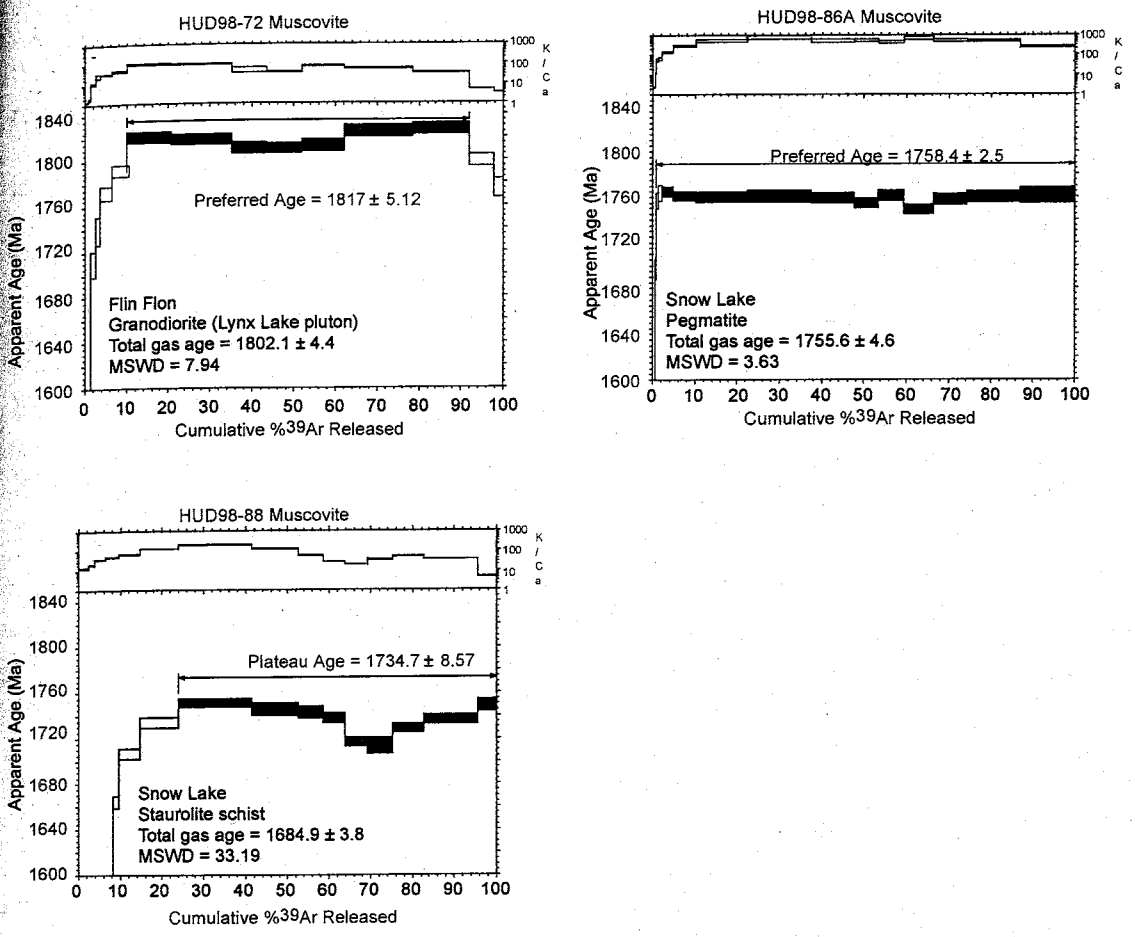

Figure 4. $^{40}Ar/^{39}Ar$ apparent age and apparent K/Ca spectra for muscovite samples. Analytical uncertainty is represented by width of bars. Total gas ages and plateau or preferred ages are shown on each spectrum. See figure 1 for sample locations.

Biotite analyses have been placed in two groups, those with age spectra that are relatively flat and can be assigned an age with a high degree of confidence and minimal inspection (Figures 5 and 6), and those with spectra that are more complex (usually in the form of a hump-shaped release pattern; Figure 7). For the flat spectra, there generally appears to be no consistent correlation with K/Ca. Electron microprobe analysis reveals biotites that range widely in composition. Contaminating mineral phases in samples with hump-shaped spectra include hornblende, feldspars, chlorite, and apatite.

Of the 24 biotite samples that were step-heated, 19 yielded relatively flat age spectra (Figures 5, 6; Table 1). For many of the samples, a well-defined plateau age has been assigned. For the remaining samples, preferred ages were assigned across relatively concordant steps comprising a large percentage of the gas released (Table 1, Appendix B). In general, the samples seem to define two distinct populations. Biotite analyses from the Kisseynew/Flin Flon traverse and Snow Lake region reveal plateau ages that cluster at ~1760 Ma. (Figure 5). Samples from the Hanson Lake Block (Highway 135 traverse) reveal ages of ~1720 Ma. (Figure 6). Total gas ages are generally younger than plateau and preferred ages by ~ 2 – 24 Ma.

Severe hump-shape spectra are found for five biotite samples: HUD98-72, HUD98-73, HUD98-74, HUD98-83, and HUD98-87 (Figure 7). In these spectra, apparent ages are significantly younger in the low and high temperature steps relative to the older, intermediate temperature steps (Figure 7). Ages of the intermediate temperature increments reach at least 1800 Ma for all of these samples, although the total gas ages are much younger. Backscattered electron imaging, as well as electron microprobe major element analysis (Appendix C, D), reveal that the majority of these samples contain

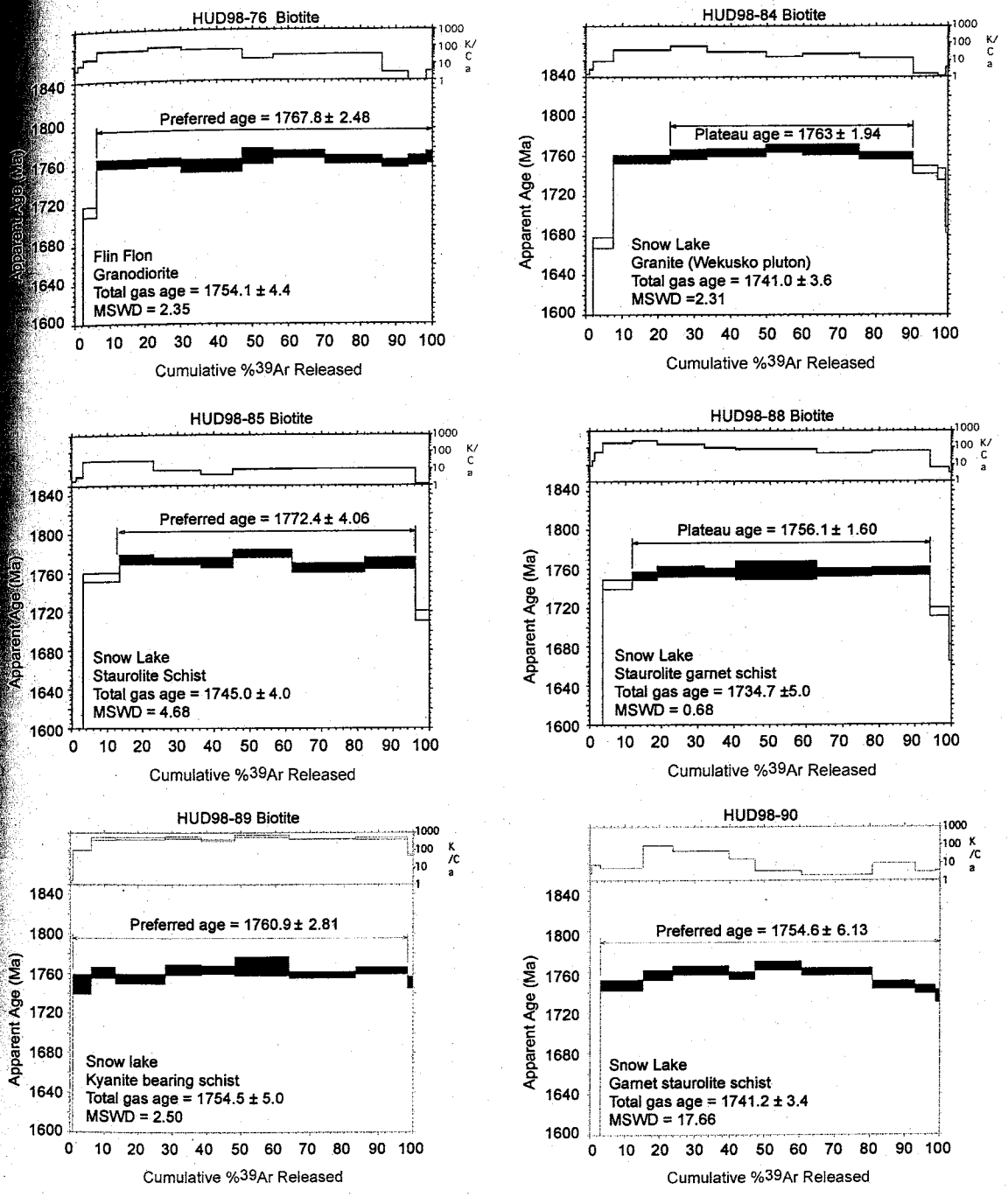

Figure 5. $^{40}Ar/^{39}Ar$ apparent age and apparent K/Ca spectra for biotites displaying flat release patterns. Analytical uncertainty is represented by width of bars. Total gas ages and plateau or preferred ages are shown on each spectrum. See figure 1 for sample locations.

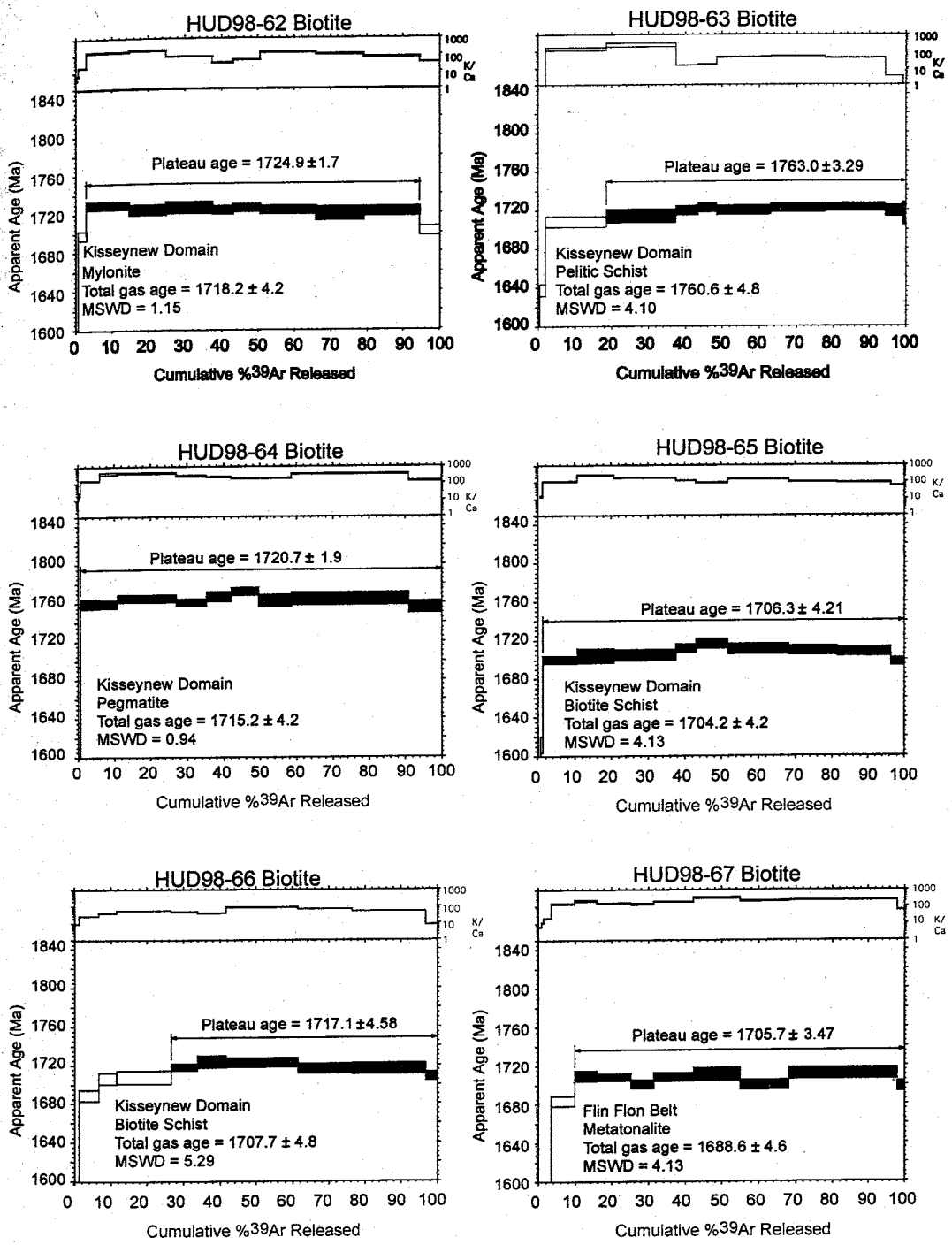

Figure 6. $^{40}Ar/^{39}Ar$ apparent age and apparent K/Ca spectra for biotites displaying flat release patterns. Analytical uncertainty is represented by width of bars. Total gas ages and plateau or preferred ages are shown on each spectrum. See Figure 1 for sample locations.

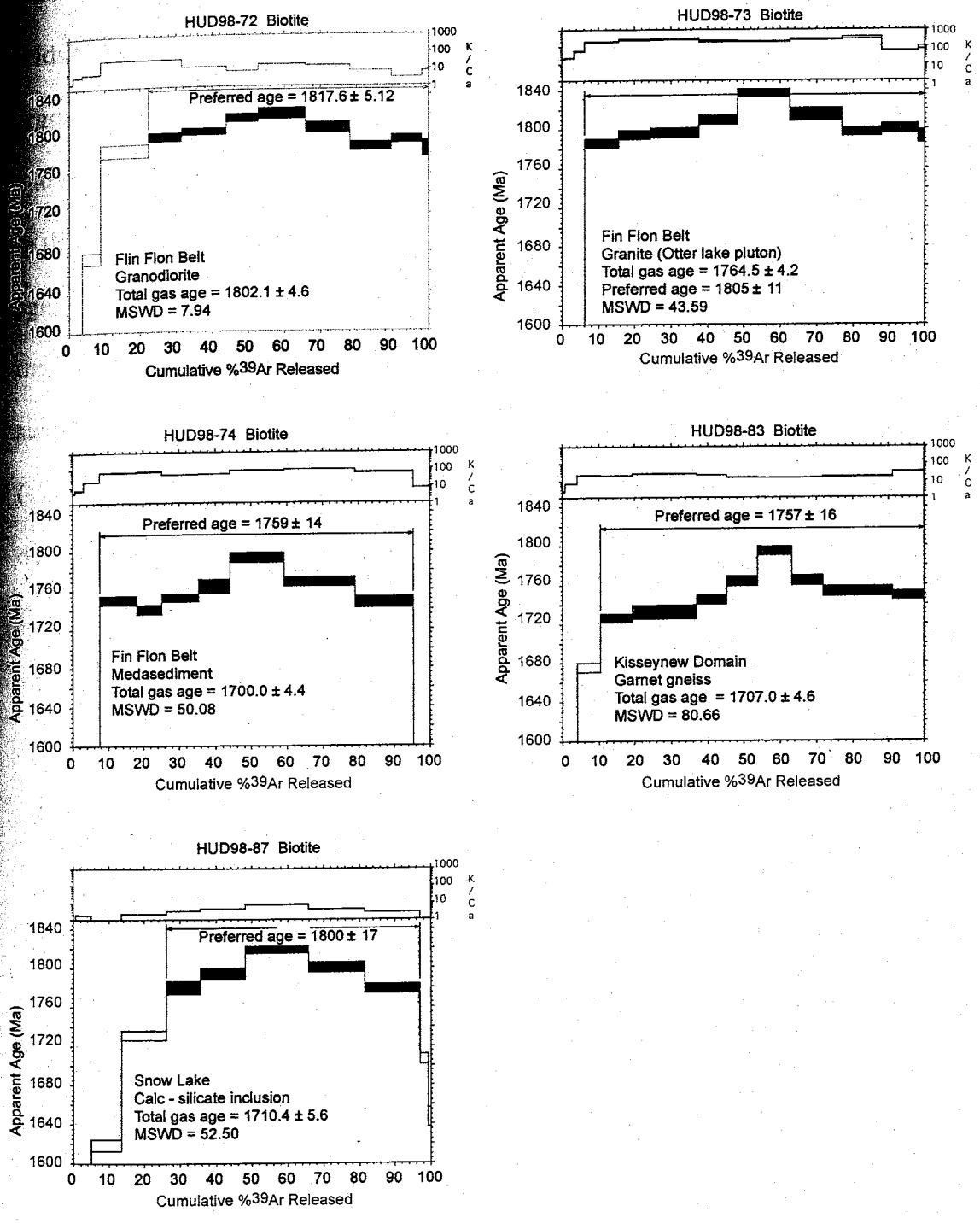

Figure 7. $^{40}Ar/^{39}Ar$ apparent age and apparent K/Ca spectra for biotites displaying hump-shaped release patterns. Analytical uncertainty is represented by width of bars. Total gas ages and plateau or preferred ages are shown on each spectrum. See Figure 1 for sample locations.

chlorite alteration and/or inclusions of potassium-bearing phases. The presence of K-feldspar inclusions may account for the shape of the spectra. K-feldspar degasses its argon throughout heating, which would explain the step- wise pattern found in the initial and final heating steps. However, K-feldspar alone can not explain the old ages attained in the intermediate steps. The biotite can not be >1800 Ma, as this would mean biotite ages older than hornblende ages, which is not possible. A more likely possibility is that the samples have been affected by recoil redistribution. It appears that for the THO samples, the "hump" is most evident in samples with the most chlorite. Lo and Onstott (1989) proposed that recoil of ^{39}Ar into intergrown chlorite was the cause for the disturbed age spectra they found in chlorite-altered granitic rocks from eastern Taiwan. During irradiation, ^{39}Ar can travel up to ~0.16um and can implant into the adjacent chlorite layers, causing a spatial variation in the $^{40}Ar/^{39}Ar$ ratio. During step-heating, differential thermal release from the two phases, where chlorite degasses during the early and late steps, corresponding to the lowest K/Ca ratios, may be the cause of the discordant age spectra (Lo and Onstott, 1989). In general, discordant age spectra are found for samples having of large number of inclusions and a high degree of chlorite alteration, whereas more pure mineral separates generate much flatter, well-behaved age spectra (Figure 8). Given this observation, recoil of ^{39}Ar is the most likely explanation for the hump-shaped pattern of the biotite age spectra. Based on the assumption that the dominant effect of recoil is the redistribution of ^{39}Ar, Lo and Onstott (1989) determined that total gas ages were the best estimate for the age of their samples. The biotites analyzed in this study show evidence of recoil as well as the effects of contaminating K-

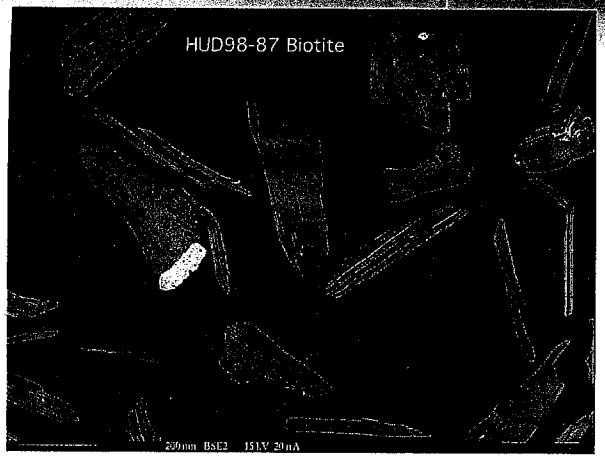

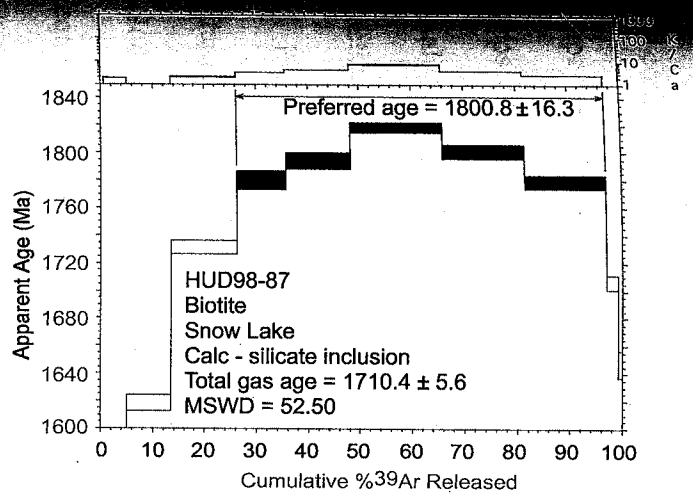

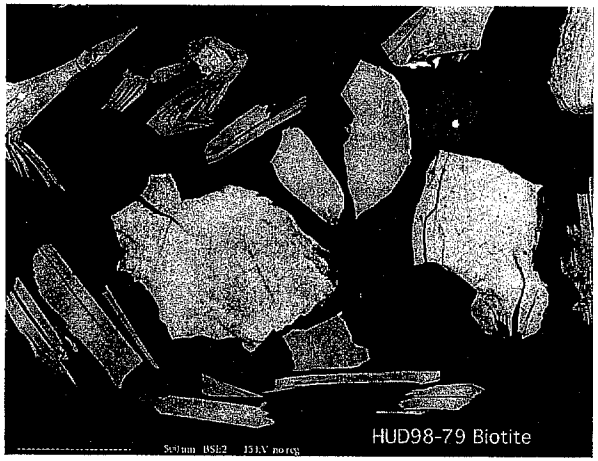

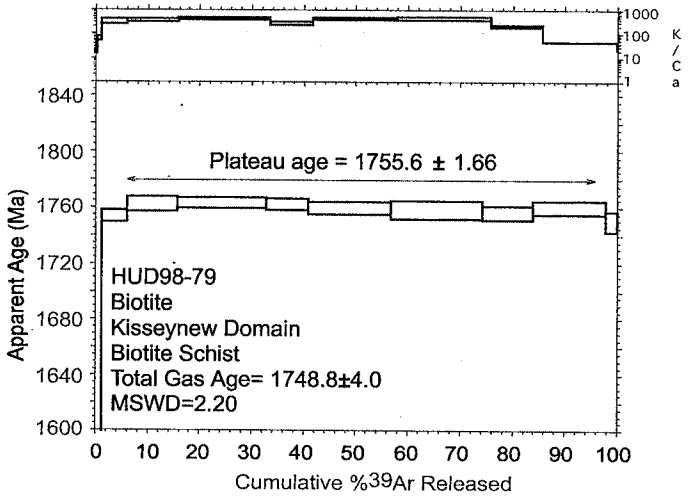

Figure 8. Backscattered electron images and apparent age and K/Ca spectra for biotite samples HUD98-87 and HUD98-79

heating phases; therefore, the total gas age is not the best estimate of the age of these samples. Although total gas ages seem to match ages found throughout the THO, they do not correspond to the general age trend for each terrane and do not make sense with respect to the entire dataset. Preferred ages have been assigned across the intermediate steps, and the very young steps have been ignored as they are likely an artifact of a low quality mineral separate and/or chlorite alteration and therefore recoil. In general, this method of age assignment provides ages that agree with nearby analyses.

Previous authors have measured, through in situ laser analysis, significant age gradients within individual mica crystals taken from slowly cooled metamorphic terranes. Hodges et al. (1994), for example, found that the diffusion domain for muscovite was equal to the size of the grain and that a concentric age gradient was the result of the diffusive argon loss. Incremental step heating of monzogranite from a low-pressure-high-temperature domain revealed ~1400 Ma mica ages and indicated a uniform distribution of $^{40}Ar^*$; however, laser mapping of the same samples revealed large age gradients ranging nearly 400 m.y. (Hodges et al., 1994). In order to determine whether plateau ages obtained by incremental heating in this study are correct or whether they are merely a homogenization of a large variation of ages within the crystal, UV laser-probe analyses were performed on a single biotite and a single muscovite crystal from a pegmatite collected in the Snow Lake region. A series of traverses were made across the cleavage surface of each grain, each consisting of 100μm x100μm ablation pits at a spacing of approximately 500μm (Figure 9).

Apparent ages from the five traverses across the muscovite range from 1640 Ma to 1916 Ma (Figures 10, 11). Ages of individual ablation pits for the three parallel traverses

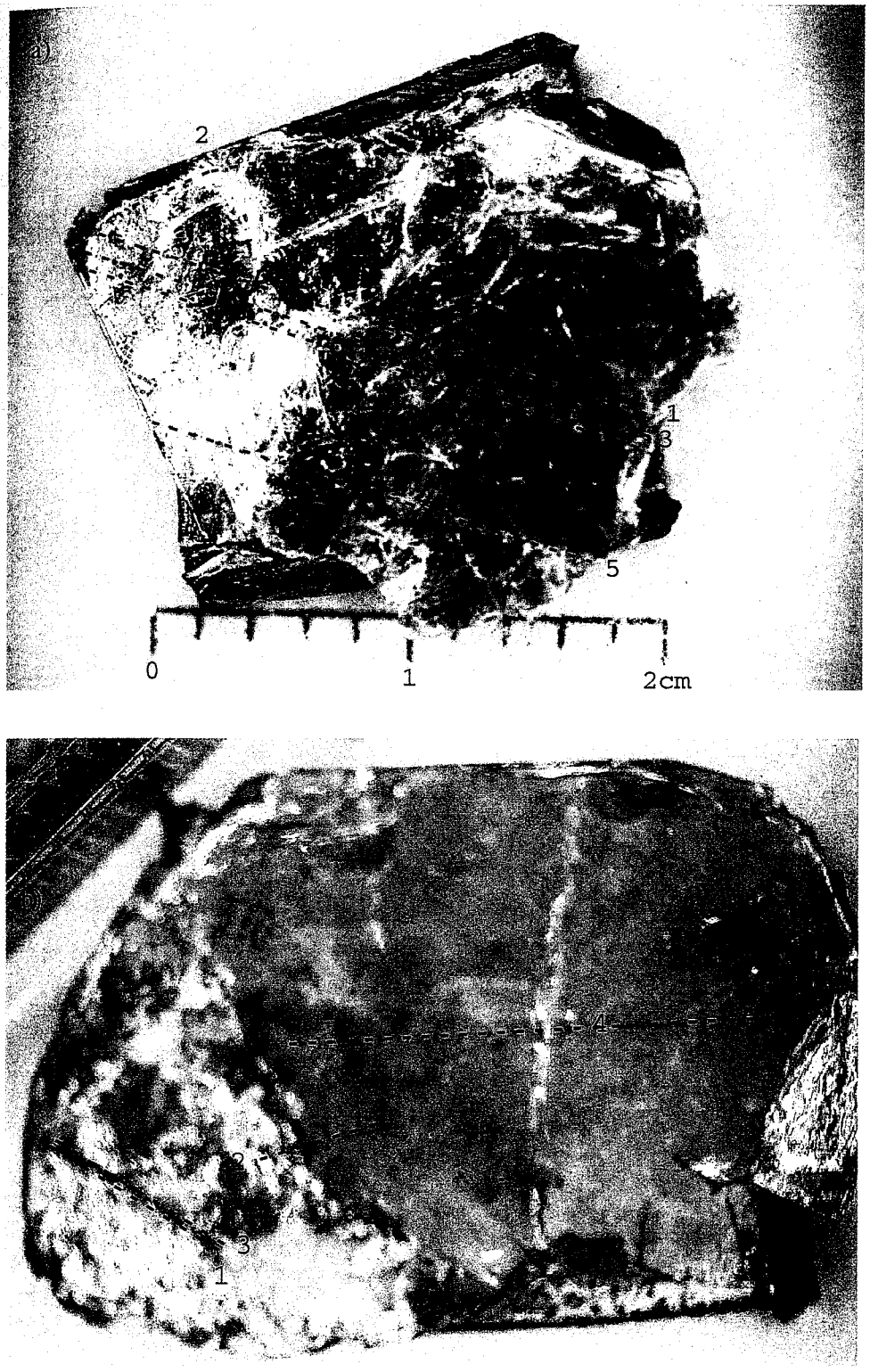

Figure 9. a)Muscovite and b) biotite crystals from sample HUD98-86A, showing location of U-V laser traverses.

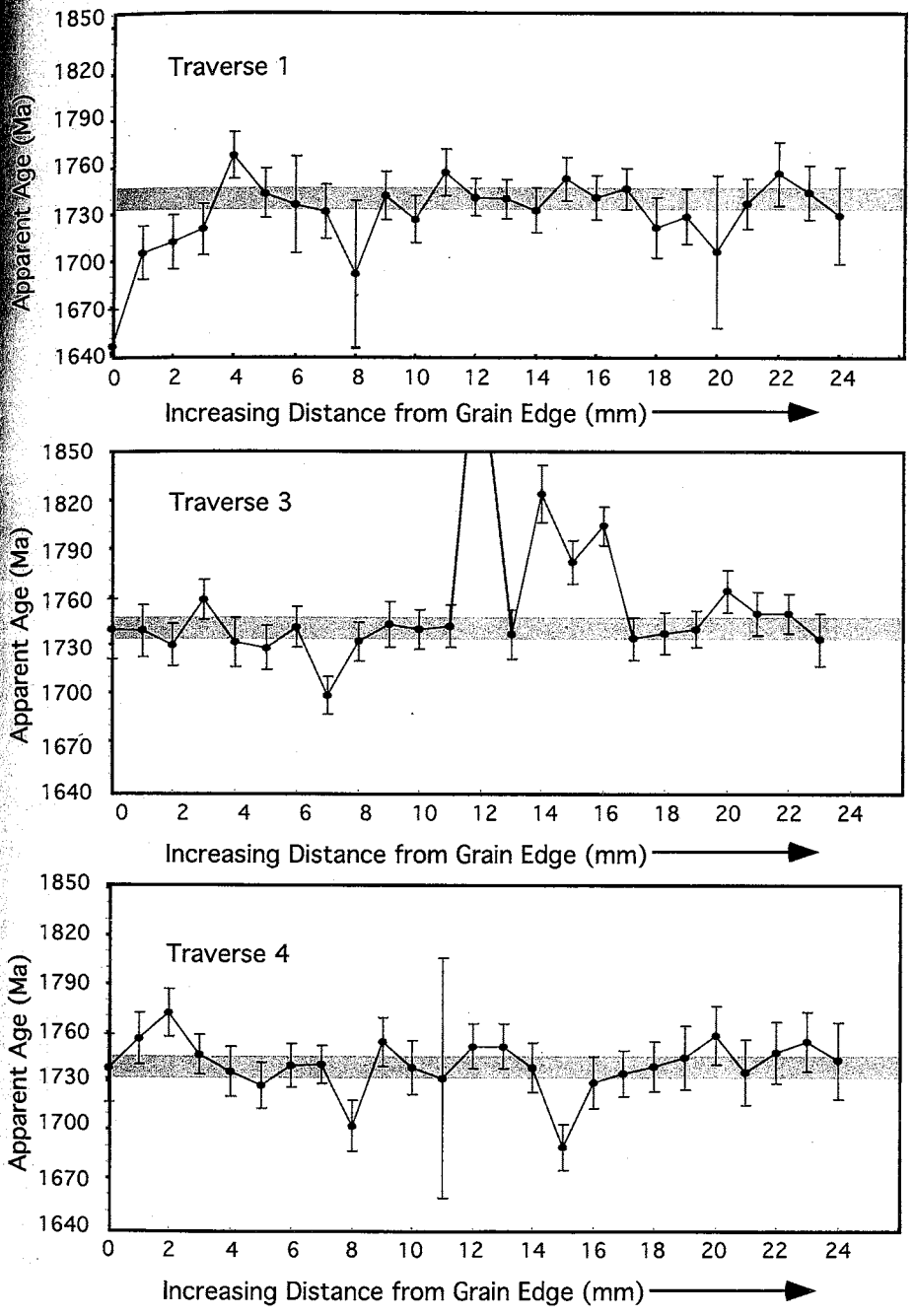

Figure 10. Age versus distance from the edge of the grain for UV laser traverses across the center portion of a muscovite grain from sample HUD98-86A. Traverse locations are shown in Figure 9. The mean weighted total fusion age of ~1740 Ma is shown as a gray bar for reference.

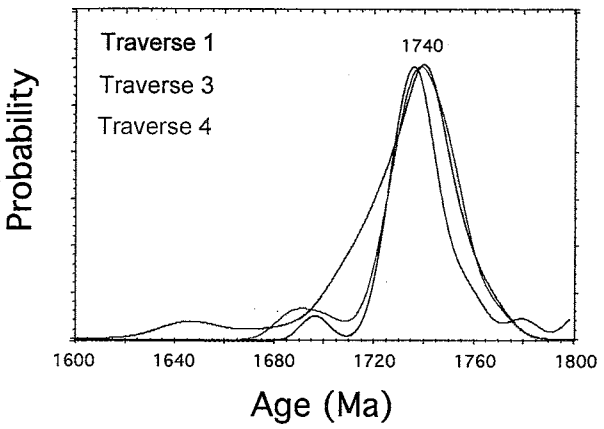

Figure 11. Age probability diagram of muscovite UV laser traverses for HUD98-86A. Traverse locations are shown on Figure 9.

rough the center of the grain have been plotted on age probability diagrams and cluster at ~1740 Ma. Note, however, that three points in the center of the middle traverse (traverse 3) yield apparent ages of 1916, 1823, and 1803 Ma, which are not reproduced in the adjacent traverses. The preservation of such old ages in the center of this grain seems unlikely given that the sample was collected from rocks of nearly sillimanite grade; at temperatures required for sillimate grade metamorphism, bioitite would still be open to argon loss. The observed old ages may be the result of excess argon ($^{40}Ar_E$). Unfortunately, all the analyses are too radiogenic (nearly 100%) to be plotted on an isochron diagram and therefore it is difficult to evaluate this possibility. The youngest ages, <1700 Ma, are found at the very edge of the grain, or are associated with steps of low radiogenic yield. The initial ablation pit of traverse 1 is quite young, (~1645 Ma) and the 3 subsequent steps get progressively older until the ages level off at ~1740. The increase in age from the grain edge may be evidence of an overall age gradient within the grain, however, this trend is not reproduced at the opposite grain edge or in either of the adjacent traverses. A traverse following the edge of the grain seems to have significant analytical error, and gives a bimodal distribution of ages when plotted on an age probability diagram (Figure 12). Ablation ages from traverse 5 (Fiure 9) are only slightly younger (1734 Ma) than those through the center. Overall, this grain does not show the concentric age gradients that have been reported for slowly cooled micas (e.g. Hodges et al., 1994).

Laser ablation of the biotite crystal demonstrates more age variation, apparent ages range between 1661.5 ± 7.8 and 1761 ± 10 Ma. There is no clear pattern of age zoning, as ages do not become consistently older with increasing distance from the grain edge

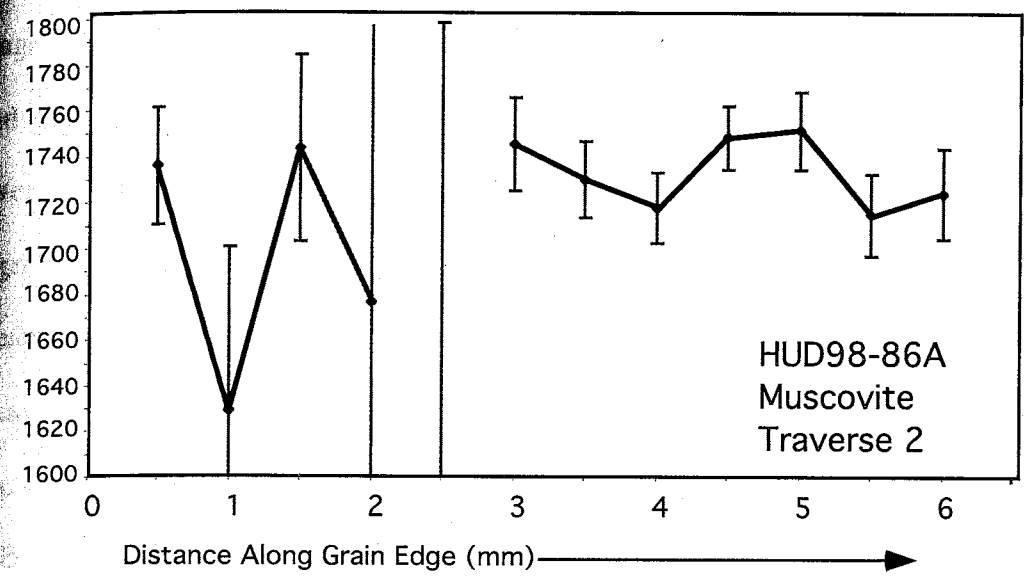

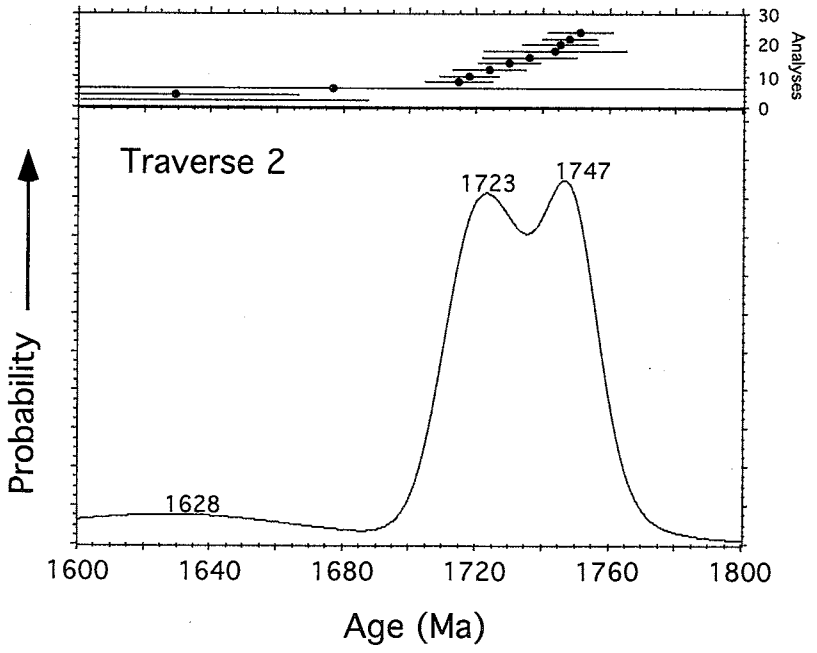

Figure 12. a) Age versus distance along grain edge for muscovite traverse 2 (HUD98-86A), b) age probability diagram of total fusion ages for the same sample.

ures 9, 13). Traverse 1 yields initially young ages that level out at ~1750 Ma, llowed by slightly older ages. Traverse 3, which runs adjacent to traverse 1, reveals nger ages that average ~1720 Ma, with the last analysis reaching 1750 Ma. Traverses nd 2, taken across the center of the grain show more structure and in general yield ages tween 1710 and 1740 Ma. Traverse 2, which crosses from the central, pristine part of he grain into the edge of the grain, shows no obvious correlation between grain ppearance and age. Virgil Lueth (personal communication, 2000) has indicated that the ppearance of the grain edge is not due to alteration

In a follow-up study to the work of Hodges et al., (1994), Hodges and Bowring (1995) utilized three different methods to evaluate the distribution of argon in a biotite crystal from the Horse Mountain monzogranite of Arizona. Although step heating revealed a flat age spectrum, total fusion of 25 biotite fragments revealed apparent ages that varied as much as 200 m.y. Therefore, Hodges and Bowring (1995) suggested that incremental heating can homogenize intracrystalline age gradients in hydrous minerals. In order to determine intra-grain age gradients for the micas in my study, CO_2 laser total fusion was performed on fragments of the two large mica crystals. Total fusion results from 32 muscovite crystal fragments do not display any significant age variation. An age probability diagram reveals a well-defined unimodal distribution, with a weighted mean age of 1751.4 ± 1.6 Ma and a MSWD of 2.17(Figure 14). This age compares favorably with the total gas age of 1755.6 ± 4.0 Ma obtained during step-heating (Figure 4). Total fusion of biotite crystal fragments (broken from an edge of the large crystal used for UV laser analysis) yields a broad distribution of ages with a mean of 1748.7 ± 5.7 Ma and a MSWD of 23 (Figure 14). Although incremental step heating was not done on this

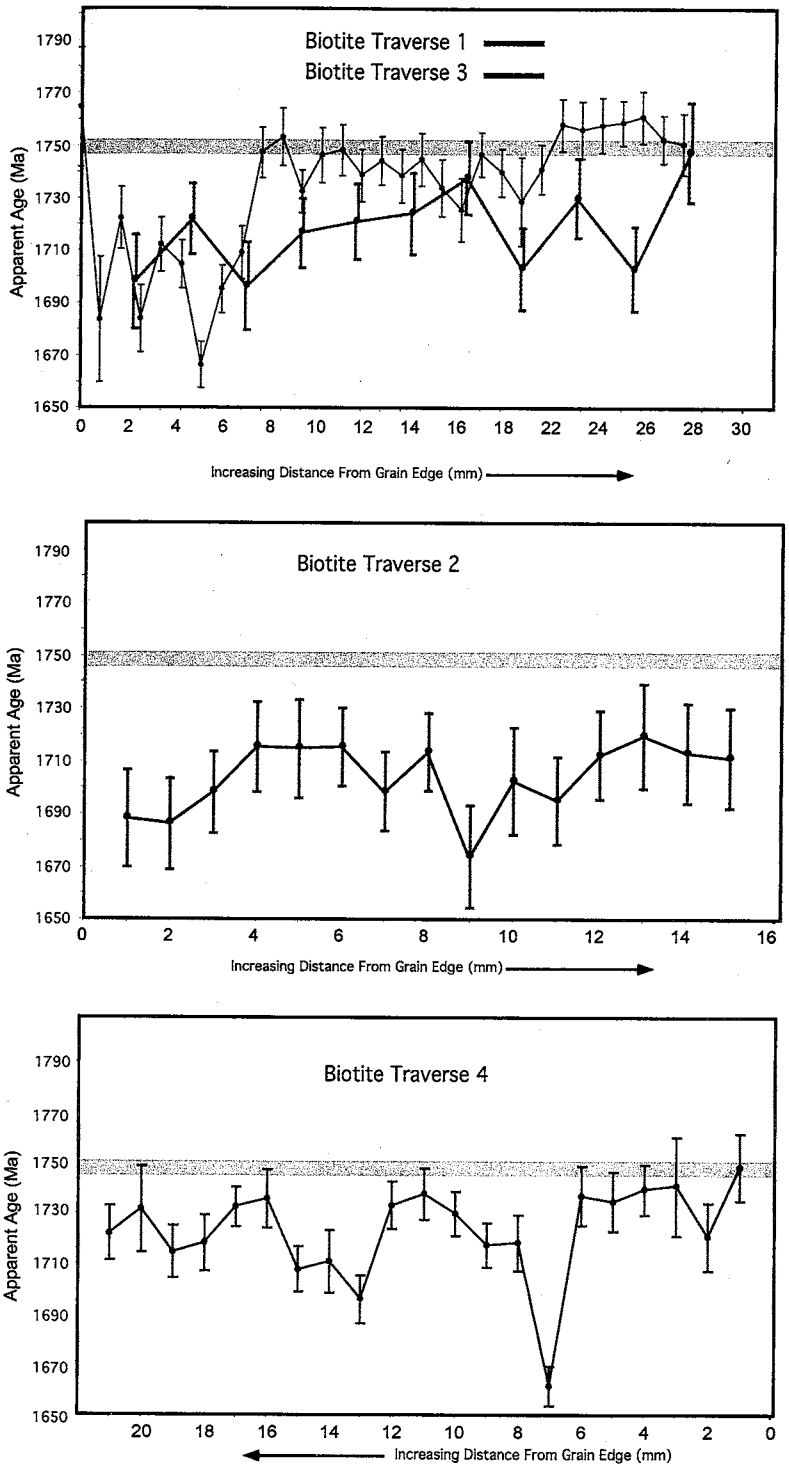

Figure 13. Age versus distance from the edge of the grain for UV laser traverses across a biotite grain from sample HUD98-86A. Traverse locations are shown in Figure 9. The weighted mean total fusion age of ~1748 Ma is shown as a gray bar for reference.

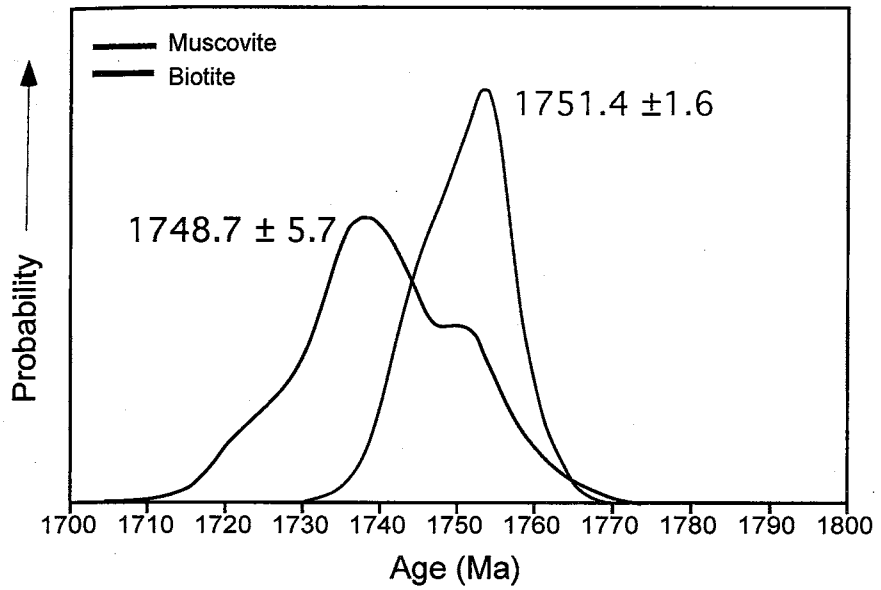

Figure 14. Age probability diagram for total fusion ages from fragments of a biotite and muscovite crystal from sample HUD98-86A.

ample, the mean total fusion age is somewhat older than the ages found for UV laser analysis. This discrepancy is possibly the result of a systematic analytical error between the two laboratory methods. Due to the typically small signal size of the UV laser data compared with total fusion, the UV laser data is much more sensitive to small systematic errors. Also, typical variation in J-factor across an irradiation tray is on the order of 1%, which correlates to a ~10 Ma difference in age. The biotite crystal that was crushed for this analysis was roughly the diameter of an irradiation tray and therefore we would expect the J-factor to vary accordingly. However, unlike the UV laser traverses, a single J value was assigned for all total fusion analyses and this may explain the age discrepancy between the two methods. The single muscovite crystals were not broken from the large crystal; they were hand separated and irradiated in the normal configuration, and therefore have been assigned a more accurate J-value.

K-feldspar thermochronology

The closure temperature theory (Dodson, 1973) states that above its closure temperature, a mineral effectively diffuses all its $^{40}Ar^*$ as soon as it is formed, and that below the closure temperature, loss of radiogenic ^{40}Ar is negligible - allowing it to accumulate in the crystal lattice, and that there is a continuous transition between these two endmember states. Lovera et al. (1989) recognized that K-feldspars typically contain age gradients that do not conform to a single diffusion length scale or closure temperature. This observation, and the recognition of nonlinear Arrhenius relationships, led them to construct a model assuming multiple diffusion domains (MDD) for K-feldspar. The MDD method (Lovera et al., 1989) is based on Dodson's concept, but

assumes that K-feldspars consist of a number of discrete diffusion domains of varying length scale and closure temperature. Since argon diffusing out of the largest domains will have farther to travel to get to a diffusion boundary, the large domains have a higher closure temperature relative to the small domains.

The MDD theory requires the assumption that the transport of argon occurs by volume diffusion in both the laboratory and in nature (McDougall and Harrison, 1999). Other assumptions include: 1) ^{40}K must be uniformly distributed; 2) the domains can be described by a simple geometry; 3) the domains are non-interacting; and 4) the formation of the domains must occur at temperatures above the closure temperature of each domain (McDougall and Harrison, 1999). Controversy exists as to whether the stringent conditions of the MDD model are actually met. Parsons et al. (1999), through direct observation of microtextures using electron microscopy (TEM), has suggested that the geometry, size, and boundaries of diffusion domains evolve continuously over time and temperature. Mechanisms for the modification of diffusion domains include metasomatism and diagenesis. In addition, Parsons et al. (1999) states that for temperatures reached during furnace heating, K-feldspar microtextures are only metastable, leading to structural and chemical changes. However, Lovera et al, (1993) state that the structural stability of K-feldspar during step heating, the kinetic parameters of argon can be accurately measured, and meaningful thermal histories can be constructed (Lovera et al., 1993). The MDD model is supported by the agreement between K-feldspar thermochonolgy and other methods of dating minerals that record a similar portion of the thermal history (apatite fission track studies) and the identical and geologically reasonable thermal histories that have been obtained for samples from a

area with very different kinetic parameters (e.g. Heizler et al., 1988; Lovera et al., 89).

K-feldspar bearing samples were collected at six sites within the study area; their age pectra are shown in Figure 15. In general, the K-feldspars show similar age spectra and vidence of non-uniform $^{40}Ar^*$ concentrations (e.g. variation in age). Three K-feldspar amples from the Kisseynew/Flin Flon traverse (HUD98-78, HUD98-80 and HUD98-83), show a monotonic increase in age beginning at ~900 - 1100 Ma rising to between 1600 and 1700 Ma (Figure 15, Appendices E, F). HUD98-86A, (from a pegmatite in the Snow Lake region), yields a much flatter spectrum, which starts at 1500 Ma and gets no older than 1600 Ma.

HUD98-69 and HUD98-84 display alternating old and young steps during the initial isothermal heating steps. Harrison et al. (1993) found that for a heating schedule containing duplicate isothermal steps, K-feldspars reveal a reproducible pattern where the first step of the pair yields a much older age and higher Cl/K than the second. These authors suggested that the old ages are the result of excess argon ($^{40}Ar_E$) that degasses during the first of each set of duplicate heating steps and is correlated to Cl. After examination of electron microprobe back-scatter images of the samples, they concluded that fluid inclusions were the source of the Cl-related excess argon ($^{40}Ar_E$). Since decrepitation of the inclusion occurs primarily during the first of the duplicate steps, very little release of $^{40}Ar_E$ occurs during the second step. In a subsequent study, Harrison et al. (1994) examined the argon to chlorine ratios for a number of basement K-feldspars. A plot of $\Delta^{40}Ar^*/K$ (apparent age) versus $\Delta Cl/K$ yields a well-defined line that enables a correction to be made for $^{40}Ar_E$, so that thermochronologic information may be obtained.

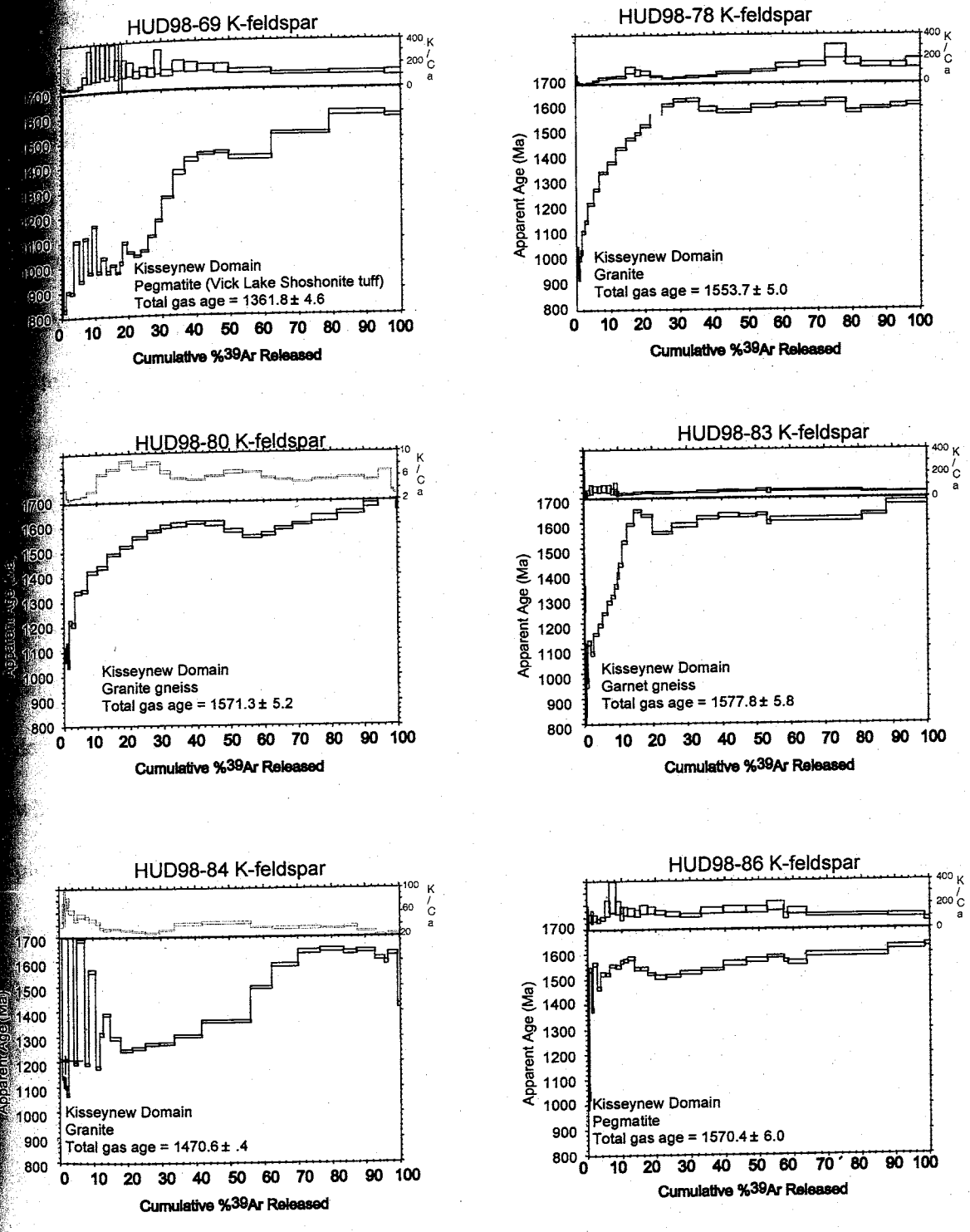

Figure 15. $^{40}Ar/^{39}Ar$ apparent age and apparent K/Ca spectra for K-feldspars. Analytical uncertainty is represented by width of bars. Total gas ages are shown on each spectrum. See Figure 1 for sample locations.

ages obtained from the second of the duplicate steps are thought for the reasons ted above to record a more accurate age, although it is difficult to know if all the xcess argon has degassed during the first step. For the samples in this study, the first tep of each duplicate pair has been corrected to fall between the second step of the receding duplicate pair and the second step for modeling purposes (Figure 16).

Argon diffusion coefficients have been calculated, assuming a slab geometry, for each K-feldspar by examining the heating time and fraction of argon released, and are plotted on Arrhenius diagrams (Figure 17, Appendix G). The activation energy for each sample is obtained by determining the slope of the initial linear segment of the Arrhenius plot. Activation energy has been calculated (using the Lovera program) to fall between 33 and 54 kcal/mol for the six samples used in this study (Table 2). Lovera et al. (1997) calculated an average activation energy for 115 K-feldspars and showed that these data define a normal distribution at 46±6 kcal/mol. In general, the samples from this study whose smallest diffusion domain is well defined by the initial points on the Arrhenius plot yield activation energies that fall within the normal distribution calculated by Lovera et al. (1997). However, for those samples whose activation energy falls outside 46 ±6 kcal/mol, the initial diffusion domain is generally not well defined. Therefore the initial points on the Arrenhius plot are not reliable and should not be used to calculate an activation energy, and an activation energy of 46 kcal/mol has been assigned to all six K-feldspars from the southern THO. Relative diffusion domain sizes are obtained by applying the activation energy and modeling the diffusion coefficients (Table 2). $Log(r/r_o)$ plots for each sample are shown in Appendix G and an example is given in Figure 17. The $log(r/r_o)$ plot is a visual representation of the amount of ^{39}Ar contained in

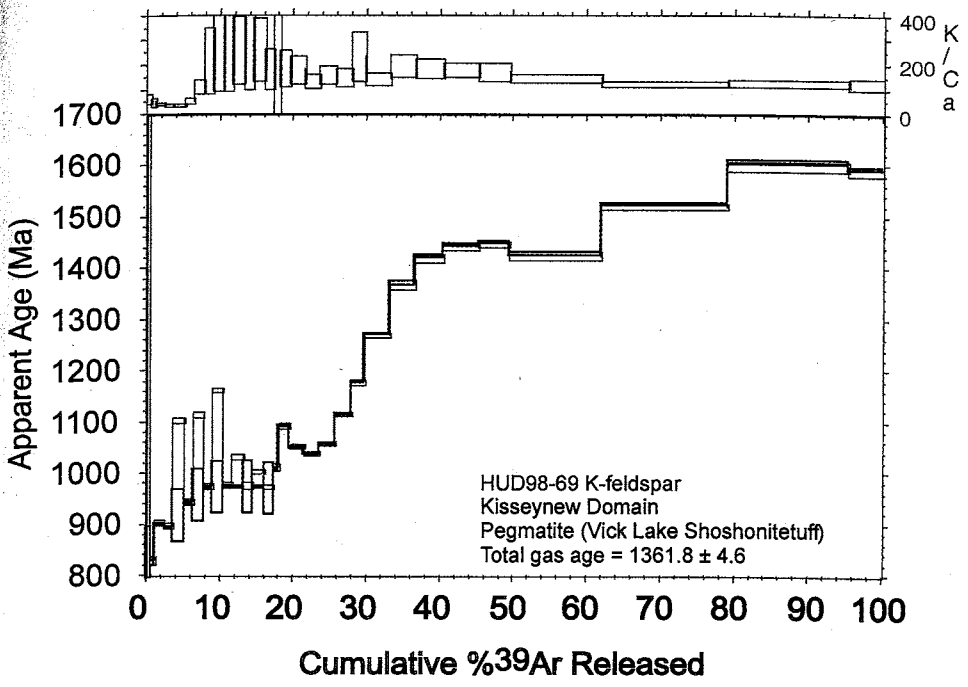

Figure 16. Age spectrum for K-feldspar from sample HUD98-69. Black line is the measured age spectrum. Red line shows the modeled age spectrum, where the initial heating steps have been corrected for excess argon.

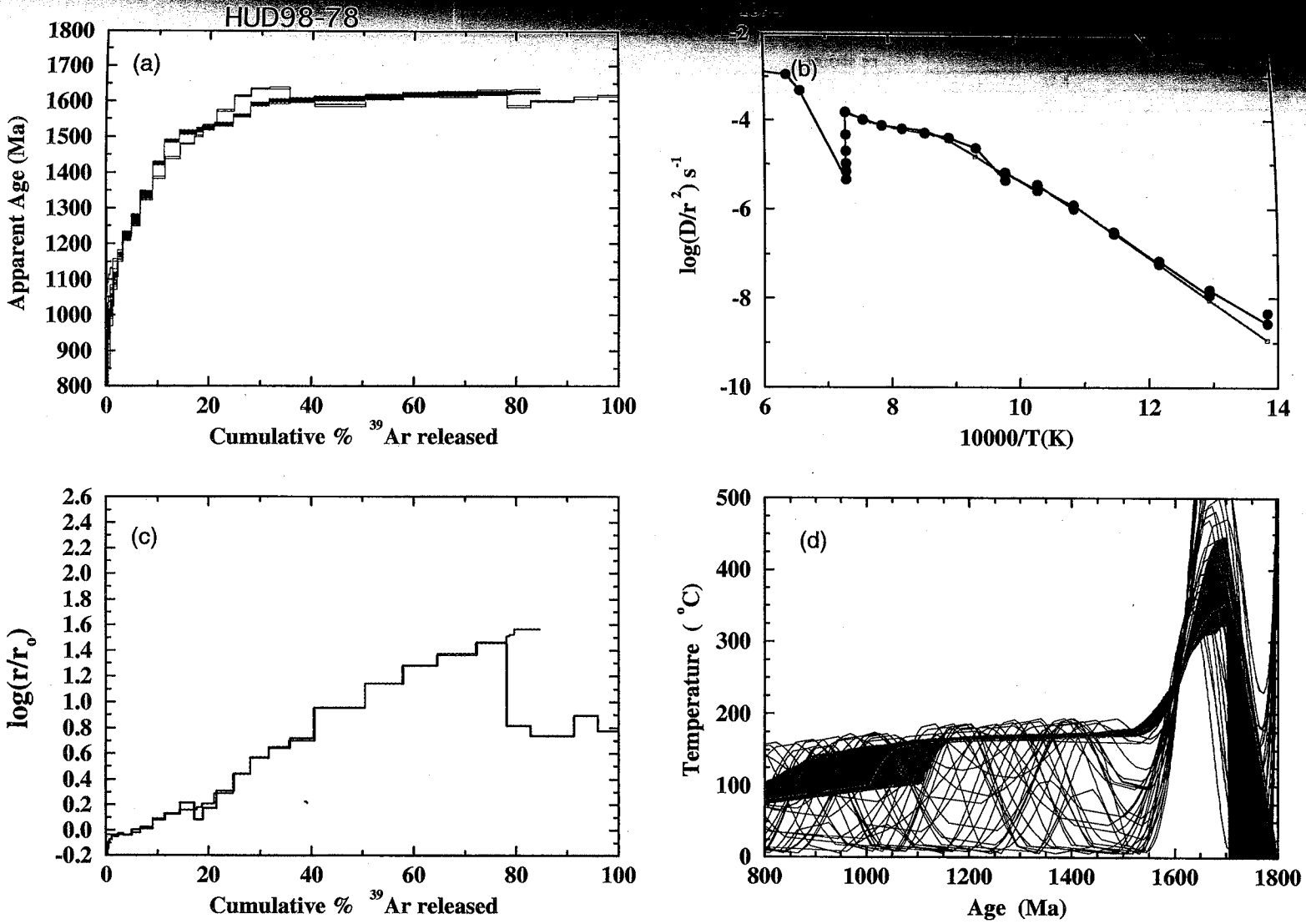

Figure 17. Example of kinetic parameters for HUD98-78, measured (black) and modeled (red) a) age spectrum, b) log (Dr^2)s^{-1} versus temperature (Arrhenius diagram), c) log r/r_o, and d) unconstrained cooling history ("spaghetti" plot) and monotonic cooling history.

2) Table of kinetics for K-feldspar

Samlple	HUD98-69	HUD98-78	HUD98-80	HUD98-83	HUD98-84	HUD98-86
Calculated Ea	**50.6**	**37.4**	**42.2**	**41.3**	**33.4**	**54.2**
Assigned Ea	**46**	**46**	**46**	**46**	**46**	**46**
Number of Domains	8	7	8	7	6	7
Ea	46	46	46	46	46	46
D/r^2	9.265777	7.0838873	7.7323221	7.080989	8.1852034	8.1183907
f	0.03239186	0.03817593	0.03387112	0.05221332	0.01572485	0.00912294
Ea	46	46	46	46	46	46
D/r^2	8.1359847	5.7899255	6.7728777	6.1769792	7.3865751	7.1894229
f	0.03740351	0.16730387	0.08528107	0.02904417	0.04921768	0.04076132
Ea	46	46	46	46	46	46
D/r^2	7.0285094	4.4987638	5.8934845	4.009081	5.9256353	6.1468361
f	0.0405902	0.07626741	0.12159268	0.13979229	0.09473677	0.06773021
Ea	46	46	46	46	46	46
D/r^2	5.6893804	4.4983641	5.4479185	3.4282337	4.042548	4.4271918
f	0.07970126	0.08358358	0.11674043	0.05499573	0.32250924	0.10136197
Ea	46	46	46	46	46	46
D/r^2	4.7546393	3.5938204	4.621932	2.9769995	3.0254408	3.250277
f	0.0825875	0.10168694	0.14395957	0.14543728	0.13292202	0.13484809
Ea	46	46	46	46	46	46
D/r^2	3.5086904	2.6607567	4.3648383	2.9507781	2	2.2934133
f	0.02691465	0.20215606	0.06982477	0.00042161	0.38488944	0.16405244
Ea	46	46	46	46		46
D/r^2	1.8402913	1.7	2.940306	1.1		1.2
f	0.194162	0.33082621	0.17771709	0.57809561		0.48212303
Ea	46		46			
D/r^2	1.3		2.4			
f	0.50624902		0.25101327			

For each domain:

Ea = activation energy

D/r^2 , D=diffusion coefficient, r=diffusion radius

f = fraction loss

domain and is independent of the heating schedule (Lovera et al., 1991). This plot generated by comparing the measured diffusion coefficients to the diffusion coefficient erated using a reference Arrhenius law. The initial linear segment of the Arrhenius is used here as the reference law and is shown as a black line on Figure 17. The ffusion length associated with the reference law is denoted as r_o, and r is the deviation om the reference line. Arrhenius plots as well as log r/r_o for each sample can be found Appendix G.

Thermal histories are obtained by repeated modeling of a given age spectrum using he kinetic parameters. Two programs were used to create thermal histories. The continuous monotonic cooling model is constrained in that it only allows cooling, the free model is completely unconstrained and therefore allows re-heating events. Results of modeling using both methods are shown in Figures 18 and 19. K-feldspar was analyzed from several locations throughout the southern THO in a reconnaissance effort to describe the low temperature thermal history of the area. Results for samples from the Flin Flon/Kisseynew traverse indicate that the samples cooled rapidly through the closure temperature of the largest domains between 1600 and 1700 Ma and that final closure through the smallest domains did not occur any earlier than 1100 Ma. Modeling of the data allowing only monotonic cooling shows accelerated cooling between 1650 –1525 Ma from ~350 -175°C, followed by protracted slow cooling until 1150 Ma, when the samples begin to cool through their lowest closure temperature (Figure 18). Below 150°C the models are not well constrained as evidenced by the broad distribution of acceptable thermal histories. Modeling allowing reheating reveals similar results (Figure 19). All three samples from the traverse record accelerated cooling from at least 325°C

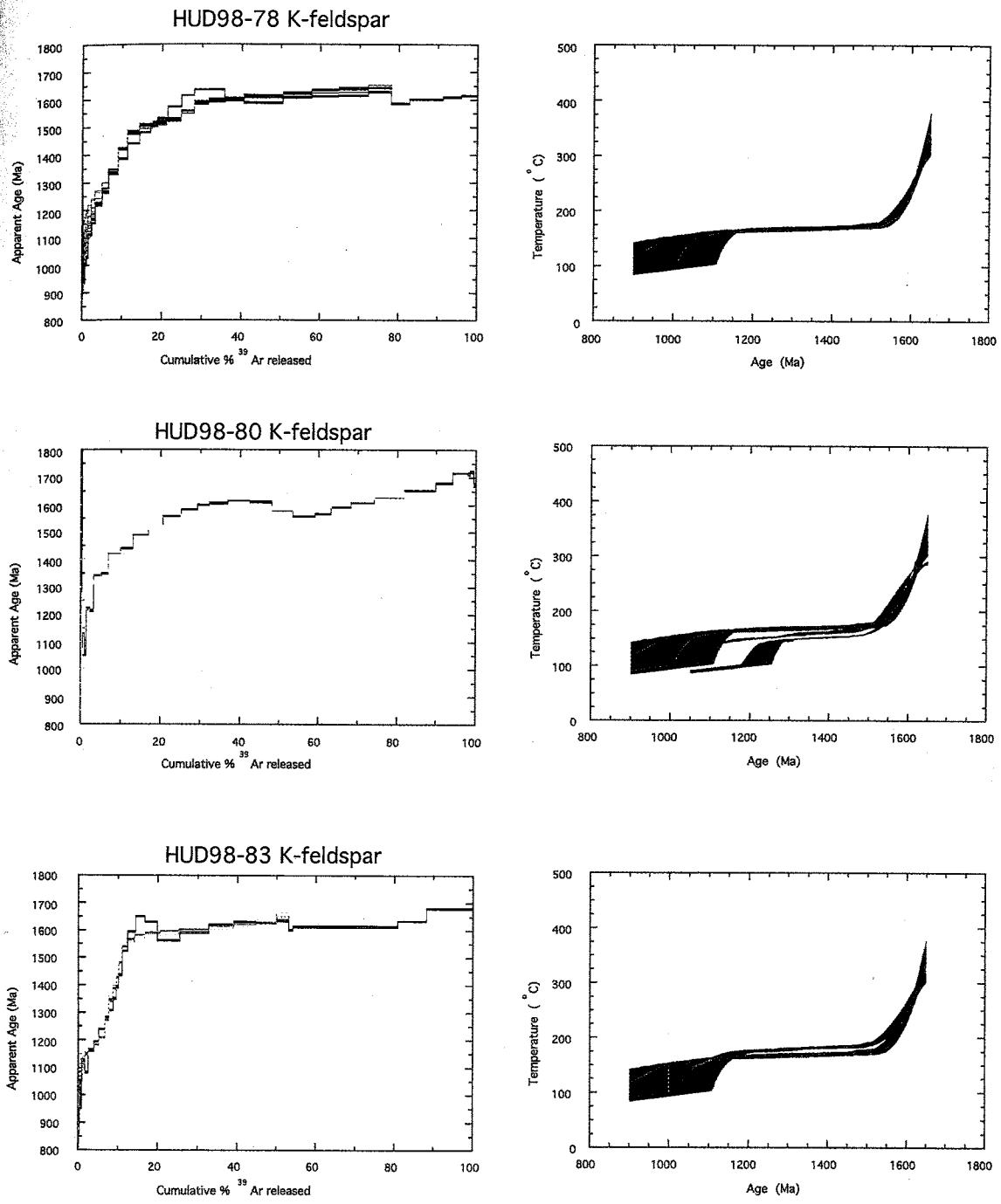

Figure 18. Age spectra and monotonic cooling models for K-feldspar samples. For each sample the measured age spectrum is shown in black whereas the modeled spectrum appears in color. The green area represents a less precise fit than the colored areas. The cooling history for sample HUD98-78 is plotted with each thermal history for reference.

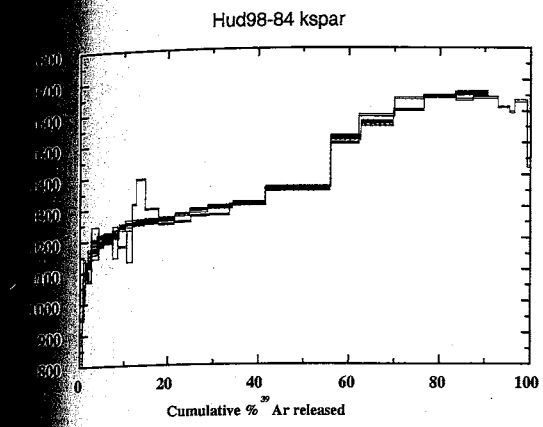

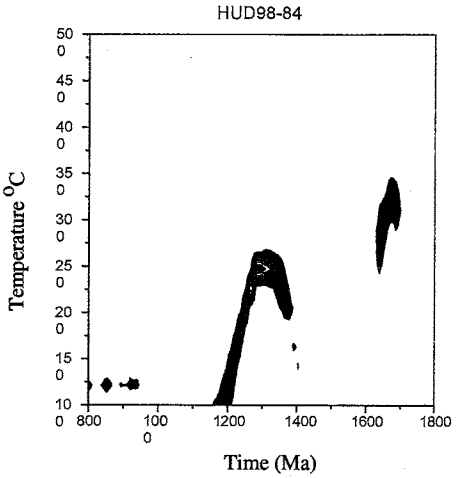

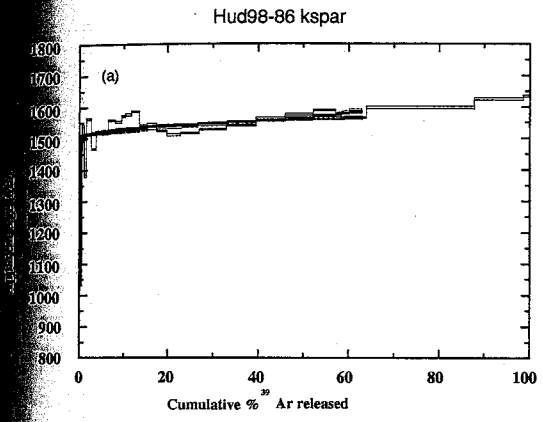

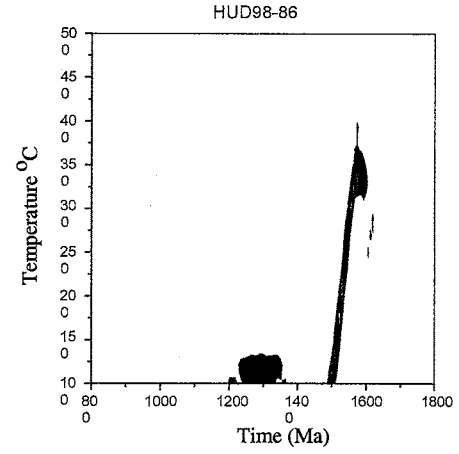

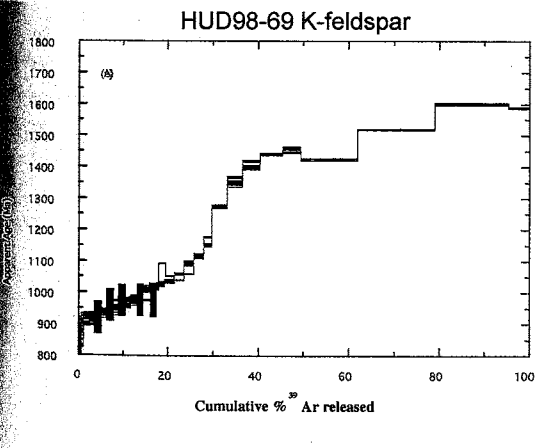

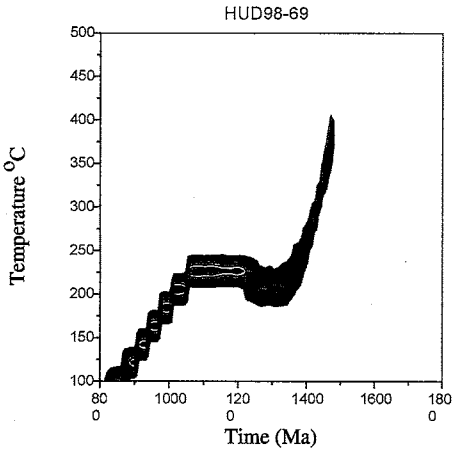

Figure 18. (continued)

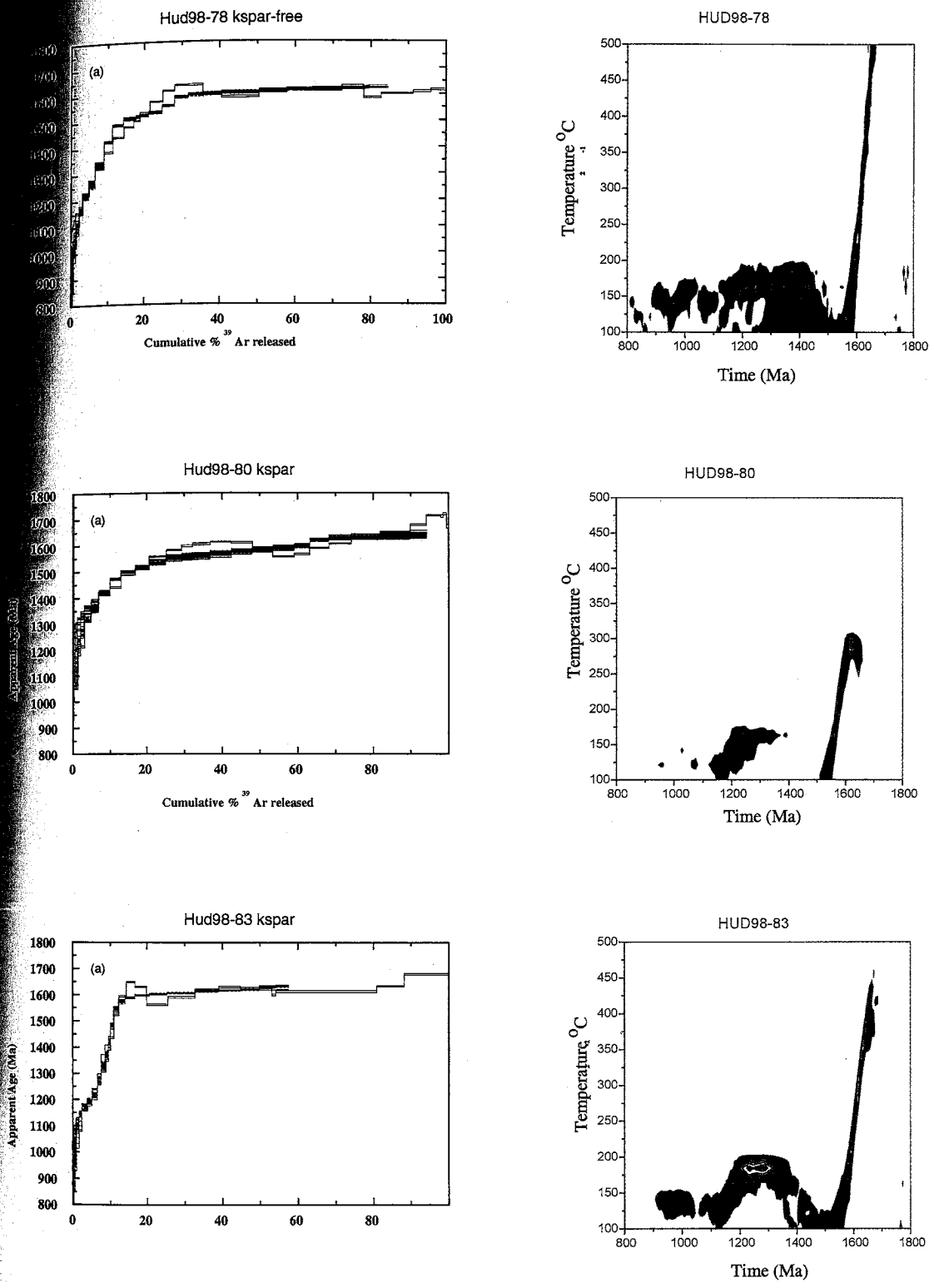

Figure 19. Age spectra and unconstrained thermal models for K-feldspar samples. For each sample the measured age spectrum is shown in black whereas the modeled spectrum appears in red.

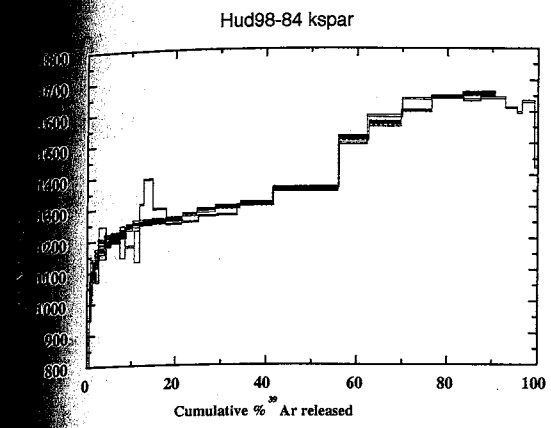

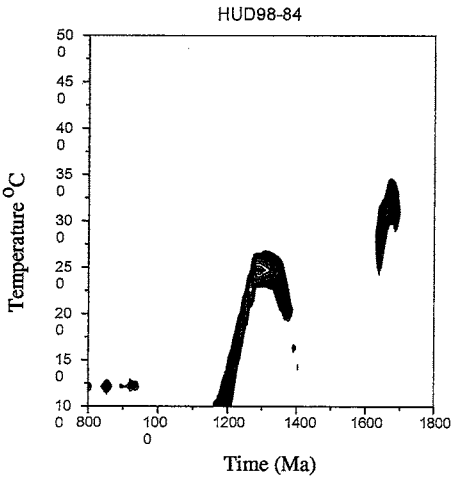

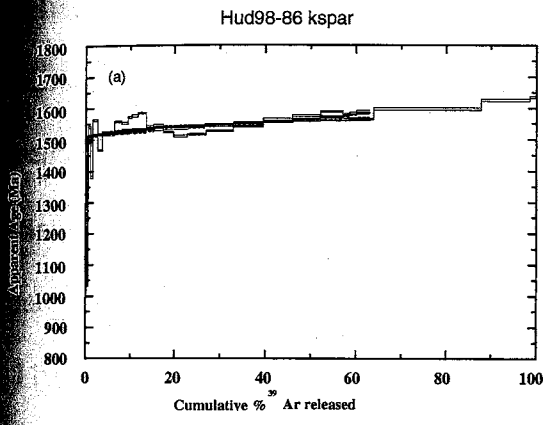

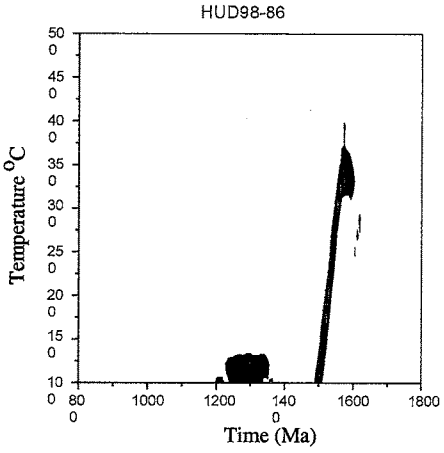

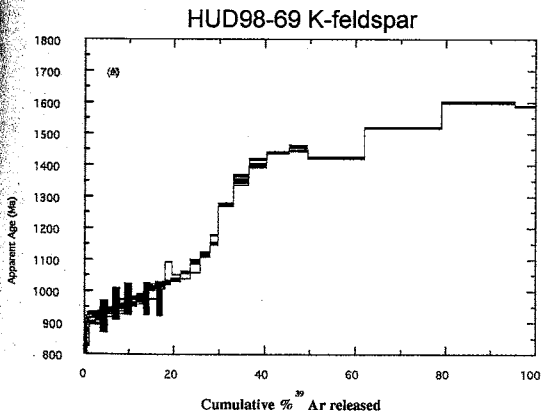

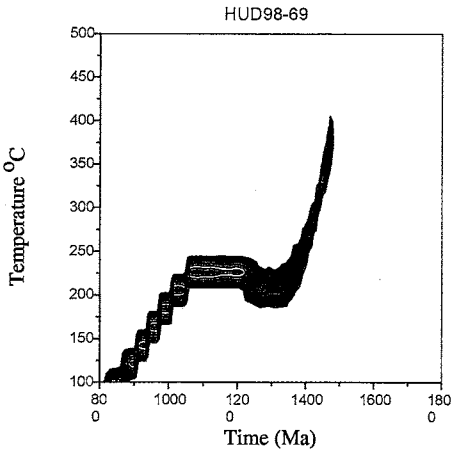

Figure 18. (continued)

to ~200°C at ~1600 Ma. Since these models allow thermal events, the program has constructed multiple heating events from 1400 – 1200 Ma, which give an equally good fit to the age spectra (Figure 17, 19). The free models for both HUD98-83 and HUD98-78 produce histories with a thermal pulse at ~1200 - 1300 Ma, whereas HUD98-78 requires more uniform temperature for the period between 1400 – 1200 Ma. The age spectrum for K-feldspar HUD98-69, from a pegmatite collected <50 km west of the traverse in the central Flin Flon Belt, reveals a similar release pattern to those from the traverse, but a different thermal history. The monotonic cooling model does not reveal the accelerated cooling seen for the traverse samples, but rather a more gradual, continuous cooling beginning at ~1500 Ma. The sample also remains warmer (~100°C) than the thermal history of the area to the east throughout cooling. Both the free and monotonic cooling models require more uniform temperatures and very slow cooling between 1300 and 1100 Ma. The agreement of the two models for this sample, as well as the agreement of the free and monotonic models for HUD98-78 and HUD98-83 support the use of monotonic cooling for the interpretation of the thermal history of this area.

The two samples collected in the Snow Lake region (HUD98-84 and HUD98-86a), exhibit strikingly different age spectra and thermal histories given their close proximity in the field. Modeling of HUD98-84 (from a granite of the Wekuso Lake pluton) is characterized by very slow cooling until 1300 Ma when more rapid cooling begins (Figure 18). Modeling without the monotonic cooling constraint reveals a possible thermal spike at ~1300 Ma. However, the lack of information provided by the contour plot between 1600 and 1400 Ma suggests that uniform continuous temperatures over this time period are possible as well. HUD98-86a displays rapid cooling from 325° to 150°C

ween 1600 to 1500 Ma. Subsequent slow cooling after 1525 Ma is an artifact of the gram, as it can be seen in the spectrum that there is no information for ages younger ~1400 Ma. Manual modeling of this sample to better resolve the age gradient in the rial heating steps does not eliminate the difference in cooling history between HUD98- and HUD98-86. Free modeling of this sample shows a possible thermal peak at 1300 a as well, but again, the age spectrum does not provide any information at ages less han 1400 Ma and therefore the monotonic cooling model is taken as the most likely ooling history of this sample.

Apatite Fission-Track Results

Naturally occurring fission tracks have an average length of ~16.5μm (Wagner and Van Den Haute, 1992). The stability of fission tracks is dependent mainly upon temperature, time, and chlorine-fluorine ratios. With increasing time and temperature, tracks anneal. Various laboratory experiments have shown that there is a temperature zone where partial track stability occurs. This zone is termed the partial annealing zone (PAZ) where tracks are retained but continuously anneal with time. The partial annealing zone generally occurrs between 60-70°C and 120-140 °C, depending on the chemistry of the apatite. Tracks in a chlorapatite anneal at temperatures ~30°C higher compared to those in flourapatite (Carlson et al., 1999). Temperatures greater than ~120°C will cause tracks to anneal quickly and not be retained; below ~60°C tracks are retained, with only slight annealing. As is true for all thermochronometers, apatite fission-track ages record the formation age of the rock only in rare cases, usually in rapidly cooled (>5°C/Ma) volcanic rocks that have not been deeply buried. Rocks that have undergone slow

cooling or have experienced re-heating will record an age that is less than the formation age, depending on the thermal history (Gleadow et al., 1986).

Fission-track ages will record events that promote cooling and thereby move samples through the partial annealing zone. Examples of such events include tectonic denudation, uplift, and erosion, removal of a heat source or change in geothermal gradient. Gleadow et al. (1986) have shown that average track-length distributions can be used to determine qualitative thermal histories. Tracks that formed in quickly cooled samples will have an average track length of 14-15.6μm and show a unimodal distribution, whereas samples that have cooled slowly will reveal a distribution skewed toward longer tracks and have a mean track length between 13 and 14μm. Samples that have experienced long residence within the PAZ will have mean track lengths between 10 and 12μm with a much broader distribution. If a sample has suffered a re-heating event, it will yield a geologically meaningless age and a bimodal track-length distribution. If re-heating does not erase all the tracks, but significantly shortens them, the resultant track-length distribution will reveal a bimodal population of tracks: shortened tracks caused by the heating event and longer ones that formed after the event.

A modeling program has been developed by Ketchum et al. (2000) for deriving thermal history information from fission track ages and track length measurements. The program utilizes mathematical formulations to characterize the annealing of fission tracks with temperature and time based on laboratory experiments extrapolated to geologic time scales. In addition to age and length data, chemical composition data can be incorporated to accommodate the relationship between annealing rates and composition. For the purpose of this study, an inverse model was run, where age, track length, and

positional data were entered and the program was allowed to generate a range of mal histories consistent with the entered measurements. Geologic constraints can be posed in order to restrict the thermal histories to those that are geologically feasible.

For fifteen samples from the study area at least 20 apatite grains were separated, making it possible to obtain an age for each sample. Three of these were collected on either side of and within the Tabbernor Fault Zone (Figure 1, Table 3). Ages on either side of the fault zone are slightly older (403 ± 23 and 392 ± 41 Ma; samples HUD98-58 and HUD98-60) than within the zone where the apparent age is 378 ± 19 Ma (HUD98-59). A single sample (HUD98-63) collected from a pelitic schist along the northern boundary between the Flin Flon Belt and the Kisseynew Domain was dated as well; it revealed an apparent age of 477 ± 26 Ma. The remaining samples were collected along a N-S traverse extending from the southern Flin Flon Belt into the Kisseynew Domain. The traverse extends northward from the craton edge nearly 80 km where the rocks are largely granites, schists and gniesses. Of the 12 samples along this traverse, eight were datable, although for HUD98-80 and HUD98-81 only 7 and 5 apatite grains were separated, respectively (Table 3). Apparent apatite fission-track ages of these samples range from 401 to 466 Ma, although there is no clear correlation with distance from the craton edge (Figure 20). Three samples collected to the west of this traverse (HUD86-9, 86-23, and 86-26) yield ages of 384 ± 36, 540 ± 36 and 530 ± 47 Ma.

Track-length measurements were made on all dated samples. Whenever possible, at least 75 confined tracks were measured for each sample. Track length measurements

Fission track data summary table.

Sample	Location	No. of Grains Dated	ρs x10^5 (t/cm^2)	ρi x10^5 (t/cm^2)	ρd (10^5) x10^5 (t/cm^2)	Central Age (Ma) (±2σ)	P(X^2)^5 (%)	Mean Track Length (±1σ)	Standard Deviation Track Length (μm)
[illegible]	Flin Flon	17	5.228 (1307)	3.784 (946)	1.14	383.95 ± 35.7	28	11.47±0.53 (73)	2.3
[illegible]-29	Flin Flon	20	14.369 (4167)	6.983 (2025)	1.15	539.59 ± 35.6	55	11.08±0.53 (71)	1.6
[illegible]-26	Flin Flon	19	6.252 (1813)	3.328 (965)	1.15	531.28 ± 46.7	82	11.18±0.47 (75)	2.1
[illegible]98-58	Hanson Lake	19	7.815 (2579)	4.212 (1390)	0.86	403.11 ± 23.0	50	11.6 (60)	2.2
[illegible]98-59	Hanson Lake	23	13.454 (5516)	8.200 (3362)	0.87	377.52 ± 19.0	45	11.55±0.59 (39)	1.9
[illegible]98-60	Hanson Lake	19	20.886 (5848)	12.168 (3407)	0.87	392.15 ± 41.4	7	10.83±0.47 (72)	2.0
[illegible]98-63	Kisseynew	20	24.217 (7023)	13.631 (93953)	0.88	476.77 ± 25.9	63	11.8±.044 (76)	2.0
[illegible]98-72	Flin Flon	20	11.673 (3852)	6.645 (2193)	1.14	456.95 ± 29.8	82	12.34±0.52 (85)	2.4
[illegible]98-77	Flin Flon	20	14.073 (4644)	7.882 (2601)	1.13	466.06 ± 28.8	67	12.14±.042 (122)	2.4
[illegible]98-78	Flin Flon	20	7.142 (2357)	4.133 (1364)	1.13	453.15 ± 35.2	>99	11.74±0.54 (96)	2.7
[illegible]98-79	Kisseynew	20	21.924 (7235)	13.055 (4308)	1.13	447.00 ± 23.0	60	12.19±0.47 (57)	1.8
[illegible]98-80	Kisseynew	7	7.323 (952)	4.885 (635)	1.12	400.71 ± 43.6	49	10.66 (14)	1.5
[illegible]98-81	Kisseynew	5	18.878 (1699)	12.011 (1081)	1.11	436.47 ± 37.7	<5	12.1±0.68 (27)	1.8
[illegible]98-82	Kisseynew	20	25.997 (8579)	16.124 (5321)	1.12	427.29 ± 22.0	47	11.44±0.32 (96)	1.6
[illegible]98-83	Kisseynew	19	14.369 (4598)	8.156 (2610)	1.12	460.06 ± 28.4	35	12.1±0.47 (63)	1.9

ρs = spontaneous track density ρi = induced track density

Number of tracks in parenthesis is the number of tracks counted for ages and fluence calibration or the number of tracks measured for lengths

ρd = track density in muscovite detector covering CN-6; Reported value determined from interpolation of valued for detectors covering standards a the top and bottom of the reactor packages (fluence gradient correction)

P(X^2)^5 = Chi-squared probability analyst zeta = 4808

λ_f = 1.551x10^{-10}yr^{-1}, g=0.5

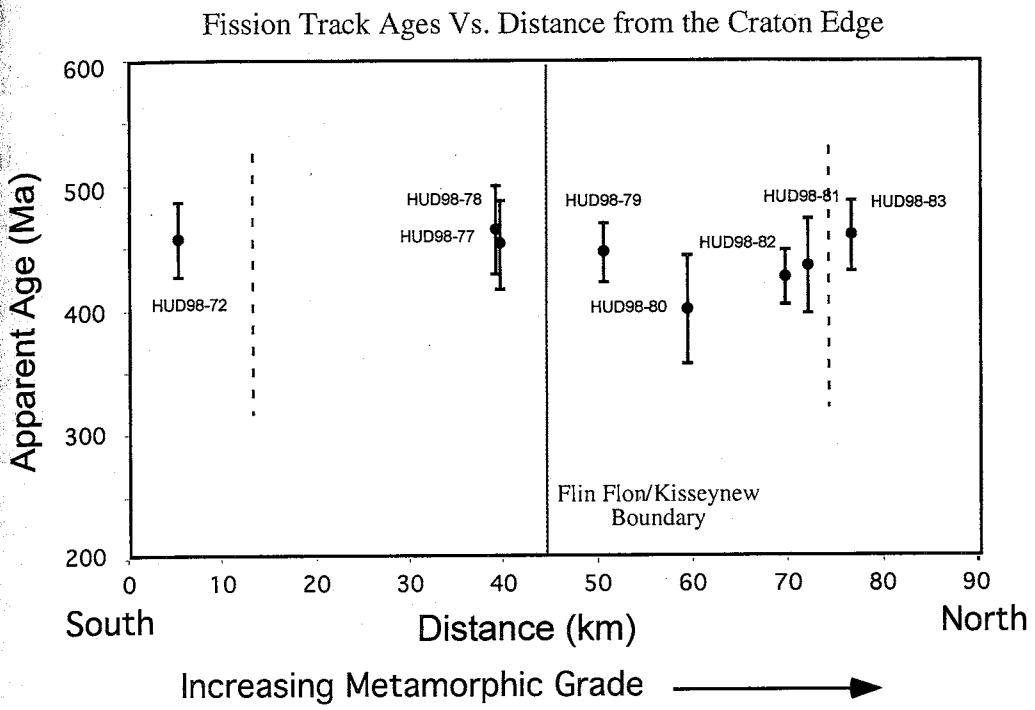

Figure 20. Fission-track ages versus distance northward from the craton edge. Red line shows the location of the boundary between the Flin Flon Belt and the Kissyenew Domain. Dashed lines show the locations of fault zones.

ically display a broad, unimodal, Gaussian distribution (Figure 21 and Table 3), with short track lengths indicating long residence time within the partial annealing zone (PAZ). Samples from the Flin Flon-Kisseynew traverse have mean track lengths between 11.6 and 12.2μm, whereas those from the Tabbernor Fault Zone have shorter mean track lengths, 10.8-11.6μm. HUD86-9, 86-23, and 86-26 give mean track lengths of 11.47, 11.08, and 11.18μm.

Major element compositions were determined on at least ten dated apatite grains from HUD98-63, HUD98-79, HUD98-82, and HUD98-83 (Appendix C). Major element analysis is necessary to determine whether the dated apatite grains are chlor-apatites or flour-apatites. Carlson et al. (1999) looked at annealing rates for fission tracks in apatites with near end-member occupancy of the halogen site by F, Cl, and OH. In general, the species will behave differently during residence within the partial annealing zone, with tracks in chlorapatite more resistant to annealing than those in flourapatite or hydroxylapatite. Totals for the apatite samples in this study are generally greater than 95%, and H_2O accounts for less than 0.6 wt% in all cases. All samples from the study area are flour- apatite with fluorine values ranging between ~2.3 – 3.8 wt.%, and chlorine values between .01-.1 wt.%.

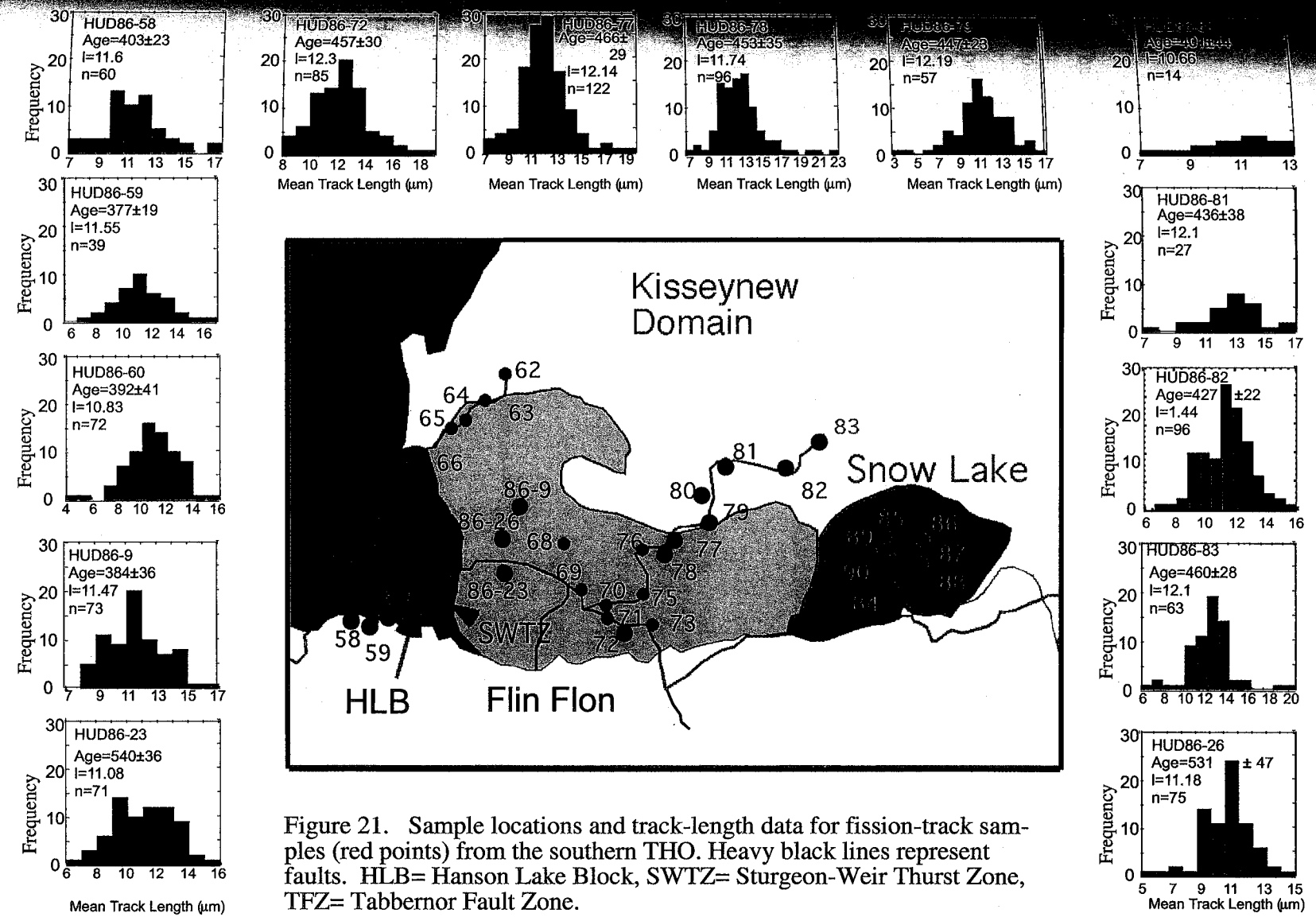

Figure 21. Sample locations and track-length data for fission-track samples (red points) from the southern THO. Heavy black lines represent faults. HLB= Hanson Lake Block, SWTZ= Sturgeon-Weir Thurst Zone, TFZ= Tabbernor Fault Zone.

DISCUSSION

Closure Temperature and Age of Standards

The largest source of uncertainty in $^{40}Ar/^{39}Ar$ thermochronology of old, high –K, samples is generally not the analytical error, but rather the determination of closure temperatures of dated minerals and the age assignment of secondary standards. Of the minerals used in $^{40}Ar/^{39}Ar$ dating, hornblende is the most retentive of $^{40}Ar^*$. Harrison (1981) reported the first argon diffusion study of hornblende and determined an activation energy of 66 ± 4 kcal/mol. Dahl (1996) has used an ionic porosity model (Fortier and Giletti, 1989) to predict the effect of composition on diffusivity in a hornblende mineral structure. He reports that diffusivity increases with an increase in ionic porosity and corresponds to a ~70°C range in closure temperature for hornblende. Closure temperature for hornblende was determined by Harrison (1981) to vary between 580°C for extremely rapidly cooled terranes (~1,000°C/Ma) and 480°C for more slowly cooled metamorphic terranes (< 5°C/Ma), given a diffusion radius between 40 - 80μm. Hornblendes analyzed in this study have been separated mainly from metamorphic and plutonic rocks. In general, cooling rates for the THO range between 1 ad 20°C/Ma, corresponding to a closure temperature of ~500°C (Harrison, 1981).

Muscovite is generally considered to have good retention properties for argon, and in contrast to biotite age spectra, muscovite age spectra can sometimes be interpreted as revealing the spatial distribution of argon in a crystal (McDougall and Harrison, 1999). $^{40}Ar/^{39}Ar$ laser studies conducted on muscovite by Hames and Bowring (1994) suggest that diffusion in muscovite occurs via cylindrical volume diffusion and that the effective

fusion length scale is equal to the crystal diameter. They also point out that the 350°C closure temperature typically assigned to muscovite (Purdy and Jager, 1976) is only appropriate for moderately cooled samples; samples with much slower cooling rates may have a lower closure temperature. Hames and Cheney (1997) looked at argon diffusivity in muscovite during polymetamorphism and found that large crystals may retain the majority of their argon through metamorphic events of temperatures up to 425°C and a time span of less than a few million years. This observation lead them to the conclusion that muscovite is more retentive of argon than previously thought. Cooling rates for the rocks of the THO fall between 1 - 20°C/Ma; with the above-mentioned studies in mind, a closure temperature range for argon in muscovite of 350 - 400°C has been assigned.

Biotite is one of the most commonly dated minerals. Harrison et al. (1985) reported a diffusion radius for biotite of 150μm and calculated an activation energy of 47kcal/mol. Given these parameters, a closure temperature for cooling rates of 100°C, 10°C, and 1°C/Ma are calculated to be 345°C, 310°C, and 280°C, respectively. However, the results of several studies indicate that caution should be exercised when assigning a common value as the diffusion radius for all biotites. Copeland et al. (1987) measured a diffusion radius of 340μm for a biotite from a granodiorite from Tibet, whereas Hess et al. (1993) reported a correlation between grain size and age that suggests that grain size is the effective diffusion radius up to ~500μm. In addition, in situ laser studies (e.g. Hodges et al., 1994) also indicate that the effective diffusion radius for micas is equivalent to the grain size. It should be noted that although the diffusion domain size does affect the closure temperature, even a doubling of the diffusion domain radius will only increase the closure temperature by ~20°C (McDougall and Harrison, 1999). The

Interpretation of $^{40}Ar/^{39}Ar$ results

The results of $^{40}Ar/^{39}Ar$ dating of micas and amphiboles reveal rapid cooling across the central THO between 500 and 300°C, followed by somewhat slower cooling. These results are shown in a summary time–temperature diagram (Figure 22). The definition of the boundary between the Kisseynew Domain and Flin Flon Belt has been continuously modified since the 1950's (e.g. Harrison, 1951; Connors, 1996). In order to better understand the relationship between the rocks of the Kisseynew Domain and those of the Flin Flon Belt, a sampling traverse was taken at a high angle to the terrane boundary (Figure 23). In an attempt to constrain possible differential cooling of the two terranes, hornblende, biotite and K-feldspar were analyzed from either side of the boundary. Both hornblende and biotite cooling ages from either side of the sillimanite isograd reveal strikingly similar ages that cluster around 1760 Ma. The concordant mineral ages suggest that cooling was rapid and that the events that led to the formation of the boundary took place well before hornblende closure temperature (500°C) was reached. It is noted, however, that Fedorowich et al., (1995) reported $^{40}Ar/^{39}Ar$ hornblende and mica ages that reveal much more age variation as the Kisseynew/Flin Flon boundary is approached. Fedorowich et al., (1995) measure hornblende ages that cluster near 1840 Ma, muscovite ages between 1782 and 1788Ma, and biotite ages that range between 1782 and 1814 Ma from the central Flin Flon Belt. Low-temperature thermal histories provided by modeling of K-feldspars from samples HUD98-78, 80 and 83 agree well with mica and amphibole results from this study. All three samples have very similar cooling histories where rapid cooling between 1650 – 1525 Ma was followed

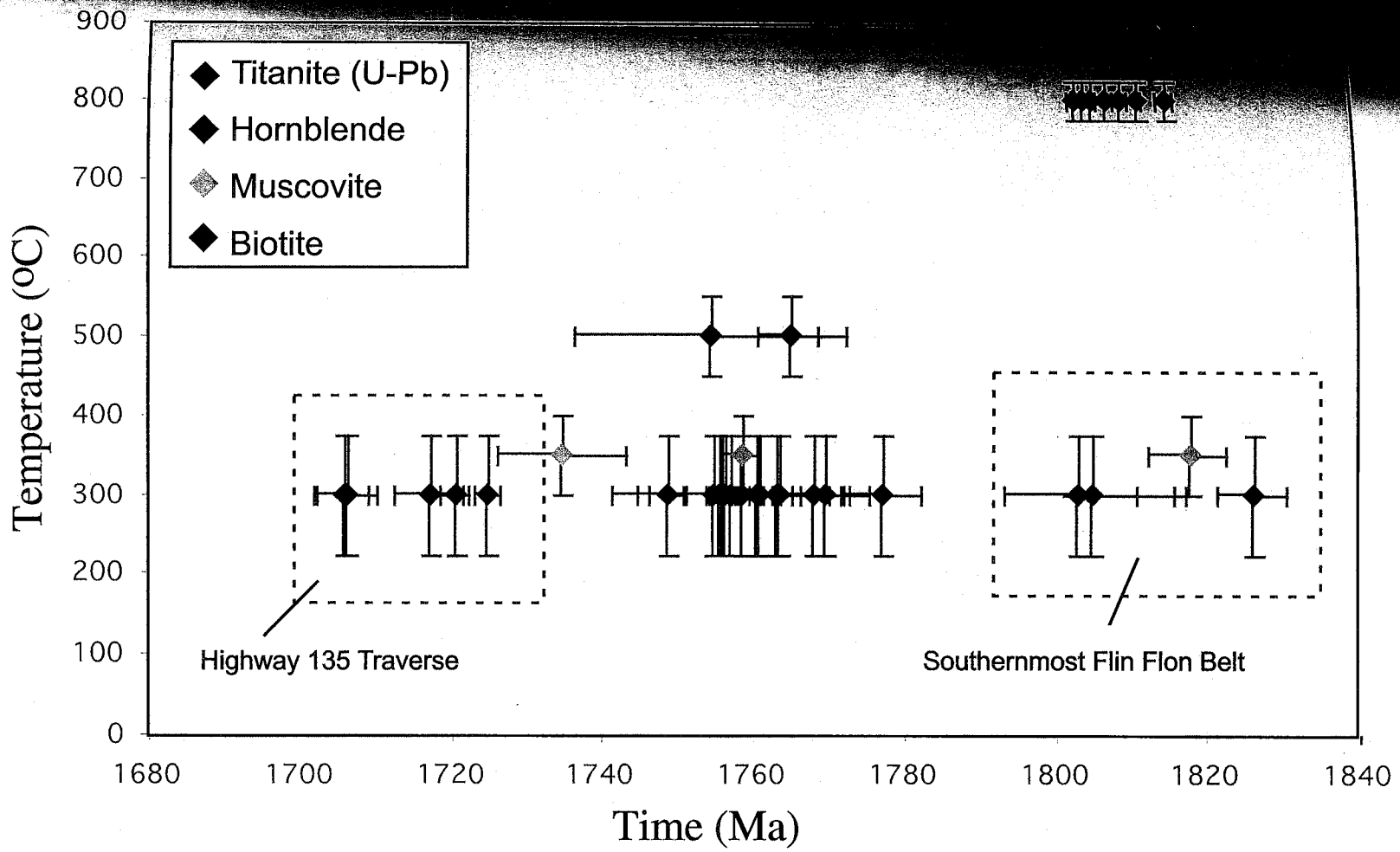

Figure 22. Summary time-temperature plot for the central terranes of the THO. $^{40}Ar/^{39}Ar$ plateau or preferred ages are shown for hornblende (purple), muscovite (green), and biotite (red). U-Pb titanite dates obtained at from Bickford (personal communication, 2000) are shown in blue. Dashed boxes indicate samples from the Highway 135 traverse and southernmost Flin Flon Belt. The remaining sample points are from the Kisseynew/Flin Flon traverse (see Figure 1 for traverse locations).

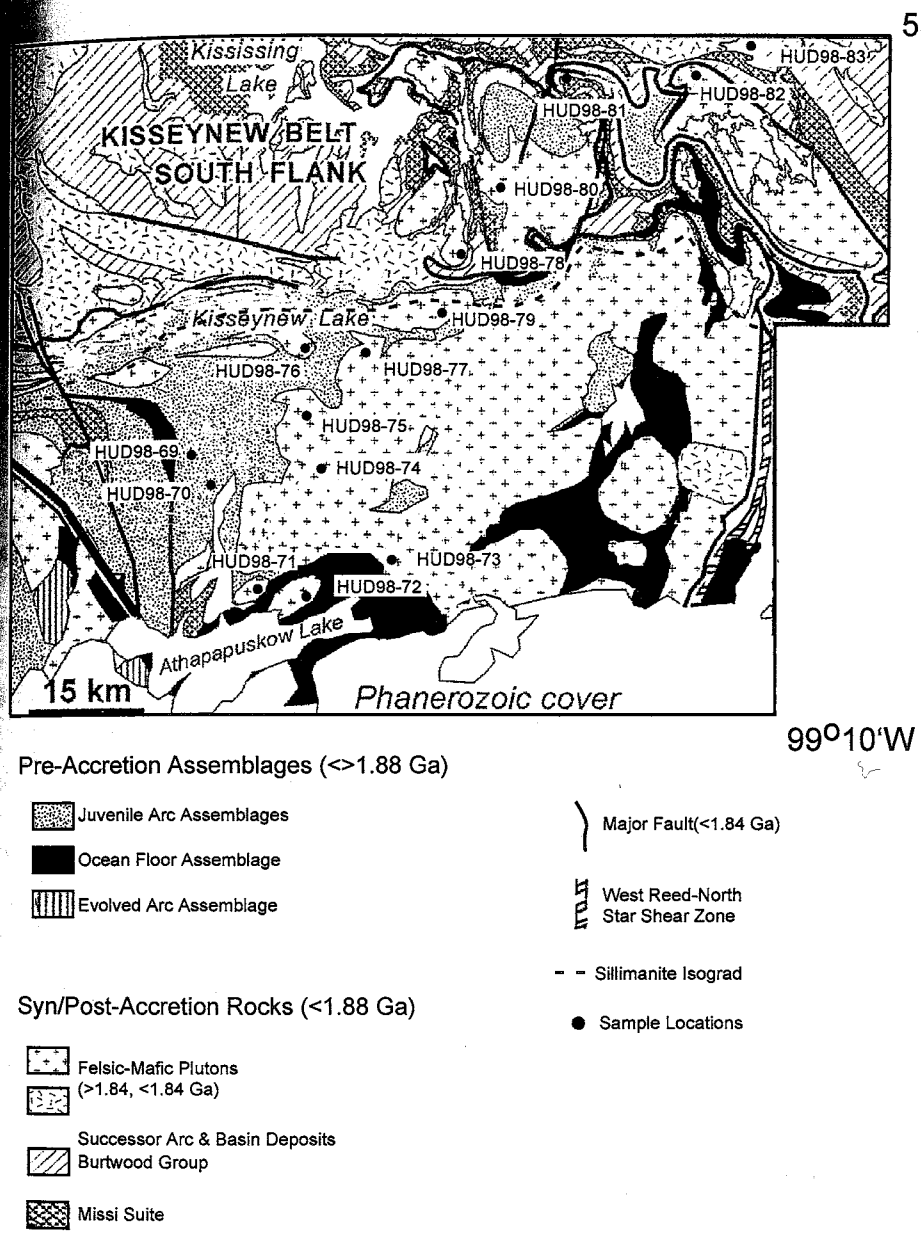

Figure 23. Simplified geology of the central portion of the Flin Flon Domain showing sample locations. Dashed line representing the sillimanite isograd approximates the Kisseynew/Flin Flon boundary. Modified from Bailes and Galley, 1999.

by dramatically slower cooling beginning at roughly 1500 Ma when the samples apparently remained at ~150 - 175°C for at least 300 m.y. (Figures 18, 19). A single hornblende from the traverse (HUD98-75) gives an apparent age of 1799.7 ± 3.22. Examination of the age spectra and electron microprobe analyses of the mineral separate (Appendices A and D), indicate that it is difficult to objectively assign an age to this sample. The mineral separate contains chlorite as well as other contaminating phases that may have contributed to the resulting hump-shaped age spectrum. As mentioned in the discussion of the hump-shaped biotite spectra described previously, the presence of chlorite may indicate that recoil is responsible for the older age of this sample. With respect to the samples located in the northern part of the Kisseynew/Flin Flon traverse, this hornblende result is an outlier. In light of the discordance of the age spectrum, and the lack of confidence in the assigned age, this sample could be eliminated from the discussion. However, samples just to the south cluster at ~1800 Ma, and it may be that this hornblende is representative of the old ages found in the southern Flin Flon Belt. Samples HUD98-80 and HUD98-82 yield flat hornblende spectra with preferred ages of 1764.8 ± 3.9 and 1758.2 ± 2.7 Ma, respectively. The concordance of the hornblende and biotite ages from the Kisseynew/Flin Flon traverse indicate that these rocks cooled quickly, in a matter of a few million years, between 500 and 300°C.

One possible explanation for the agreement between biotite and hornblende cooling ages across the boundary is that a large-scale plutonic event occurred at ~1760Ma. Although such an event could reset the $^{40}Ar/^{39}Ar$ ages and facilitate raped cooling, it would have had to occur on a very large scale in order to produce resetting across such a large area (100s of km) and there is no evidence for widespread plutonism in the

Kisseynew after 1.83 Ga (Ansdell et al., 1995a). A more plausible scenario is that the rocks of the northern Flin Flon Belt and southern Kisseynew Domain simply cooled quickly from peak metamorphic conditions. Cooling may have occurred through denudation or isobaric relaxation. Briggs and Foster (1992) have estimated peak metamorphic conditions in the southern flank of the Kisseynew at 560-625°C and 3.3-4.6kbar (~50°C/km). Assuming cooling to 500°C by 1760Ma orogen wide, the geothermal gradient would have decreased to ~40°C/kmby1760Ma. However, at 500°C biotite is still open to argon loss. Given the concordance of hornblende and biotite ages in this study, we know that cooling was rapid between 500 and 300°C. This raped cooling would imply a decrease in the geothermal gradient from 40°C/km to 25°C/km. Unless high goetherms are preserved by plutonism between 1800 and 1760 Ma, it is difficult to imagine such an abrupt geotherm change, making denudation a more likely cause for cooling. Two major metamorphic events are recorded in the Kisseynew: the first, M1, is attributed to back arc extension and advective heat transfer from rising plutons between 1840 –1830 Ma (Ansdell and Norman, 1995). The origin of the second event, M2 (1820 – 1805 Ma), is uncertain. Gordon (1989) and Kraus and Menard (1997) have estimated peak M2 metamorphic conditions in the central portion of the Kisseynew Belt at 750°± 50°C at a depth of 15 km (less than 5.5 kbar), corresponding to a linear thermal gradient of 50°C/km. In addition, Gordon (1989) reported no mineralogical evidence for the rocks being buried to much greater depths, indicating that the elevated thermal gradient is not the result of crustal thickness alone, but rather that elevated mantle heat flow or heat transfer from rising plutons must have contributed to the high geothermal gradient. In the adjacent Flin Flon Belt, temperature-pressure estimates in the

50°C/km. In addition, Gordon (1989) reported no mineralogical evidence for the rocks being buried to much greater depths, indicating that the elevated thermal gradient is not the result of crustal thickness alone, but rather that elevated mantle heat flow or heat transfer from rising plutons must have contributed to the high geothermal gradient. In the adjacent Flin Flon Belt, temperature-pressure estimates in the File Lake area range from 560 to 625°C and 3.3 to 4.6 kbar (Briggs and Foster, 1992), suggesting an anomalously warm thermal regime in the Kisseynew Domain (Ansdell et al., 1995). Ansdell et al. (1995) have suggested that southward-directed-thrusting of the Kisseynew Domain occurred synchronously with M2 deformation and that cooling from peak metamorphic conditions can be attributed to "thermal relaxation and exhumation of tectonically thickened basinal rocks that were anomalously hot because of heat retained from 1.84 – 1.83 Ga metamorphism". Therefore, the concordant $^{40}Ar/^{39}Ar$ ages found here are likely to represent continuing cooling associated with denundation, assuming the monazite ages record peak metamorphism. The $^{40}Ar/^{39}Ar$ ages can be combined with U/Pb data to determine cooling rates. U/Pb monazite dating of sample HUD98-83, the northernmost sample of this traverse, yields concordant single crystal ages between 1814 ± 1 and 1803 ± 1 Ma for 10 grains analyzed (Bickford, personal communication, 2000). The ages of single grains do not overlap at 2σ, suggesting that monazite growth was either episodic or occurred continuously over this time period. Due to the severe hump-shape biotite age spectrum for HUD98-83, a sample with a better behaved spectrum, HUD98-82, is used here to calculate a cooling rate for the southern flank of the Kisseynew Domain. These data together imply a cooling rate of ~ 2.5°C/Ma between 1800 and 1760 Ma. The

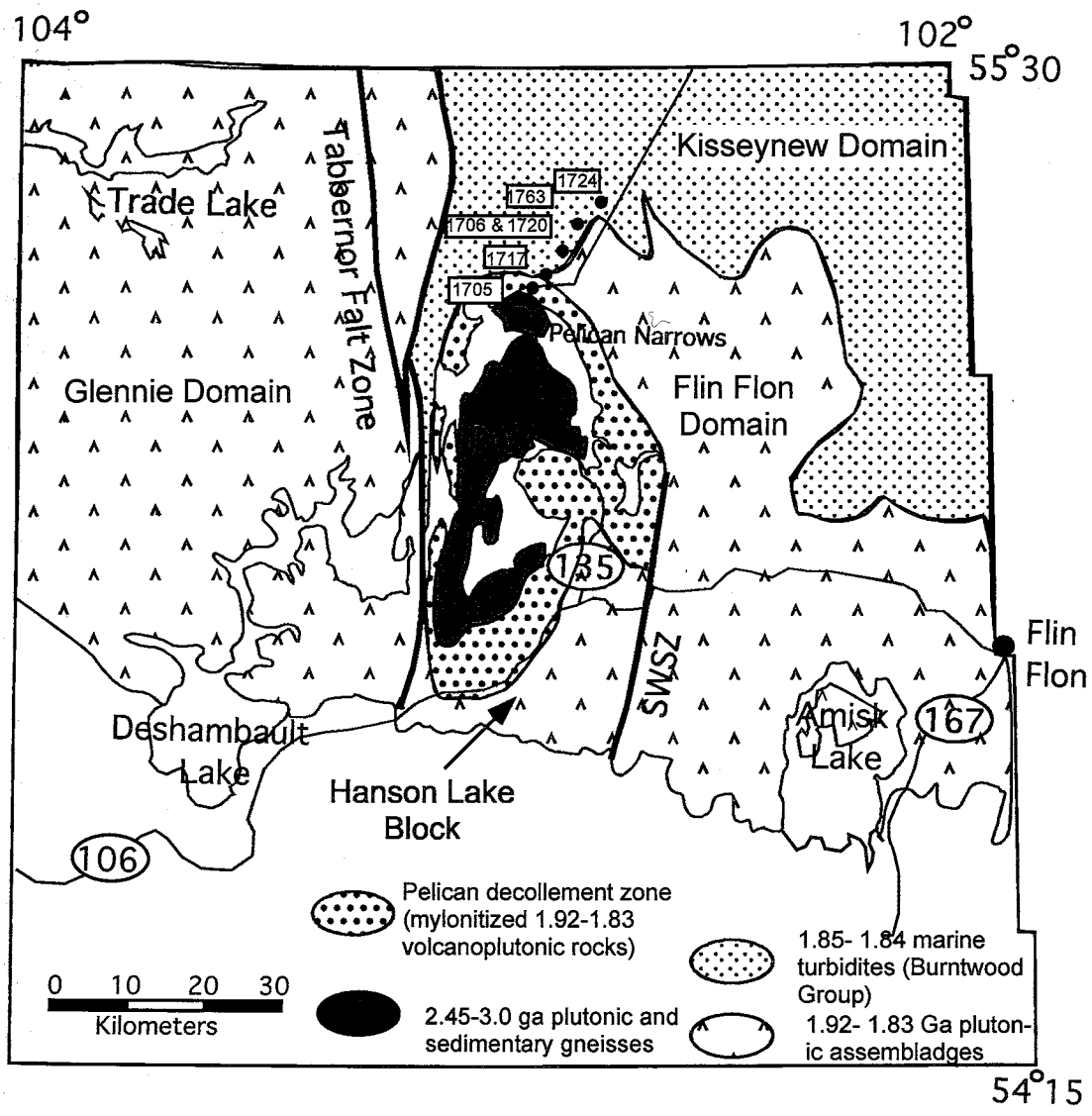

Figure 24. Location and apparent ages of highway 135 samples. PW = Pelican Window, SWSZ= Sturgeon-Weir Shear Zone. Modified from Maxeiner et al, 1999.

1763Ma. This sample is from a pelitic schist of the Burntwood Group, collected in the Kisseynew Domain just north of the Kisseynew-Hanson Lake boundary. The age spectrum is well behaved with essentially identical plateau and total gas ages. Therefore, although it is at odds with the surrounding samples, there is no analytical reason to disregard this analysis. It is interesting that this sample is of the same age as those from the Kisseynew - Flin Flon traverse, suggesting that a laboratory mix-up is a possibility.

Several possible geological histories can be constructed that would explain the slightly younger ages found for the highway 135 traverse. A 1758 ±1Ma titanite age (Tc 660-700°C, Scott and Onge, 1995) obtained by Wortman and Bickford (1999) from the Hanson Lake Block is very similar to the 1760 Ma hornblende ages found by Heizler et al. (2000) in the same area. The agreement in age suggests a plutonic event may have occurred that reset both the U/Pb and $^{40}Ar/^{39}Ar$ ages. However, plutonism in the Hanson Lake Block is not recorded after peak metamorphism (1804 – 1808 Ma; Maxeiner et al., 1999). Another possibility is that the rocks in this area simply cooled slightly later than those of the Kisseynew/Flin Flon traverse to the east. This later cooling could result from differential uplift and erosion across the Reindeer Zone. This hypothesis may be supported by the 1758 ±1Ma titanite age obtained by Wortman and Bickford (1999), which is significantly younger than the >1800 Ma ages they have found across the southern THO.

The Hanson Lake Block is separated from the Flin Flon Belt by the Sturgeon-Weir thrust zone, where the rocks of the Flin Flon Belt have been thrust over those of the Hanson Lake Block (Figure 22; Lewry et al., 1990b; Pandit et al., 1998). Heizler et al. (1999, 2000) reported $^{40}Ar/^{39}Ar$ biotite ages from the western THO (Rottenstone, Glennie,

and Hanson Lake Domains) of 1740 – 1710 Ma and hornblende ages of ~1760 Ma from all terranes west of the Sturgeon Weir fault. They calculated cooling rates of ~5°C/Ma from 500 to 300°C west of the fault and cooling rates of 10 - 20°C/Ma east of the fault. The results of this large dataset indicate that movement of the Sturgeon-Weir thrust can be bracketed between 1760 and 1720 Ma and between ~500 and 300°C. Tectonism in the Sturgeon-Weir – Tabbernor fault zone area created a large thermochronologic boundary. The older (1760 Ma) rocks to the east of this zone (Flin Flon and Kisseynew) were uplifted relative to the younger (1720 Ma) rocks to the west (Hanson Lake and Glennie).

A K-feldspar collected in the central Flin Flon Belt, east of the city of Flin Flon (HUD98-69), reveals a thermal history that is characterized by more gradual cooling than those of the Kisseynew/Flin Flon traverse to the east (Figures 17, 18, 21). In addition, this sample remained warmer (~100°C) between 1500 and 1100Ma compared to those to the east. Considering the younger ages of the Highway 135 traverse, we would expect this sample to have cooled later than those of the traverse and therefore this result seems counterintuitive. Unfortunately, this is the only K-feldspar analyzed from this area, and therefore it is not possible to make any geologic interpretations based on the results of this analysis alone.

In the southern Flin Flon Domain, three samples reveal noticeably older $^{40}Ar/^{39}Ar$ biotite ages relative to those from the Kisseynew/Flin Flon traverse to the north (Figure 23, Table 1). The Minks Narrows pluton, (a non-deformed stitching pluton), the Lynx Lake pluton, and the Otter Lake pluton reveal biotite plateau ages of 1825.9 ± 4.62 and 1802.7 ±8.12 Ma (HUD98-71, HUD98-73, respectively), and a muscovite age of 1817.6 ± 5.12 Ma (HUD98-72). Peak metamorphism at 1815 Ma postdated the major plutonic

events (1860 – 1840 Ma). The only other heat source would be the presence of a buried 1815 Ma pluton (Fedorowich et al., 1995). One possible explanation for the older ages seen in the southern Flin Flon Belt is that crustal thickening due to the ongoing collision resulted in continuing denudation and that the southernmost Flin Flon was uplifted early relative to those samples to the north, giving them slightly older cooling ages. However, Fedorowich et al. (1995) performed $^{40}Ar/^{39}Ar$ analysis on hornblende and micas from the west-central Flin Flon Belt and found hornblende and mica ages similar to those found to the south. They measured hornblende ages of 1841 ± 6, and 1844 ± 7 Ma, as well as muscovite ages of 1791 ± 4 and 1782 ±6 Ma. The old ages found in this study and by Fedorowich et al. (1995) suggest that the southern Flin Flon may have escaped the 1.8 Ga metamorphism that affected the Kisseynew and other parts of the southern THO.

In the Snow Lake region (Figure 25), samples were collected both from juvenile arc rocks and rocks of the Burntwood Group, as well as one sample (HUD98-84) from the Wekusko lake pluton (crystallization age: 1.83 –1.84 Ga; Gordon et al., 1990). Plateau spectra of micas in the Snow Lake area yield well defined cooling ages of ~1760 Ma, indicating that cooling through biotite closure temperature in this area is similar to that of samples HUD98-76 –HUD98-83 (Table 1). The exception is HUD98-87, which shows the characteristic hump-shaped spectrum discussed earlier. Alteration as well as inclusions of feldspar indicate that recoil likely caused the shape of the spectrum observed for this sample. The results of this study compare favorably with those of Marshall et al. (1997) who reported $^{40}Ar/^{39}Ar$ biotite and hornblende ages of 1720-1769 Ma and 1747-1764 Ma, respectively, in the Wekusko Lake area. K-feldspar modeling (both monotonic and unconstrained) indicate HUD98-84 cooled to 250°C at 1300 Ma,

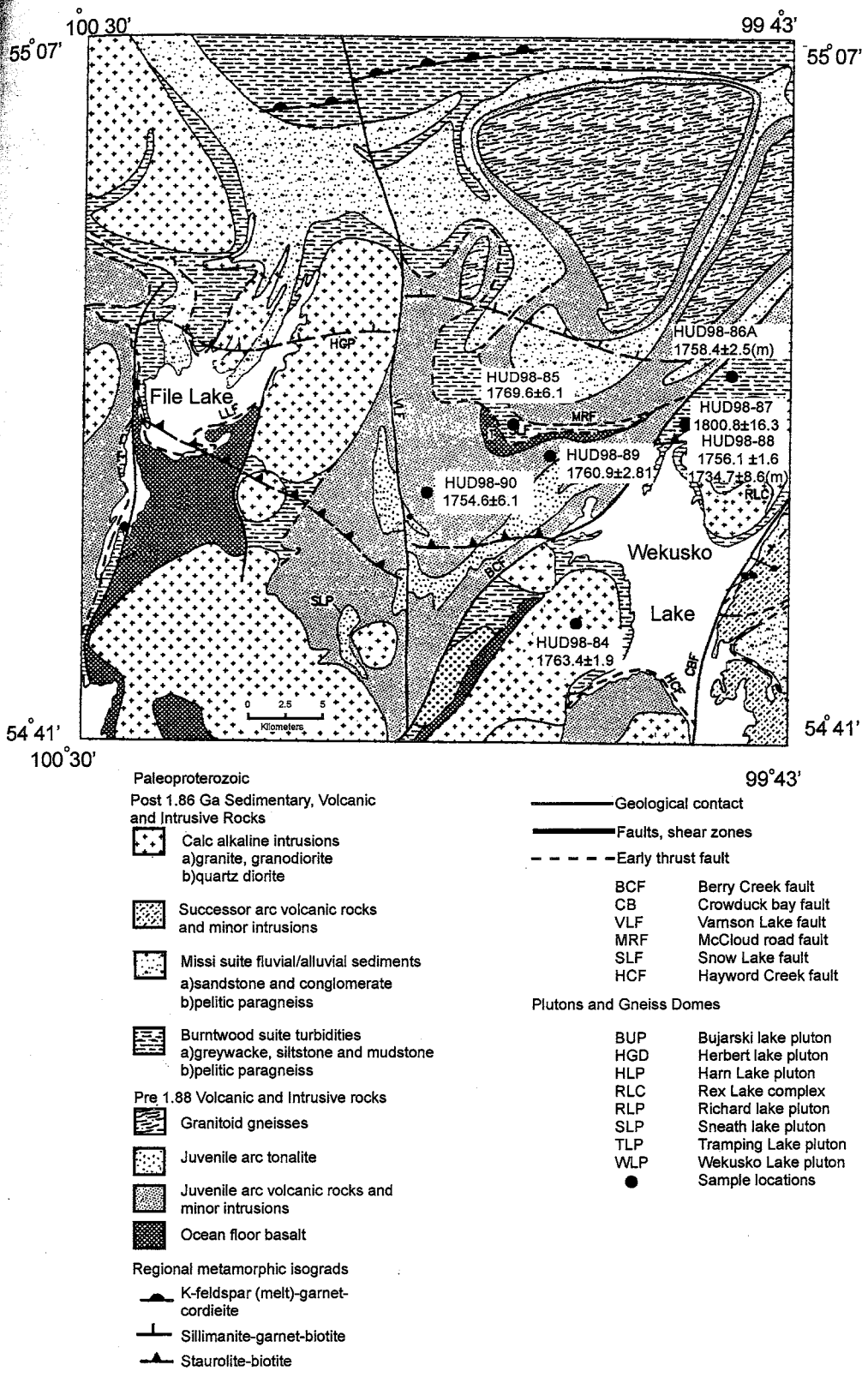

Figure 25. Apparent ages and location on Snow Lake samples. Modified from David et al., 1996.

much warmer than samples from the Kisseynew-Flin Flon traverse, with accelerated cooling beginning between 1250 and 1300 Ma (Figures 18, 19) and lasting through 1150 Ma, when the mineral closed to argon loss. HUD98-86a, a pegmatite within the Burntwood Group, yields a flat muscovite age spectrum that defines a plateau age of 1758.7 ± 1.4 Ma. K-feldspar modeling shows a nearly opposite cooling history to HUD98-84 where initially rapid cooling lasted until 1500 Ma. Considering the higher metamorphic grade of the host rock for HUD98-86A, we would expect it to have cooled later than HUD98-84, if denudation were acting alone. The Berry Creek fault runs adjacent to the two sample locations and has offset the staurolite – biotite isograd (David et al., 1996; Figure 23). A scissor-like motion along this fault may have produced the disparate cooling history of these two samples. In general, the Snow Lake area has experienced a similar cooling history to the Kissynew Domain, until the K-feldspar temperatures when differential uplift caused HUD98-86A to cool faster than those samples to the south.

Interpretation of Apatite fission-track results

Fission track ages from a traverse extending from the southern Flin Flon Belt northward into the Kisseynew Domain range between 401 ± 44 Ma and 466 ± 29 Ma, although there is no systematic variation in age with metamorphic grade or distance from the craton edge (Figure 20). The results presented here are in agreement with those of Osadetz et al. (2000), who report ages of 423, 455, and 445 Ma and track lengths of 12.1 – 12.6μm for three samples in the Flin Flon Belt. Our traverse begins in the low grade rocks of the southern Flin Flon. The first sample of the traverse (HUD98-72) is roughly

5 km from the southernmost exposure of the craton where Ordovician limestones uncomformably overlie the Precambrian rocks of the THO. The traverse was taken northward through rocks of increasing metamorphic grade, across the Flin Flon – Kisseynew boundary and ending in the southern flank of the Kisseynew Domain, approximately 77 km from the southern craton edge (sample HUD98-83; Figure 23). The traverse was designed to test whether there are systematic trends in the Phanerozoic unroofing history of the craton or any evidence of reactivation of ancient structures. As illustrated in Figure 20, the variation in apparent ages does not follow a systematic increase with distance from the craton edge. Potential causes for the observed variation in age on Figure 20 include chemical composition of apatite, structural influences, and/or differences in burial thickness. Electron microprobe data (Appendix C) shows that all samples have similar flourine and chlorine concentrations. In addition, the apatite fission-track ages do not seem to be controlled by the major structures crossing the traverse. Ages from samples collected across the fault zone that defines the Kisseynew/Flin Flon boundary overlap within 2σ error and are therefore considered to be of equal age. Given that we know vertical displacement along this fault is significant, we can infer that the lack of age variation across the fault indicates that movement occurred prior to cooling below ~100°C and that there is no evidence for significant reactivation. This observation is confirmed by other authors (e.g., Ansdell et al., 1995; Connors, 1996) as well as $^{40}Ar/^{39}Ar$ from this study, in which concordant mica and amphibole ages are found across the fault zone. Thus, the observed apatite fission-track age variation may be due to slight differences in thickness of the Phanerozoic cover.

Samples from this traverse have short mean track lengths, and generally broad distributions, suggesting slow cooling and long residence within the PAZ. Modeling of these samples was completed using two geologic constraints. Given the presence of Ordovician cover which overlies the basement rocks adjacent to the southernmost exposure of the craton, as well as the presence of Ordovician limestone found adjacent to fault blocks within the craton(Elliot, 1996), we can infer that the samples of the traverse were near the surface at ~ 400 Ma. Therefore, a fairly tight constraint at ~400 Ma was used for sample HUD98-72, which is closest to the Ordovician cover and must therefore have been at the surface at this time (Figure 26). The second constraint was placed at ~60 Ma and reflects the presence of rocks of Cretaceous age that lie in close proximity to the traverse and suggest recent burial, possibly related to the Cretaceous Interior Seaway. Because samples further north are less geologically constrained, the model constraints were loosened. Comparing best-fit time-temperature models with K-feldspar cooling histories shows that the samples remained in the PAZ for a long period of time (~400 Ma) and cooled slowly prior to Ordovician denudation. This was followed by burial between ~160 and 80 Ma and subsequent cooling to surface temperatures (Figure 26). The AFT model predicts that samples from the Kisseynew/Flin Flon traverse reached at least 50°C at roughly 80 Ma. Using heat flow measurements, Mareschal et al. (1999) determined current geothermal gradients in the Flin Flon/Snow Lake area. A measurement from a borehole in the southernmost Flin Flon Belt reveals a geothermal gradient of 13.9 °C/km. If this gradient is applied to our samples it would imply ~3.5 km of sediment have been denuded since the Cretaceous. However, these results are somewhat puzzling in that there is not enough Pherozoic section preserved in the eastern

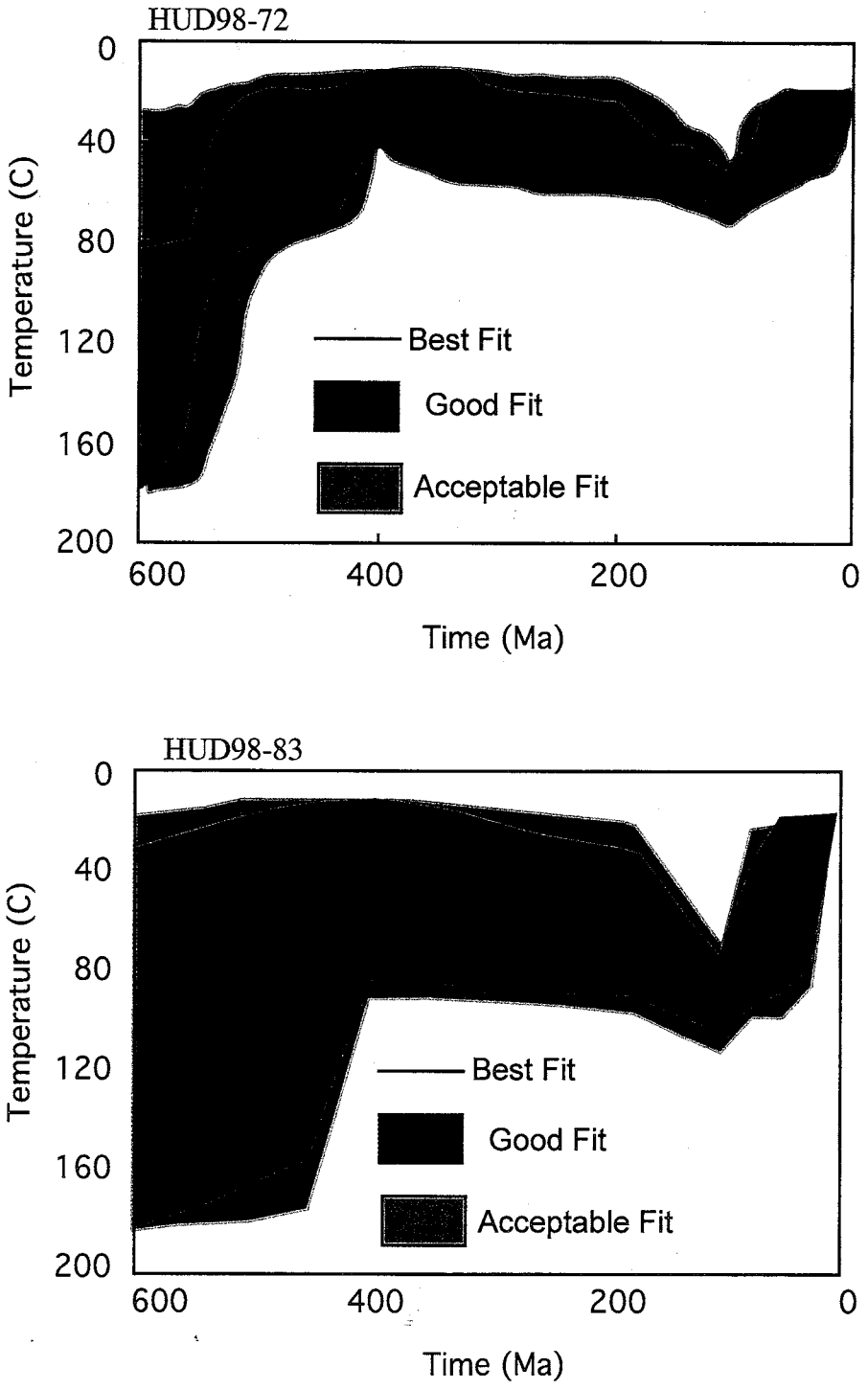

Figure 26. AFTsolve modeling of HUD98-72 and HUD98-83. For each the black line shows the best fit to the data. The purple shows the area containing solutions that provide a good fit whereas the green shows the area of solutions that provide only an acceptable fit.

Canadian Basin to verify this result (Stockmal et al., 1992; Leckie and Smith, 1992). Possible mechanisms for post-Cretaceous denudation include 1) falling eustatic sea level causing isostatic rebound and denudation, 2) changes in climate leading to a corresponding increase in denudation rates, and 3) epeirogenic uplift. Mitrovica et al. (1989) proposed a mechanism for the epeirogenic movement of cratons in response to the geometry of shallow subduction zones. They suggest that a shallowly dipping subduction zone could account for horizontal platform sedimentation over areas much larger than individual basins. Their results from analysis of the cratonic tilt of North America indicate Late Cretaceous tilt toward the subduction zone at the margin of the continent, followed by Teriary denudation. In a more recent study, Lithgow-Bertelloni and Gurnis (1997) suggested that dynamic topography (that generated by flow within the mantle) may be responsible for long-term regional uplift. They predicted significant uplift of the North American Craton in the Cenozoic with the amount of uplift increasing northward. The timing of uplift that their model predicts is somewhat later (35 Ma) than is predicted by the fission-track results of this study. Although the scope of this paper does not allow for a more in-depth discussion of the mechanisms for uplift, future work will have to be done in order to better understand the events producing the Cretaceous denudation of the central THO.

Apatite fission-track ages for rocks collected on either side of (HUD98-58 and HUD98-60), and within the Tabbernor fault zone (HUD98-59), can be used to determine the timing of faulting relative to the time that the samples passed through the PAZ. Although major displacement along the fault is strike-slip, dip-slip slickenlines found in outcrop provide evidence of at least some dip-slip movement. Within uncertainty, the

ages of the two samples on either side of the fault are indistinguishable and that within the fault zone is slightly younger (Table 3). If faulting occurred after the samples had cooled to temperatures less than that of the PAZ, and vertical displacement was significant, then there would be an age difference across the fault. If faulting occurred before cooling, rocks at the same elevation would have come through the PAZ at the same time and therefore be of the same apparent age. If there was no vertical movement, or if vertical motion were negligible, there would be no significant age difference across the fault. There are several possibilities for the young age of the sample collected from within the fault zone (HUD98-59). This sample contains a considerable amount of pyrite, which may record fluid flow through the fault zone. If this fluid were warm enough (>60°C), the increased temperature could anneal the tracks, thus lowering the age. Another possibility is that the heat generated by the slip along the fault was enough to lower the age. However, this seems unlikely as heat generated by slip in generally very localized (Kelley, unpublished data). Mapping across the Tabbernor fault shows brittle, strike-slip motion (Elliot, 1994; Hajnal et al., 1995). Apatite fission track ages across the Tabbernor fault do not show significant age variation, suggesting that either 1) dip-slip movement along the fault occurred before cooling or 2) vertical offset was not enough to be recorded by the apatite fission-track method.

All three samples have relatively short mean track lengths and broad track length distributions, indicating that these samples had a long residence time within the PAZ (Figure 21, Table 3). Modeling of these data using the computer program AFTSolve to create time-temperature histories reveals that the samples were near the surface at ~ 400 Ma, buried to ~3.5km and subsequently exhumed (Figure 27). The models for samples

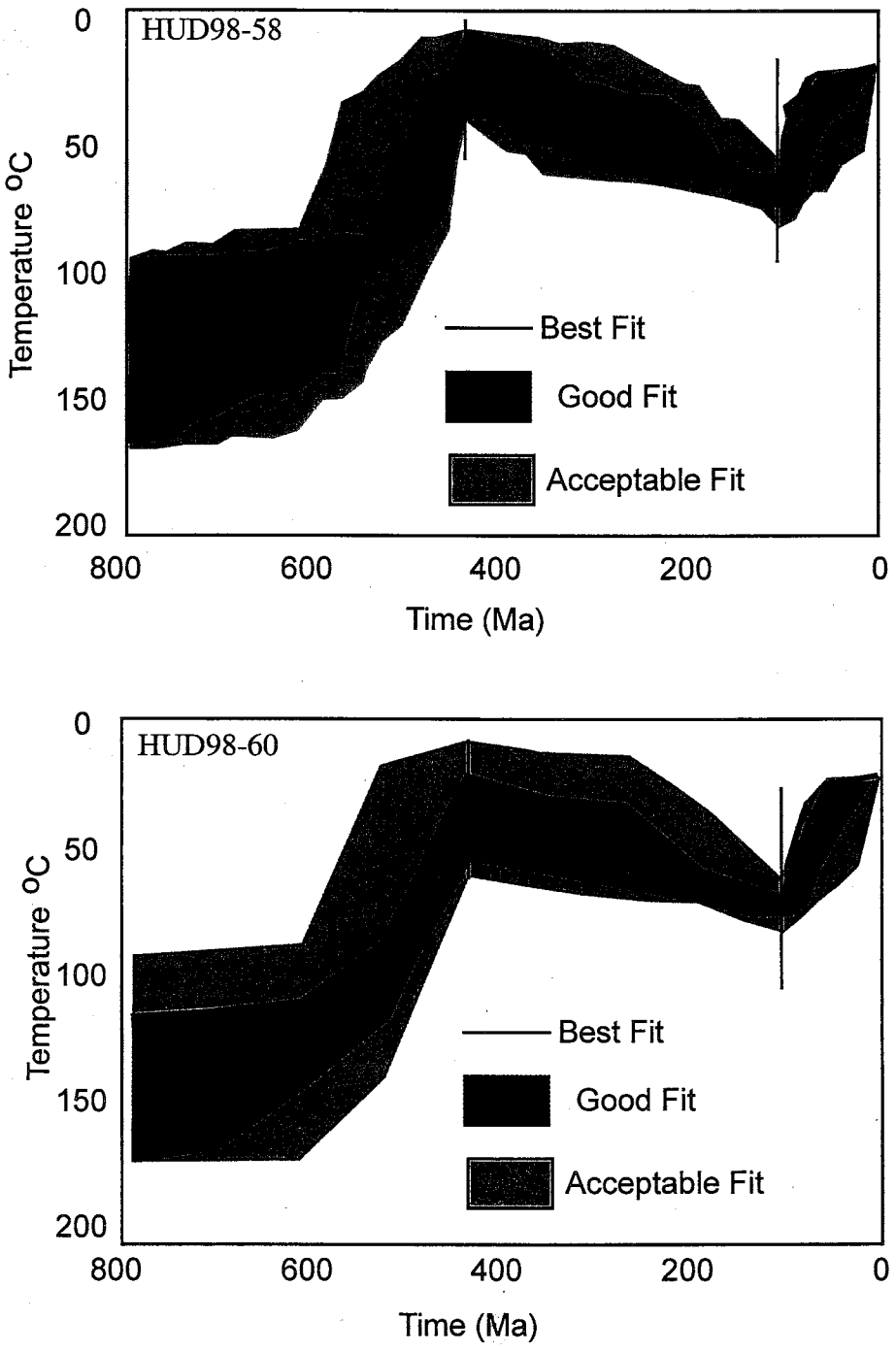

Figure 27. AFT Solve modeling of fission-track samples from either side of the Tabbernor fault For each the black line shows the best fit to the data. The purple shows the area containing solutions that provide a good fit whereas the green shows the area of solutions that provide only an acceptable fit.

from the Kisseynew/Flin Flon traverse are similar. The early segment of the thermal history is not well constrained as indicated by the wide range in acceptable thermal histories prior to ~300 Ma. Feinstein et al. (2000) proposed Pennsylvanian heating for apatite fission-track samples from the Williston Basin located in Manitoba, Saskatchewan, and the north central USA. When a constraint placing maximum heating during the Pennsylvanian is imposed for the samples in this study, the results of the AFTSolve model still yield cooling beginning in the Cretaceous.

West of the Flin Flon/Kisseynew traverse, three samples (HUD86-9, 86-23, 86-26) reveal much different apparent ages. HUD86-23, the northernmost of the three, gives the youngest age, 384 ± 36 Ma, (Table 3) whereas HUD86-26 and HUD86-9 yield ages >530 Ma. IF the craton had been simply stripped form north to south, the apatite fission-track age should decrease toward the south; however, the opposite trend if observed here. The data imply that Phanerozoic cover was not of uniform thickness. Some areas may have been buried more deeply than others. The areas with younger fission-track ages may correlate to thicker pockets of sediment.

In summary, the apatite fission-track data reveal long term Phanerozoic residence within the PAZ and subsequent post-Cretaceous denudation. Fission-track ages across the Tabbernor fault indicate that vertical offset was likely insignificant. Samples across the Kisseynew-Flin Flon boundary imply that movement along the fault predated cooling through 120 -60°C and there has been no Phanerozoic reactivation of this strucure.

CONCLUSIONS

The $^{40}Ar/^{39}Ar$ result for this study demonstrate that the Kissyenew and northern Flin Flon Belt cooled as a unit below 500°C, rather than retaining individual cooling histories. Variation in cooling histories of individual samples are the result of differential uplift and erosion (e.g. southward tilting of Flin Flon to preserve old ages to the south) and/or movement along faults (e.g. the Sturgeon – Weir fault zone), Across the Reindeer zone, rocks apparently cooled from peak metamorphism related to the ongoing collision. Concordant mineral ages across the Kisseynew/Flin Flon boundary and in the Snow Lake region suggest that the events leading to the creation of the mapped terrane boundary occurred prior to 1760 Ma and at temperatures above 500°C. The southernmost Flin Flon terrane appears to have escaped regional metamorphism at 1.8 Ga that affected a large region of the southern THO. Younger mica ages in the Hanson Lake Block and western Kisseynew Domain are representative of the entire western portion of the THO, which is separated from the 1760 Ma ages of the Kisseynew/Flin Flon traverse and Snow Lake region by the Sturgeon-Weir and Tabbernor fault zones. K-feldspar dating from across the region reveals generally similar cooling histories with accelerated cooling through ~275°C, followed by protracted cooling through 150°C. Initial rapid cooling between 1815 and 1760 Ma in the Kisseynew Domain and Flin Flon Belt was followed by somewhat slower cooling and long-term residence in the PAZ. Apatite fission track analysis show that the southern portion of the Flin Flon was denuded prior to Ordovician

sedimentation, buried and/or heated between Middle Paleozoic and Late Mesozoic, and subsequently denuded starting in the late Cretaceous to their present day surface level.

REFERENCES CITED

ANSDELL, K.M., LUCAS, S.B., CONORS, C., STERN R.A. (1995) Kisseynew metasedimentary gneiss belt, Trans-Hudson Orogen (Canada): Back-arc origin an collisional inversion. *Geology*, **23**(11), 1039-1043.

ANSDELL, K.M., NORMAN, A.R. (1995) U-Pb geochronolgy and tectonic development of the southern flank of the Kisseynew Domain, Trans-Hudson Orogen, Canada. *Precambrian Research*, **72**, 147-167.

ASHTON, K.E., LEWRY, J.F. (1994) Vergence of the 'Pelican slide' and Sturgeon-weir shear zone. *Lithoprobe Trans-Hudson Orogen Transect, Report of fourth Transect meeting April 11-12*, **38**, 12-15.

BAILES, A.H. (1980) Geology of the File Lake area. *Manitoba Energy and Mines, Geological Report 78-1.*

BAILES, A.H., GALLEY, A.G. (1999) Evolution of the Paleoproterozoic Snow Lake arc assemblage and geodynamic setting for associated volcanic-hosted massive sulfide deposites, Flin FLon Belt, Manitoba, Canada. *Canadian Journal of Earth Science*, **36**, 189 - 1805.

BICKFORD, M.E., COLLERSON, K.S., LEWRY, J.F., VAN SCHMUS, R.W., CHIARENZELLI, J.R. (1990) Proterozoic collisional tectonism in the Trans Hudson Orogen, Saskatchewan. *Geology*, **18**, 14-18.

BICKFORD, M.E., VAN SCHMUS, W.R., MACDONALD, R., LEWRY, J.F., PEARSON, J.G. (1986) U-Pb geochronology project for the Trans-Hudson: current sampling and recent results. *Summary of Investigations 1982. Sask. Geol. Surv. Energ. Min., Misc. Rep.*, **86-4**, 101-107.

BRIGGS, W., FOSTER, C.T. (1992) Pressure-temperature conditions of Early Proterozoic metamorphism during the Trans-Hudson Orogen as determined from rocks straddling the Flin Flon - Kisseynew boundary at Niblock and File Lakes, Manitoba. *Canadian Journal of Earth Science*, **29**, 2497-2507.

BROWN, M. (1993) P-T-t evolution of orogenic belts and the causes of regional metamorphism. *J. Geol. Soc. Lond.*, **150**, 227-241.

CARLSON, W.D., DONELICK, R.A., KETCHUM, R.A. (1999) Variability of apatite fission-track annealing kinetics: I. Experimental results. *American Mineralogist*, **84**(9), 1213-1223.

CONNORS, K.A. (1996) Unravelling the boundary between turbidites of the Kisseynew Domain and the volcano-plutonic rocks of the Flin Flon Belt, Trans-Hudson orogen, Canada. *Canadian Journal of Earth Science*, **33**, 811 - 829.

COPELAND, P., HARRISON, T.M., KIDD, W.S.F., RONGHUA, X., YUQUAN, Z. (1987) Rapid early Miocene acceleration of uplift in the Gangdese Belt, Xizang (southern Tibet) and its bearing on accommodation mechanisms of the India-Asia collision. *Earth and Planetary Science Letters*, **86**, 240-252.

DAHL, P.S. (1996) The effects of composition on retentivity of argon and oxygen in hornblende and related amphiboles: A field-tested empirical model. *Geochimica et Cosmochimica Acta*, **19**, 3687-3700.

DAVID, J., BAILES, A.H., MACHADO, N. (1996) Evolution of the Snow Lake portion of the Paleoproterozoic Flin Flon and Kisseynew Belts, Trans-Hudson Orogen, Manitoba, Canada. *Precambrian Research*, **80**, 107-124.

DODSON, M.H. (1973) Closure temperature in cooling geochronological and petrological systems. *Contributions to Mineralogy and Petrology*, **40**(3), 259-274.

ELLIOT, C.G. (1994) Structural relationships across the Tabbernor Fault, Neilson Lake area, Trans-Hudson Orogen, Saskatchewan. *Geological Survey of Canada, Current Research*, **1994-C, 19**, 113-120.

ELLIOT, C.G. (1996) Phanerozoic deformation in the "stable" craton, Manitoba, Canada. *Geology*, **24**(10), 909-912.

FEDOROWICH, J.S., KERRICH, R., STAUFFER, M.R. (1995) Geodynamic evolution and thermal history of the central Flin Flon Domain, Trans-Hudosn Orogen: Constraints from structural development, $^{40}Ar/^{39}Ar$, and stable isotope geothermometry. *Tectonics*, **14**, 472-503.

EINSTEIN, S., KOHN, B.P., OSADETZ, K.G., O'SULLIVAN, P.B. (2000) Implications for the tectonics and petroleum generation history of Williston basin from apatite fission track thermochronology. *GeoCanada Program with Abstracts.*

FORTIER, S.M., GILETTI, B.J. (1989) An empirical model for predicting diffusion coefficients in silicate minerals. *Science*, **245**, 1481-1484.

GALA, M.G., SYMONS, D.T.A., PALMER, H.C. (1998) Geotectonics of the Hanson Lake Block, Trans-Hudson Orogen, central Canada: a preliminary report. *Precambrian Research*, **90**, 85-101.

GLEADOW, A.J.W., DUDDY, I.R., GREE, P.F., AND LOVERING, J.F. (1986) Confined fission track lengths in apatite: a diagnostic tool for thermal history analysis. *Contributions to Mineralogy and Petrology*, **94**, 405-415.

GORDON, T.M. (1989) Thermal evolution of the Kisseynew sedimentary gneiss belt, Manitoba: metamorphism at an early Proterozoic accretionary margin. In: *Evolution of Metamorpic Belts, Geological Society Special Publication NO. 40* (Ed. by J. S. Daly, Cliff, R.A., Yardley, B.W.D.), pp. 233-243. Blackwell Scientific Publications, Oxford.

GORDON, T.M., HUNT, P.A., BAILES, A.H., SYME, E.C. (1990) U-Pb Ages from the Flin Flon and Kisseynew Blets, Manitoba: chronology of crust formation at an early proterozoic accretionary margin. In: *The Early Proterozoic Trans Hudson Orogen of North America* (Ed. by J. F. Lewry, and Stauffer, M.R).

GROVE, M., HARRISON T.M. (1996) $^{40}Ar^*$ diffusion in Fe-rich biotite. *American Mineralogist*, **81**, 940-951.

HAJNAL, Z., LUCAS, S., WHITE, D., LEWRY, J., BEZDAN, S., STAUFFER, M.R., THOMAS, M.J. (1996) Post-collisional tectonics of the Trans-Hudson Orogen: seismic reflection evidence for linked strike-slip and detachment fault systems. *Tectonophysics*, **15**(2), 427-439.

HAMES, W.E., BOWERING, S.A. (1994) An empirical evaluation of the argon diffusion geometry in muscovite. *Earth and Planetary Science Letters*, **124**, 161-167.

HAMES, W.E., CHENEY, J.T. (1997) On the loss of $^{40}Ar^*$ from muscovite during polymetamorphism. *Geochimica et Cosmochimica Acta*, **61**(18), 3863-3872.

HARRISON, J.M. (1951) Precambrian correlation and nomenclature, and problems of the Kisseynew gneisses in Manitoba. *Geological Survey of Canada, Bulletin 20.*

HARRISON, T.M. (1981) Diffusion of ^{40}Ar in hornblende. *Contributions to Mineralogy and Petrology*, **78**, 324-331.

HARRISON, T.M., DUNCAN, I., AND MCDOUGALL, I. (1985) Diffusion of ^{40}Ar in biotite: Temperature, pressure and compositional effects. *Geochimica et Cosmochimica Acta*, **49**, 2461-2468.

HARRISON, T.M., HEIZLER, M.T., LOVERA. O.M. (1993) In vacuo crushing experiments and K-feldspar thermochronology. *Earth and Planetary Science Letters*, **117**, 169-180.

HARRISON, T.M., HEIZLER, M.T., LOVERA. O.M., CHEN, W., GROVE, M. (1994) A chlorine disinfectant for excess argon released from K-feldspar thermochronology. *Earth and Planetary Science Letters*, **123**, 95-104.

HEIZLER, M.T., KELLEY, S.A., CONDIE, K.C., LEWRY, J.F. (1999) Evolution of the Trans-Hudson Orogen into a craton. *Geological Society of America Abstracts with Programs.*

HEIZLER, M.T., KELLEY, S.A., CONDIE, PERILLI, S.L., BICKFORD, M.E., WORTMAN, G.L. (2000) The thermal history of the Trans-Hudson Orogen. *GeoCanada Program with Abstracts.*

HEIZLER, M.T., LUX, D.R., AND DECKER, E.R. (1988) The age and cooling history of the Chain of Ponds and Big Island plutons and the Spider Lake granite, west-central Maine and Quebec. *American Journal of Science*, **288**, 925-952.

HESS, J.C., LIPPOLT, H.J., WIRTH, R. (1993) The cooling history of the late Pliocene Eldzhurtinskiy granite (Caucasus Russia) and the thermochronological potential of grain size/age relationships. *Earth and Planetary Science Letters*, **117**, 393-406.

HODGES, K.V., BOWERING, S.A. (1995) $^{40}Ar/^{39}Ar$ thermochronology of isotopically zoned micas: insights from the southwestern USA Proterozoic orogen. *Geochimica et Cosmochimica Acta*, **59**(15), 3205-3220.

HODGES, K.V., HAMES, W.E., BOWRING, S.A. (1994) $^{40}Ar/^{39}Ar$ age gradients in micas from a high-temperature-low-pressure metamorphic terrain: Evidence for very

slow cooling and implication for the interpretation of age spectra. *Geology*, **22**, 55-58.

HOFFMAN, P.F. (1981) Autopsy of Ahapuscow Aulacogen: a failed arm affected by three collisions. In: *Proterozoic basins of Canada, Geological Survey of Canada, Special Paper 91-10* (Ed. by F. H. A. Campbell), pp. 523-549.

HOFFMAN, P.F. (1988) United plates of America, the birth of a craton: Early proterozoic assembly and growth of Laurentia. *Annual Review of Earth and Planetary Sciences*, **16**, 543-603.

KETCHUM, R.A., DONELICK, R.A., AND DONELICK, M.B. (2000) AFTSolve: A program for multi-kinetic modeling of apatite fission-track data. *Geological Materials Research*, **2**(1), 1-32.

KRAUS, J., MENARD, T. (1997) A Thermal Gradient at Constant Pressure: Implications for low-to medium-Pressure Metamorphism in a Compressional Tectonic Setting, Flin FLon and Kisseynew Domain, Trans-HUdson Orogen, Central Canada. *THe Canadian Mineralogist*, **35**, 1117-1136.

LANPHERE, M.A., DALRYMPLE, G.B. (2000) First-principles calibration of ^{38}Ar tracers: Implications for the ages of $^{40}Ar/^{39}Ar$ fluence monitors, pp. 10. U.S. Geological Survey Professional paper 1621.

Leckie, D.A., (1992) Regional setting, evolution, and depositional cycles of the Western Canada Foreland Basin. *In Foreland Basins and Fold Belts*, AAP Memoir 55, pp 9-47(Ed.by R.W. Macqween and D.A. Leckie).

LEWRY, J.F., COLLERSON, K.D. (1990a) The Trans-Hudson Orogen: Extent, subdivision, and problems. In: *The Early Proterozoic Trans Hudson Orogen of North America, Geological Association of Canada Special Paper 37, p. 1-14* (Ed. by J. F. Lewry, and Stauffer, M.R.).

LEWRY, J.F., HAJNAL, Z.,LUCAS S.B., WHITE, D., STAUFFER, M.R., ASHTON, K.E., WEBER, W., CLOWES, R. (1994) Structure of a Paleoproterozoic continent-continent collison zone: a LITHOPROBE seismic reflection profile across the Trans-Hudson Orogen, Canada. *Tectonophysics*, **232**, 143-160.

LEWRY, J.F.T., D.J., MACDONALD, R.; CHIARENZELLE, J. (1990b) Structural relations in accreted terranes of the Trans Hudson Orogen, Saskatchewan: Telescoping in on a

collisional regime? In: *The early Proterozoic Trans-Hudson Orogen of North America, Geological Association of Canada Special Paper 37, p. 75-94* (Ed. by J. F. Lewry, and Stauffer, M.R.).

GURNIS, M. (1997) Cenozoic subsidence and uplift of continents from time-varying dynamic topography. *Geology*, **25**(8), 735-738.

ONSTOTT, T.C. (1989) ^{39}Ar recoil artifacts in chloritized biotite. *Geochimica et Cosmochimica Acta*, **53**, 2697-2711.

GROVE, M., HARRISON, M.T., MAHON, K.I. (1997) Syatematic analysis of K-feldspar ^{40}Ar/^{39}Ar step-heating results: I. Significance of activation energy determinations. *Geochimica et Cosmochimica Acta*, **61**(15), 3171-3192.

HARRISON, M.T., HARRISON, T.M. (1991) Diffusion domains determined by ^{39}Ar released during step heating. *Journal of Geophysical Research*, **96**, 2057-2067.

HEIZLER, M.T., HARRISON, M.T. (1993) Argon diffusion domains in K-feldspar II: kinetic properties of MH-10. *Contributions to Mineralogy and Petrology*, **113**, 381-393.

RICHTER, F.M., AND HARRISON, T.M. (1989) ^{40}Ar/^{39}Ar thermochronology for slowly cooled samples having a distribution of diffusion domain sizes. *Journal of Geophysical Research*, **94**, 17,917-17,936.

SYME, E.C., REILLY, B.A., THOMAS, D.J. (1996) Intracratonic tectonics and the development of continental crust: 1.92 -1.84 Ga evolution of the Flin Flon Blet, Canada. *GSA Bulletin*, **108**(5), 602-629.

JAUPART, L.Z., ROLANDONE, F., GARIEPY, C., BIENFAIT, G., GUILLOU-FROTTIER, L., LAPOINTE, R. (1999) Heat flow in the Trans-Hudson Orogen of the Canadian Shield: Implications for Proterozoic continental growth. *Journal of Geophysical Research*, **104**(B14), 29007-29024.

CONNORS, K., ANSDELL, K.,. (1997) Thermochronology of hornblende and biotite from Wekusko Lake area, Flin Flon Domain, Trans-Hudson Orogen, Manitoba. *Radiogenic Age and Isotopic Studies: Report 10; Geological Survey of Canada, Current Research 1997-F*, 89-100.

MAXEINER, R.O., SIBBALD, T.I.I., SLIMMON, W.L., MEAMAN, L.M., WATTERS, B.R. (1999) Lithogeochemistry of volcano-plutonic assemblages of the southern Hanson Lake Block and southeastern Glennie Domain, Trans-Hudson Orogen: evidence for a single island arc complex. *Canadian Journal of Earth Science*, **36**, 209-225.

MCDOUGALL, I., HARRISION, T.M. (1999) *Geochronology and Thermochronology by the $^{40}Ar/^{39}Ar$ Method.* Oxford University Press, Oxford.

MENARD, T., GORDON, T.M. (1997) Metamorphic P-T paths from the eastern Flin Flon Belt and Kisseynew Domain, Snow Lake, Manitoba., **35**(5), 1093-1115.

MIN, K., MUNDIL, R., RENNE, P.R., AND LUWIG, K.R. (2000) A test for systematic errors in $^{40}Ar/^{39}Ar$ geochronology through comparison with U/Pb analysis of a 1.1Ga rhyolite. *Geochimica et Cosmochimica Acta*, **64**(1), 73-98.

MITROVICA, J.X., BEAUMONT, C., JARVIS, G.T.,. (1989) Tilting of continental interiors by the dynamical effects of subduction. *Tectonics*, **8**(5), 1079-1094.

NORMAN, A.R., WILLIAMS, P.F., ANSDELL, K.M.,. (1995) Early Proterozoic deformaion along the southern margin of the Kisseynew gneiss belt, Trans-Hudson Orogen: a 30Ma progressive deformation cycle. *Canadian Journal of Earth Science*, **32**(7), 875-894.

OSADETZ, K.G., KOHN, B.P., FEINSTEIN, S., O'SULLIVAN, P.B. (2000) Clues to the origin, tectonics and hydrocarbon generation history of Williston Basin from apatite fission track thermochronology. *GeoCanada Program with Abstracts.*

PANDIT, B.I., HAJNAL, Z., STAUFFER, M.R., ASHTON, K.E. (1998) New seismic images of the crust in the central Trans-Hudson Orogen of Saskatchewan. *Tectonophysics*, **290**, 211-219.

PARRISH, R.R. (1990) U-Pb dating of monazite and its application to geological problems. *Canadian Journal of Earth Science*, **27**(11), 1431-1450.

PARSONS, I., BROWN, W.L., SMITH, J.V. (1999) $^{40}Ar/^{39}Ar$ thermochronology using alkali feldspars: real thermal history or mathmatical mirage of microtexture. *Contributions to Mineralogy and Petrology*, **136**, 92-110.

PURDY, J.W., JAGER, E. (1976) K-Ar ages on rock forming minerals from the Central Alps. *Mem.1st. Geol.Min.Univ.*, **30**, 31.

RENNE, P.R., SWISHER, C.C., DEINO, A.L., KARNER, D.B., OWENS, T.L., DEPAOLO, D.J. (1998) Intercalibration of standard, absolute ages and uncertainties in $^{40}Ar/^{39}Ar$ dating. *Chemical Geology*, **145**, 117-152.

SCOTT, D.J., ONGE, M.R.S. (1995) Constraints on Pb closure temperature in titanite based on rocks from the Ungava orogen, Canada: Implications for U-Pb geochronology and P-T-t path determinations. *Geology*, **23**(12), 1123-1126.

Stockmal, G.S., Cant, D.J., Bell, J.S., (1992) Relationship of the Stratigraphy of the Western Canadian Foreland Basin to Cordilleran Tectonics, . *In Foreland Basins and Fold Belts*, AAP Memoir 55, pp 9-47(Ed.by R.W. Macqween and D.A. Leckie).

VAN SCHMUS, W.R., BICKFORD, M.E., LEWRY, J.F., MACDONALD, R. (1987) U-Pb geochronology in the Trans-Hudson Orogen, northern Saskatchewan, Canada. *Canadian Journal of Earth Science*, **24**, 407-424.

WAGNER, G.A., VAN DEN HAUTE, P. (1992) *Fission-track dating*. Kluwer Acedemic Publishers, Dordrecht, The Netherlands.

WORTMAN, G.L., BICKFORD, M.E., LEWRY, J.F. (1999) Thermochronology of the southern Trans-Hudson Orogen, Canada; U-Pb data from monazite and titanite. *Geological Society of America Abstracts with Programs*, **31**(7).

ZWANZIG, H.V. (1998) Synoptic stratigraphy and large-scale structure south flank of Kisseynew Domain in Trans-Hudson Orogen, Manitoba: Implication for 1.845 to 1.77 Ga collision tectonics. *Canadian Journal of Earth Science*, **36**(11), 1859-1880.

Appendix A

Explanation of Appendix A

Appendix A contains all of the $^{40}Ar/^{39}Ar$ analytical data for the hornblende, muscovite, and biotite analyzed in this study. The information for the individual samples includes mineral dated, lab ID number, J-value, and irradiation ID number. The irradiation ID numbers can be correlated with the information in Table A to determine nuclear interference correction factors. All errors are quoted at the 1σ level (except those followed by a *, which are quoted at 2σ) and propagate errors in J-value, mass discrimination and system blank measurements. Ages given for each sample are the total gas age and the plateau or preferred age. Also included are the number of steps used to calculate the age, and the MSWD.

Table A. Nuclear interference correction factors listed by irradiation number.

Irradiation number	$(^{39}Ar/^{37}Ar)_{Ca}$	$(^{36}Ar/^{37}Ar)_{Ca}$	$(^{38}Ar/^{39}Ar)_{K}$	$(40Ar/^{39}Ar)_{K}$
NM-97	0.00073 ± 0.0001	0.00025 ± 0.0000	0.0119	.0291 ± 0.0008
NM-102	0.00073 ± 0.0002	0.00028 ± 0.0001	0.0119	.0282 ± 0.0006

ID	Temp (°C)	$^{40}Ar/^{39}Ar$	$^{37}Ar/^{39}Ar$	$^{36}Ar/^{39}Ar$ (x 10^{-3})	$^{39}Ar_K$ (x 10^{-15} mol)	K/Ca	$^{40}Ar^*$ (%)	^{39}Ar (%)	Age (Ma)	± 1 s (Ma)
HUD-98-62, Biotite, 2.79 mg, J=0.015695, NM-97, Lab#=9705-01										
A	*530*	*45.34*	*0.1394*	*31.07*	*2.54*	*3.7*	*79.7*	*0.3*	*810.8*	*5.8*
B	*600*	*64.99*	*0.0729*	*11.30*	*2.92*	*7.0*	*94.8*	*0.6*	*1220.8*	*4.6*
C	*680*	*100.6*	*0.0232*	*3.269*	*19.3*	*22.0*	*99.0*	*2.8*	*1698.2*	*2.1*
D	760	102.6	0.0032	0.5745	104.0	157.2	99.8	14.7	1728.9	2.1
E	830	102.1	0.0026	0.2827	88.1	197.3	99.9	24.7	1724.0	2.7
F	900	102.3	0.0060	0.2699	111.1	85.4	99.9	37.3	1726.5	3.0
G	950	102.0	0.0143	0.2352	51.0	35.8	99.9	43.1	1723.7	2.1
H	1010	102.2	0.0096	0.2043	64.7	53.0	99.9	50.5	1726.2	2.2
I	1070	102.0	0.0036	0.2925	134.5	142.8	99.9	65.8	1723.8	2.0
J	1130	101.7	0.0048	0.3100	116.5	107.4	99.9	79.1	1720.2	3.5
K	1230	101.9	0.0069	0.2675	136.3	73.8	99.9	94.6	1722.4	2.4
L	*1580*	*100.4*	*0.0142*	*1.407*	*47.5*	*35.9*	*99.6*	*100.0*	*1701.9*	*2.3*
total gas age			n=12		878.5	105.2			1718.2	2.1
plateau		**MSWD = 1.15**	n=8	steps D-K	806.3	112.0		91.8	1724.9	1.7*
HUD-98-63, 1.29 mg biotite, J=0.0157621, NM-97, Lab#=9631-01										
A	*530*	*110.0*	*0.0319*	*249.1*	*0.475*	*16.0*	*33.0*	*0.1*	*816.7*	*30.6*
B	*600*	*63.12*	*0.0328*	*30.35*	*0.628*	*15.5*	*85.7*	*0.3*	*1112.8*	*8.5*
C	*680*	*88.75*	*0.0224*	*14.18*	*1.30*	*22.8*	*95.2*	*0.6*	*1527.9*	*6.3*
D	760	105.4	0.0034	1.980	22.9	149.0	99.4	6.0	1758.9	2.6
E	830	105.0	0.0014	0.4785	20.0	376.3	99.8	10.8	1759.3	2.1
F	900	105.4	0.0012	0.3055	67.9	412.8	99.9	27.0	1764.7	2.2
G	950	105.0	0.0019	0.3565	34.2	267.8	99.9	35.2	1760.7	1.8
H	1010	105.6	0.0021	0.2512	29.1	240.4	99.9	42.1	1766.9	2.6
I	1070	106.1	0.0026	0.3823	30.7	197.2	99.9	49.4	1772.2	2.2
J	1130	105.2	0.0026	0.3919	37.9	196.4	99.9	58.5	1762.7	3.2
K	1230	105.4	0.0015	0.1834	136.5	345.9	99.9	91.0	1764.5	3.3
L	1580	104.7	0.0038	0.6407	37.5	132.7	99.8	100.0	1755.7	3.2
total gas age			n=12		418.9	288.4			1760.6	2.4
plateau		**MSWD=4.10**	n=9	steps D-L	416.5	289.9		99.4	1763.0	3.29*

ID	Temp (°C)	$^{40}Ar/^{39}Ar$	$^{37}Ar/^{39}Ar$	$^{36}Ar/^{39}Ar$ (x 10^{-3})	$^{39}Ar_K$ (x 10^{-15} mol)	K/Ca	$^{39}Ar_K$ (%)	$^{40}Ar^*$ (%)	Age (Ma)	± 2σ (Ma)
HUD-98-64, Biotite, 0.32 mg, J=0.0157981, NM-97, Lab#=9610-02										
B	*600*	*79.09*	*0.0000*	*20.84*	*0.575*	-	*92.2*	*0.3*	*1382.4*	*10.0*
C	*680*	*95.96*	*0.0000*	*7.948*	*3.09*	-	*97.5*	*2.0*	*1637.4*	*3.2*
D	*760*	*100.5*	*0.0037*	*2.068*	*29.4*	*138.0*	*99.4*	*18.4*	*1708.0*	*2.8*
E	830	100.6	0.0022	0.4467	33.9	232.4	99.8	37.3	1714.1	3.4
F	900	101.1	0.0353	0.6294	11.0	14.5	99.8	43.5	1719.7	2.7
G	950	101.6	0.0304	1.282	9.18	16.8	99.6	48.6	1723.1	2.6
H	1010	101.2	0.0112	0.6218	25.8	45.5	99.8	63.0	1720.2	2.4
I	1070	101.3	0.0101	0.6555	26.8	50.3	99.8	78.0	1721.8	2.3
J	1130	101.4	0.0129	0.6485	29.5	39.5	99.8	94.4	1722.5	2.2
K	1230	101.3	0.1537	1.435	8.58	3.3	99.6	99.2	1719.1	2.8
L	1580	105.9	1.439	18.62	1.45	0.35	94.9	100.0	1716.0	6.0
total gas age			n=11		179.2	90.9			1715.2	2.4
plateau		**MSWD=0.94**	n=8	steps E-L	146.2	81.4		81.6	1720.7	1.9*
HUD-98-65, 1.32 mg biotite, J=0.0157680, NM-97, Lab#=9632-01										
A	*530*	*69.37*	*0.0487*	*55.81*	*1.84*	*10.5*	*76.2*	*0.4*	*1093.6*	*6.9*
B	*600*	*82.90*	*0.0396*	*21.58*	*0.795*	*12.9*	*92.3*	*0.6*	*1427.5*	*11.2*
C	*680*	*94.24*	*0.0360*	*8.913*	*3.01*	*14.2*	*97.2*	*1.2*	*1612.2*	*4.2*
D	760	100.7	0.0048	4.536	44.3	105.5	98.6	10.6	1700.0	2.2
E	830	99.90	0.0019	0.7303	47.4	261.7	99.8	20.7	1703.9	3.8
F	900	99.92	0.0030	0.3867	79.3	168.7	99.9	37.6	1705.2	3.0
G	950	100.6	0.0043	0.5764	25.6	118.3	99.8	43.1	1711.6	2.3
H	1010	101.0	0.0055	0.4266	41.1	92.3	99.8	51.8	1716.8	2.8
I	1070	100.4	0.0033	0.2956	76.7	152.9	99.9	68.1	1711.0	2.8
J	1130	100.3	0.0050	0.4445	63.1	101.6	99.8	81.6	1709.7	2.3
K	1230	100.2	0.0058	0.3601	69.7	87.5	99.9	96.4	1708.3	2.4
L	1580	99.72	0.0088	2.012	17.0	58.0	99.4	100.0	1697.7	2.1
total gas age			n=12		469.8	133.2			1704.2	2.4
plateau		**MSWD-6.24**	n=9	steps D-L	464.1	134.6		98.8	1706.3	4.21*

ID	Temp (°C)	$^{40}Ar/^{39}Ar$	$^{37}Ar/^{39}Ar$	$^{36}Ar/^{39}Ar$ (x 10^{-3})	$^{39}Ar_K$ (x 10^{-15} mol)	K/Ca	$^{40}Ar^*$ (%)	^{39}Ar (%)	Age (Ma)	± 1s (Ma)
HUD-98-66, 1.02 mg biotite, J=0.0157694, NM-97, Lab#=9633-01										
C	*680*	*57.83*	*0.0550*	*7.189*	*5.88*	*9.3*	*96.3*	*1.3*	*1137.1*	*2.4*
D	*760*	*99.06*	*0.0194*	*2.420*	*24.4*	*26.3*	*99.2*	*6.6*	*1689.1*	*2.9*
E	*830*	*100.2*	*0.0122*	*1.018*	*22.6*	*41.7*	*99.7*	*11.6*	*1706.5*	*2.9*
F	*900*	*100.1*	*0.0092*	*0.3110*	*68.6*	*55.5*	*99.9*	*26.6*	*1707.8*	*3.4*
G	950	101.1	0.0104	0.2642	32.8	49.2	99.9	33.8	1718.2	1.9
H	1010	101.6	0.0127	0.3074	35.6	40.2	99.9	41.6	1723.8	3.1
I	1070	101.5	0.0059	0.1244	90.1	86.9	99.9	61.4	1723.2	2.4
J	1130	100.9	0.0074	0.1752	68.8	69.1	99.9	76.5	1717.1	2.6
K	1230	100.9	0.0100	0.2145	92.7	50.9	99.9	96.8	1716.8	3.1
L	1580	100.6	0.0629	1.721	14.7	8.1	99.5	100.0	1708.7	2.2
total gas age			n=10		456.2	56.8			1707.7	2.4
plateau		**MSWD=5.29**	n=6	steps G-L	334.7	61.2		73.4	1717.1	4.58*
HUD-98-67, Biotite, 2.43 mg, J=0.0157105, NM-97, Lab#=9707-01										
A	*530*	*41.38*	*0.0839*	*64.19*	*4.66*	*6.1*	*54.1*	*0.9*	*543.8*	*5.8*
B	*600*	*59.48*	*0.0472*	*22.83*	*3.53*	*10.8*	*88.6*	*1.5*	*1088.4*	*3.7*
C	*680*	*87.03*	*0.0256*	*8.043*	*10.8*	*19.9*	*97.2*	*3.5*	*1525.6*	*2.5*
D	*760*	*98.76*	*0.0034*	*1.932*	*34.9*	*151.8*	*99.4*	*9.8*	*1683.3*	*2.5*
E	830	100.7	0.0022	0.5541	32.9	229.6	99.8	15.8	1709.0	2.6
F	900	100.6	0.0031	0.6256	50.6	162.2	99.8	25.1	1707.8	1.8
G	950	99.96	0.0036	0.6610	34.4	140.7	99.8	31.4	1700.7	2.2
H	1010	100.6	0.0026	0.6633	59.8	197.2	99.8	42.3	1707.7	2.2
I	1070	100.8	0.0015	0.3668	69.5	333.7	99.9	54.9	1710.7	3.3
J	1130	99.80	0.0023	0.4693	71.5	221.5	99.8	68.0	1699.6	2.6
K	1230	100.8	0.0021	0.2464	164.4	240.1	99.9	98.0	1711.5	2.9
L	1580	102.4	0.0087	9.710	11.0	58.9	97.2	100.0	1698.1	2.6
total gas age			n=12		547.9	213.7			1688.6	2.3
plateau		**MSWD=4.13**	n=8	steps E-L	494.1	225.7		90.2	1705.7	3.47*

ID	Temp (°C)	$^{40}Ar/^{39}Ar$	$^{37}Ar/^{39}Ar$	$^{36}Ar/^{39}Ar$ (x 10^{-3})	$^{39}Ar_K$ (x 10^{-15} mol)	K/Ca	$^{40}Ar^*$ (%)	^{39}Ar (%)	Age (Ma)	±1s (Ma)
HUD-98-71, 1.26 mg biotite, J=0.0157040, NM-97, Lab#=9646-01										
A	*530*	*87.35*	*0.1676*	*151.9*	*1.44*	*3.0*	*48.6*	*0.3*	*921.6*	*18.7*
B	*600*	*46.02*	*0.1507*	*9.203*	*2.77*	*3.4*	*94.1*	*0.9*	*935.8*	*2.8*
C	*680*	*101.7*	*0.0467*	*5.551*	*7.62*	*10.9*	*98.4*	*2.6*	*1703.5*	*2.3*
D	*760*	*109.1*	*0.0111*	*1.208*	*35.0*	*46.1*	*99.6*	*10.4*	*1796.4*	*3.4*
E	830	110.7	0.0075	0.2404	44.7	68.2	99.9	20.3	1816.9	2.3
F	900	111.2	0.0077	0.1769	59.8	66.3	99.9	33.6	1822.2	2.8
G	950	112.0	0.0096	0.2214	43.5	53.1	99.9	43.2	1829.7	2.9
H	1010	111.9	0.0135	0.3455	29.4	37.9	99.9	49.8	1828.2	2.7
I	1070	112.8	0.0131	0.2213	52.3	38.9	99.9	61.4	1837.7	2.3
J	1130	111.3	0.0345	0.2665	47.0	14.8	99.9	71.8	1822.2	2.2
K	1230	111.8	0.1159	0.2290	98.6	4.4	99.9	93.7	1828.3	2.2
L	1580	111.7	0.0711	1.490	28.5	7.2	99.6	100.0	1822.9	2.1
total gas age			n=12		450.8	34.4			1813.6	2.1
plateau		**MSWD=7.39**	n=8	steps E-L	404.0	34.2		89.6	1825.9	4.62*
HUD-98-72, Biotite, 0.55 mg, J=0.0158105, NM-97, Lab#=9709-01										
A	*530*	*40.18*	*0.2435*	*29.62*	*2.03*	*2.1*	*78.2*	*1.1*	*727.7*	*5.3*
B	*600*	*34.56*	*0.1027*	*5.183*	*4.95*	*5.0*	*95.5*	*3.6*	*757.6*	*2.4*
C	*680*	*97.73*	*0.0748*	*2.847*	*10.1*	*6.8*	*99.1*	*8.9*	*1675.7*	*2.9*
D	*760*	*107.3*	*0.0125*	*1.207*	*25.8*	*40.8*	*99.6*	*22.4*	*1785.3*	*3.3*
E	830	108.3	0.0129	0.4884	17.6	39.4	99.8	31.6	1798.8	2.2
F	900	108.8	0.0359	0.4885	23.4	14.2	99.8	43.8	1803.8	2.0
G	950	110.1	0.0639	0.6822	17.2	8.0	99.8	52.7	1817.0	2.3
H	1010	110.5	0.0279	0.4594	25.0	18.3	99.9	65.8	1821.9	3.0
I	1070	109.2	0.0340	0.6735	23.7	15.0	99.8	78.2	1807.1	2.8
J	1130	107.4	0.0734	0.9047	22.0	7.0	99.7	89.7	1787.9	2.5
K	1230	108.3	0.1692	1.692	16.1	3.0	99.5	98.1	1795.1	2.2
L	1580	115.3	0.0736	28.19	3.66	6.9	92.8	100.0	1785.3	4.0
total gas age			n=12		191.6	17.5			1756.7	2.2
plateau		**MSWD=21.75**	n=8	steps E-L	148.7	14.8		77.6	1802.7	8.12*

ID	Temp (°C)	$^{40}Ar/^{39}Ar$	$^{37}Ar/^{39}Ar$	$^{36}Ar/^{39}Ar$ (x 10^{-3})	$^{39}Ar_K$ (x 10^{-15} mol)	K/Ca	$^{40}Ar^*$ (%)	^{39}Ar (%)	Age (Ma)	±1s (Ma)
HUD-98-72, Muscovite, 0.28 mg, J=0.0157542, NM-97, Lab#=9711-01										
A	*580*	*38.48*	*0.3604*	*30.09*	*1.14*	*1.4*	*76.9*	*0.7*	*690.5*	*9.7*
B	*630*	*79.74*	*0.3064*	*21.13*	*0.312*	*1.7*	*92.2*	*0.9*	*1387.7*	*19.3*
C	*680*	*90.36*	*0.2490*	*13.59*	*0.758*	*2.0*	*95.5*	*1.4*	*1549.4*	*10.6*
D	*730*	*101.1*	*0.0436*	*2.582*	*1.83*	*11.7*	*99.2*	*2.6*	*1709.6*	*5.6*
E	*770*	*104.1*	*0.0188*	*3.945*	*1.43*	*27.1*	*98.9*	*3.5*	*1738.6*	*6.2*
F	*810*	*106.9*	*0.0156*	*3.030*	*4.58*	*32.7*	*99.1*	*6.5*	*1771.9*	*2.9*
G	*850*	*108.7*	*0.0111*	*2.608*	*5.51*	*45.9*	*99.3*	*10.1*	*1791.4*	*2.7*
H	890	111.0	0.0050	1.047	16.3	101.8	99.7	20.7	1821.0	2.4
I	930	110.7	0.0051	0.7623	22.4	100.6	99.8	35.2	1818.6	2.3
J	970	110.1	0.0108	1.144	12.7	47.3	99.7	43.4	1811.0	2.3
K	1010	110.0	0.0138	0.9790	13.1	37.1	99.7	52.0	1810.7	2.2
L	1050	110.2	0.0069	0.7944	15.8	73.6	99.8	62.2	1812.9	2.6
M	1090	111.3	0.0092	0.5611	25.2	55.7	99.8	78.6	1825.1	2.6
N	1130	111.7	0.0147	1.096	20.5	34.8	99.7	91.9	1827.3	2.4
O	*1230*	*109.3*	*0.1047*	*2.213*	*9.15*	*4.9*	*99.4*	*97.8*	*1799.2*	*2.6*
P	*1580*	*112.3*	*0.1571*	*20.28*	*3.35*	*3.2*	*94.6*	*100.0*	*1774.7*	*4.1*
total gas age			n=16		154.1	57.1			1802.1	2.3
plateau		**MSWD=7.94**	n=7	steps H-N	126.0	65.7		81.8	1817.6	5.12*
HUD-98-73, 0.82 mg biotite, J=0.0157155, NM-97, Lab#=9647-01										
A	*530*	*68.95*	*0.0259*	*105.4*	*2.41*	*19.7*	*54.8*	*0.8*	*840.8*	*7.4*
B	*600*	*33.08*	*0.0227*	*10.10*	*6.70*	*22.5*	*90.9*	*3.2*	*698.3*	*1.8*
C	*680*	*90.04*	*0.0089*	*5.862*	*9.28*	*57.6*	*98.0*	*6.4*	*1569.9*	*2.2*
D	760	108.3	0.0026	2.322	27.3	195.7	99.3	16.0	1785.4	2.4
E	830	108.6	0.0020	0.5313	24.9	258.2	99.8	24.7	1794.7	2.4
F	900	108.8	0.0018	0.4402	39.1	280.4	99.9	38.4	1796.4	2.7
G	950	110.0	0.0024	0.4368	31.0	215.6	99.9	49.2	1809.2	2.5
H	1010	112.7	0.0026	0.4842	41.3	193.1	99.8	63.6	1837.0	2.2
I	1070	110.5	0.0020	0.3804	42.2	256.7	99.9	78.4	1815.1	3.4
J	1130	108.9	0.0016	0.5920	31.7	315.1	99.8	89.5	1797.0	2.2
K	1230	109.2	0.0091	0.5647	30.0	56.0	99.8	100.0	1800.4	2.4
L	1580	110.7	0.0061	8.161	0.001	83.4	97.8	100.0	1792.6	3.3
total gas age			n=12		285.9	212.0			1764.5	2.1
plateau		MSWD=43.59	n=9	steps D-L	267.5	223.9		93.6	1804.6	11.10*

ID	Temp (°C)	$^{40}Ar/^{39}Ar$	$^{37}Ar/^{39}Ar$	$^{36}Ar/^{39}Ar$ (x 10^{-3})	$^{39}Ar_K$ (x 10^{-15} mol)	K/Ca	$^{40}Ar^*$ (%)	^{39}Ar (%)	Age (Ma)	±1s (Ma)
HUD-98-74, Biotite, 0.87 mg, J=0.0158309, NM-97, Lab#=9713-01										
A	*530*	*44.23*	*0.1191*	*109.0*	*1.61*	*4.3*	*27.1*	*0.6*	*313.4*	*10.7*
B	*600*	*31.59*	*0.0822*	*7.968*	*6.60*	*6.2*	*92.5*	*3.1*	*685.7*	*1.6*
C	*680*	*76.78*	*0.0270*	*3.664*	*11.7*	*18.9*	*98.6*	*7.6*	*1420.8*	*2.0*
D	760	103.8	0.0078	1.068	27.6	65.4	99.7	18.0	1750.1	2.3
E	830	102.8	0.0070	0.8028	18.8	72.9	99.7	25.1	1740.3	2.5
F	900	103.9	0.0110	0.7064	27.1	46.4	99.8	35.4	1752.2	2.1
G	950	105.0	0.0098	0.6190	22.9	52.1	99.8	44.0	1763.9	3.5
H	1010	107.7	0.0062	0.3753	39.7	82.2	99.9	59.1	1793.5	2.5
I	1070	105.3	0.0055	0.3164	53.0	92.8	99.9	79.1	1768.5	2.5
J	1130	103.4	0.0083	0.5030	42.7	61.5	99.8	95.3	1747.2	2.9
K	*1230*	*87.49*	*0.0719*	*2.054*	*11.0*	*7.1*	*99.3*	*99.5*	*1560.7*	*1.8*
L	*1580*	*78.70*	*0.0652*	*50.63*	*1.44*	*7.8*	*81.0*	*100.0*	*1258.3*	*7.2*
total gas age			n=12		264.0	63.6			1700.0	2.2
plateau		MSWD=50.08	n=7	steps D-J	231.7	70.9		87.7	1758.4	13.56*
HUD-98-75, Hornblende, 1.21 mg, J=0.0157584, NM-97, Lab#=9648-01										
A	*730*	*61.74*	*0.3065*	*44.34*	*0.005*	*1.7*	*78.8*	*6.9*	*1026.5*	*3.3*
B	*830*	*98.71*	*0.1771*	*6.624*	*0.008*	*2.9*	*98.0*	*18.0*	*1670.8*	*2.8*
C	*930*	*101.8*	*0.6607*	*2.459*	*0.009*	*0.77*	*99.3*	*31.1*	*1719.2*	*2.6*
D	*980*	*106.2*	*1.860*	*2.050*	*0.007*	*0.27*	*99.5*	*40.5*	*1770.1*	*3.0*
E	1010	108.9	2.947	1.917	0.007	0.17	99.7	49.8	1801.3	2.6
F	1040	108.9	4.165	1.909	0.010	0.12	99.7	63.6	1802.7	2.8
G	1060	108.1	2.851	1.529	0.011	0.18	99.8	79.1	1793.4	3.0
H	*1080*	*106.1*	*0.6276*	*1.249*	*0.005*	*0.81*	*99.7*	*86.3*	*1770.3*	*2.7*
I	*1100*	*106.4*	*0.8601*	*3.038*	*0.003*	*0.59*	*99.2*	*91.0*	*1767.8*	*2.8*
J	*1150*	*106.3*	*3.945*	*4.694*	*0.002*	*0.13*	*98.9*	*93.7*	*1766.7*	*3.3*
K	*1230*	*105.5*	*4.293*	*4.597*	*0.004*	*0.12*	*99.0*	*99.4*	*1759.3*	*3.5*
L	*1580*	*127.1*	*4.666*	*91.93*	*0.000*	*0.11*	*78.9*	*100.0*	*1713.6*	*13.9*
total gas age			n=12		0.072	0.72			1710.7	2.6
plateau		**MSWD=2.93**	n=3	steps E-G	0.028	0.16		38.6	1799.7	3.22*

ID	Temp (°C)	$^{40}Ar/^{39}Ar$	$^{37}Ar/^{39}Ar$	$^{36}Ar/^{39}Ar$ (x 10^{-3})	$^{39}Ar_K$ (x 10^{-15} mol)	K/Ca	$^{40}Ar^*$ (%)	^{39}Ar (%)	Age (Ma)	± 1s (Ma)
HUD-98-76, Biotite, 1.58 mg, J=0.0157157, NM-97, Lab#=9715-01										
A	*530*	*67.20*	*0.0973*	*38.53*	*4.11*	*5.2*	*83.0*	*0.9*	*1135.9*	*3.4*
B	*600*	*75.41*	*0.0494*	*6.700*	*6.77*	*10.3*	*97.3*	*2.3*	*1384.1*	*2.3*
C	*680*	*101.8*	*0.0231*	*2.335*	*18.6*	*22.1*	*99.3*	*6.3*	*1716.3*	*2.6*
D	760	105.8	0.0075	0.6409	67.3	67.6	99.8	20.7	1764.9	2.3
E	830	105.9	0.0051	0.2795	44.5	100.8	99.9	30.2	1766.5	2.1
F	900	105.4	0.0073	0.2518	79.2	70.3	99.9	47.1	1762.0	3.4
G	950	106.4	0.0264	0.3098	39.9	19.3	99.9	55.6	1772.0	4.1
H	1010	106.6	0.0159	0.3396	67.9	32.1	99.9	70.2	1773.7	2.0
I	1070	106.1	0.0144	0.3447	74.4	35.5	99.9	86.1	1768.2	2.2
J	1130	105.8	0.1686	0.6870	33.8	3.0	99.8	93.3	1764.1	2.0
K	1230	106.0	0.7282	0.8293	24.0	0.70	99.8	98.4	1767.4	2.6
L	1580	109.2	0.1511	10.47	7.41	3.4	97.2	100.0	1770.1	3.0
total gas age			n=12		467.9	44.5			1754.1	2.2
plateau		**MSWD=2.35**	n=9	steps D-L	438.4	46.4		93.7	1767.8	2.48*
HUD-98-77, Biotite, 1.74 mg, J=0.0157794, NM-97, Lab#=9608-01										
A	*530*	*63.24*	*0.1498*	*80.26*	*3.13*	*3.4*	*62.5*	*0.6*	*874.2*	*5.7*
B	*600*	*58.16*	*0.1109*	*17.62*	*3.04*	*4.6*	*91.0*	*1.2*	*1095.5*	*4.3*
C	*680*	*94.94*	*0.0286*	*4.237*	*13.6*	*17.9*	*98.7*	*3.7*	*1637.0*	*2.6*
D	760	105.1	0.0059	0.8667	70.5	87.1	99.7	17.1	1761.0	3.7
E	830	106.0	0.0047	0.4014	47.4	108.3	99.9	26.0	1771.9	2.6
F	900	106.6	0.0093	0.3888	81.3	54.7	99.9	41.4	1778.0	4.0
G	950	107.1	0.0320	0.5077	49.5	16.0	99.8	50.8	1782.9	2.7
H	1010	107.1	0.0725	0.3827	91.0	7.0	99.9	68.0	1784.3	1.8
I	1070	105.6	0.0746	0.3813	63.1	6.8	99.9	79.9	1768.3	2.8
J	1130	105.5	0.0385	0.5382	51.6	13.3	99.8	89.7	1766.7	3.4
K	1230	106.7	0.3544	0.5009	42.8	1.4	99.9	97.8	1780.1	2.2
L	1580	107.5	0.3350	6.968	11.7	1.5	98.1	100.0	1768.1	2.2
total gas age			n=12		528.7	35.2			1761.5	2.5
plateau		**MSWD=9.80**	n=9	steps D-L	508.9	36.0		96.3	1777.1	5.36*

ID	Temp (°C)	$^{40}Ar/^{39}Ar$	$^{37}Ar/^{39}Ar$	$^{36}Ar/^{39}Ar$ (x 10^{-3})	$^{39}Ar_K$ (x 10^{-15} mol)	K/Ca	$^{40}Ar^*$ (%)	^{39}Ar (%)	Age (Ma)	±1s (Ma)
HUD-98-78, 1.19 mg biotite, J=0.0156080, NM-97, Lab#=9699-01										
A	*530*	*51.52*	*0.0470*	*46.36*	*3.23*	*10.8*	*73.4*	*0.8*	*836.5*	*4.4*
B	*600*	*63.45*	*0.0418*	*5.667*	*4.04*	*12.2*	*97.3*	*1.8*	*1217.5*	*2.8*
C	*680*	*89.93*	*0.0364*	*2.527*	*6.64*	*14.0*	*99.1*	*3.4*	*1573.1*	*3.3*
D	*760*	*103.1*	*0.0222*	*1.160*	*26.2*	*22.9*	*99.6*	*9.7*	*1725.9*	*1.9*
E	*830*	*104.6*	*0.0053*	*0.4139*	*34.8*	*97.0*	*99.9*	*18.1*	*1744.6*	*2.1*
F	900	106.1	0.0056	0.2305	72.2	91.5	99.9	35.6	1760.7	2.6
G	950	106.0	0.0081	0.3088	36.3	63.4	99.9	44.4	1760.5	2.1
H	1010	106.3	0.0090	0.2642	56.3	56.4	99.9	58.0	1763.3	2.6
I	1070	105.8	0.0090	0.2160	55.3	56.8	99.9	71.3	1757.9	2.4
J	*1130*	*105.5*	*0.0155*	*0.3130*	*49.4*	*32.9*	*99.9*	*83.3*	*1754.2*	*1.9*
K	*1230*	*105.5*	*0.1691*	*0.4292*	*49.2*	*3.0*	*99.9*	*95.2*	*1754.7*	*2.6*
L	*1580*	*105.5*	*0.1734*	*1.503*	*19.8*	*2.9*	*99.6*	*100.0*	*1750.7*	*3.9*
total gas age			n=12		413.5	51.3			1739.6	2.0
plateau		**MSWD=0.78**	n=4	steps F-I	220.0	69.2		53.2	1760.4	2.12*
HUD-98-79, 1.06 mg biotite, J=0.0157784, NM-97, Lab#=9649-01										
A	*530*	*62.58*	*0.0220*	*105.6*	*0.948*	*23.2*	*50.1*	*0.2*	*724.9*	*12.3*
B	*600*	*53.88*	*0.0152*	*22.91*	*0.391*	*33.6*	*87.4*	*0.3*	*1002.2*	*16.7*
C	*680*	*80.22*	*0.0065*	*7.904*	*3.69*	*79.1*	*97.1*	*1.2*	*1445.6*	*2.9*
D	*760*	*104.3*	*0.0013*	*1.810*	*19.9*	*392.2*	*99.5*	*6.0*	*1748.8*	*2.1*
E	830	104.7	0.0011	0.6217	40.6	445.3	99.8	15.7	1757.4	2.6
F	900	104.7	0.0010	0.1571	70.9	490.2	99.9	32.8	1758.2	1.8
G	950	104.6	0.0016	0.2695	33.9	317.7	99.9	40.9	1757.0	2.1
H	1010	104.3	0.0010	0.1988	65.9	486.2	99.9	56.7	1754.4	2.1
I	1070	104.2	0.0010	0.0975	72.5	503.0	99.9	74.2	1753.5	3.2
J	1130	104.0	0.0021	0.3384	40.3	246.5	99.9	83.8	1751.0	2.5
K	1230	104.3	0.0089	0.2105	57.8	57.4	99.9	97.7	1754.6	2.4
L	1580	105.1	0.0187	5.561	9.41	27.2	98.4	100.0	1745.5	3.5
total gas age			n=12		416.2	369.3			1748.8	2.0
plateau		**MSWD=2.20**	n=8	steps E-L	391.2	372.1		94.0	1755.6	1.66*

ID	Temp (°C)	$^{40}Ar/^{39}Ar$	$^{37}Ar/^{39}Ar$	$^{36}Ar/^{39}Ar$ (x 10^{-3})	$^{39}Ar_K$ (x 10^{-15} mol)	K/Ca	$^{40}Ar^*$ (%)	^{39}Ar (%)	Age (Ma)	±1s (Ma)
HUD-98-80, Biotite, 0.60 mg, J=0.0158104, NM-97, Lab#=9612-01										
A	*530*	*52.89*	*0.2490*	*94.29*	*0.384*	*2.0*	*47.3*	*0.2*	*601.3*	*20.7*
B	*600*	*59.34*	*0.0727*	*7.114*	*3.14*	*7.0*	*96.4*	*1.8*	*1162.4*	*3.0*
C	*680*	*102.4*	*0.0307*	*2.281*	*7.05*	*16.6*	*99.3*	*5.5*	*1729.0*	*2.3*
D	760	103.8	0.0052	0.5439	24.6	98.6	99.8	18.2	1749.9	2.1
E	830	103.8	0.0039	0.0497	20.2	129.6	100.0	28.6	1751.8	2.5
F	900	104.1	0.0120	0.2844	27.9	42.7	99.9	43.1	1754.5	2.3
G	950	105.4	0.0321	0.5023	20.5	15.9	99.8	53.6	1767.5	2.1
H	1010	104.6	0.1232	0.4965	31.1	4.1	99.8	69.7	1758.5	1.9
I	1070	104.2	0.0536	0.2603	30.2	9.5	99.9	85.3	1755.3	2.3
J	1130	103.7	0.0415	0.8893	18.2	12.3	99.7	94.7	1747.8	2.2
K	*1230*	*103.1*	*0.0381*	*2.209*	*10.3*	*13.4*	*99.3*	*100.0*	*1737.7*	*2.1*
total gas age			n=11		193.6	38.7			1741.4	1.8
plateau		**MSWD=9.69**	n=7	steps D-J	172.8	41.7		89.2	1756.0	5.13*
HUD-98-80, Hornblende, 1.3 mg, J=0.0157892, NM-97, Lab#=9614-01										
A	*730*	*78.19*	*1.167*	*56.60*	*0.005*	*0.44*	*78.7*	*2.7*	*1225.3*	*4.2*
B	*830*	*101.9*	*0.3050*	*3.768*	*0.011*	*1.7*	*98.9*	*8.3*	*1718.0*	*2.5*
C	930	104.3	0.8264	1.427	0.013	0.62	99.6	14.8	1752.3	2.6
D	980	105.6	2.425	1.183	0.035	0.21	99.8	32.5	1769.9	1.8
E	1010	104.0	2.821	1.078	0.055	0.18	99.9	60.4	1753.9	5.0
F	1040	105.1	2.751	0.8519	0.022	0.19	99.9	71.8	1766.1	2.4
G	1060	105.4	2.551	0.8421	0.012	0.20	99.9	77.9	1768.5	2.7
H	1080	104.8	2.561	1.322	0.009	0.20	99.8	82.6	1761.1	2.3
I	1100	104.8	2.743	2.267	0.009	0.19	99.5	87.1	1758.4	2.8
J	1150	104.9	2.984	1.286	0.018	0.17	99.8	96.3	1762.7	2.9
K	1230	105.8	3.164	2.623	0.005	0.16	99.5	99.1	1768.8	3.1
L	1580	112.7	1.995	25.93	0.002	0.26	93.3	100.0	1766.4	6.2
total gas age			n=12		0.196	0.31			1744.6	2.9
plateau		**MSWD=5.27**	n=10	steps C-L	0.180	0.22		91.7	1764.8	3.90*

ID	Temp (°C)	$^{40}Ar/^{39}Ar$	$^{37}Ar/^{39}Ar$	$^{36}Ar/^{39}Ar$ (x 10^{-3})	$^{39}Ar_K$ (x 10^{-15} mol)	K/Ca	$^{40}Ar^*$ (%)	^{39}Ar (%)	Age (Ma)	±1s (Ma)
HUD-98-81, J7:97, 0.89 mg biotite, J=0.01578998±0.10%, D=1.00362±0.00105, NM-97, Lab#=9650-01										
A	*530*	*65.54*	*0.0343*	*98.72*	*0.776*	*14.9*	*55.4*	*0.2*	*818.1*	*15.2*
B	*600*	*57.67*	*0.0309*	*20.38*	*0.689*	*16.5*	*89.5*	*0.4*	*1075.4*	*10.9*
C	*680*	*85.41*	*0.0077*	*6.007*	*2.37*	*65.9*	*97.9*	*1.0*	*1518.4*	*4.3*
D	*760*	*103.1*	*0.0027*	*1.870*	*18.6*	*188.8*	*99.4*	*5.8*	*1736.4*	*2.3*
E	*830*	*102.2*	*0.0006*	*0.4255*	*38.6*	*810.4*	*99.8*	*15.7*	*1731.7*	*3.0*
F	900	103.4	0.0008	0.2345	74.3	606.2	99.9	34.9	1745.3	3.1
G	950	103.6	0.0016	0.2249	25.0	322.2	99.9	41.3	1747.7	2.3
H	1010	103.8	0.0014	0.2465	43.4	369.5	99.9	52.5	1749.9	2.7
I	1070	103.9	0.0011	0.1450	70.2	468.1	99.9	70.5	1750.5	2.2
J	*1130*	*102.8*	*0.0013*	*0.4495*	*35.4*	*380.3*	*99.8*	*79.7*	*1738.4*	*2.1*
K	*1230*	*103.2*	*0.0008*	*0.2148*	*59.4*	*617.5*	*99.9*	*94.9*	*1743.0*	*2.9*
L	*1580*	*104.1*	*0.0012*	*2.877*	*19.6*	*429.1*	*99.2*	*100.0*	*1744.1*	*2.8*
total gas age			n=12		388.3	503.5			1739.7	2.3
plateau		**MSWD=0.74**	n=4	steps F-I	212.9	479.0		54.8	1748.8	2.50*
HUD-98-82, Hornblende, 1.70 mg, J=0.0157784, NM-97, Lab#=9651-01										
A	*730*	*170.2*	*3.187*	*493.9*	*0.000*	*0.16*	*14.4*	*0.9*	*590.2*	*51.7*
B	*830*	*99.52*	*2.942*	*166.9*	*0.000*	*0.17*	*50.6*	*1.3*	*1057.1*	*31.2*
C	*930*	*91.58*	*3.536*	*30.60*	*0.000*	*0.14*	*90.4*	*2.1*	*1509.9*	*13.5*
D	*980*	*99.81*	*5.634*	*16.11*	*0.001*	*0.091*	*95.6*	*3.2*	*1661.8*	*7.9*
E	*1010*	*102.2*	*6.813*	*10.04*	*0.001*	*0.075*	*97.6*	*5.2*	*1710.9*	*6.6*
F	1040	104.3	8.096	3.410	0.008	0.063	99.6	21.1	1756.6	2.7
G	1060	104.3	8.244	2.705	0.026	0.062	99.8	71.9	1759.2	2.2
H	*1080*	*98.57*	*7.437*	*5.992*	*0.001*	*0.069*	*98.7*	*74.2*	*1684.5*	*5.8*
I	*1100*	*103.8*	*7.751*	*7.649*	*0.001*	*0.066*	*98.4*	*76.2*	*1737.9*	*5.7*
J	1150	105.2	8.132	3.770	0.004	0.063	99.5	83.1	1765.8	3.5
K	1230	104.3	8.085	4.418	0.008	0.063	99.3	98.8	1754.2	2.7
L	*1580*	*118.0*	*6.038*	*58.29*	*0.001*	*0.085*	*85.8*	*100.0*	*1726.6*	*11.1*
total gas age			n=12		0.051	0.065			1738.9	3.1
plateau		**MSWD=2.44**	n=4	steps F-K	0.046	0.062		89.3	1758.2	2.7*

ID	Temp (°C)	$^{40}Ar/^{39}Ar$	$^{37}Ar/^{39}Ar$	$^{36}Ar/^{39}Ar$ (x 10^{-3})	$^{39}Ar_K$ (x 10^{-15} mol)	K/Ca	$^{40}Ar^*$ (%)	^{39}Ar (%)	Age (Ma)	±1s (Ma)
HUD-98-83, Biotite, 0.78 mg, J=0.0158122, NM-97, Lab#=9616-01										
A	*530*	*59.31*	*0.2182*	*156.0*	*1.51*	*2.3*	*22.2*	*0.6*	*341.8*	*17.4*
B	*600*	*37.17*	*0.2029*	*36.20*	*0.843*	*2.5*	*71.2*	*0.9*	*630.7*	*9.6*
C	*680*	*41.82*	*0.0796*	*8.476*	*8.84*	*6.4*	*94.0*	*4.1*	*871.9*	*1.9*
D	*760*	*98.57*	*0.0247*	*4.879*	*17.2*	*20.7*	*98.5*	*10.4*	*1678.4*	*2.4*
E	830	101.7	0.0267	1.203	24.4	19.1	99.6	19.4	1725.0	2.6
F	900	102.1	0.0209	0.4312	47.9	24.4	99.8	36.9	1731.8	3.5
G	950	103.2	0.0237	0.4038	22.8	21.5	99.9	45.3	1744.7	2.3
H	1010	105.1	0.0343	0.7365	22.7	14.9	99.8	53.6	1763.7	2.5
I	1070	108.0	0.0354	0.5446	25.8	14.4	99.8	63.1	1795.1	2.2
J	1130	105.2	0.0364	0.7464	23.9	14.0	99.8	71.9	1764.7	2.6
K	1230	104.0	0.0307	0.2848	52.2	16.6	99.9	91.0	1753.2	2.6
L	1580	104.3	0.0151	2.613	24.4	33.9	99.2	100.0	1748.6	2.2
total gas age			n=12		272.5	19.4			1707.0	2.3
plateau		MSWD=80.66	n=8	steps E-L	244.1	19.9		89.6	1757.1	15.77*
HUD-98-84, Biotite, 1.10 mg, J=0.0158347, NM-97, Lab#=9617-01										
A	*530*	*58.22*	*0.3325*	*61.04*	*3.85*	*1.5*	*69.0*	*0.9*	*888.4*	*5.9*
B	*600*	*60.06*	*0.1796*	*12.28*	*4.29*	*2.8*	*93.9*	*2.0*	*1151.8*	*4.0*
C	*680*	*97.56*	*0.0572*	*3.688*	*23.9*	*8.9*	*98.9*	*7.7*	*1672.6*	*2.6*
D	*760*	*104.4*	*0.0127*	*0.8453*	*65.1*	*40.0*	*99.7*	*23.4*	*1757.2*	*2.0*
E	830	104.7	0.0079	0.4463	41.6	64.7	99.8	33.4	1761.9	2.5
F	900	104.9	0.0169	0.4547	67.0	30.2	99.8	49.6	1763.6	2.1
G	950	105.3	0.0328	0.6254	42.2	15.6	99.8	59.8	1767.7	2.0
H	1010	105.1	0.0228	0.3322	64.5	22.4	99.9	75.4	1766.6	2.7
I	1070	104.6	0.0407	0.5153	62.4	12.5	99.8	90.4	1760.2	1.8
J	*1130*	*103.6*	*0.3513*	*1.828*	*27.9*	*1.5*	*99.5*	*97.2*	*1745.7*	*2.0*
K	*1230*	*103.5*	*0.4706*	*2.978*	*9.57*	*1.1*	*99.2*	*99.5*	*1741.0*	*3.0*
L	*1580*	*108.5*	*0.1402*	*31.93*	*2.23*	*3.6*	*91.3*	*100.0*	*1701.4*	*7.0*
total gas age			n=12		414.5	25.3			1741.0	1.8
plateau		**MSWD=2.31**	n=5	steps E-I	277.7	27.4		67.0	1763.4	1.94*

ID	Temp (°C)	$^{40}Ar/^{39}Ar$	$^{37}Ar/^{39}Ar$	$^{36}Ar/^{39}Ar$ (x 10^{-3})	$^{39}Ar_K$ (x 10^{-15} mol)	K/Ca	$^{40}Ar^*$ (%)	^{39}Ar (%)	Age (Ma)	±1s (Ma)
HUD-98-85, Biotite, 1.00 mg, J=0.0157894, NM-97, Lab#=9615-01										
A	*530*	*37.99*	*0.2499*	*54.54*	*2.79*	*2.0*	*57.6*	*0.9*	*535.2*	*7.4*
B	*600*	*46.87*	*0.2223*	*20.81*	*0.797*	*2.3*	*86.9*	*1.2*	*895.6*	*10.4*
C	*680*	*73.14*	*0.1469*	*7.811*	*6.35*	*3.5*	*96.8*	*3.3*	*1354.1*	*2.7*
D	*760*	*105.0*	*0.0179*	*2.366*	*30.7*	*28.5*	*99.3*	*13.5*	*1755.5*	*2.1*
E	830	106.3	0.0180	1.107	29.1	28.4	99.7	23.2	1773.8	2.5
F	900	106.0	0.0636	0.6996	39.8	8.0	99.8	36.5	1771.9	1.9
G	950	105.9	0.1157	0.7362	26.5	4.4	99.8	45.3	1770.4	2.5
H	1010	106.6	0.0554	0.3167	49.6	9.2	99.9	61.8	1779.7	2.1
I	1070	105.3	0.0541	0.4849	60.7	9.4	99.8	82.0	1764.9	2.4
J	1130	105.8	0.0519	0.7149	42.8	9.8	99.8	96.2	1769.5	2.9
K	*1230*	*101.2*	*0.4079*	*2.243*	*11.3*	*1.3*	*99.3*	*100.0*	*1715.3*	*2.6*
total gas age			n=11		300.4	12.1			1745.0	2.0
plateau		**MSWD=12.69**	n=6	steps E-J	248.4	10.9		82.7	1772.4	4.06*
HUD-98-86A, Muscovite, 1.40 mg, J=0.0158125, NM-97, Lab#=9611-01										
A	*580*	*51.61*	*0.2164*	*37.30*	*1.85*	*2.4*	*78.6*	*0.3*	*894.3*	*6.2*
B	*630*	*89.56*	*0.2145*	*18.57*	*0.827*	*2.4*	*93.9*	*0.5*	*1525.5*	*9.2*
C	*680*	*102.2*	*0.0413*	*11.71*	*1.89*	*12.4*	*96.6*	*0.9*	*1697.0*	*4.4*
D	730	106.1	0.0097	6.233	2.60	52.5	98.2	1.4	1756.7	3.7
E	770	106.4	0.0075	5.187	4.01	67.9	98.5	2.1	1763.6	3.5
F	810	106.2	0.0037	4.079	14.3	138.3	98.8	4.8	1764.7	2.2
G	850	105.5	0.0018	2.818	28.8	289.7	99.2	10.3	1761.0	2.1
H	890	104.9	0.0010	1.084	64.3	532.5	99.7	22.4	1760.1	2.2
I	930	104.7	0.0007	0.2887	78.7	749.0	99.9	37.3	1760.7	2.5
J	970	104.6	0.0010	0.5474	54.4	505.7	99.8	47.6	1759.0	2.2
K	1010	104.3	0.0010	1.003	30.3	505.5	99.7	53.4	1754.2	2.0
L	1050	104.9	0.0012	0.8205	31.6	441.5	99.7	59.3	1761.4	2.2
M	1090	103.8	0.0007	0.7007	37.4	686.9	99.8	66.4	1749.3	1.9
N	1130	104.6	0.0010	0.7605	41.2	527.4	99.8	74.2	1758.1	2.4
O	1230	104.7	0.0010	0.4875	67.2	497.3	99.8	86.9	1760.3	2.4
P	1580	104.9	0.0020	0.6961	69.1	255.9	99.8	100.0	1761.5	3.4
total gas age			n=16		528.5	490.6			1755.6	2.0
plateau		**MSWD=3.63**	n=13	steps D-P	523.9	494.8		99.1	1758.4	2.49*

ID	Temp (°C)	$^{40}Ar/^{39}Ar$	$^{37}Ar/^{39}Ar$	$^{36}Ar/^{39}Ar$ (x 10^{-3})	$^{39}Ar_K$ (x 10^{-15} mol)	K/Ca	$^{40}Ar^*$ (%)	^{39}Ar (%)	Age (Ma)	±1s (Ma)
HUD-98-87, Biotite, 1.50 mg, J=0.0154999, NM-97, Lab#=9696-01										
A	*530*	*104.8*	*0.6917*	*269.6*	*1.75*	*0.74*	*24.0*	*0.6*	*593.9*	*82.7*
B	*600*	*32.78*	*0.2741*	*23.88*	*2.01*	*1.9*	*78.4*	*1.3*	*605.3*	*17.1*
C	*680*	*29.29*	*0.2891*	*8.116*	*10.7*	*1.8*	*91.8*	*5.1*	*628.6*	*1.8*
D	*760*	*95.87*	*0.8343*	*7.567*	*23.6*	*0.61*	*97.7*	*13.4*	*1618.6*	*3.1*
E	*830*	*104.3*	*0.2428*	*1.252*	*36.1*	*2.1*	*99.6*	*26.1*	*1731.0*	*2.4*
F	900	108.7	0.1511	0.6811	27.1	3.4	99.8	35.7	1780.0	3.5
G	950	110.1	0.1190	0.5505	35.0	4.3	99.8	48.0	1794.2	2.9
H	1010	112.4	0.0674	0.3941	50.1	7.6	99.9	65.7	1818.6	2.0
I	1070	110.7	0.1262	0.3484	44.8	4.0	99.9	81.5	1800.8	2.7
J	1130	108.5	0.1872	0.3291	43.6	2.7	99.9	96.9	1778.9	2.3
K	*1230*	*102.0*	*2.373*	*2.411*	*6.77*	*0.22*	*99.4*	*99.3*	*1706.2*	*2.7*
L	*1580*	*100.6*	*4.952*	*17.19*	*2.05*	*0.10*	*95.3*	*100.0*	*1646.6*	*4.8*
total gas age			n=12		283.6	3.7			1710.4	2.8
plateau		MSWD=52.50	n=5	steps F-J	200.7	4.6		70.8	1800.8	16.30*
HUD-98-87, Hornblende, 1.15 mg, J=0.0155191, NM-97, Lab#=9697-01										
A	730	93.94	7.991	201.0	0.002	0.064	37.4	9.4	788.6	12.7
B	830	72.63	12.39	35.35	0.001	0.041	86.8	14.1	1239.4	7.8
C	930	69.16	11.81	17.59	0.001	0.043	93.7	20.8	1263.5	5.8
D	980	74.56	10.74	12.03	0.001	0.047	96.3	24.9	1357.9	8.1
E	1010	78.72	10.99	14.64	0.001	0.046	95.5	28.6	1402.7	9.3
F	1040	82.47	11.54	14.21	0.000	0.044	95.9	31.2	1453.2	11.2
G	1060	97.72	14.39	5.944	0.003	0.035	99.3	46.5	1668.3	4.0
H	1080	81.93	12.09	11.36	0.001	0.042	97.0	50.7	1458.0	6.7
I	1100	83.37	12.78	8.996	0.000	0.040	97.9	53.0	1485.9	11.1
J	1150	103.3	15.96	7.523	0.002	0.032	99.0	63.2	1727.8	3.9
K	1230	103.3	15.69	6.666	0.006	0.033	99.2	98.3	1729.8	2.8
L	1580	94.35	19.51	70.99	0.000	0.026	79.3	100.0	1403.7	18.7
total gas age			n=12		0.019	0.039			1520.3	5.6
plateau			n=12	steps A-L	0.019	0.039		100.0	1606.3	58.4

ID	Temp (°C)	$^{40}Ar/^{39}Ar$	$^{37}Ar/^{39}Ar$	$^{36}Ar/^{39}Ar$ (x 10^{-3})	$^{39}Ar_K$ (x 10^{-15} mol)	K/Ca	$^{40}Ar^*$ (%)	^{39}Ar (%)	Age (Ma)	±1s (Ma)
HUD-98-88, Biotite, 1.94 mg, J=0.0158345, NM-97, Lab#=9618-01										
A	*530*	*47.13*	*0.0572*	*55.31*	*5.17*	*8.9*	*65.3*	*0.7*	*715.9*	*3.7*
B	*600*	*43.90*	*0.0293*	*7.496*	*5.40*	*17.4*	*94.9*	*1.5*	*914.0*	*2.3*
C	*680*	*85.50*	*0.0093*	*2.662*	*14.9*	*54.7*	*99.0*	*3.6*	*1534.5*	*2.0*
D	*760*	*103.1*	*0.0027*	*0.6618*	*58.4*	*191.9*	*99.8*	*11.8*	*1744.3*	*2.4*
E	830	103.8	0.0019	0.3048	48.9	268.2	99.9	18.7	1752.6	2.2
F	900	104.3	0.0032	0.2807	92.6	159.3	99.9	31.8	1757.5	2.8
G	950	104.1	0.0051	0.1517	60.7	100.6	99.9	40.4	1756.2	2.1
H	1010	104.3	0.0064	0.1447	158.2	79.3	99.9	62.7	1758.6	4.8
I	1070	104.1	0.0109	0.1777	109.2	47.0	99.9	78.1	1756.4	2.2
J	1130	104.2	0.0081	0.2007	114.7	63.3	99.9	94.3	1757.3	2.0
K	*1230*	*100.4*	*0.0813*	*0.3516*	*37.0*	*6.3*	*99.9*	*99.5*	*1715.2*	*2.3*
L	*1580*	*101.3*	*0.1588*	*16.12*	*3.66*	*3.2*	*95.3*	*100.0*	*1673.3*	*4.2*
total gas age			n=12		708.8	100.6			1734.7	2.5
plateau		**MSWD=0.68**	n=6	steps E-J	584.3	100.8		82.4	1756.1	1.60*
HUD-98-88, Muscovite, 1.25 mg, J=0.0158511, NM-97, Lab#=9635-01										
A	*580*	*32.80*	*0.0376*	*37.87*	*11.1*	*13.6*	*65.8*	*2.3*	*530.8*	*2.6*
B	*630*	*45.04*	*0.0257*	*8.694*	*7.31*	*19.9*	*94.2*	*3.9*	*928.2*	*1.9*
C	*680*	*80.08*	*0.0139*	*5.644*	*12.3*	*36.7*	*97.9*	*6.4*	*1456.9*	*2.2*
D	*730*	*89.60*	*0.0103*	*4.639*	*8.53*	*49.5*	*98.4*	*8.2*	*1578.0*	*2.3*
E	*770*	*96.18*	*0.0101*	*1.869*	*6.59*	*50.4*	*99.4*	*9.6*	*1664.1*	*2.5*
F	*810*	*99.89*	*0.0078*	*1.654*	*24.1*	*65.5*	*99.5*	*14.6*	*1706.5*	*2.3*
G	*850*	*102.1*	*0.0041*	*0.7661*	*44.6*	*125.6*	*99.8*	*24.0*	*1734.0*	*2.1*
H	890	103.6	0.0027	0.3564	83.8	191.2	99.9	41.5	1751.1	2.0
I	930	103.1	0.0042	0.3599	52.4	121.1	99.9	52.5	1745.7	2.9
J	970	102.8	0.0094	0.4020	28.9	54.3	99.9	58.6	1742.9	2.5
K	1010	102.5	0.0197	0.8262	24.7	25.9	99.7	63.7	1737.8	2.4
L	1050	100.6	0.0263	0.7948	25.8	19.4	99.7	69.1	1717.0	1.9
M	1090	100.2	0.0150	0.7667	28.9	34.1	99.7	75.2	1713.4	3.5
N	1130	101.6	0.0101	0.5263	35.8	50.7	99.8	82.7	1728.7	1.8
O	1230	102.2	0.0148	0.3473	61.7	34.4	99.9	95.6	1736.4	2.0
P	1580	104.0	0.1095	2.594	21.1	4.7	99.2	100.0	1748.8	2.5
total gas age			n=16		477.5	81.2			1684.9	1.9
plateau		**MSWD=33.19**	n=9	steps H-P	363.0	82.9		76.0	1734.7	8.57*

ID	Temp (°C)	$^{40}Ar/^{39}Ar$	$^{37}Ar/^{39}Ar$	$^{36}Ar/^{39}Ar$ (x 10^{-3})	$^{39}Ar_K$ (x 10^{-15} mol)	K/Ca	$^{40}Ar^*$ (%)	^{39}Ar (%)	Age (Ma)	±1s (Ma)
HUD-98-89, Biotite, 1.70 mg, J=0.0158117, NM-97, Lab#=9613-01										
A	*530*	*39.34*	*0.4450*	*68.61*	*1.20*	*1.1*	*48.5*	*0.2*	*475.7*	*11.4*
B	*600*	*53.60*	*0.4134*	*32.78*	*0.573*	*1.2*	*81.9*	*0.3*	*951.5*	*12.3*
C	*680*	*66.78*	*0.2793*	*15.46*	*2.59*	*1.8*	*93.1*	*0.8*	*1235.7*	*4.1*
D	760	104.7	0.0054	3.962	29.2	95.2	98.9	6.2	1749.2	5.1
E	830	104.9	0.0011	0.7801	38.2	444.1	99.8	13.3	1761.1	2.7
F	900	104.2	0.0010	0.6446	79.4	491.7	99.8	28.1	1754.7	2.7
G	950	105.0	0.0009	0.2008	56.1	540.1	99.9	38.5	1763.7	2.8
H	1010	105.0	0.0013	0.2758	52.0	382.4	99.9	48.1	1763.8	2.4
I	1070	105.3	0.0008	0.2173	85.4	656.7	99.9	64.0	1767.3	4.7
J	1130	104.6	0.0012	0.4028	103.6	436.1	99.9	83.2	1758.9	1.8
K	1230	104.9	0.0011	0.2914	81.6	480.4	99.9	98.4	1762.9	1.8
L	*1580*	*105.9*	*0.0096*	*7.461*	*8.81*	*53.1*	*97.9*	*100.0*	*1751.3*	*3.0*
total gas age			n=12		538.6	464.0			1754.5	2.5
plateau		**MSWD=2.50**	n=8	steps D-K	525.4	474.7		97.6	1760.9	2.81*
HUD-98-90, 2.90 mg biotite, J=0.0157938, NM-97, Lab#=9607-01										
A	*530*	*46.95*	*0.1994*	*46.38*	*1.93*	*2.6*	*70.8*	*0.5*	*761.2*	*6.0*
B	*600*	*54.47*	*0.0687*	*5.547*	*4.64*	*7.4*	*96.9*	*1.7*	*1094.3*	*2.7*
C	*680*	*90.72*	*0.0690*	*3.195*	*5.08*	*7.4*	*98.9*	*2.9*	*1592.6*	*2.7*
D	760	103.7	0.1024	0.7045	48.6	5.0	99.8	15.2	1747.1	2.7
E	830	104.5	0.0056	0.3608	33.5	90.9	99.9	23.7	1756.8	2.4
F	900	104.9	0.0114	0.1686	63.4	44.7	99.9	39.8	1761.5	2.2
G	950	104.4	0.0331	0.2947	30.0	15.4	99.9	47.3	1756.4	1.9
H	1010	105.3	0.1490	0.2240	52.6	3.4	99.9	60.6	1766.0	2.1
I	1070	104.7	0.2497	0.2594	79.1	2.0	99.9	80.7	1760.2	1.9
J	1130	103.6	0.0566	0.3535	48.3	9.0	99.9	92.9	1747.0	2.0
K	1230	103.2	0.1685	0.6053	23.0	3.0	99.8	98.7	1742.5	2.2
L	1580	104.2	0.1473	6.183	5.12	3.5	98.2	100.0	1735.7	3.1
total gas age			n=12		395.3	19.0			1741.2	1.7
plateau		MSWD=17.66	n=9	steps D-L	383.6	19.4		97.1	1754.6	6.13*

ID	$^{40}Ar/^{39}Ar$	$^{37}Ar/^{39}Ar$	$^{36}Ar/^{39}Ar$ (x 10^{-3})	$^{39}Ar_K$ (x 10^{-15} mol)	K/Ca	$\%^{40}Ar^*$	Age (Ma)	±1s (Ma)
HUD98-86A, NM-97, biotite, CO2 laser, J=0.01595, NM-97, Lab#=9704								
168	148.3	0.0000	23765.8	0.032	-	%-4636.2	0.0	195.4
171	94.04	0.0000	10.19	0.222	-	96.8	1617.7	5.3
152	101.4	0.0000	1.199	0.780	-	99.6	1731.9	3.5
178	102.8	181.2	5.940	0.281	0.003	98.3	1732.0	5.5
155	102.9	0.0000	5.025	0.342	-	98.5	1735.7	4.7
174	103.6	0.0000	6.468	0.218	-	98.1	1738.3	5.6
160	104.5	72.98	9.614	0.285	0.007	97.3	1738.4	5.3
183	105.9	34.43	13.73	0.752	0.015	96.1	1740.3	2.9
151	103.2	0.0000	3.807	0.404	-	98.9	1743.0	4.3
187	102.9	67.38	2.039	0.512	0.008	99.4	1744.9	3.2
182	102.7	38.64	1.373	0.932	0.013	99.6	1745.3	2.9
156	103.5	0.0000	3.904	0.662	-	98.9	1746.0	3.3
172	103.2	0.0000	2.683	1.28	-	99.2	1746.1	2.6
180	102.8	21.94	1.370	0.857	0.023	99.6	1746.4	2.8
154	103.0	45.48	1.985	0.834	0.011	99.4	1746.4	3.4
184	103.3	0.0000	2.516	0.314	-	99.3	1748.3	4.6
159	104.7	0.0000	6.911	0.071	-	98.0	1748.9	13.8
173	104.0	8.642	4.603	0.788	0.059	98.7	1749.0	3.1
164	103.3	36.00	1.959	0.940	0.014	99.4	1750.2	2.8
167	103.5	0.0000	2.084	1.42	-	99.4	1752.0	2.7
157	104.8	0.0000	6.227	0.415	-	98.2	1752.5	4.8
161	103.9	20.91	2.928	0.714	0.024	99.1	1752.9	3.1
181	103.5	69.15	1.387	0.237	0.007	99.6	1753.6	5.3
166	103.6	35.68	1.757	1.10	0.014	99.5	1753.8	2.6
185	103.8	74.60	2.245	0.255	0.007	99.3	1754.3	6.1
186	104.1	93.59	3.031	0.199	0.005	99.1	1755.4	6.0
162	104.2	115.5	3.136	0.560	0.004	99.1	1755.7	3.7
176	104.3	33.79	3.464	1.13	0.015	99.0	1755.9	2.5

ID	$^{40}Ar/^{39}Ar$	$^{37}Ar/^{39}Ar$	$^{36}Ar/^{39}Ar$ (x 10^{-3})	$^{39}Ar_K$ (x 10^{-15} mol)	K/Ca	% $^{40}Ar^*$	Age (Ma)	±1s (Ma)
177	104.4	78.93	3.097	0.856	0.006	99.1	1757.9	2.8
150	105.9	0.0000	8.087	0.127	-	97.7	1758.3	10.2
175	104.9	60.62	4.252	0.414	0.008	98.8	1759.5	4.3
158	105.1	0.0000	5.084	0.241	-	98.5	1759.7	5.6
179	105.7	75.21	6.941	0.417	0.007	98.0	1760.1	4.0
165	104.5	0.0000	2.444	0.647	-	99.3	1761.4	2.7
163	104.8	0.0000	3.118	0.654	-	99.1	1762.3	2.9
170	104.4	0.0000	1.002	0.483	-	99.7	1765.2	3.6
169	104.7	0.0000	0.4102	0.310	-	99.9	1770.4	4.9
153	1017.7	8548.7	2215.6	0.003	0.000	35.7	3455.4	612.6
weighted mean ± Taylor err			n=38		0.013 ±0.009		1748.7	5.7

ID	$^{40}Ar/^{39}Ar$	$^{37}Ar/^{39}Ar$	$^{36}Ar/^{39}Ar$ (x 10^{-3})	$^{39}Ar_K$ (x 10^{-15} mol)	K/Ca	$\%^{40}Ar^*$	Age (Ma)	±1s (Ma)
HUD98-86A, muscovite, CO2 laser, J=0.0158125, NM-97, Lab#=9611								
166	221.0	179922.4	938.6	0.000	0.000	-25.5	-4005.5	189471.9
170	118.7	68564.1	422.0	0.001	0.000	-5.1	-181.5	3557.9
157	103.2	22.27	0.8876	1.12	0.023	99.7	1742.4	2.7
153	103.6	0.0000	2.043	0.945	-	99.4	1743.8	2.6
151	103.6	0.0000	1.646	0.401	-	99.5	1744.3	4.2
176	103.4	0.0000	0.8924	0.796	-	99.7	1744.4	2.7
175	103.8	16.57	2.216	0.752	0.031	99.3	1744.6	3.0
156	103.6	62.16	1.433	1.14	0.008	99.6	1745.7	2.7
154	104.2	67.58	3.227	0.898	0.008	99.1	1746.3	3.0
165	104.3	25.92	3.137	3.32	0.020	99.1	1747.1	2.5
181	103.8	46.35	1.540	1.05	0.011	99.5	1747.3	2.5
163	103.8	53.61	1.576	0.923	0.010	99.5	1747.4	2.7
161	104.1	0.0000	2.071	1.25	-	99.4	1748.6	2.8
177	103.7	2.526	0.8071	15.6	0.20	99.7	1748.7	2.4
158	103.8	0.0000	0.8159	1.11	-	99.7	1749.4	2.8
178	104.2	38.04	1.885	2.26	0.013	99.4	1749.9	2.5
172	104.1	0.0000	1.582	0.745	-	99.5	1750.7	3.1
179	104.5	0.0000	2.556	0.482	-	99.2	1751.4	4.5
162	104.6	8.401	2.635	1.94	0.061	99.2	1752.1	2.2
159	104.4	0.0000	1.603	0.803	-	99.5	1753.4	2.9
155	104.6	22.73	2.133	0.821	0.022	99.4	1753.5	2.6
169	104.2	11.78	0.6441	3.28	0.043	99.8	1753.7	2.5
152	104.5	0.0000	1.730	2.78	-	99.5	1754.2	2.2
180	104.4	10.81	1.275	3.39	0.047	99.6	1754.2	1.9
174	105.0	4.168	3.318	0.992	0.12	99.0	1754.3	2.9
164	104.8	39.54	2.692	0.635	0.013	99.2	1754.5	3.1
167	104.4	0.0000	1.066	1.35	-	99.7	1754.7	2.6

ID	$^{40}Ar/^{39}Ar$	$^{37}Ar/^{39}Ar$	$^{36}Ar/^{39}Ar$ (x 10^{-3})	$^{39}Ar_K$ (x 10^{-15} mol)	K/Ca	$\%^{40}Ar^*$	Age (Ma)	±1s (Ma)
171	105.0	2.917	2.856	1.65	0.17	99.2	1755.9	2.5
173	104.7	27.67	1.612	1.44	0.018	99.5	1756.8	2.4
160	104.8	0.0000	1.480	0.470	-	99.6	1758.2	3.4
150	105.6	0.0000	3.317	0.486	-	99.0	1760.6	3.5
168	108.4	1012.4	-19.1009	0.016	0.001	105.2	1858.9	45.9
weighted mean ± Taylor err			n=32		0.041 ±0.046		1751.4	1.6

ID	Temp	$^{40}Ar/^{39}Ar$	$^{37}Ar/^{39}Ar$	$^{36}Ar/^{39}Ar$	$^{39}Ar_K$	K/Ca	$^{40}Ar^*$	^{39}Ar	Age	±1σ
	(°C)			(x 10^{-3})	(x 10^{-15} mol)		(%)	(%)	(Ma)	(Ma)
HUD 98-86A, Biotite large crystal UV, J=0.01595±0.10%, NM-97, Lab#=9704-01										
1	0	108.2	0.0039	13.97	0.169	130.0	96.2	0.3	1764.5	11.3
2	0	137.6	0.0822	138.1	0.234	6.2	70.3	0.8	1683.6	11.9
3	0	104.7	0.0224	15.26	0.308	22.8	95.7	1.3	1722.1	5.9
4	0	101.7	0.0178	16.62	0.373	28.6	95.1	2.0	1683.9	6.4
5	0	101.3	0.0059	6.778	0.553	86.8	98.0	3.1	1712.0	5.1
6	0	102.6	0.0109	13.65	0.564	46.7	96.0	4.1	1704.5	4.6
7	0	100.00	0.0250	16.13	0.606	20.4	95.2	5.2	1666.3	4.4
9	0	92.50	0.0109	-17.8394	0.613	46.9	105.7	6.4	1695.1	4.5
10	0	96.29	0.0153	-9.1821	0.593	33.4	102.8	7.5	1709.0	5.0
11	0	103.0	0.0316	2.006	0.530	16.1	99.4	8.5	1747.1	4.8
12	0	106.4	0.0321	11.60	0.535	15.9	96.8	9.5	1753.0	5.5
13	0	102.9	0.0226	6.087	0.529	22.6	98.2	10.5	1732.3	4.0
14	0	109.7	0.0364	24.75	0.520	14.0	93.3	11.4	1746.1	5.2
15	0	110.2	0.0321	25.73	0.768	15.9	93.1	12.9	1748.1	4.9
16	0	106.1	0.0524	14.87	0.671	9.7	95.8	14.1	1738.4	4.9
17	0	107.0	0.0362	16.27	0.624	14.1	95.5	15.3	1743.9	4.6
18	0	106.0	0.0444	14.65	0.635	11.5	95.9	16.5	1738.2	5.1
19	0	106.0	0.0000	12.83	0.549	-	96.4	17.5	1744.5	5.0
20	0	104.1	0.0000	9.798	0.531	-	97.2	18.5	1733.7	5.4
21	0	104.2	0.0000	12.72	0.492	-	96.4	19.4	1725.4	6.0
22	0	104.5	0.0008	7.007	0.776	604.6	98.0	20.9	1746.3	4.2
23	0	104.8	0.0046	10.14	0.734	110.8	97.1	22.3	1739.5	4.5
24	0	145.8	0.0000	152.3	0.694	-	69.1	23.6	1728.6	8.4
25	0	104.5	0.0000	8.806	0.698	-	97.5	24.9	1740.8	4.7
26	0	104.6	0.0000	3.863	0.637	-	98.9	26.0	1757.7	5.0
27	0	107.6	0.0118	14.62	0.537	43.1	96.0	27.0	1755.9	5.4
28	0	106.7	0.0000	11.17	0.619	-	96.9	28.2	1757.6	5.3
29	0	108.1	0.0046	15.55	0.656	112.1	95.7	29.4	1758.5	4.3

ID	Temp (°C)	$^{40}Ar/^{39}Ar$	$^{37}Ar/^{39}Ar$	$^{36}Ar/^{39}Ar$ (x 10^{-3})	$^{39}Ar_K$ (x 10^{-15} mol)	K/Ca	$^{40}Ar^*$ (%)	^{39}Ar (%)	Age (Ma)	±1σ (Ma)
30	0	108.3	0.0004	15.41	0.628	1190.6	95.8	30.6	1760.7	5.0
31	0	105.6	0.0411	8.939	0.647	12.4	97.5	31.8	1752.2	4.6
32	0	115.1	0.0450	41.84	0.656	11.3	89.2	33.0	1750.4	5.8
33	0	106.4	0.0208	10.39	0.681	24.5	97.1	34.3	1756.6	5.3
40	0	102.0	1.606	14.66	0.485	0.32	95.7	35.2	1688.7	9.2
41	0	100.5	1.504	9.989	0.434	0.34	97.0	36.0	1686.7	8.7
42	0	101.9	2.505	11.42	0.471	0.20	96.7	36.9	1698.6	7.8
43	0	103.7	0.4741	11.84	0.407	1.1	96.6	37.7	1715.8	8.5
44	0	99.02	0.0000	-3.9619	0.346	-	101.2	38.3	1715.1	9.3
45	0	101.2	1.243	3.391	0.380	0.41	99.0	39.0	1715.8	7.3
46	0	101.1	0.0000	7.925	0.376	-	97.7	39.7	1698.8	7.5
47	0	101.7	0.0000	5.438	0.356	-	98.4	40.4	1713.9	7.3
48	0	102.7	0.6841	21.11	0.323	0.75	93.9	41.0	1674.3	9.7
49	0	101.0	0.0000	6.357	0.310	-	98.1	41.6	1702.9	10.1
50	0	99.56	0.0000	3.825	0.306	-	98.8	42.1	1695.6	8.2
51	0	102.7	0.0000	9.144	0.327	-	97.3	42.8	1712.8	8.4
52	0	101.0	1.134	1.596	0.326	0.45	99.5	43.4	1719.9	9.8
53	0	104.0	0.0000	13.42	0.303	-	96.2	43.9	1713.4	9.5
54	0	101.5	0.0000	5.498	0.281	-	98.4	44.5	1711.7	9.4
55	0	102.5	0.0000	15.13	0.329	-	95.6	45.1	1698.2	8.9
56	0	102.4	0.0000	7.685	0.483	-	97.8	46.0	1721.7	6.7
57	0	100.3	0.0000	8.206	0.489	-	97.6	46.9	1696.6	8.3
58	0	100.8	0.0000	3.741	0.531	-	98.9	47.9	1716.5	6.6
59	0	102.0	0.0000	6.430	0.491	-	98.1	48.8	1720.9	7.1
60	0	100.8	0.0000	1.616	0.489	-	99.5	49.7	1723.9	7.8
61	0	106.5	0.0000	16.48	0.530	-	95.4	50.7	1737.6	6.9
62	0	100.1	0.3537	5.350	0.456	1.4	98.4	51.6	1703.2	7.7
63	0	100.9	0.0000	0.2281	0.475	-	99.9	52.4	1729.7	7.5
64	0	99.90	0.0000	4.800	0.493	-	98.6	53.4	1703.1	7.8

ID	Temp (°C)	$^{40}Ar/^{39}Ar$	$^{37}Ar/^{39}Ar$	$^{36}Ar/^{39}Ar$ (x 10^{-3})	$^{39}Ar_K$ (x 10^{-15} mol)	K/Ca	$^{40}Ar^*$ (%)	^{39}Ar (%)	Age (Ma)	±1σ (Ma)
65	0	103.2	1.500	2.921	0.458	0.34	99.1	54.2	1747.1	9.5
66	0	123.2	3.709	76.98	1.09	0.14	81.5	56.3	1722.0	5.4
67	0	153.5	2.675	176.6	1.11	0.19	66.0	58.3	1731.4	8.4
68	0	115.8	3.237	54.04	1.11	0.16	86.2	60.4	1714.6	5.1
69	0	117.3	2.843	58.14	1.37	0.18	85.3	62.9	1718.2	5.5
70	0	103.9	2.482	8.179	1.30	0.21	97.6	65.4	1732.2	4.0
71	0	114.1	0.1988	41.06	1.02	2.6	89.3	67.3	1735.7	5.7
72	0	110.1	2.179	37.32	1.31	0.23	90.0	69.7	1707.6	4.4
73	0	128.5	0.6832	98.33	1.29	0.75	77.4	72.1	1710.6	6.2
74	0	101.9	3.383	13.20	1.40	0.15	96.1	74.8	1695.8	4.7
75	0	105.2	4.293	13.32	0.933	0.12	96.2	76.5	1732.9	4.7
76	0	108.7	2.801	23.51	1.19	0.18	93.6	78.7	1737.4	5.1
77	0	102.4	1.583	4.223	1.11	0.32	98.8	80.8	1729.4	4.4
78	0	102.3	4.107	8.471	1.14	0.12	97.5	82.9	1717.1	4.4
79	0	100.3	0.7791	1.185	0.729	0.65	99.6	84.3	1718.1	5.6
80	0	97.42	0.1394	8.258	1.22	3.7	97.5	86.6	1661.5	3.9
81	0	102.9	0.0000	3.900	0.670	-	98.9	87.8	1736.7	5.8
82	0	102.4	0.0000	3.047	0.690	-	99.1	89.1	1734.3	5.9
83	0	102.3	0.0000	1.287	0.676	-	99.6	90.4	1739.1	5.0
84	0	136.4	0.0000	116.4	0.670	-	74.8	91.6	1740.4	9.7
85	0	107.2	0.0000	23.57	0.612	-	93.5	92.8	1720.4	6.7
86	0	104.4	3.710	6.560	0.641	0.14	98.1	94.0	1747.9	6.6
87	0	100.9	3.359	7.489	0.670	0.15	97.8	95.2	1706.0	6.0
89	0	101.1	0.0000	7.726	0.556	-	97.7	96.2	1705.3	7.4
90	0	102.0	0.0000	-0.0840	0.539	-	100.0	97.3	1740.1	6.3
91	0	101.5	0.5958	1.668	0.660	0.86	99.5	98.5	1729.8	5.1
95	0	102.1	0.5298	1.453	0.808	0.96	99.6	100.0	1736.6	3.9

ID	Temp (°C)	$^{40}Ar/^{39}Ar$	$^{37}Ar/^{39}Ar$	$^{36}Ar/^{39}Ar$ (x 10^{-3})	$^{39}Ar_K$ (x 10^{-15} mol)	K/Ca	$^{40}Ar^*$ (%)	^{39}Ar (%)	Age (Ma)	±1σ (Ma)
HUD98-86a, muscovite large srystal UV, J=0.01595±0.10%, NM-97, Lab#=9703-01										
1	0	100.5	4.659	25.06	0.208	0.11	92.6	0.5	1645.1	11.8
2	0	103.2	2.835	15.85	0.314	0.18	95.4	1.2	1705.3	8.6
3	0	102.8	1.054	12.20	0.331	0.48	96.5	1.9	1712.1	8.6
4	0	102.0	2.950	7.525	0.383	0.17	97.8	2.8	1720.3	8.1
5	0	104.0	0.2121	-1.2508	0.398	2.4	100.3	3.7	1767.7	7.5
6	0	101.1	0.2071	-3.2681	0.423	2.5	100.9	4.7	1743.4	7.8
7	0	156.0	0.0000	184.6	0.399	-	65.0	5.6	1736.2	15.5
8	0	100.6	0.6539	-1.2143	0.405	0.78	100.3	6.5	1731.7	8.7
9	0	259.3	1.919	548.4	0.419	0.27	37.5	7.4	1691.2	23.8
10	0	101.7	1.007	-0.7090	0.444	0.51	100.2	8.4	1742.0	7.7
11	0	100.9	3.775	1.798	0.482	0.14	99.4	9.5	1726.6	7.5
12	0	102.9	1.921	-1.1221	0.451	0.27	100.3	10.5	1756.5	7.3
13	0	101.8	0.5367	-0.0521	0.479	0.95	100.0	11.6	1740.7	6.1
14	0	101.7	1.395	-0.0349	0.503	0.37	100.0	12.8	1739.5	6.3
15	0	106.9	1.308	19.98	0.497	0.39	94.5	13.9	1732.3	7.2
16	0	105.5	2.025	9.167	0.474	0.25	97.4	15.0	1752.4	6.9
17	0	102.1	3.780	1.579	0.449	0.13	99.5	16.0	1740.6	7.1
18	0	103.5	1.607	4.279	0.463	0.32	98.8	17.0	1746.1	6.6
19	0	102.8	5.919	10.69	0.282	0.086	96.9	17.7	1721.1	9.6
20	0	111.2	1.120	35.67	0.332	0.46	90.5	18.4	1728.4	8.8
21	0	100.4	4.757	6.657	0.379	0.11	98.0	19.3	1705.8	24.4
22	0	102.5	0.5207	3.474	0.332	0.98	99.0	20.0	1736.6	7.9
23	0	103.2	0.0000	-0.1830	0.296	-	100.0	20.7	1755.7	10.0
24	0	100.7	0.8039	-4.5839	0.327	0.63	101.3	21.4	1743.8	8.6
25	0	99.44	0.0000	-4.6690	0.153	-	101.4	21.8	1729.0	15.5
26	0	103.7	0.0000	7.479	0.204	-	97.8	22.3	1736.1	12.8
27	0	94.93	0.0000	9.855	0.186	-	96.9	22.7	1629.3	35.8
28	0	102.3	0.0000	0.5156	0.179	-	99.8	23.1	1743.8	20.3

ID	Temp (°C)	$^{40}Ar/^{39}Ar$	$^{37}Ar/^{39}Ar$	$^{36}Ar/^{39}Ar$ (x 10^{-3})	$^{39}Ar_K$ (x 10^{-15} mol)	K/Ca	$^{40}Ar^*$ (%)	^{39}Ar (%)	Age (Ma)	±1σ (Ma)
29	0	117.3	0.0000	71.58	0.005	-	81.9	23.1	1676.9	323.5
30	0	84.75	0.0000	-8.8607	0.185	-	103.1	23.5	1574.1	112.0
31	0	104.7	0.0000	8.128	0.354	-	97.7	24.3	1745.4	10.1
32	0	104.9	0.0000	13.54	0.407	-	96.2	25.2	1730.1	8.2
33	0	100.8	0.0530	3.214	0.358	9.6	99.0	26.0	1718.0	7.7
34	0	103.5	0.4939	3.325	0.432	1.0	99.0	27.0	1748.2	6.9
35	0	102.7	2.361	0.0433	0.367	0.22	100.0	27.9	1751.4	8.4
36	0	103.0	3.339	12.38	0.341	0.15	96.4	28.6	1714.8	9.0
37	0	102.7	4.912	9.065	0.292	0.10	97.4	29.3	1724.0	9.7
38	0	112.9	0.0000	37.63	0.338	-	90.1	30.1	1739.6	9.3
39	0	102.8	0.9543	3.908	0.320	0.53	98.8	30.8	1738.7	8.1
40	0	100.9	0.0000	-0.1073	0.383	-	100.0	31.6	1729.9	6.6
41A	0	103.4	0.0000	-0.0144	0.583	-	100.0	33.0	1757.7	6.2
43	0	109.1	0.0000	27.45	0.406	-	92.5	33.9	1731.5	7.7
44	0	101.3	0.0000	2.000	0.502	-	99.4	35.0	1728.1	7.0
45	0	102.6	0.0000	2.268	0.527	-	99.3	36.2	1740.9	6.4
46	0	98.32	1.821	1.337	0.506	0.28	99.6	37.4	1698.3	5.9
47	0	102.9	2.576	6.933	0.557	0.20	98.0	38.6	1731.9	6.1
48	0	106.6	1.508	15.82	0.515	0.34	95.6	39.8	1742.7	7.1
49	0	103.0	1.887	4.807	0.518	0.27	98.6	41.0	1739.4	6.2
50	0	101.7	0.0000	-0.8968	0.483	-	100.2	42.1	1741.4	6.6
51	0	118.7	0.0000	-0.0776	0.518	-	100.0	43.2	1916.6	6.4
52A	0	103.9	0.2793	8.179	0.416	1.8	97.6	44.2	1736.4	7.5
53	0	112.1	0.0000	8.316	0.510	-	97.8	45.3	1823.7	8.9
54	0	107.0	0.0000	4.687	0.485	-	98.7	46.4	1781.4	6.7
55	0	108.2	1.216	2.088	0.471	0.42	99.4	47.5	1803.7	5.9
56	0	105.5	0.0000	14.54	0.516	-	95.9	48.7	1733.7	6.6
57	0	102.3	0.1457	2.489	0.525	3.5	99.3	49.9	1737.1	6.4
58	0	102.3	3.091	2.668	0.474	0.17	99.2	50.9	1739.7	5.6

ID	Temp (°C)	$^{40}Ar/^{39}Ar$	$^{37}Ar/^{39}Ar$	$^{36}Ar/^{39}Ar$ (x 10^{-3})	$^{39}Ar_K$ (x 10^{-15} mol)	K/Ca	$^{40}Ar^*$ (%)	^{39}Ar (%)	Age (Ma)	±1σ (Ma)
59	0	108.6	0.0000	15.77	0.449	-	95.7	51.9	1763.2	6.6
60	0	103.2	0.0000	1.785	0.489	-	99.5	53.1	1749.3	6.7
61	0	102.6	0.6375	0.1862	0.512	0.80	99.9	54.2	1749.1	6.1
62	0	101.7	0.0000	1.773	0.326	-	99.5	55.0	1733.0	8.1
63	0	116.4	0.0000	50.31	0.348	-	87.2	55.7	1737.4	10.5
64	0	105.1	0.0000	6.061	0.403	-	98.3	56.6	1755.9	8.0
65	0	103.8	0.0000	-3.1383	0.462	-	100.9	57.7	1772.0	7.4
66	0	103.5	0.0000	3.717	0.485	-	98.9	58.8	1746.2	6.2
67	0	101.6	3.223	1.277	0.386	0.16	99.6	59.7	1735.6	7.7
68	0	101.5	4.410	3.889	0.442	0.12	98.8	60.7	1727.3	7.0
69	0	101.7	2.016	0.1301	0.473	0.25	99.9	61.7	1739.4	6.7
70	0	102.0	2.996	1.197	0.517	0.17	99.6	62.9	1740.2	5.9
71	0	99.29	0.0000	3.005	0.451	-	99.1	63.9	1702.2	7.8
72	0	106.9	0.0000	12.91	0.514	-	96.4	65.1	1753.9	7.4
73	0	103.3	0.0000	5.617	0.474	-	98.4	66.2	1738.0	8.3
74	0	383.8	0.0000	957.0	0.519	-	26.3	67.3	1731.5	37.0
75	0	103.3	2.182	2.124	0.455	0.23	99.4	68.4	1751.4	6.8
76	0	104.0	0.6451	4.087	0.471	0.79	98.8	69.4	1751.4	6.9
77	0	103.2	0.3316	5.131	0.486	1.5	98.5	70.5	1738.3	7.6
78B	0	102.8	0.0000	18.83	0.481	-	94.6	71.6	1689.4	7.1
79B	0	101.2	1.621	1.763	0.417	0.31	99.5	72.6	1729.3	8.0
80A	0	101.9	0.0000	2.093	0.429	-	99.4	73.5	1734.4	7.0
81A	0	102.4	0.0993	2.454	0.420	5.1	99.3	74.5	1739.1	7.6
82A	0	102.2	4.457	0.9245	0.615	0.11	99.7	75.9	1744.4	9.9
83A	0	103.5	2.922	0.7714	0.649	0.17	99.8	77.4	1758.2	9.1
84A	0	102.5	2.953	4.620	0.646	0.17	98.6	78.8	1735.2	10.2
85A	0	102.2	4.593	0.0829	0.630	0.11	99.9	80.3	1747.5	9.5
86A	0	103.3	0.9179	0.9748	0.656	0.56	99.7	81.7	1754.3	9.2
87A	0	104.5	0.0000	8.574	0.351	-	97.5	82.5	1742.2	11.8

ID	Temp (°C)	$^{40}Ar/^{39}Ar$	$^{37}Ar/^{39}Ar$	$^{36}Ar/^{39}Ar$ (x 10^{-3})	$^{39}Ar_K$ (x 10^{-15} mol)	K/Ca	$^{40}Ar^*$ (%)	^{39}Ar (%)	Age (Ma)	±1σ (Ma)
88A	0	102.3	6.708	7.355	0.557	0.076	97.8	83.8	1726.6	7.2
89A	0	104.3	1.471	14.43	0.535	0.35	95.9	85.0	1721.8	8.7
90	0	105.5	3.313	14.08	0.636	0.15	96.0	86.4	1737.8	5.7
91	0	105.9	0.0000	4.854	0.427	-	98.6	87.4	1769.2	9.0
92	0	100.6	0.0000	4.231	0.510	-	98.7	88.6	1712.3	8.4
93	0	103.3	0.7337	7.273	0.557	0.70	97.9	89.8	1733.7	5.6
94	0	102.8	0.0000	10.42	0.495	-	97.0	91.0	1716.7	7.3
95	0	103.6	0.7289	5.328	0.454	0.70	98.5	92.0	1742.6	9.9
96	0	103.0	2.549	1.086	0.552	0.20	99.7	93.2	1751.8	7.0
97	0	115.1	8.279	43.96	0.184	0.062	88.7	93.6	1749.3	9.3
98	0	102.7	6.639	6.170	0.242	0.077	98.2	94.2	1734.4	6.4
99	0	105.9	8.861	17.20	0.220	0.058	95.2	94.7	1735.9	7.5
100	0	101.1	6.942	4.547	0.253	0.073	98.6	95.3	1722.4	6.3
101	0	104.0	0.0000	1.141	0.306	-	99.6	96.0	1759.8	5.0
102	0	172.5	2.666	237.8	0.280	0.19	59.2	96.6	1746.3	11.7
103	0	102.8	1.152	3.395	0.253	0.44	99.0	97.2	1740.6	5.8
104	0	117.8	1.394	56.85	0.207	0.37	85.7	97.6	1732.1	8.3
105	0	105.0	0.2783	12.83	0.261	1.8	96.4	98.2	1734.1	6.8
106	0	104.6	0.0000	11.18	0.376	-	96.8	99.1	1734.4	4.7
107	0	103.2	0.0000	9.340	0.407	-	97.3	100.0	1724.9	4.8

Appendix B

Explanation of Appendix B

The following section contains plots that graphically display the data for the resistance step-heated micas and amphiboles. Each spectra consists of the age of the individual heating steps plotted against the total $\%^{39}Ar$ released. The double headed arrow shows steps that were used in calculating a plateau or preferred age. Each plot is also accompanied by the K/Ca for the individual heating steps.

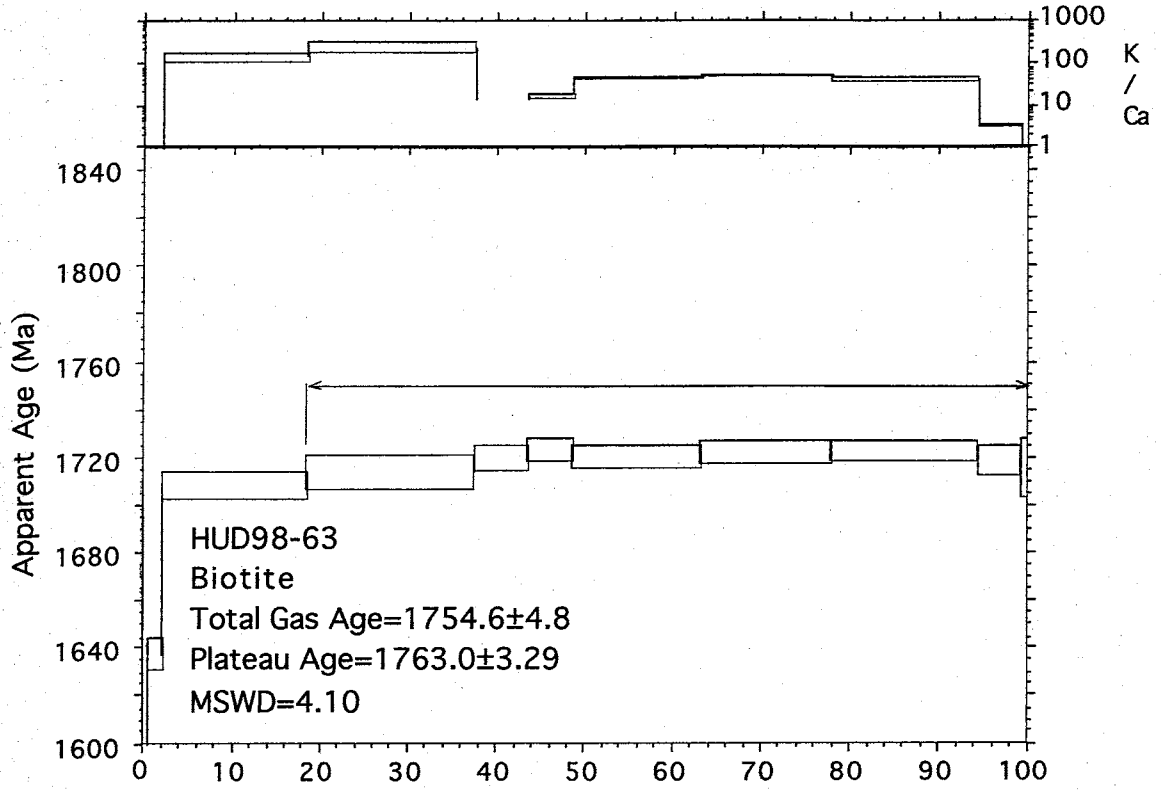
1000
100
10
1
K
/
Ca
1840
1800
1760
1720
1680
1640
1600
Apparent Age (Ma)
HUD98-63
Biotite
Total Gas Age=1754.6±4.8
Plateau Age=1763.0±3.29
MSWD=4.10
0
10
20
30
40
50
60
70
80
90
100

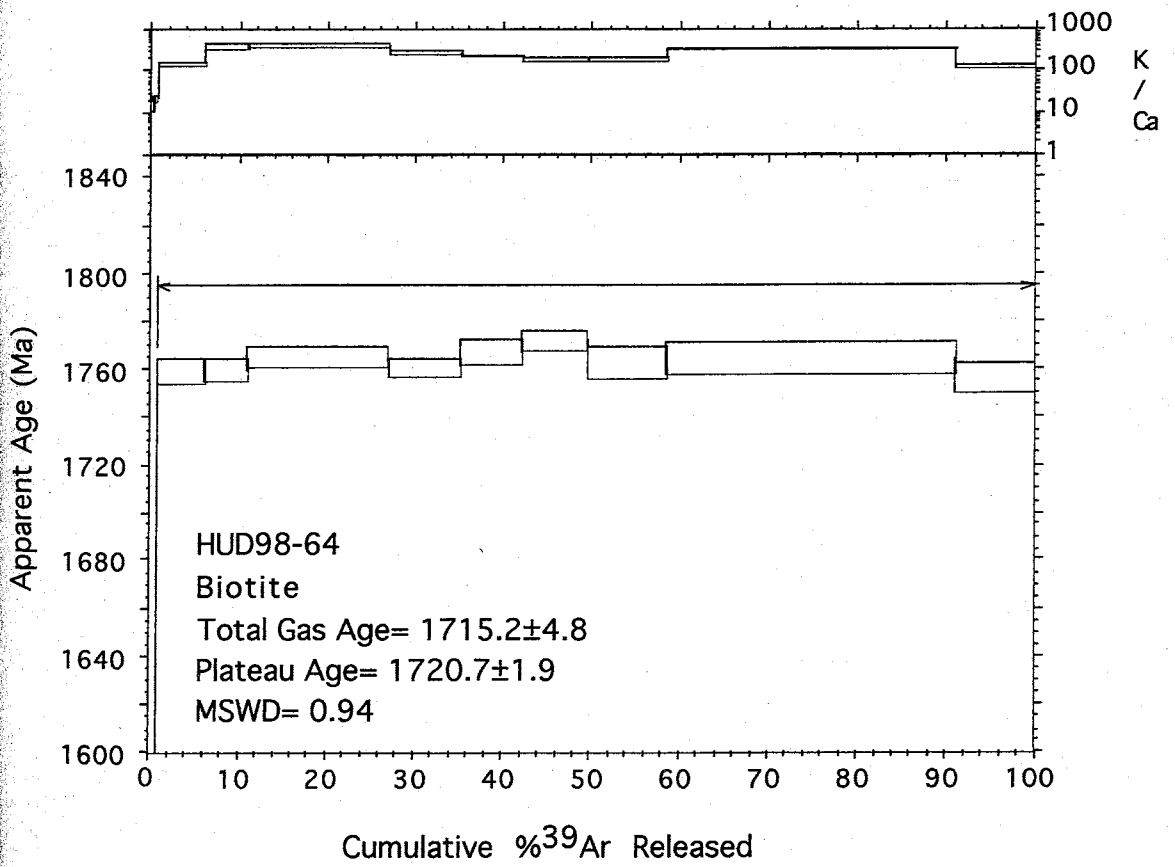
1000
100
10
1
K
/
Ca
1840
1800
1760
1720
1680
1640
1600
Apparent Age (Ma)
HUD98-64
Biotite
Total Gas Age= 1715.2±4.8
Plateau Age= 1720.7±1.9
MSWD= 0.94
0
10
20
30
40
50
60
70
80
90
100
Cumulative %39Ar Released

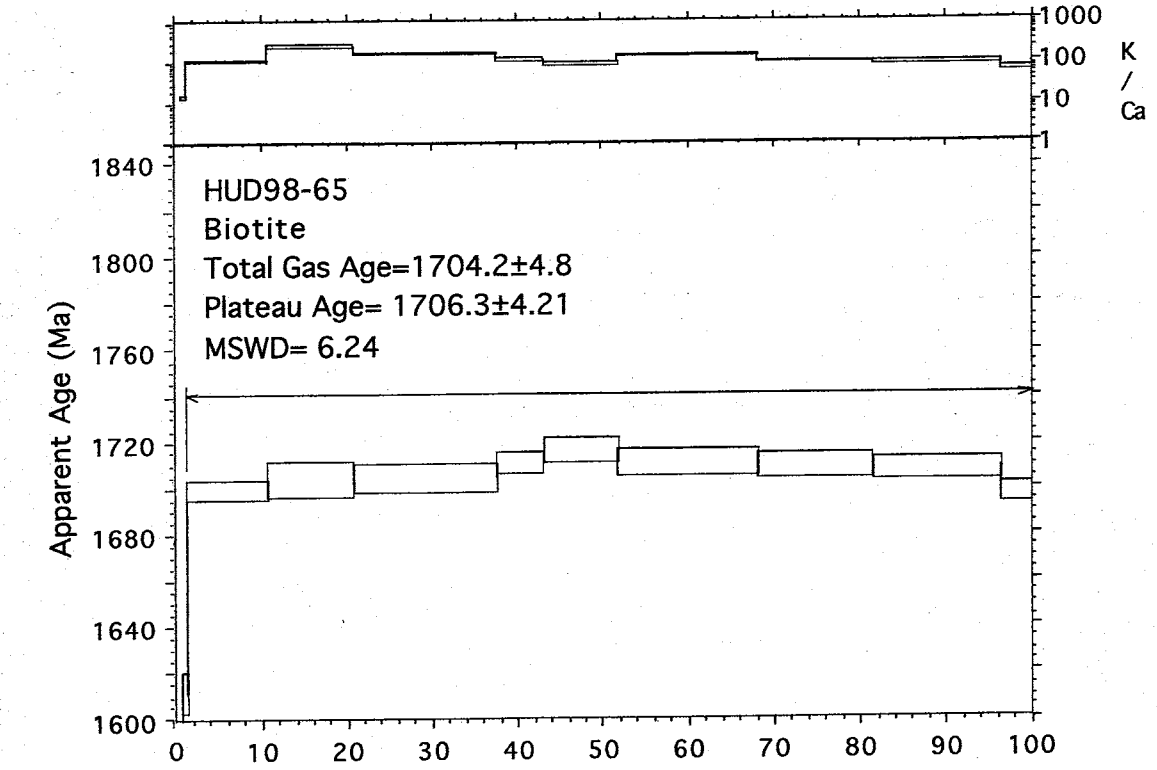
1000
100
10
1
K
/
Ca
HUD98-65
Biotite
Total Gas Age=1704.2±4.8
Plateau Age= 1706.3±4.21
MSWD= 6.24
Apparent Age (Ma)
1840
1800
1760
1720
1680
1640
1600
0
10
20
30
40
50
60
70
80
90
100

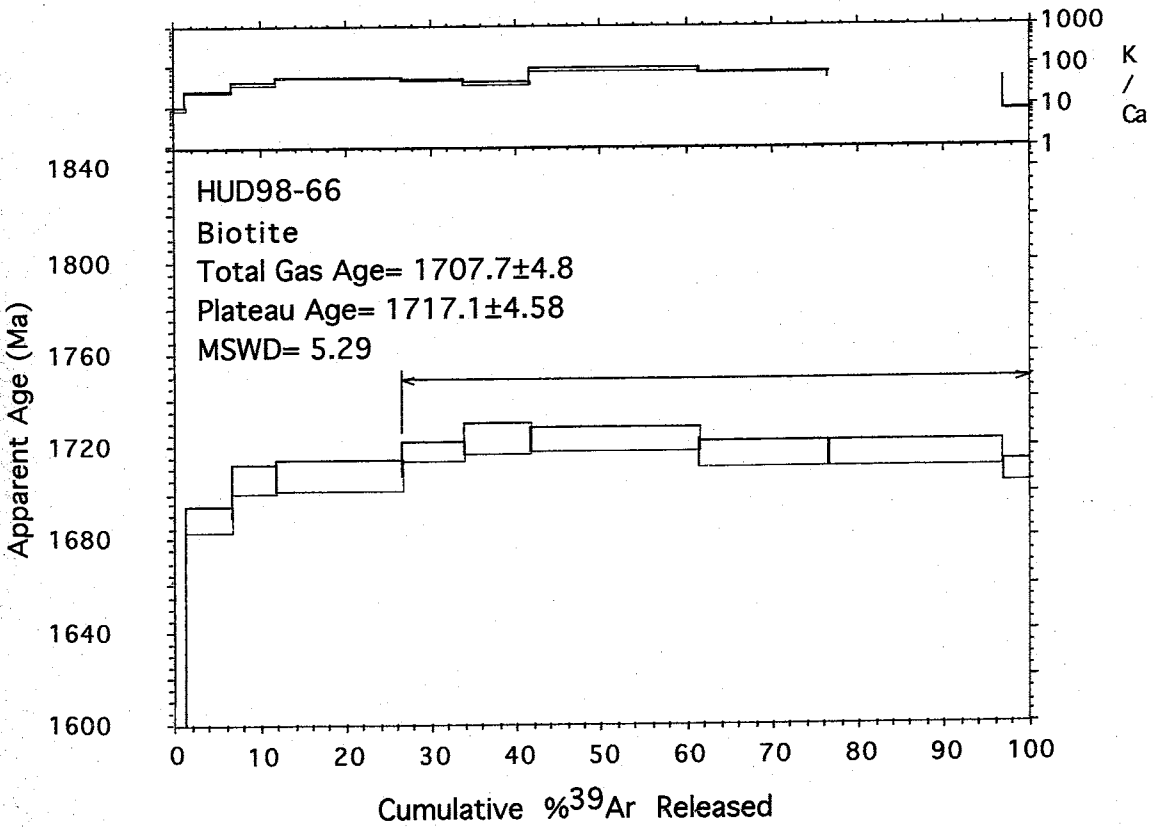
1000
100
10
1
K
/
Ca
HUD98-66
Biotite
Total Gas Age= 1707.7±4.8
Plateau Age= 1717.1±4.58
MSWD= 5.29
Apparent Age (Ma)
1840
1800
1760
1720
1680
1640
1600
0
10
20
30
40
50
60
70
80
90
100
Cumulative %39Ar Released

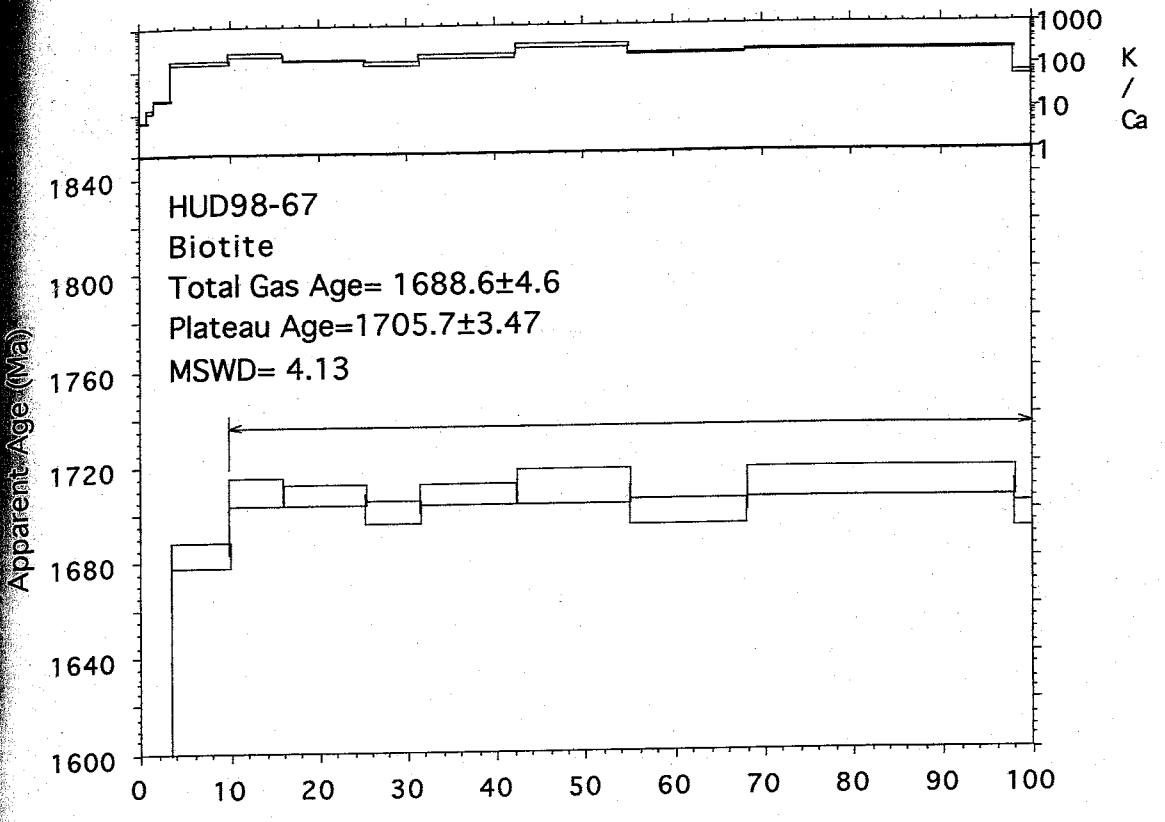
1000
100
10
1
K
/
Ca
HUD98-67
Biotite
Total Gas Age= 1688.6±4.6
Plateau Age=1705.7±3.47
MSWD= 4.13
Apparent Age (Ma)
1840
1800
1760
1720
1680
1640
1600
0
10
20
30
40
50
60
70
80
90
100

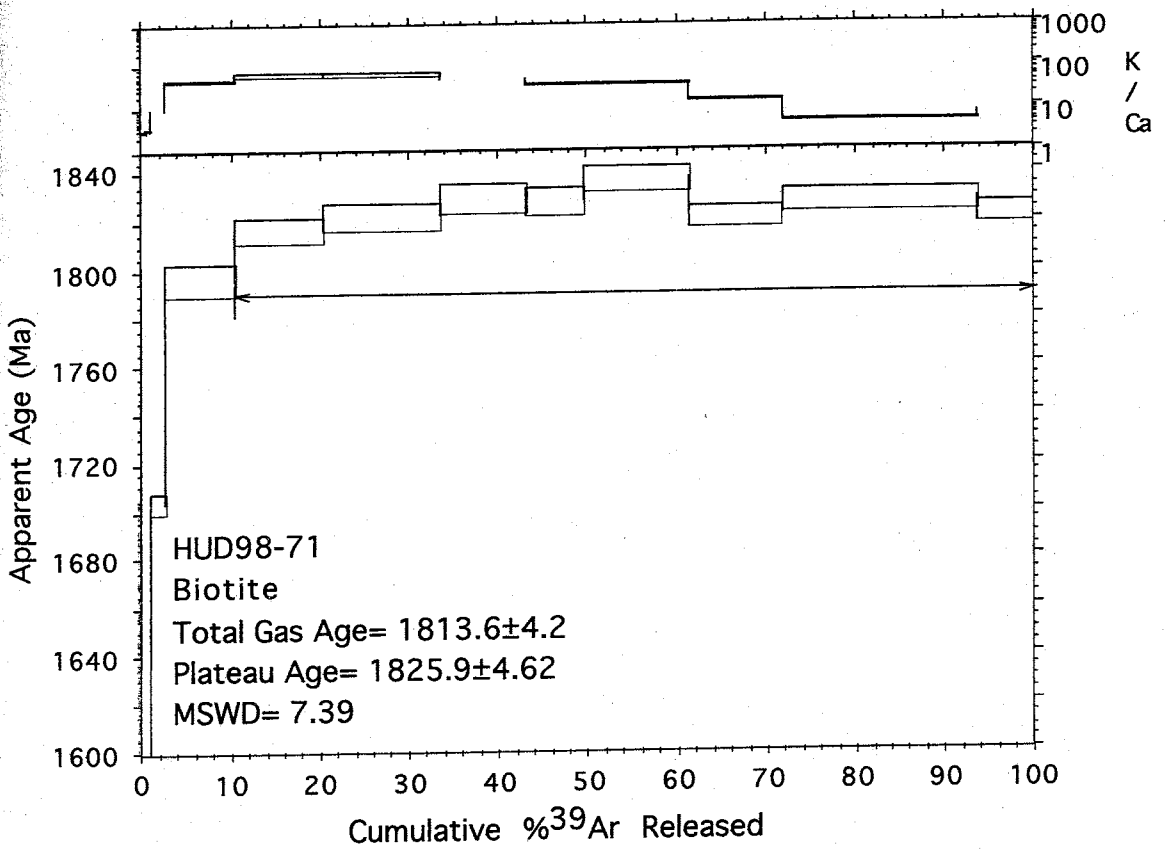
1000
100
10
1
K
/
Ca
HUD98-71
Biotite
Total Gas Age= 1813.6±4.2
Plateau Age= 1825.9±4.62
MSWD= 7.39
Apparent Age (Ma)
1840
1800
1760
1720
1680
1640
1600
0
10
20
30
40
50
60
70
80
90
100
Cumulative %39Ar Released

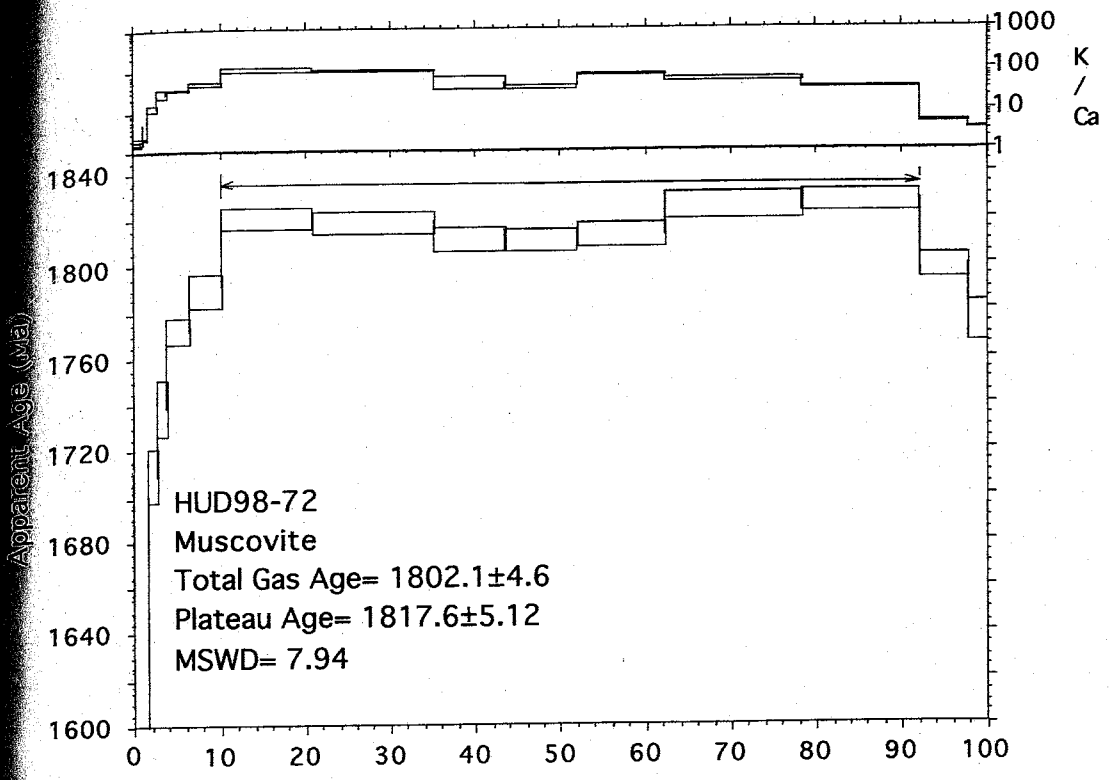
1000
100
10
1
K
/
Ca
1840
1800
1760
1720
1680
1640
1600
Apparent Age (Ma)
HUD98-72
Muscovite
Total Gas Age= 1802.1±4.6
Plateau Age= 1817.6±5.12
MSWD= 7.94
0
10
20
30
40
50
60
70
80
90
100

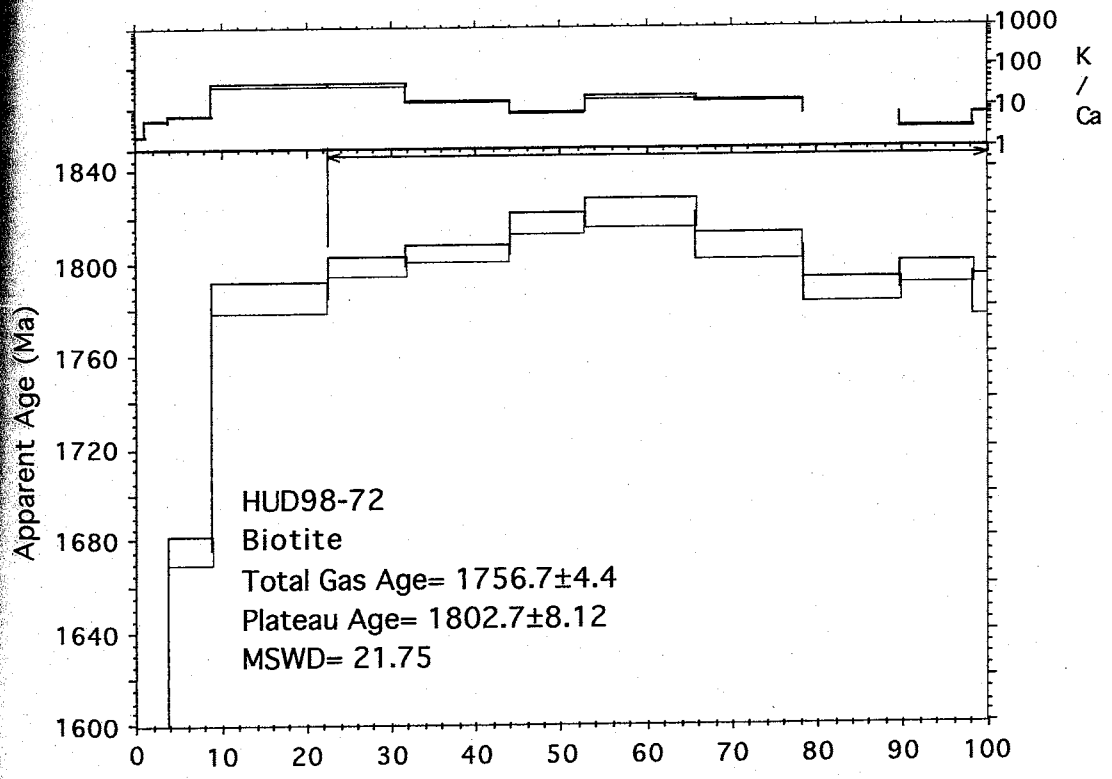
1000
100
10
1
K
/
Ca
1840
1800
1760
1720
1680
1640
1600
Apparent Age (Ma)
HUD98-72
Biotite
Total Gas Age= 1756.7±4.4
Plateau Age= 1802.7±8.12
MSWD= 21.75
0
10
20
30
40
50
60
70
80
90
100

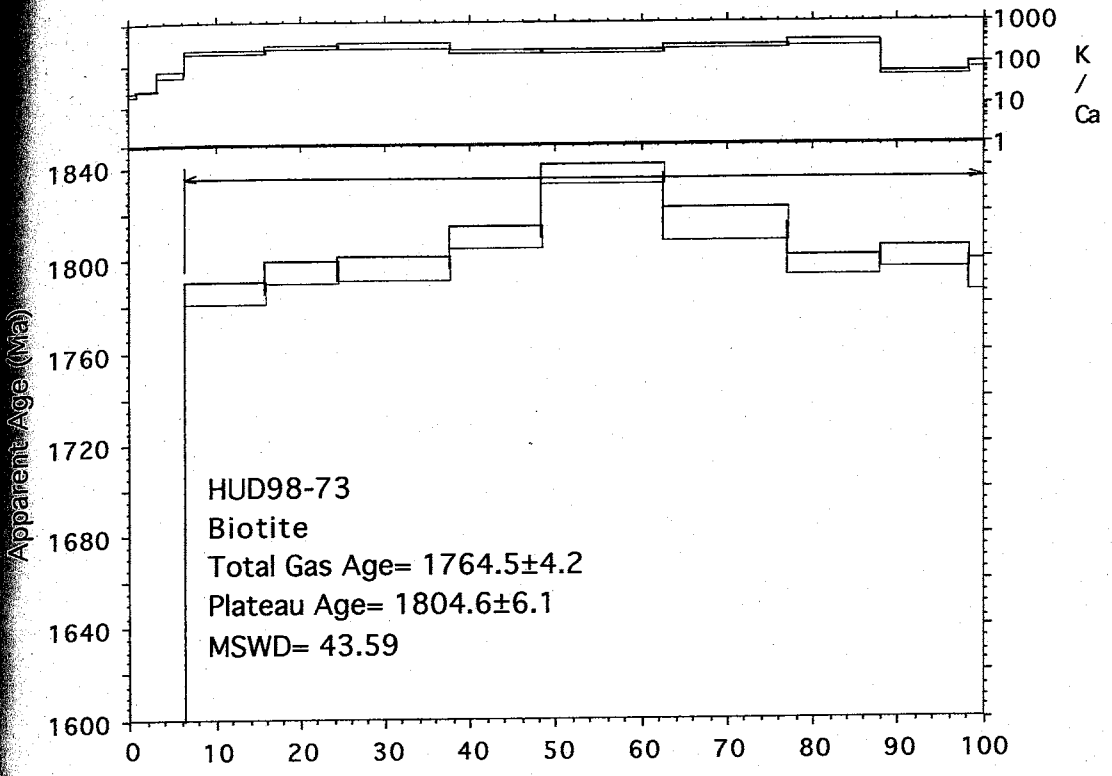
1000
100
10
1
K
/
Ca
1840
1800
1760
1720
1680
1640
1600
Apparent Age (Ma)
HUD98-73
Biotite
Total Gas Age= 1764.5±4.2
Plateau Age= 1804.6±6.1
MSWD= 43.59
0
10
20
30
40
50
60
70
80
90
100

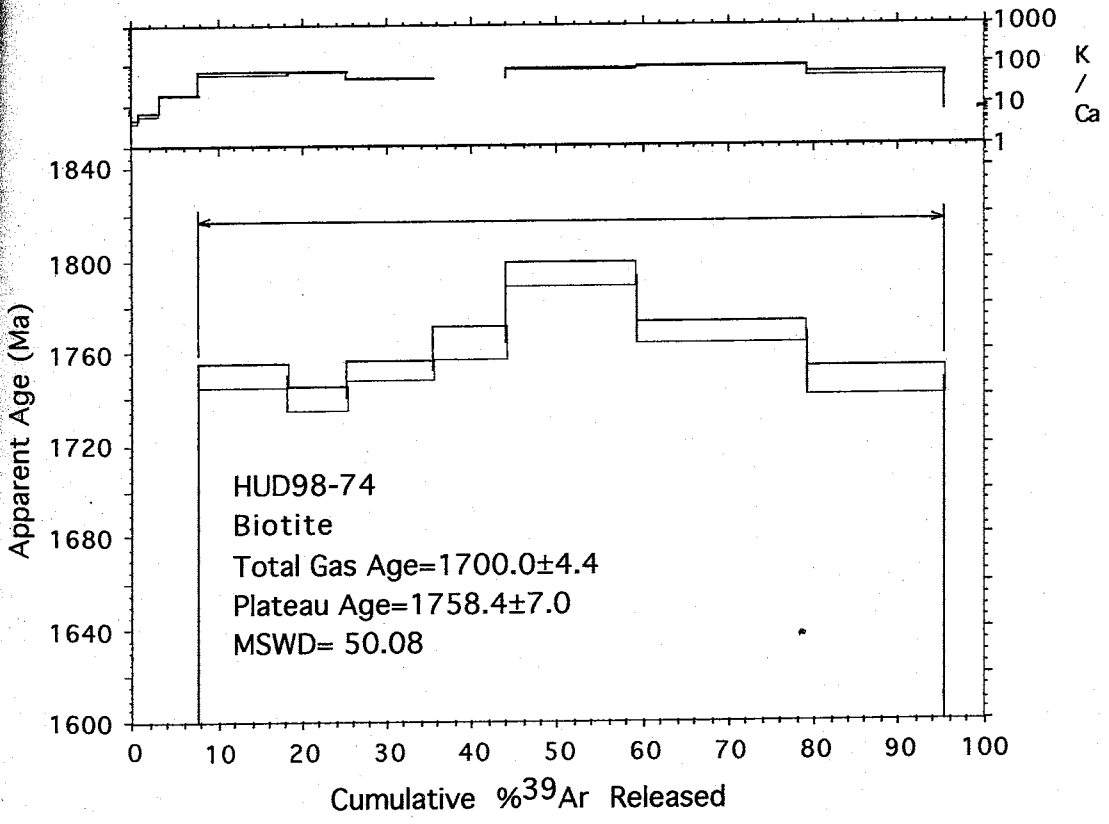
1000
100
10
1
K
/
Ca
1840
1800
1760
1720
1680
1640
1600
Apparent Age (Ma)
HUD98-74
Biotite
Total Gas Age=1700.0±4.4
Plateau Age=1758.4±7.0
MSWD= 50.08
0
10
20
30
40
50
60
70
80
90
100
Cumulative %39Ar Released

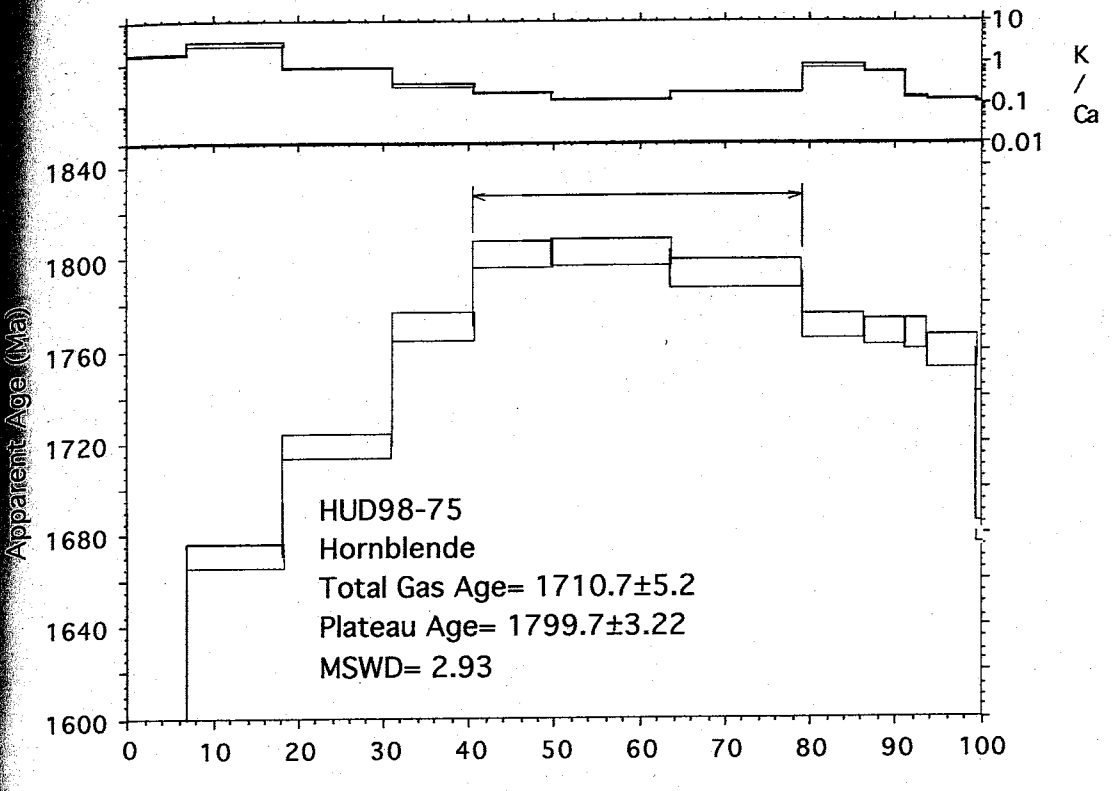
10
1
0.1
0.01
K
/
Ca
1840
1800
1760
1720
1680
1640
1600
Apparent Age (Ma)
HUD98-75
Hornblende
Total Gas Age= 1710.7±5.2
Plateau Age= 1799.7±3.22
MSWD= 2.93
0
10
20
30
40
50
60
70
80
90
100

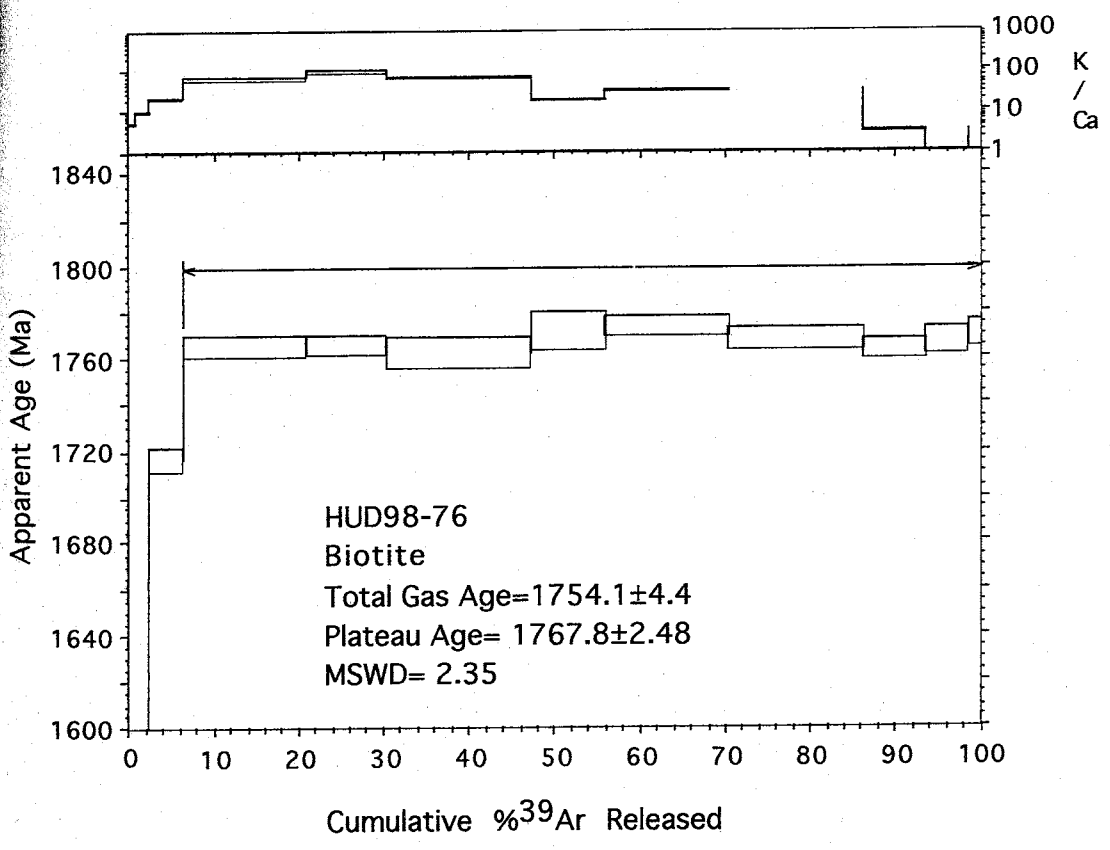
1000
100
10
1
K
/
Ca
1840
1800
1760
1720
1680
1640
1600
Apparent Age (Ma)
HUD98-76
Biotite
Total Gas Age=1754.1±4.4
Plateau Age= 1767.8±2.48
MSWD= 2.35
0
10
20
30
40
50
60
70
80
90
100
Cumulative %39Ar Released

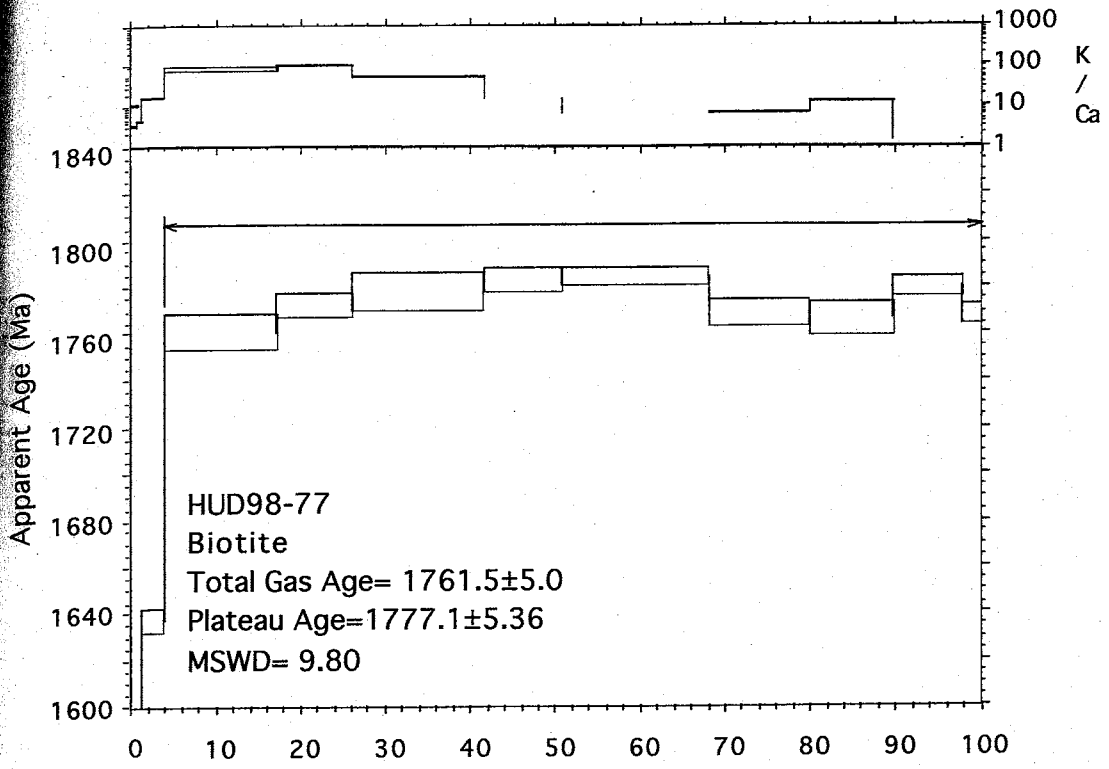
1000
100
10
1
K
/
Ca
1840
1800
1760
1720
1680
1640
1600
Apparent Age (Ma)
HUD98-77
Biotite
Total Gas Age= 1761.5±5.0
Plateau Age=1777.1±5.36
MSWD= 9.80
0
10
20
30
40
50
60
70
80
90
100

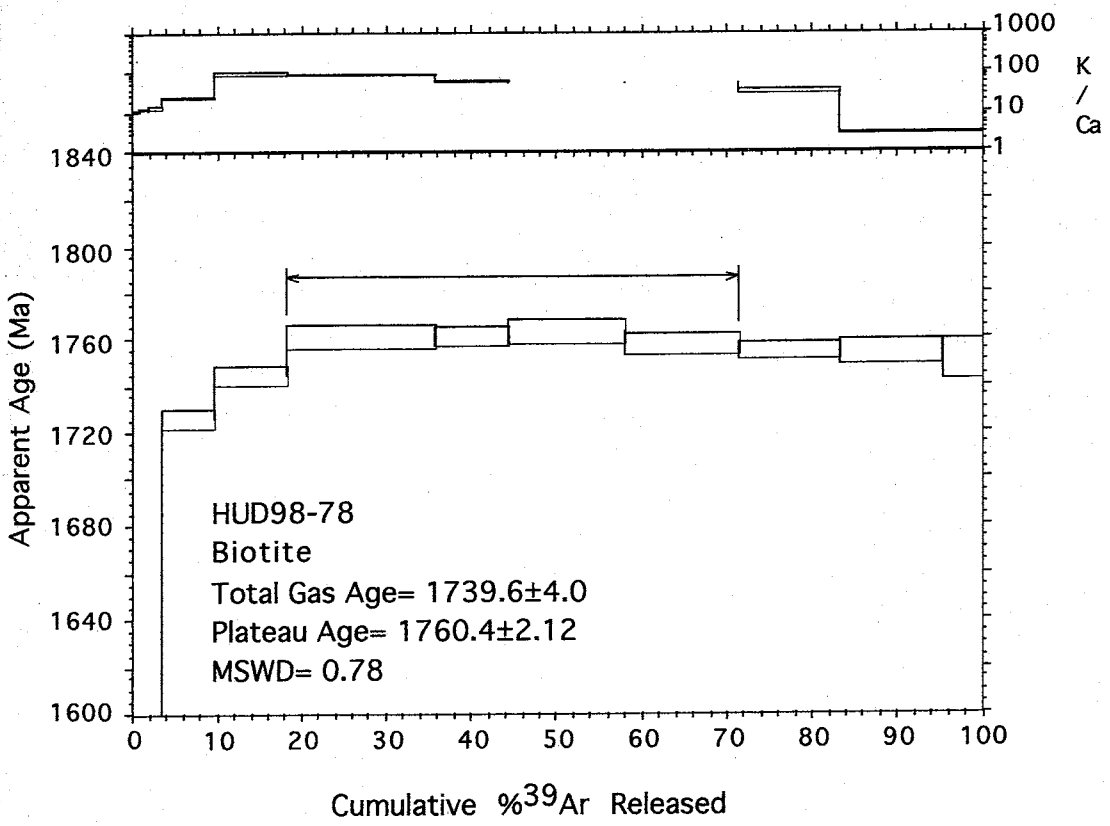
1000
100
10
1
K
/
Ca
1840
1800
1760
1720
1680
1640
1600
Apparent Age (Ma)
HUD98-78
Biotite
Total Gas Age= 1739.6±4.0
Plateau Age= 1760.4±2.12
MSWD= 0.78
0
10
20
30
40
50
60
70
80
90
100
Cumulative %39Ar Released

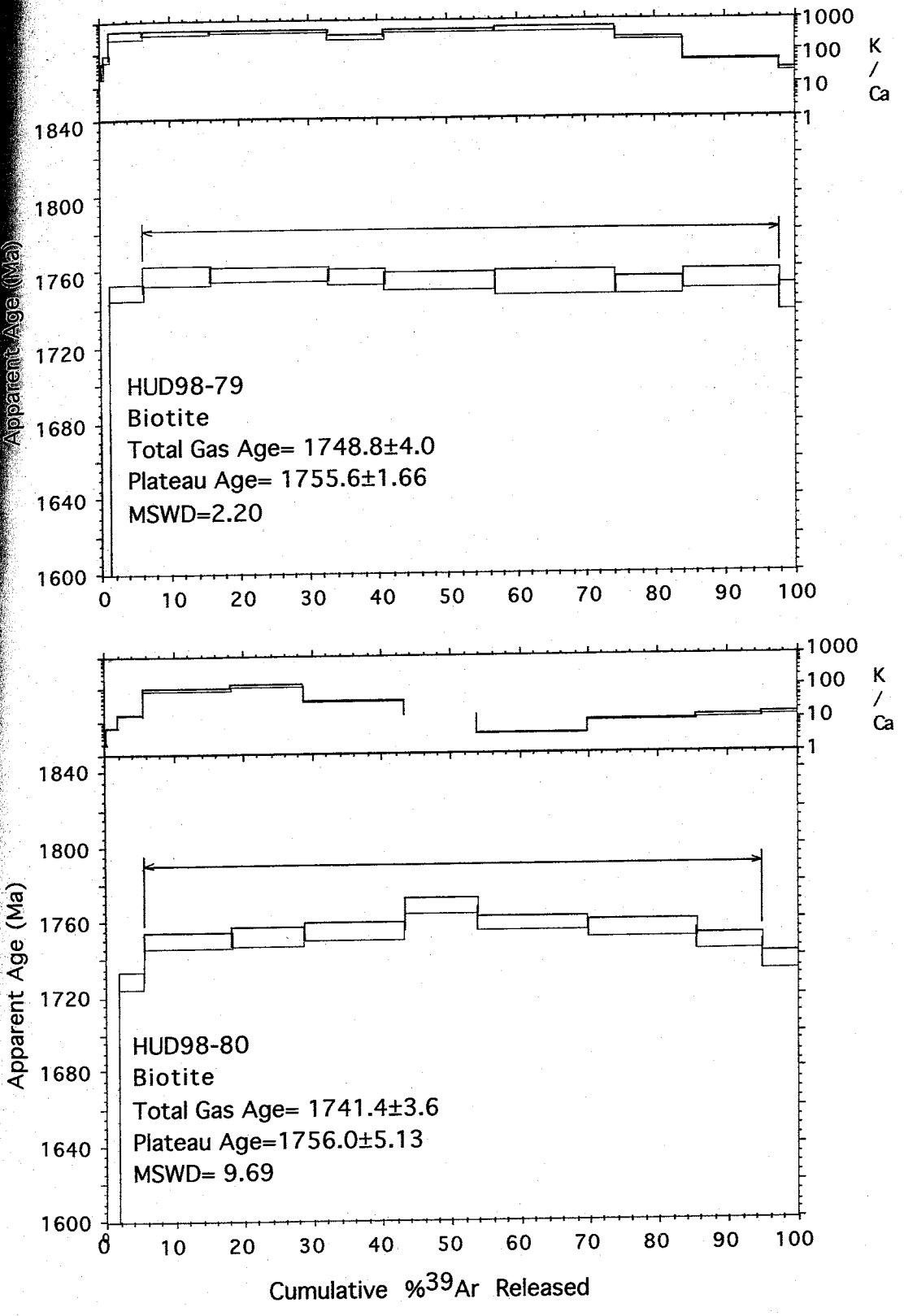
Apparent Age (Ma)
1840
1800
1760
1720
1680
1640
1600
1000
100
10
1
K / Ca
HUD98-79
Biotite
Total Gas Age= 1748.8±4.0
Plateau Age= 1755.6±1.66
MSWD=2.20
0
10
20
30
40
50
60
70
80
90
100
HUD98-80
Biotite
Total Gas Age= 1741.4±3.6
Plateau Age=1756.0±5.13
MSWD= 9.69
Cumulative %39Ar Released

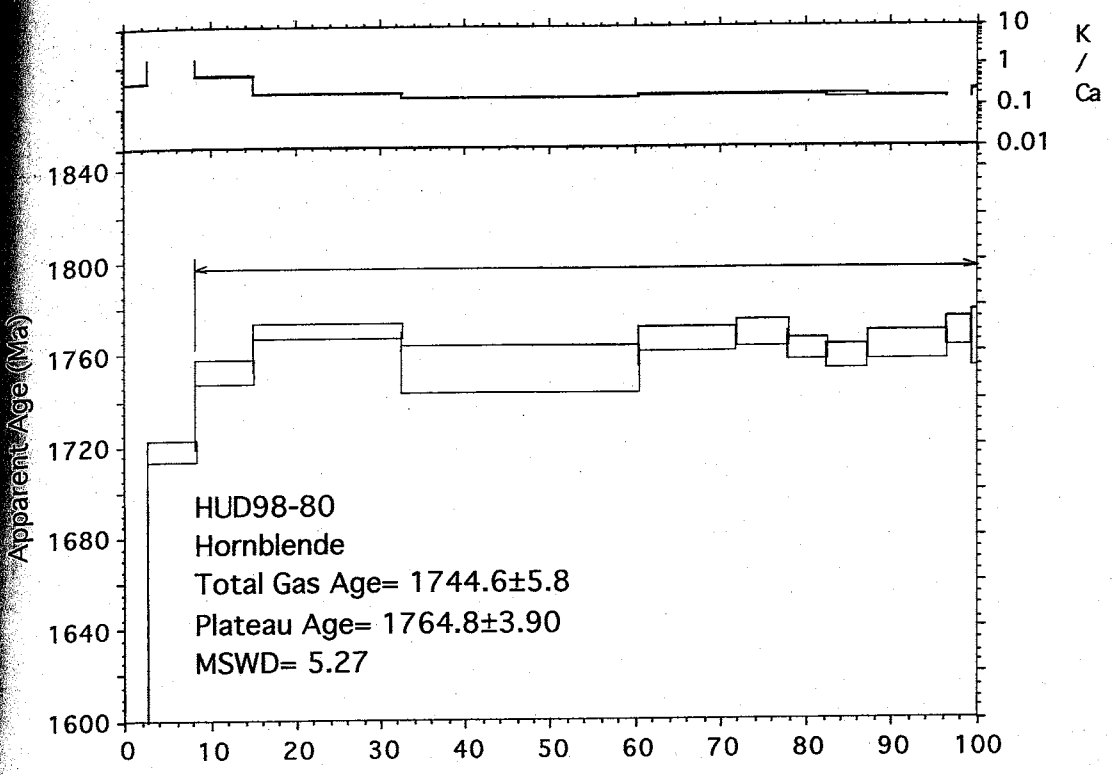
10
1
0.1
0.01
K
/
Ca
1840
1800
1760
1720
1680
1640
1600
Apparent Age (Ma)
HUD98-80
Hornblende
Total Gas Age= 1744.6±5.8
Plateau Age= 1764.8±3.90
MSWD= 5.27
0
10
20
30
40
50
60
70
80
90
100

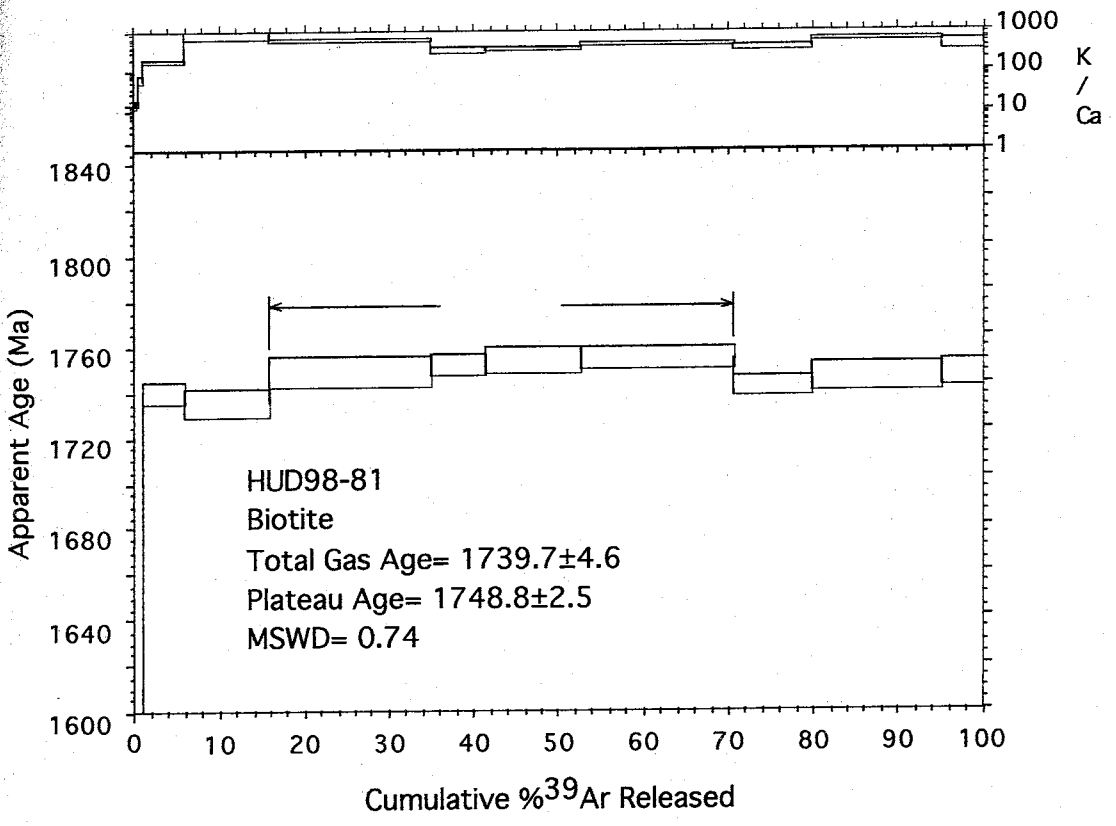
1000
100
10
1
K
/
Ca
1840
1800
1760
1720
1680
1640
1600
Apparent Age (Ma)
HUD98-81
Biotite
Total Gas Age= 1739.7±4.6
Plateau Age= 1748.8±2.5
MSWD= 0.74
0
10
20
30
40
50
60
70
80
90
100
Cumulative %39Ar Released

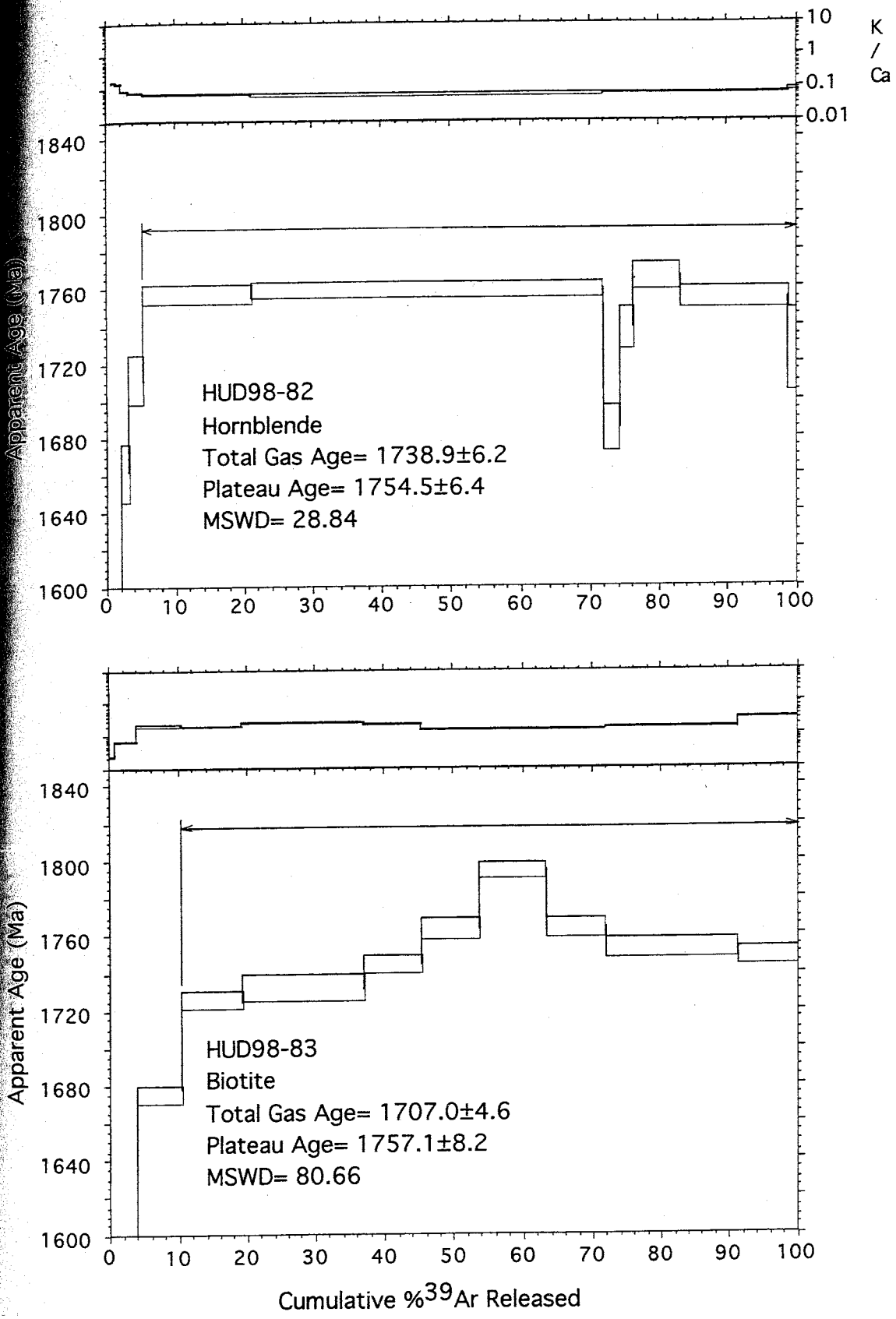
10
1
0.1
0.01
K
/
Ca
Apparent Age (Ma)
1840
1800
1760
1720
1680
1640
1600
HUD98-82
Hornblende
Total Gas Age= 1738.9±6.2
Plateau Age= 1754.5±6.4
MSWD= 28.84
0
10
20
30
40
50
60
70
80
90
100
HUD98-83
Biotite
Total Gas Age= 1707.0±4.6
Plateau Age= 1757.1±8.2
MSWD= 80.66
Cumulative %39Ar Released

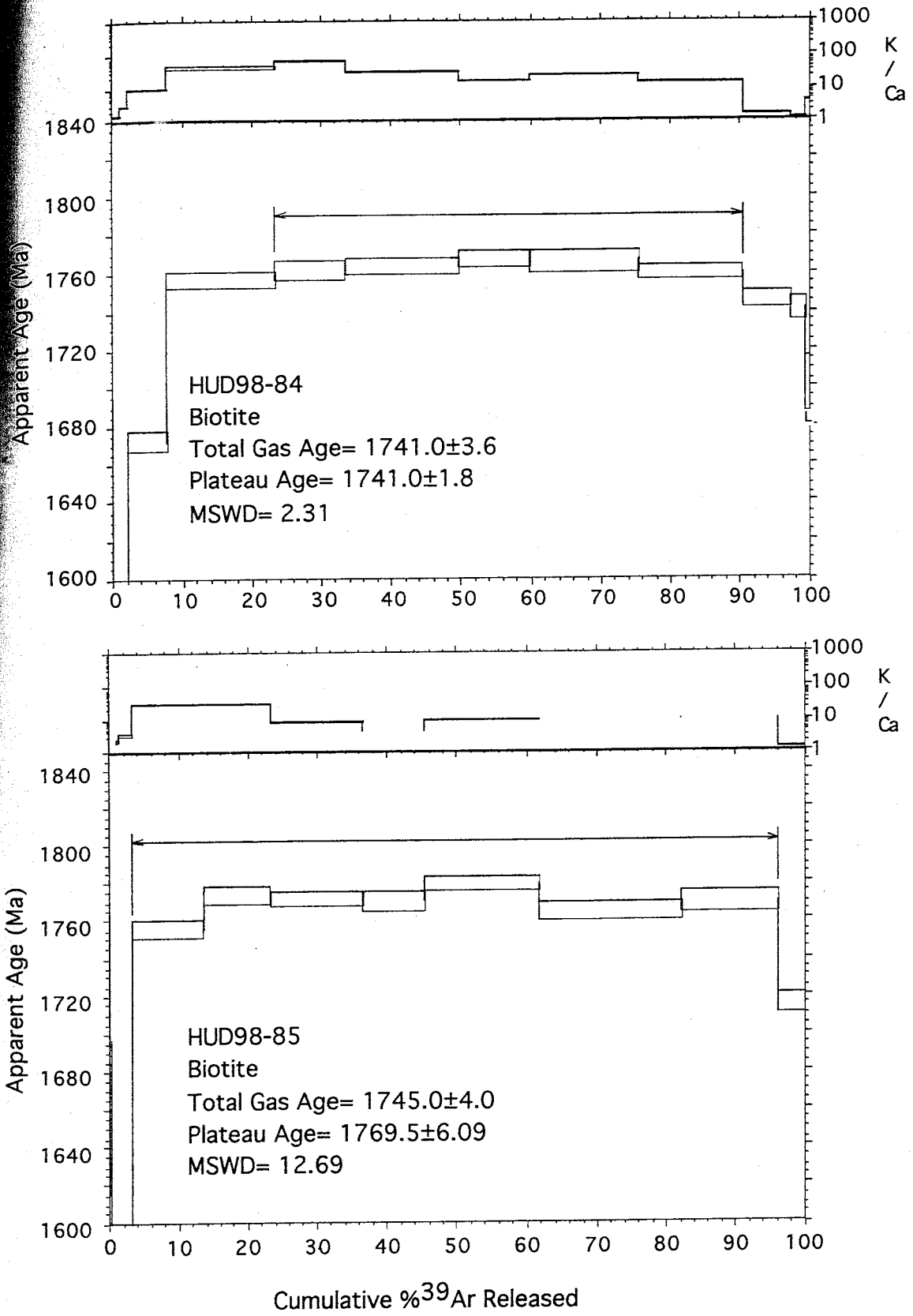
1000
100
10
1
K
/
Ca
1840
1800
1760
1720
1680
1640
1600
Apparent Age (Ma)
HUD98-84
Biotite
Total Gas Age= 1741.0±3.6
Plateau Age= 1741.0±1.8
MSWD= 2.31
0
10
20
30
40
50
60
70
80
90
100
HUD98-85
Biotite
Total Gas Age= 1745.0±4.0
Plateau Age= 1769.5±6.09
MSWD= 12.69
Cumulative %39Ar Released

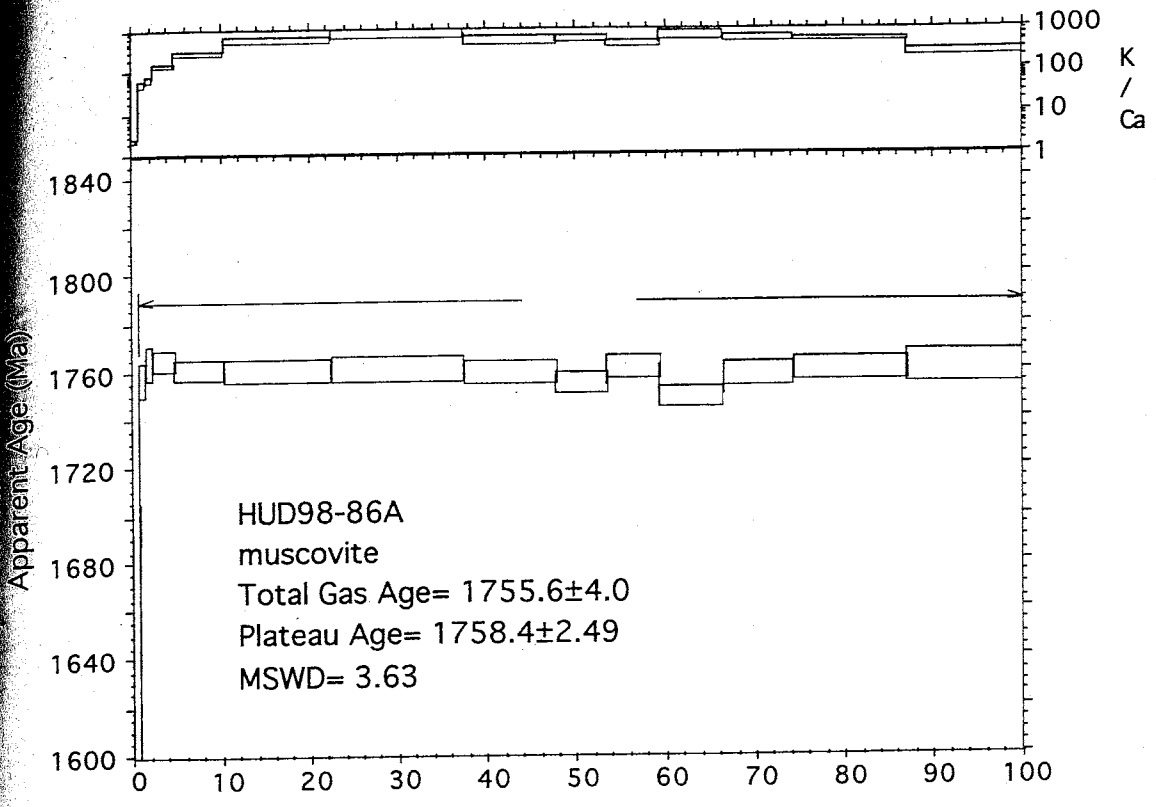
1000
100
10
1
K
/
Ca
1840
1800
1760
1720
1680
1640
1600
Apparent Age (Ma)
HUD98-86A
muscovite
Total Gas Age= 1755.6±4.0
Plateau Age= 1758.4±2.49
MSWD= 3.63
0
10
20
30
40
50
60
70
80
90
100

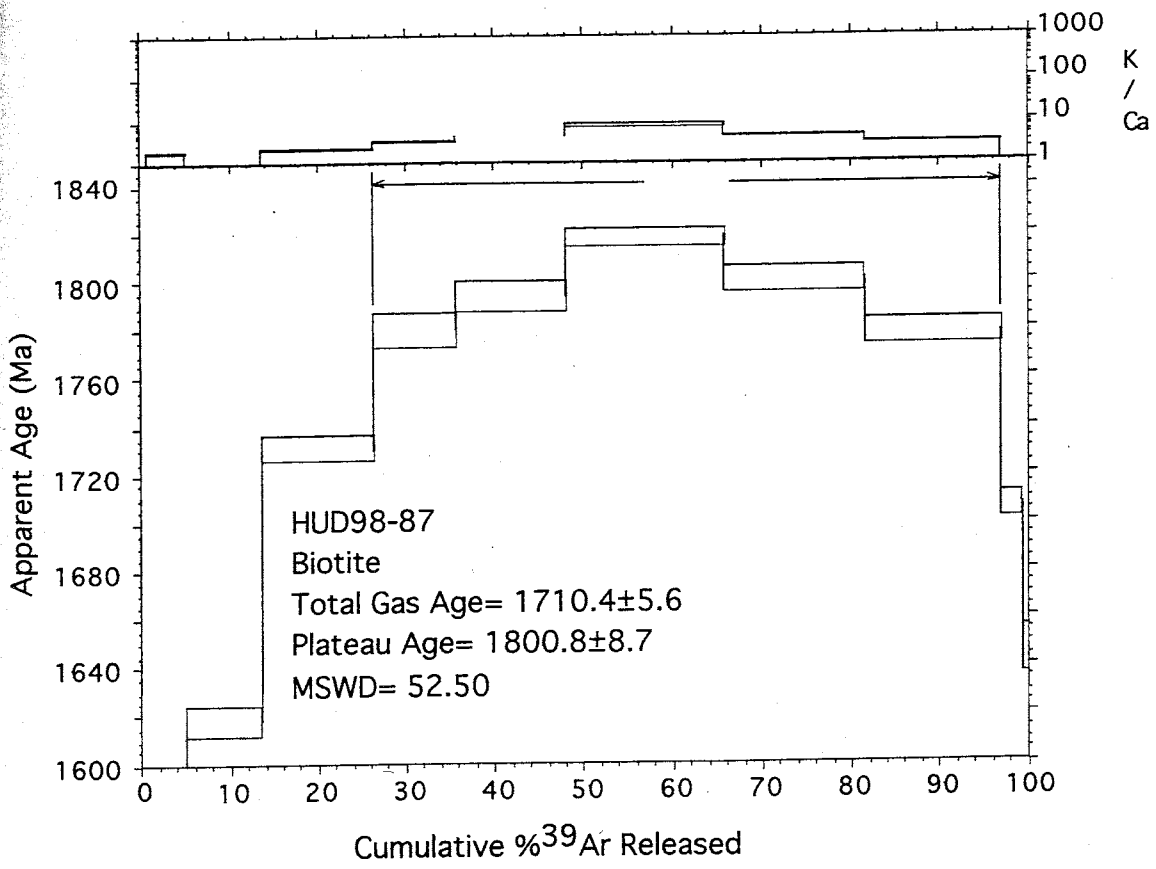
1000
100
10
1
K
/
Ca
1840
1800
1760
1720
1680
1640
1600
Apparent Age (Ma)
HUD98-87
Biotite
Total Gas Age= 1710.4±5.6
Plateau Age= 1800.8±8.7
MSWD= 52.50
0
10
20
30
40
50
60
70
80
90
100
Cumulative %39Ar Released

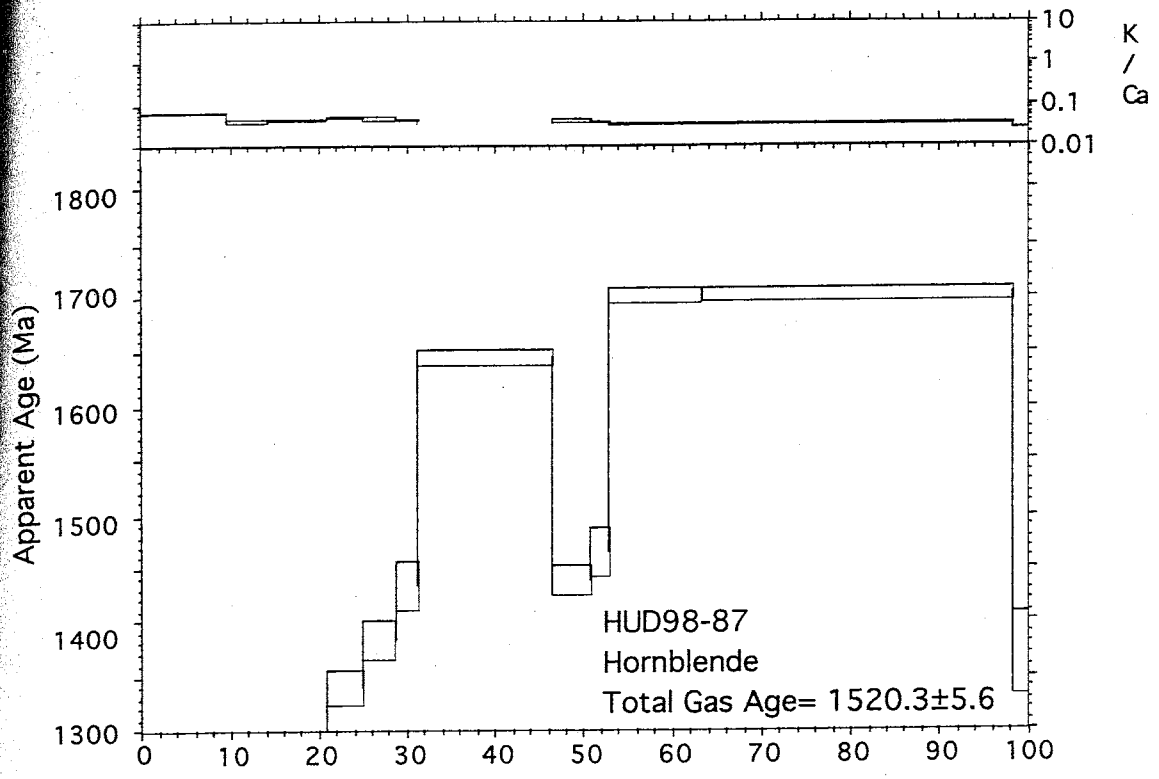
10
1
0.1
0.01
K
/
Ca
1800
1700
1600
1500
1400
1300
Apparent Age (Ma)
HUD98-87
Hornblende
Total Gas Age= 1520.3±5.6
0
10
20
30
40
50
60
70
80
90
100

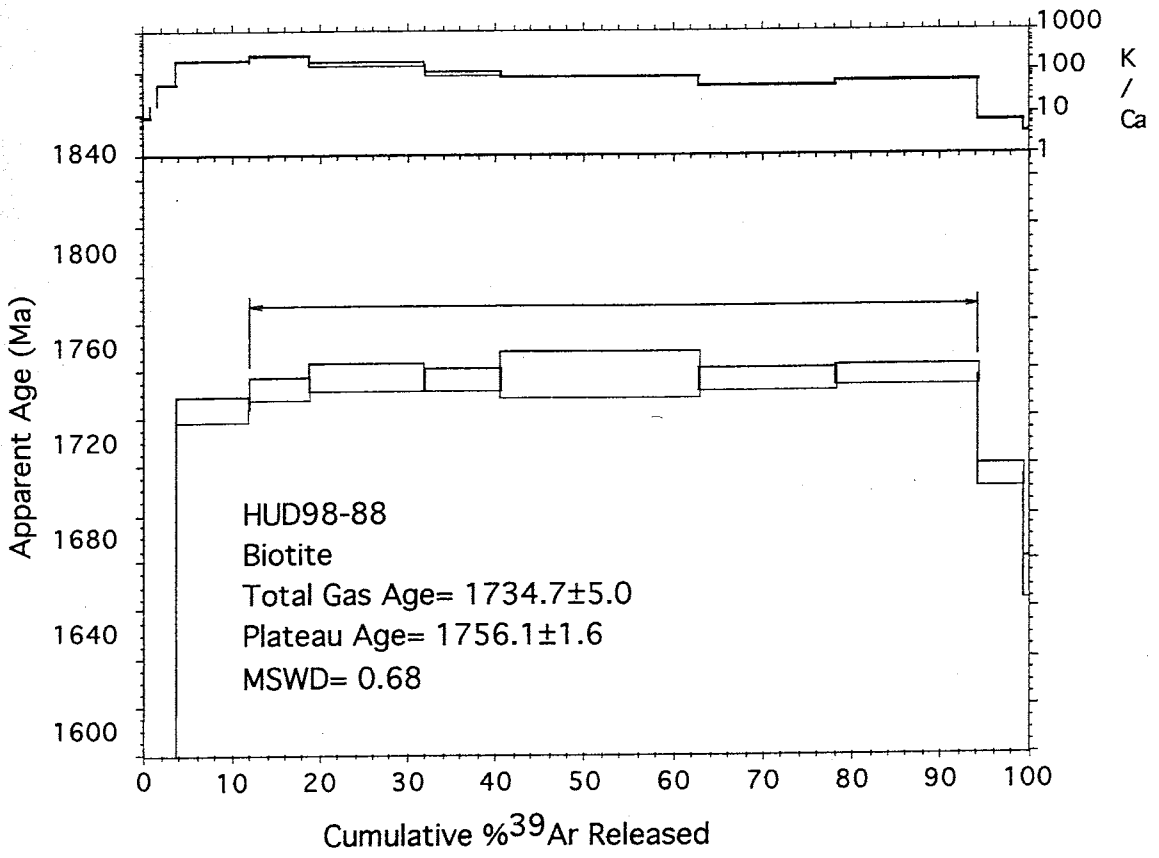
1000
100
10
1
K
/
Ca
1840
1800
1760
1720
1680
1640
1600
Apparent Age (Ma)
HUD98-88
Biotite
Total Gas Age= 1734.7±5.0
Plateau Age= 1756.1±1.6
MSWD= 0.68
0
10
20
30
40
50
60
70
80
90
100
Cumulative %39Ar Released

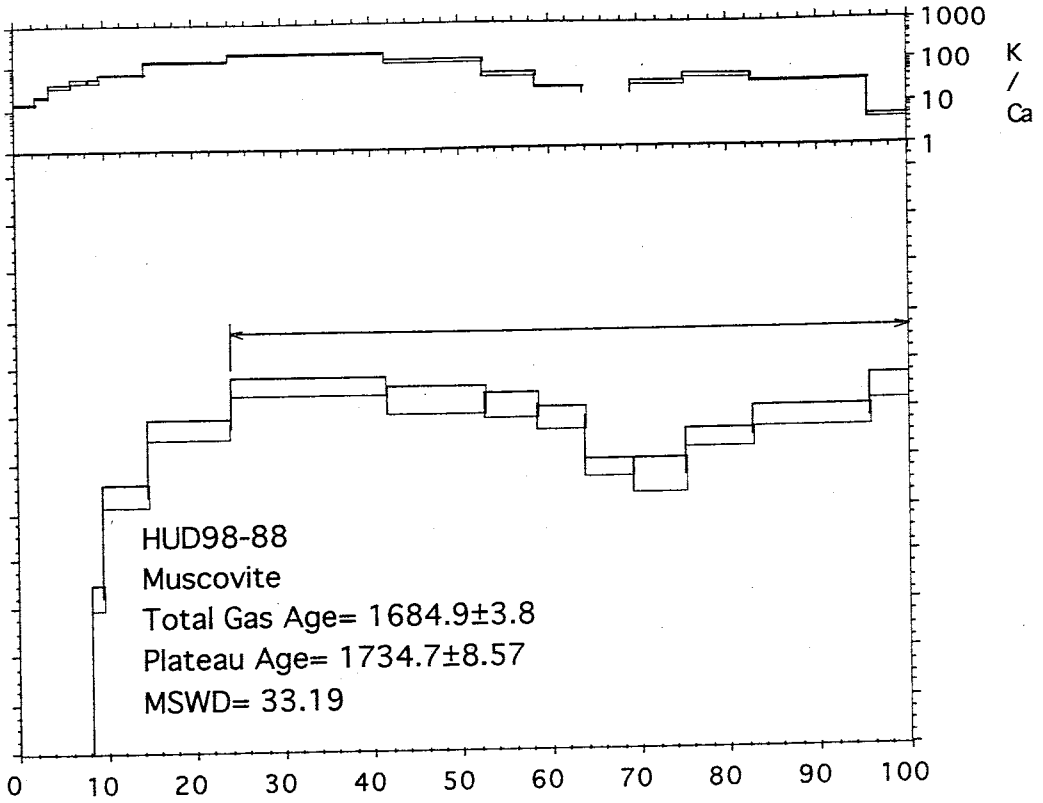
1000
100
10
1
K
/
Ca
HUD98-88
Muscovite
Total Gas Age= 1684.9±3.8
Plateau Age= 1734.7±8.57
MSWD= 33.19
0
10
20
30
40
50
60
70
80
90
100

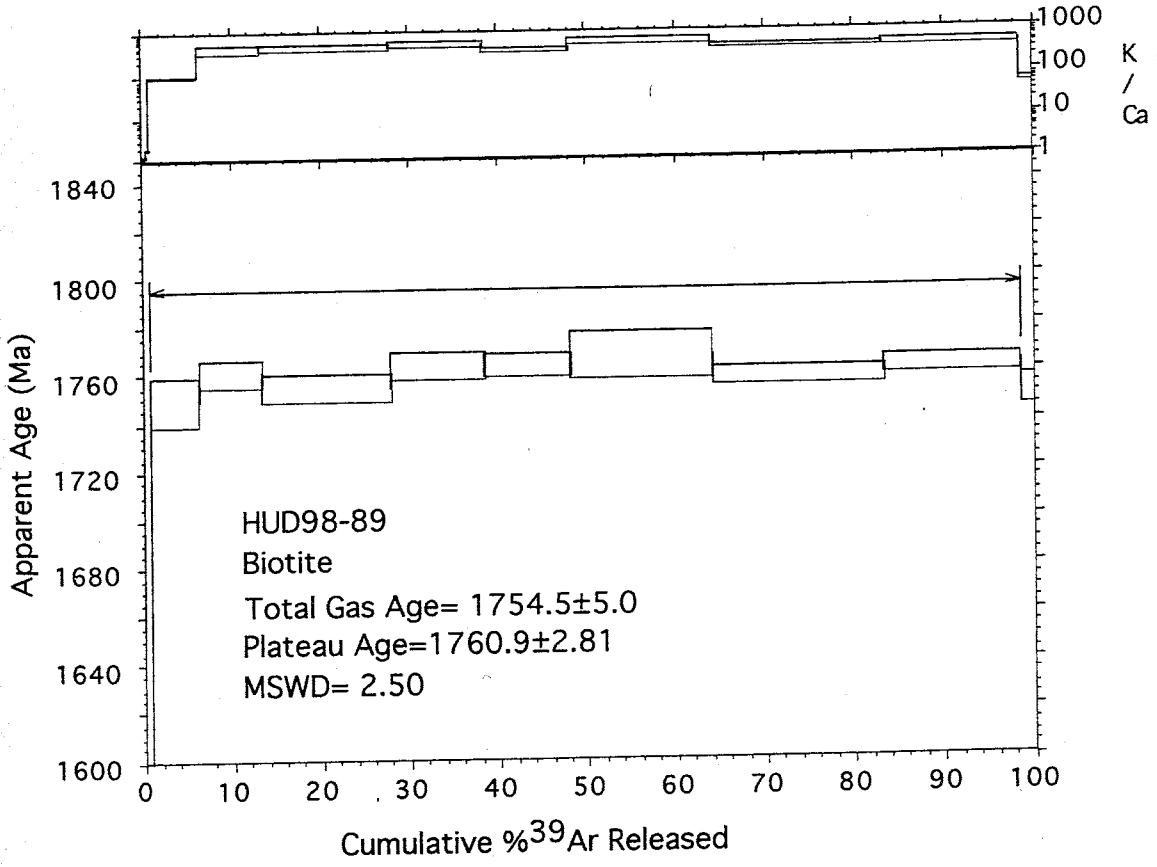
1000
100
10
1
K
/
Ca
1840
1800
1760
1720
1680
1640
1600
Apparent Age (Ma)
HUD98-89
Biotite
Total Gas Age= 1754.5±5.0
Plateau Age=1760.9±2.81
MSWD= 2.50
0
10
20
30
40
50
60
70
80
90
100
Cumulative %39Ar Released

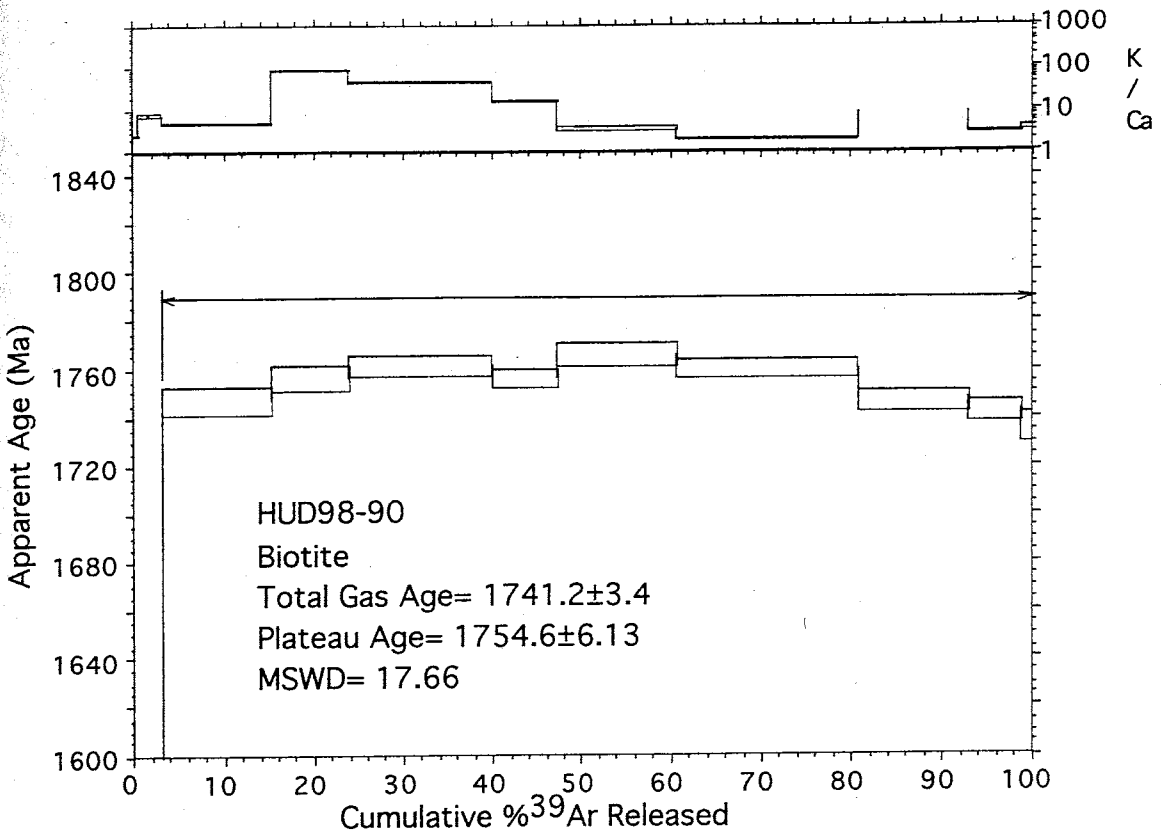
1000
100
10
1
K
/
Ca
1840
1800
1760
1720
1680
1640
1600
Apparent Age (Ma)
HUD98-90
Biotite
Total Gas Age= 1741.2±3.4
Plateau Age= 1754.6±6.13
MSWD= 17.66
0
10
20
30
40
50
60
70
80
90
100
Cumulative %39Ar Released

Appendix C

Explanation of Appendix C

The following section contains the results of electron microprobe analyses of micas and amphiboles analyzed by $^{40}Ar/^{39}Ar$ dating as well as four apatite grains used for apatite fission-track analysis. Samples are listed in numerical order and major elements are listed across the top. Sample numbers can be correlated with sample points on the electron microprobe images in Appendix D. All numbers are weight percentages normalized to 100%.

Mica and hornblende electron microprobe results

HUD98-62 Biotite

	SiO2	TiO2	Al2O3	Cr2O3	MgO	CaO	MnO	FeO	BaO	Na2O	K2O	H2O	F	Cl	P2O5	SrO	Total
1	35.061	3.257	18.733	0.059	9.271	0.009	0	18.65	0	0.128	9.518	3.664	0.526	0.029			98.905
2	34.891	3.28	18.777	0.077	9.081	0	0.054	18.639	0	0.101	9.864	3.562	0.729	0.023			99.078
3	35.081	3.303	19.149	0.082	9.249	0.009	0.02	17.886	0	0.136	9.72	3.716	0.442	0.018			98.811
4	34.859	3.279	18.924	0.064	9.538	0.006	0	18.089	0	0.077	9.768	3.582	0.702	0.023			98.911

HUD98-63 Biotite

	SiO2	TiO2	Al2O3	Cr2O3	MgO	CaO	MnO	FeO	BaO	Na2O	K2O	H2O	F	Cl	P2O5	SrO	Total
1	33.848	4.329	17.579	0.057	9.898	0.032	0.027	17.365	0	0.101	9.575	3.706	0.273	0.019			96.809
2	0.053	0.039	0.119		0.014	0.004	0.036	89.598		0.028	0.008				0.014		89.907
3	33.54	4.468	17.158	0.055	9.852	0.019	0.057	17.902	0	0.095	9.617	3.686	0.27	0.024			96.743
4	34.077	4.489	17.489	0.062	9.687	0.017	0.062	17.55	0.002	0.079	9.32	3.73	0.236	0.015			96.815

HUD98-64 Biotite

	SiO2	TiO2	Al2O3	Cr2O3	MgO	CaO	MnO	FeO	BaO	Na2O	K2O	H2O	F	Cl	P2O5	SrO	Total
1	101.364	0	0.007		0	0.008	0	0.349		0	0.015				0		101.757
2	100.256	0.045	0.004		0.004	0.034	0	0.275		0	0.017				0		100.635
3	36.74	2.18	15.696	0.188	13.416	0.041	0.209	16.158	0.141	0.072	9.804	3.84	0.209	0.035			98.729
4	35.765	1.413	15.209	0.076	13.999	0.227	0.243	16.661	0.068	0.051	8.799	3.753	0.201	0.043			96.508
5	36.408	2.203	15.601	0.219	13.743	0.022	0.254	16.458	0.032	0.118	9.701	3.843	0.2	0.034			98.836
6	36.67	2.095	15.35	0.178	13.342	0.02	0.289	16.677	0.106	0.095	9.838	3.836	0.182	0.047			98.725
7	50.668	0.236	5.601		14.581	12.21	0.449	13.074		0.66	0.364				0.057		97.843

HUD98-65 Biotite

	SiO2	TiO2	Al2O3	Cr2O3	MgO	CaO	MnO	FeO	BaO	Na2O	K2O	H2O	F	Cl	P2O5	SrO	Total
1	34.038	3.162	18.114	0.03	9.567	0.016	0.164	17.369	0	0.118	9.704	3.645	0.356	0.023			96.306
2	33.863	2.258	17.34	0.04	12.94	0.296	0.041	14.788	0	0.082	7.736	3.615	0.296	0.118			93.413
3	34.542	3.202	17.935	0.038	9.726	0.001	0.043	17.643	0	0.149	9.572	3.844	0	0.019			96.714
4	34.708	3.034	17.999	0.011	9.905	0.009	0.106	17.341	0.037	0.105	9.846	3.713	0.293	0.026			97.133

HUD98-66 Biotite

	SiO2	TiO2	Al2O3	Cr2O3	MgO	CaO	MnO	FeO	BaO	Na2O	K2O	H2O	F	Cl	P2O5	SrO	Total
1	34.895	2.224	17.062	0.075	11.583	0.027	0.035	17.09	0.069	0.177	8.796	3.651	0.382	0.024			96.09
2	35.037	1.838	16.943	0.056	12.003	0.032	0.114	16.48	0	0.152	8.803	3.648	0.363	0.029			95.498
3	33.739	1.974	16.567	0.085	11.66	0.175	0.055	16.132	0.066	0.173	7.777	3.541	0.317	0.073			92.334

HUD98-67 Biotite

	SiO2	TiO2	Al2O3	Cr2O3	MgO	CaO	MnO	FeO	BaO	Na2O	K2O	H2O	F	Cl	P2O5	SrO	Total
1	36.081	3.98	13.972	0.019	10.531	0.017	0.188	20.907	0.021	0.029	9.658	3.722	0.283	0.102			99.51
2	35.813	3.951	14.135	0	10.594	0.016	0.167	20.998	0.081	0.038	9.69	3.762	0.196	0.094			99.535
3	37.353	3.686	14.908		10.564	0.058	0.215	21.67		0.043	9.091				0.01		97.645
4	35.896	4.2	14.119	0.019	10.289	0.005	0.183	20.903	0.015	0.026	9.477	3.787	0.126	0.111			99.156

HUD98-72 Muscovite

	SiO2	TiO2	Al2O3	Cr2O3	MgO	CaO	MnO	FeO	BaO	Na2O	K2O	H2O	F	Cl	P2O5	SrO	Total
1	12.98	64.24	1.27		0.08	15.67	0.09	0.94		0.01	0.05				0.04		95.34
1	26.28	0.3	18.39	0.01	12.84	0.21	0.77	na	29.93	0.03	0.21	3.45	0.23	0			92.66
2	26.2	0.4	18.3	0.03	12.83	0.28	0.76	na	29.63	0	0.19	3.42	0.28	0			92.33
3	35.82	2.41	15.31	0	9.2	0	0.41	na	22.34	0.01	9.78	3.5	0.73	0.02			99.55
4	70.53	0.05	21.17		0.01	0.89	0.02	0.5		10.99	0.4				0		104.58
5	34.57	2.72	16.02	0	8.72	0.5	0.59	na	22.64	0.02	9.57	3.48	0.73	0.02			99.59
6	29.88	0.49	17.88		12.54	0.08	0.8	26.03		0.01	3.52				0		91.23
7	43.63	0.94	29.92		3.68	0.11	0.21	8.92		0.27	6.24				0.02		93.91
8	28.5	0.52	17.64		13.18	0.24	0.81	26.37		0	2.11				0.05		89.38
9	25.51	0.04	20.25		11.82	0.07	0.93	29.73		0.02	0.02				0		88.45
10	51.01	0.55	32.05		2.46	0.03	0.09	5.92		0.19	7.67				0.02		100.01
11	35.02	2.28	16.79	0	8.87	0.07	0.57	na	23.39	0.05	9.69	3.52	0.77	0.03			101.03

HUD98-73 Biotite

	SiO2	TiO2	Al2O3	Cr2O3	MgO	CaO	MnO	FeO	BaO	Na2O	K2O	H2O	F	Cl	P2O5	SrO	Total
1	25.792	0.046	16.493	0.012	13.787	0.027	0.804	27.905	0	0	0	3.315	0.219	0			88.4
2	36.149	2.757	12.628	0	9.535	0.073	0.718	21.488	0	0.031	9.152	3.335	0.823	0.09			96.779
3	23.611	0.1	18.558	0	9.711	0.014	1.553	31.878	0	0.001	0.003	3.271	0.142	0.021			88.863
5	24.919	0.047	16.983	0.002	12.779	0.044	0.995	28.389	0.037	0.002	0.069	3.308	0.117	0.031			87.722
6	30.92	1.615	14.548	0	10.793	0.129	0.655	25.196	0	0.015	3.909	3.426	0.24	0.05			91.496
7	97.869		0.507			0.051		1.199	0	0	0.095					0.02	99.741
8	99.524		0.034			0.01		0.704	0	0.004	0					0.027	100.303
9	67.1		20.705			0.737		0.137	0	11.305	0.092					0.014	100.09
10	63.599		18.605			0.017		0.443	0	0.031	16.984					0.029	99.708

HUD98-74 Biotite

	SiO2	TiO2	Al2O3	Cr2O3	MgO	CaO	MnO	FeO	BaO	Na2O	K2O	H2O	F	Cl	P2O5	SrO	Total
1	34.81	1.523	18.897	0.041	10.829	0.027	0.047	17.418	0.035	0.262	8.935	3.718	0.317	0.02			96.879
2	34.687	1.483	18.71	0.028	10.875	0.037	0.015	17.679	0.105	0.23	8.77	3.748	0.229	0.014			96.61
3	35.596	1.523	19.095	0.031	11.143	0.045	0	17.691	0.038	0.279	8.944	3.812	0.273	0.012			98.482
4	35.217	1.5	18.891	0.03	11.381	0.061	0	17.787	0.037	0.234	8.467	3.648	0.548	0.032			97.833

HUD98-75 Hornblende

	SiO2	TiO2	Al2O3	Cr2O3	MgO	CaO	MnO	FeO	BaO	Na2O	K2O	H2O	F	Cl	P2O5	SrO	Total
1	40.25	0.3	12.09		7.49	10.67	0.57	21.94		1.39	0.63	1.9					97.22
10	34.21	1.32	16.61		9.95	0.03	0.26	23.16		0.05	8.17				0.01		93.77
11	40.28	0.44	12.89		7.12	10.23	0.51	21.53		1.52	0.49				0.04		95.03
12	24.15	0.06	21.32		13.13	0.03	0.44	28.42		0	0				0.07		87.58
13	57.65		25.47			6.24		0.22	0.01	7.79	0.07					0.03	97.49
2	41.4	0.23	11.8		7.68	10.7	0.54	21.6		1.39	0.68	1.92					97.94
3	35.21	2.2	15.79		8.8	0.04	0.22	23.1		0.07	9.16	1.83					96.42
4	35.6	2.07	16.46		9.2	0.08	0.18	22.66		0.08	9.19	1.86					97.38
5	33.91	1.83	15.47		8.03	0.16	0.21	22.08		0.08	8.43				0.03		90.27
6	36.65	1.93	17.05		9.26	0.23	0.22	22.14		0.09	8.51				0.03		96.1
7	34.03	2.06	15.52	0	9.02	0.01	0.17	22.36	0.49	0.06	8.88	3.58	0.31	0.02			96.51
8	28.14	1.21	14.87		9.72	0.28	0.28	23.63		0.07	3.96				0.04		82.19
9	40.57	0.45	12.53		6.57	10.62	0.45	22.45		1.4	0.64				40.176		95.73

HUD98-76 Biotite

	SiO2	TiO2	Al2O3	Cr2O3	MgO	CaO	MnO	FeO	BaO	Na2O	K2O	H2O	F	Cl	P2O5	SrO	Total
1	0.346	0.011	0.021		0.003	55.663	0.081	0.451		0.032	0.163				0		96.947
2	36.575	1.78	18.138		7.182	0.05	0.343	23.397		0.061	9.479				0		97.005
3	35.58	1.859	17.684		7.044	0.012	0.315	23.013		0.037	9.667				0.004		95.211
4	36.42	1.978	17.761		7.038	0.003	0.313	23.413		0.016	8.775				0.019		95.721
5	35.418	1.806	16.963	0.01	7.342	0.014	0.324	22.537	0	0.039	9.868	3.527	0.606	0.004			98.458
6	35.078	1.653	16.63	0.018	7.45	0.036	0.21	22.575	0	0.036	9.576	3.008	1.602	0.021			97.893
7	35.881	1.946	17.638	0.042	7.123	0.018	0.291	20.751	0	0.018	9.854	3.543	0.602	0			97.707

HUD98-77 Biotite

	SiO2	TiO2	Al2O3	Cr2O3	MgO	CaO	MnO	FeO	BaO	Na2O	K2O	H2O	F	Cl	P2O5	SrO	Total
1	35.221	1.531	15.587	0.115	14.219	0.059	0.195	15.96	0.18	0.083	9.163	3.737	0.208	0.052			96.31
2	20.807	0.096	6.404		12.41	0.252	0.045	7.082		0.039	0.168				0		47.322
3	20.186	1.298	9.247		6.818	0.071	0.202	16.302		0.04	7.03				0.01		61.194
4	37.232	1.489	16.262	0.185	14.835	0.004	0.168	16.063	0.314	0.076	9.765	3.863	0.325	0.045			100.626
5	37.073	1.435	16.556	0.144	13.176	0.008	0.162	15.691	0.349	0.102	9.549	3.729	0.447	0.044			98.465
6	30.764	37.393	1.422		0.015	27.713	0.034	0.52		0	0.089				0.022		97.96
7	38.628	1.405	17.406		12.838	0.053	0.205	17.257		0.08	7.532				0.02		95.426

HUD98-78 Biotite

	SiO2	TiO2	Al2O3	Cr2O3	MgO	CaO	MnO	FeO	BaO	Na2O	K2O	H2O	F	Cl	P2O5	SrO	Total
1	35.59	2.09	15.24	0.03	9.33	0.08	0.29	21.96	0.11	0.06	9.39	3.5	0.65	0			98.32
10	35.48	1.82	15.44	0.02	9.99	0.01	0.27	21.29	0	0.06	9.47	3.47	0.73	0.01			98.07
11	48.06	0.55	31.38		1.55	0.03	0.06	6.09		0.15	8.4				0.04		96.3
12	62.51	0.02	18.58		0	0.01	0.01	0.16		0.47	15.69				0		97.49
13	48.23	0.82	30.57		1.45	0.02	0.02	5.13		0.19	9.72				37.58		96.14
14	0.28	0	0		0	52.85	0.08	0.55		0.07	0				0.03		91.42
15	27.24	0.05	17.04		13.68	0.02	0.56	28.82		0	0.02				0		87.46
16	27.49	0.01	16.99		14.74	0	0.55	28.13		0	0.06				0.01		87.97
17	37.24	0.11	23.16		0.03	22.3	0.22	12.99		0	0				0.04		96.06
18	27.98	0.09	15.28		13.15	0.16	0.5	24.62		0.02	0.19				0		82.02
19	36.28	0.06	23.66		0.01	22.07	0.24	12.77		0	0.02				0.03		95.13
2	35.92	2.21	15.94		8.19	0.06	0.38	23.29		0.04	9.13				0		95.2
20	49.49	1.07	32.57		1.27	0	0.02	4.86		0.21	8.8				0.03		98.31
21	49.92	1.23	31.7		1.46	0.06	0.02	5.08		0.2	8.22				38.15		97.91
22	0.24	0	0.01		0.02	53.4	0.05	0.22		0.03	0				0		92.13
23	7.27	0.03	2.58		0.27	0.29	0.06	79.87		0.01	0.26				0.07		90.64
3	35.67	2.5	14.77	0.03	8.72	0.03	0.26	22.09	0.2	0.06	9.41	3.47	0.66	0.03			97.88
4	35.42	2.63	15.27		8.72	0.09	0.35	21.64		0.08	9.16				0.04		93.43
5	36.22	2.55	15.5		8.88	0.03	0.37	21.82		0.06	9.35				0.03		94.81
6	36.3	2.52	15.5		8.99	0.02	0.34	22.1		0.05	9.59				39.22		95.43
7	0.18	0.01	0		0	54.74	0.07	0.55		0	0.08				0.01		94.85
8	34.62	2.27	15.02	0.03	9.27	0.04	0.29	21.5	0	0.06	9.62	3.38	0.78	0.02			96.9
9	34.99	2.63	15.09	0.03	8.97	0.06	0.28	21.35	0	0.06	9.58	3.47	0.63	0.02			97.15

HUD98-79 Biotite

	SiO2	TiO2	Al2O3	Cr2O3	MgO	CaO	MnO	FeO	BaO	Na2O	K2O	H2O	F	Cl	P2O5	SrO	Total
1	34.28	2.98	17.91	0.08	9.89	0.01	0	18.14	0.04	0.22	9.28	3.67	0.34	0.02			96.88
2	34.27	2.79	18	0.14	9.92	0.02	0	17.87	0	0.2	9.5	3.68	0.31	0.02			96.73
3	34.16	2.93	17.79	0.09	9.66	0	0	18.4	0	0.1	9.47	3.66	0.32	0.03			96.61
4	33.39	3	17.78	0.1	9.77	0.01	0.06	18.36	0	0.15	9.38	3.64	0.29	0.03			95.97
5	34.24	2.79	18.31	0.11	9.97	0.03	0	18.35	0.02	0.17	9.36	3.69	0.34	0.03			97.41
6	60.33	0.04	25.18		2.42	4.37	0.01	0.88		4.21	3.64				0.03		101.1
7	32.03	2	19.68		10.27	0.01	0.09	22.46		0.06	6.37				0		93
8	33.36	2.59	18.23		9.15	0.01	0.03	18.86		0.05	8.61				0		90.89
9	35.28	2.88	18.62		9.19	0.03	0.05	19.28		0.09	9.06				0		94.49

HUD98-80 Hornblende

	SiO2	TiO2	Al2O3	Cr2O3	MgO	CaO	MnO	FeO	BaO	Na2O	K2O	H2O	F	Cl	P2O5	SrO	Total
1	65.03	0.002	18.783		0	0.015	0	0.324		0.596	15.113				0		99.863
2	38.657	1.494	10.374		3.129	10.473	0.61	27.585		1.56	1.7	1.825					97.407
3	34.831	1.967	16.676		4.14	0.034	0.38	26.93		0.033	9.592	1.79					96.373
4	34.517	2.049	16.497		4.363	0.076	0.371	27.346		0.02	9.201	1.785					96.225
5	34.431	2.131	15.574		4.275	0.023	0.359	28.461		0.043	9.387	1.775					96.459
6	96.073		0.051			0.517		0.549	0	0.006	0.052					0.029	97.277
7	38.255	1.491	10.204	0	3.316	10.356	0.522	27.07	0	1.475	1.605	3.543	0.448	0.064			98.349
8	0.304	0.148	0.101		0.035	6.981	0	1.119		0.008	0				0.01		8.696

HUD98-80 Biotite

	SiO2	TiO2	Al2O3	Cr2O3	MgO	CaO	MnO	FeO	BaO	Na2O	K2O	H2O	F	Cl	P2O5	SrO	Total
1	33.598	1.63	16.429	0.007	3.591	0.035	0.34	27.304	0	0	9.206	0	26.565	0.052			118.757
2	0.029		0			52.032		1.38	0	0.004	0.04					0.022	53.507
3	32.932	1.9	15.369	0.007	4.166	0.048	0.31	28.555	0	0.032	9.033	3.118	0.989	0.054			96.513
4	37.765	1.353	10.309	0.008	3.012	10.351	0.514	27.611	0	1.405	1.62	3.528	0.425	0.048			97.949
5	33.458	1.952	15.422	0.006	4.215	0.146	0.409	27.963	0	0.041	9.223	3.046	1.199	0.066			97.146
6	33.526	2.842	14.976	0	3.641	0.022	0.146	28.344	0.094	0.042	9.136	3.368	0.513	0.053			96.703
7	33.135	2.013	15.651	0.018	3.982	0.092	0.461	27.558	0	0.026	8.762	2.863	1.516	0.074			96.151
8	32.629	2.072	16.031	0.013	3.518	0.068	0.363	27.703	0	0	9.26	3.307	0.549	0.06			95.573
9	33.69	0.084	20.843	0	0.047	16.251	0.504	12.542	0.032	0.031	0.085	3.585	0.072	0.008			87.774
1	34.37	2.87	17.7	0.08	9.99	0.01	0.04	18.12	0	0.22	9.47	3.7	0.28	0.02			96.86

HUD98-81 Biotite

	SiO2	TiO2	Al2O3	Cr2O3	MgO	CaO	MnO	FeO	BaO	Na2O	K2O	H2O	F	Cl	P2O5	SrO	Total
10	53.9		28.64			9.99		0.23	0.02	5.68	0.13					0.08	98.68
11	34.54	2.68	18.58		8.9	0.06	0.06	19.14		0.1	9.32				24.46		93.4
12	0.68	0.03	0		0	1.78	0	0.07		0	0				0.01		27.02
2	34.2	2.84	18.11	0.09	9.84	0.01	0.03	18.1	0.02	0.25	9.29	3.69	0.3	0.03			96.8
3	34.17	3.04	17.91	0.09	9.92	0.02	0.01	18.44	0	0.21	9.37	3.69	0.32	0.02			97.22
4	34.17	2.59	17.77	0.09	9.78	0.02	0	18.16	0	0.12	9.29	3.64	0.33	0.02			95.98
5	34.83	2.65	18.71		9.51	0.01	0.02	18.61		0.17	9.18				0.02		93.7
6	34.94	2.61	18.88		9.07	0.04	0.04	19.54		0.12	9.44				0.02		94.7
7	24.71	0.09	23.1		15.1	0.03	0.04	24.42		0	0.01				0.01		87.53
8	34.02	2.09	18.15	0.12	9.77	0.08	0.01	19.15	0.05	0.1	9.23	3.62	0.39	0.05			96.82
9	54.17		28.81			10.09		0.13	0	5.68	0.15					0.08	99.1

HUD98-82 Biotite

	SiO2	TiO2	Al2O3	Cr2O3	MgO	CaO	MnO	FeO	BaO	Na2O	K2O	H2O	F	Cl	P2O5	SrO	Total
1	42.31	1	11.61		9.25	10.76	0.34	19.59		1.28	0.65	1.96					98.74
10	30.65	0.04	21.67		19.44	0.39	0.03	11.89		0.05	0.03				0		84.19
2	42.15	1.01	11.24		9.17	10.81	0.31	19.84		1.34	0.62	1.95					98.43
3	41.97	0.91	11.91		8.89	11.18	0.29	19.94		1.15	0.69	1.96					98.89
4	42.2	0.96	11.34		9.37	10.76	0.34	19.92		1.33	0.61	1.96					98.78
5	41.57	0.86	11.62		9.46	10.84	0.35	19.5		1.3	0.61	1.94					98.06
6	42.62	0.88	11.51		9.13	10.63	0.35	20.03		1.3	0.59	1.96					99
7	35.05	0	0.01		0.02	0.07	0	0.7		0	0.01				0.01		35.86
8	30.87	0.03	22.01		21.68	0.27	0.04	10.39		0.04	0.04				0.05		85.4
9	30.59	0.03	23.3		19.11	0.18	0.09	13.43		0.01	0.03				0.01		86.81

HUD98-83 Biotite

	SiO2	TiO2	Al2O3	Cr2O3	MgO	CaO	MnO	FeO	BaO	Na2O	K2O	H2O	F	Cl	P2O5	SrO	Total
1	27.76	3.01	13.73	0.04	10.06	0	0.01	7.93	0	0.07	6.18	2.6	0.83	0			72.24
10	28.44	3.3	15.43		10.38	0.06	0.04	18.75		0.06	5.64				0.11		82.11
11	65.77	0.03	19.15		0	0.01	0.01	0.29		0.74	14.6				0.05		100.71
12	31.85	17.46	16.94		8.57	0.11	0.03	12.98		0.05	4.4				0.07		92.44
2	35.26	4.72	16.27	0.05	11.74	0.02	0	15.2	0	0.1	9.72	3.57	0.67	0.03			97.36
3	35.33	5.17	15.94	0.08	11.2	0	0	16.29	0	0.11	9.53	3.6	0.62	0.03			97.89
4	34.69	5.97	16.18	0.07	10.9	0	0.04	15.86	0	0.12	9.52	3.57	0.67	0.02			97.61
5	25.28	0.08	21.47	0.04	16.92	0.01	0	23.02	0	0.02	0.01	3.57	0.12	0.01			90.54
6	63.08	0.01	23.42		0	4.18	0	0.3		9.03	0.15				0.04		100.25
7	25.81	0.06	22.06		16.55	0.01	0.03	22.23		0.02	0.01				0.02		86.83
8	49.66	0.41	35.1		2.06	0.02	0	2.33		0.26	6.8				0		96.66
9	36.36	4.3	17.31		11.29	0.02	0.03	16.41		0.08	8.01				0		93.79

HUD98-84 Biotite

	SiO2	TiO2	Al2O3	Cr2O3	MgO	CaO	MnO	FeO	BaO	Na2O	K2O	H2O	F	Cl	P2O5	SrO	Total
1	34.28	1.4	15.89	0	4.48	0.01	0.21	28.19	0	0.03	9.73	3.39	0.49	0.27			98.38
10	33	1.13	16.53	0.01	4.71	0.08	0.23	28.68	0	0.03	8.7	3.58	0	0.25			96.93
11	31.55	1.34	16.88		6.13	0.95	0.34	29.11		0.03	5.74				0.02		92.06
12	32.85	1.05	16.78		5.27	0.26	0.3	29.83		0.02	7.58				0		93.97
2	33.58	2.54	14.41	0	4.25	0.02	0.18	28.86	0.02	0.05	9.33	3.35	0.38	0.41			97.37
3	33.21	1.03	16.26	0	4.26	0.04	0.2	28.96	0.02	0.06	9.4	3.39	0.38	0.29			97.49
4	33.74	1.13	15.83	0.02	4.27	0.07	0.18	28.9	0	0.03	9.27	3.42	0.32	0.32			97.49
5	34.12	2.32	14.71	0.01	4.05	0.04	0.23	28.26	0.18	0.08	9.43	3.31	0.47	0.46			97.66
6	27.18	0.18	1.77		0.15	1.35	0.05	5.4		0	0.03				38.81		36.12
7	0.2	0.03	0		0.01	52.76	0.08	0.71		0.09	0.12				35.69		92.83
8	1.4	0.03	0		0	50.63	0.06	0.89		0.03	0.19				0.002		88.94
9	29.39	27.95	7.1	0	0.02	27.87	0	0.88	0	0.01	0.05	2.72	2.53	0.02			98.55

HUD98-85 Biotite

	SiO2	TiO2	Al2O3	Cr2O3	MgO	CaO	MnO	FeO	BaO	Na2O	K2O	H2O	F	Cl	P2O5	SrO	Total
1	35.04	1.49	18.95	0.06	10.14	0.02	0	18.56	0	0.26	8.9	3.75	0.28	0.01			97.45
2	34.66	1.61	18.74	0.02	10.05	0.01	0.06	19.06	0.07	0.25	8.95	3.71	0.32	0			97.5
3	34.88	1.54	18.56	0.05	10.05	0.05	0	18.73	0.08	0.23	8.77	3.72	0.28	0.02			96.95
4	34.42	1.74	18.48	0.06	10.09	0	0	18.49	0.05	0.27	8.85	3.73	0.2	0.02			96.41
5	33.89	1.41	18.65	0.04	9.97	0.01	0	18.45	0.09	0.28	9.15	3.67	0.26	0			95.87
6	59.38	0	23.85	0.02	0.02	5.8	0	0.45	0	8.37	0.06	4.79	0	0			102.74
7	59.18	0.01	24.19	0	0	6.07	0	0.42	0	8.09	0.1	4.78	0.03	0			102.88
8	58.89	0.02	24.44	0	0.01	6.56	0	0.35	0	7.97	0.05	4.8	0	0			103.07
9	59.07	0.02	24.06	0	0.05	6.39	0	0.43	0.02	8.03	0.14	4.75	0.09	0			103.05

HUD98-86A Biotite

	SiO2	TiO2	Al2O3	Cr2O3	MgO	CaO	MnO	FeO	BaO	Na2O	K2O	H2O	F	Cl	P2O5	SrO	Total
1	46.146	0	36.152	0	0.383	0	0	1.975	0	0.523	10.056	4.386	0.251	0.01			99.882
2	46.303	0.031	35.831	0.01	0.372	0	0	2.009	0	0.511	9.893	4.382	0.247	0			99.589
3	46.272	0.049	36.019	0	0.592	0.007	0	1.941	0.013	0.561	9.904	4.345	0.359	0.002			100.064
4	47.895	0.048	36.997	0	0.418	0.016	0	2.008	0.015	0.524	10	4.51	0.289	0			102.72
5	46.558	0.093	36.223	0	0.275	0.002	0	2.062	0.013	0.489	9.536	4.246	0.585	0.006			100.088

HUD98-86A Muscovite

	SiO2	TiO2	Al2O3	Cr2O3	MgO	CaO	MnO	FeO	BaO	Na2O	K2O	H2O	F	Cl	P2O5	SrO	Total
1	34.47	2.661	18.227	0.027	7.979	0.004	0.111	21.237	0	0.077	9.793	3.629	0.4	0.127			98.742
2	29.206	0.817	19.565		10.086	0.075	0.229	29.249		0.041	2.015				0.021		91.285
3	49.423	0.908	25.389		4.453	0.017	0.068	7.927		0.011	4.871				0.031		93.088
4	28.674	0.853	18.713		8.892	0.11	0.198	27.249		0.038	2.228				0.052		86.986
5	7.846	0.766	6.971		4.344	0	0.129	19.057		0.05	4.571				0.017		43.786
6	24.793	0.035	17.936	0.032	10.863	0.078	0.182	30.122	0.005	0	0.046	3.218	0.277	0.017			87.604
7	25.938	0.069	18.855		10.96	0.082	0.236	30.596		0	0.062				0		86.815

HUD98-87 Biotite

	SiO2	TiO2	Al2O3	Cr2O3	MgO	CaO	MnO	FeO	BaO	Na2O	K2O	H2O	F	Cl	P2O5	SrO	Total
1	31.54	1.17	17.82	0.04	13.71	0.44	0.09	20.68	0	0.02	3.54	3.61	0.26	0.01			92.92
10	33.53	1.33	16.98		12.38	0.15	0.04	19.46		0.08	5.02				0.01		88.96
11	36.49	0.12	24.86		3.17	20.78	0.05	3.33		0	0.04				0.05		88.85
2	35.84	0.15	24.52	0.02	3.46	21.61	0	4.59	0	0.01	0.06	3.95	0.13	0.01			94.36
3	36.7	0.04	25.2	0	2.98	22.53	0	3.96	0	0	0.04	3.99	0.2	0.01			95.65
4	29.92	1.25	17.43	0.02	13.88	0.63	0.04	21.26	0	0.05	2.79	3.5	0.29	0.02			91.07
5	30.45	1.2	17.3	0.06	14.4	0.08	0	20.47	0	0.04	3.39	3.55	0.23	0.03			91.18
6	36.28	0.05	25.35	0.01	3.4	22.2	0	2.45	0	0	0.02	3.86	0.38	0			94
7	31.79	1.29	17.58	0.06	14.59	0.19	0	20.02	0	0	3.57	3.62	0.27	0.01			92.97
8	44.44		35.76			17.54		0.2	0	1.14	0.03					0.04	99.15
9	34.78	1.59	17.69		12.51	0.29	0.08	18.08		0.08	5.5				0.03		90.64

HUD98-87 Hornblende

	SiO2	TiO2	Al2O3	Cr2O3	MgO	CaO	MnO	FeO	BaO	Na2O	K2O	H2O	F	Cl	P2O5	SrO	Total
1	41.08	0.41	16.9		7.81	10.49	0.11	17.27		1.23	0.4	1.98					97.68
10	25.73	0.11	20.51		11.76	1.26	0.12	26.57		0.11	0.06				0.02		86.25
11	49.14	0.69	34.2		0.9	0.07	0.02	1.86		0.31	7				0.01		94.21
12	11.96	0.03	8.4		0.76	47.03	0.13	1.88		0.01	0.05				0		70.26
2	41.36	0.37	17.59		7.52	10.68	0.13	17.14		1.26	0.42	1.99					98.45
3	41.93	0.32	16.81		7.8	10.95	0.12	16.92		1.17	0.34	2					98.35
4	42.1	0.43	16.34		8	10.7	0.16	16.73		1.22	0.37	1.99					98.03
5	43.97		35.74			17.8		0.08	0.01	1.08	0.02					0.05	98.74
6	45.14		35.56			17.47		0.24	0.04	1.1	0					0.08	99.62
7	36.89	0.02	21.68		2.69	5.52	1.84	31.93		0.02	0				0.01		100.6
8	44.17	0.37	19.08		9.55	10.59	0.11	16.33		1.17	0.35				0.01		101.73
9	40.62	0.47	17.32		7.92	10.09	0.13	17.56		1.13	0.37				0.03		95.61

HUD98-88 Biotite

	SiO2	TiO2	Al2O3	Cr2O3	MgO	CaO	MnO	FeO	BaO	Na2O	K2O	H2O	F	Cl	P2O5	SrO	Total
1	33.69	1.42	18.82	0.04	9.23	0.09	0	20.19	0.01	0.26	8.21	3.62	0.34	0.02			95.95
10	44.6		36.71			0.01		1.29	0.42	1.4	8.88					0.04	93.36
11	34.6		18.93			0		20.84	0.04	0.23	8.55					0	83.19
12	34.75		19.01			0.03		20.75	0.05	0.24	8.41					0	83.23
13	34.56		19			0		20.95	0.05	0.29	8.56					0	83.41
2	34.64	1.44	18.86	0.05	9.38	0.08	0	20.33	0	0.21	7.86	3.69	0.33	0.02			96.89
3	67.7	0.02	20.97		0.15	0.32	0	0.31		0.48	10.25				0.02		100.23
4	61.58	0.01	25.14		0	5.58	0.02	0.1		8.35	0.09				0		100.89
5	35.31	1.48	19.32		8.8	0.01	0.03	21.35		0.19	8.37				0		94.86
6	36.2	1.54	20.39		9.61	0.05	0.05	20.82		0.23	7.87				0		96.77
7	44.67		36.47			0.03		1.26	0.39	1.32	7.88					0.02	92.03
8	61.73		25.08			5.35		0.17	0	8.68	0.08					0.1	101.19
9	45.6		37.22			0.04		3.31	0.35	1.56	8.32					0.02	96.43

HUD98-88 Muscovite

	SiO2	TiO2	Al2O3	Cr2O3	MgO	CaO	MnO	FeO	BaO	Na2O	K2O	H2O	F	Cl	P2O5	SrO	Total
1	47.4	0.33	36.92	0.06	0.5	0.02	0	na	0.98	1.12	9.21	4.61	0	0			101.16
10	50.05	0.39	39.33		0.52	0.03	0	1.07		1.34	7.33				0.04		100.06
11	25.09	0.08	23.89		13.09	0.07	0.09	26.56		0.03	0.12				0.04		89.06
12	0.21	56.33	0.08		0.07	0.05	0.33	33.96		0	0.14				0.02		91.2
2	47.79	0.31	36.78	0.01	0.63	0.08	0	na	1.17	1.09	8.83	4.62	0.02	0			101.33
3	34.51	1.55	18.91	0	9.29	0.01	0	na	21.01	0.22	9.2	3.74	0.28	0.01			98.74
4	45.81	0.36	37	0.04	0.47	0.03	0	na	0.95	1.12	8.94	4.47	0.1	0.01			99.3
5	100.21	0	0	0.06	0	0.02	0	na	0.05	0	0	5.47	0	0			105.82
6	99.36	0.02	0.01	0.01	0	0.01	0	na	0.05	0	0.01	5.42	0	0.01			104.91
7	24.04	0.05	23.15		13.49	0.03	0.05	26.59		0.04	0.03				0		87.49
8	47.98	0.37	38.58		0.43	0.02	0	0.96		1.31	6.71				0.01		96.33
9	49.85	0.41	39.26		0.48	0.02	0	1		1.21	7.13				0.02		99.37

HUD98-89 Biotite

	SiO2	TiO2	Al2O3	Cr2O3	MgO	CaO	MnO	FeO	BaO	Na2O	K2O	H2O	F	Cl	P2O5	SrO	Total
1	37.75	1.2	18.21	0.01	17	0	0.01	10.05	0.42	0.58	8.61	3.73	0.73	0			98.31
2	37.56	1.14	18.09	0	16.69	0	0.01	9.75	0.44	0.54	8.78	3.72	0.67	0			97.4
3	35	1.06	16.67	0.01	15.74	0	0.05	9.63	0.17	0.48	8.58	3.56	0.47	0			91.4
4	37.75	1.09	18.1	0.01	17	0.01	0.05	9.85	0.18	0.54	8.8	3.79	0.58	0			97.74
5	37.94	1.27	19.03		16.61	0.01	0.03	10.16		0.54	7.16				0.02		92.78

HUD98-90 Biotite

	SiO2	TiO2	Al2O3	Cr2O3	MgO	CaO	MnO	FeO	BaO	Na2O	K2O	H2O	F	Cl	P2O5	SrO	Total
1	35.32	1.32	18.35	0	9.78	0	0	na	20.83	0.35	9.27	3.65	0.54	0			99.42
10	24.96	0.1	23.1		12.94	0.07	0.05	26.42		0.03	0.2				0.03		87.9
11	34.4	1.45	17.98	0.03	9.63	0.02	0	na	21.23	0.37	9.31	3.56	0.59	0.05			98.6
2	35	1.41	18.38	0.02	9.86	0.01	0	na	21.13	0.39	9.28	3.59	0.66	0.02			99.76
3	35.31	1.34	18.46	0	9.68	0.01	0	na	21.11	0.4	9.33	3.61	0.64	0			99.9
4	35.09	1.52	18.02	0.04	9.85	0.02	0.02	na	21.08	0.31	9.53	3.58	0.66	0.02			99.75
5	24.09	0.09	23.79		13.09	0.02	0.05	27.97		0	0.06				0.05		89.2
6	23.74	0.11	23.58		12.77	0.03	0.05	27.81		0.03	0.02				0.01		88.19
7	34.78	1.25	18.16		9.53	0.02	0.03	20.73		0.29	8.89				0.03		93.69
8	22.99	0.07	23.76		11.99	0.02	0.04	28.17		0	0.05				0.04		87.11
9	49.82	0.28	39.11		0.79	0.06	0	1.3		1.11	7.06						99.57

Electron Micoprobe Apatite Anayses

HUD98-63

P2O5	SiO2	SO2	CaO	MnO	FeO	SrO	H2O	F	Cl	Total
41.68	0.02	0	55.53	0.14	0.32	0.04	0.43	2.83	0.03	101.02
40.31	0.05	0.05	54.43	0.18	0.37	0.01	0.42	2.67	0.18	98.66
41.07	0.04	0.25	54.47	0.15	0.46	0.01	0.41	2.81	0.05	99.72
40.36	0.16	0.2	54.34	0.2	0.56	0.08	0.53	2.51	0.07	99
41.22	0.03	0.02	55	0.27	0.5	0.04	0.38	2.89	0.05	100.4
41.03	0.01	0.02	55.21	0.24	0.44	0.04	0.36	2.94	0.04	100.33
40.1	0.03	0.03	54.17	0.22	0.44	0.08	0.54	2.48	0.04	98.15
40.94	0.02	0.01	55.71	0.13	0.16	0.05	0.19	3.3	0.02	100.54
41.71	0.04	0.04	55.29	0.16	0.34	0.08	0.48	2.71	0.04	100.88
41.71	0.03	0.04	55.28	0.19	0.17	0	0.19	3.33	0.04	100.98
39.98	0	0.1	54.65	0.2	0.48	0.09	0.32	2.92	0.06	98.8
38.06	0.18	0.37	52.29	0.21	0.4	0	0.38	2.65	0.08	94.62

HUD98-79

P2O5	SiO2	SO2	CaO	MnO	FeO	SrO	H2O	F	Cl	Total
41.29	0.06	0	54.9	0.14	0.03	0	0.16	3.35	0.02	99.95
42.17	0.05	0.01	56.02	0.2	0.04	0	0	3.83	0	102.32
41.66	0.07	0.01	53.8	0.25	0.01	0.01	0.2	3.27	0.02	99.31
41.21	0.05	0.01	54.49	0.25	0.12	0	0.16	3.35	0.01	99.64
41.64	0.06	0.02	54.98	0.13	0.07	0	0.17	3.36	0.01	100.44
40.28	0.16	0.06	53.18	0.18	0.11	0.01	0.2	3.15	0.05	97.38
41.8	0.04	0.01	54.43	0.17	0.08	0.03	0.1	3.5	0.01	100.17
41.16	0.03	0.01	54.34	0.22	0.11	0.01	0.23	3.18	0.04	99.33
41.3	0.03	0.01	55.48	0.12	0.07	0.05	0.16	3.38	0.01	100.6
41.65	0.08	0.02	54.51	0.28	0.17	0.04	0.13	3.44	0.01	100.33
40.73	0.11	0.01	53.69	0.25	0.07	0	0.27	3.07	0.03	98.22
40.69	0.13	0.03	53.17	0.27	0.19	0.04	0.02	3.57	0.03	98.15

HUD98-82

P2O5	SiO2	SO2	CaO	MnO	FeO	SrO	H2O	F	Cl	Total
42.1	0	0	55.62	0.02	0.08	0	0.25	3.24	0	101.32
42.03	0.02	0.02	55.49	0.1	0.04	0	0.38	2.96	0.01	101.04
41.77	0.02	0.04	55.24	0.07	0	0	0.2	3.3	0.01	100.66
41.39	0.09	0.01	55.48	0.07	0.02	0.03	0.14	3.43	0	100.66
41.73	0.03	0.01	55.51	0.04	0.03	0.05	0.18	3.37	0	100.94
40.63	0.19	0.04	54.61	0.07	0.08	0.03	0	3.69	0.07	99.41
41.59	0.06	0	56	0.02	0.04	0.03	0.2	3.32	0	101.26
41.44	0.04	0	55.8	0.08	0.06	0	0.09	3.54	0	101.06
41.24	0.05	0	56.13	0.01	0	0.03	0	4.14	0.01	101.63
41.47	0.04	0.02	55.35	0.02	0	0.05	0.09	3.53	0.01	100.58

HUD98-83

P2O5	SiO2	SO2	CaO	MnO	FeO	SrO	H2O	F	Cl	Total
40.05	0.05	0.02	54.03	0.02	0.14	0.02	0.05	3.47	0.09	97.94
39.83	0.19	0.1	53.2	0.02	0.3	0.05	0.19	3.15	0.09	97.12
41.8	0.02	0.04	54.66	0.02	0.21	0.01	0.04	3.59	0.11	100.5
41.52	0.02	0.01	54.93	0.01	0.1	0.01	0	3.77	0.05	100.43
41.52	0.24	0.03	55.12	0.03	0.17	0.02	0	3.9	0.06	101.08
40.91	0.04	0.09	54.32	0.01	0.14	0.05	0	3.84	0.05	99.44
37.97	0.21	0.05	53.78	0.04	0.12	0	0	3.65	0.08	95.89
41.16	0.04	0.01	55.14	0.03	0.11	0.04	0	3.69	0.08	100.3
41.71	0.03	0.02	54.65	0	0.13	0.04	0	3.95	0.09	100.61
38.99	0.12	0.02	53.58	0	0.15	0	0	3.54	0.15	96.55
41.92	0.02	0.02	54.15	0.05	0.17	0.06	0.01	3.68	0.05	100.12
41.71	0.15	0.02	54.47	0.03	0.19	0.01	0	3.9	0.05	100.54

Appendix D

Explanation of Appendix D

The following section contains electron microprobe backscattered images. A scale bar is shown in the bottom left corner of each image. Sample numbers and points can be correlated with the tables in Appendix C.

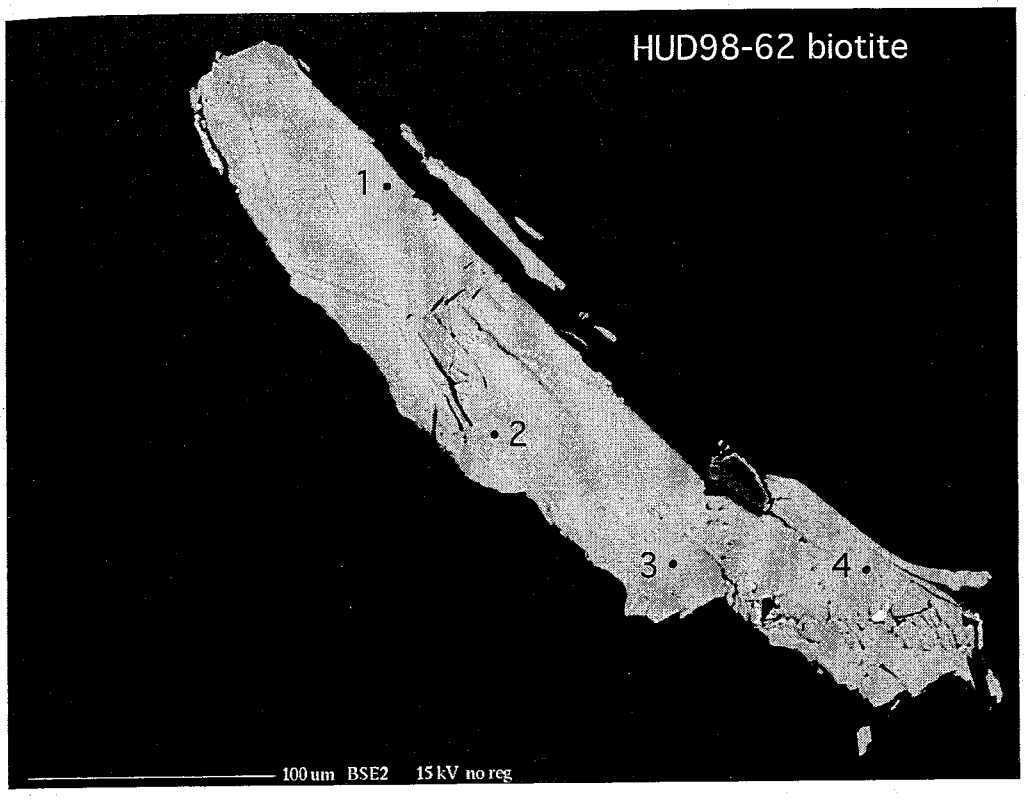
HUD98-62 biotite
1
2
3
4
100 um BSE2 15 kV no reg

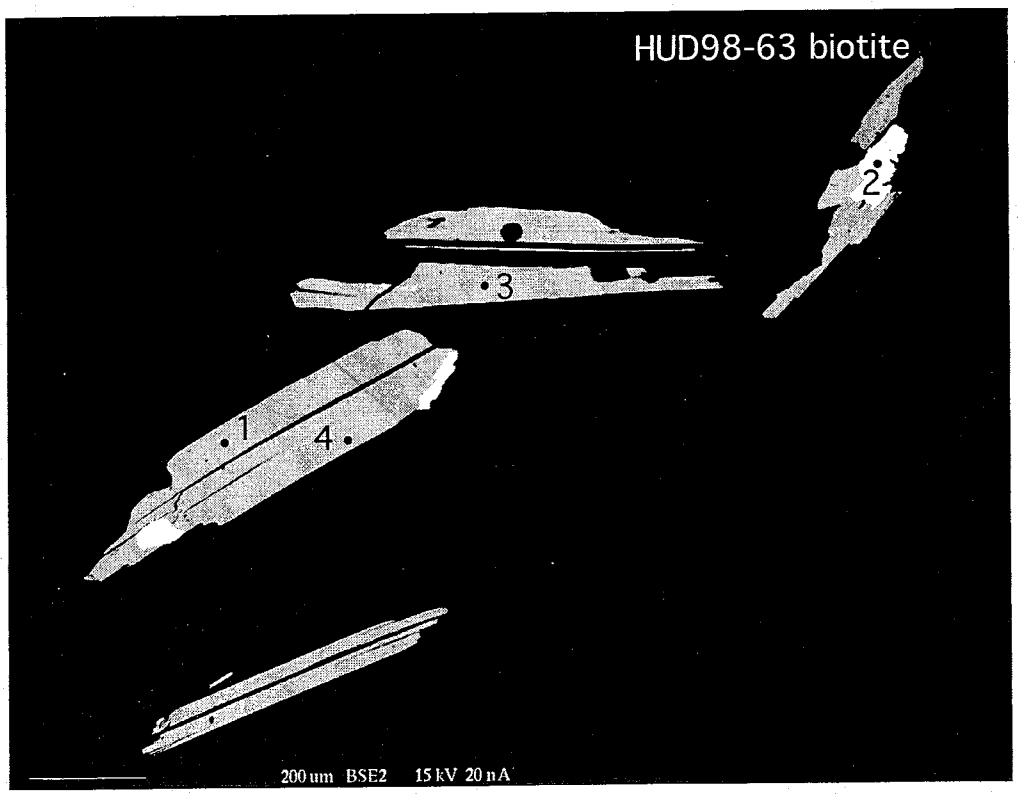
HUD98-63 biotite
1
2
3
4
200 um BSE2 15 kV 20 nA

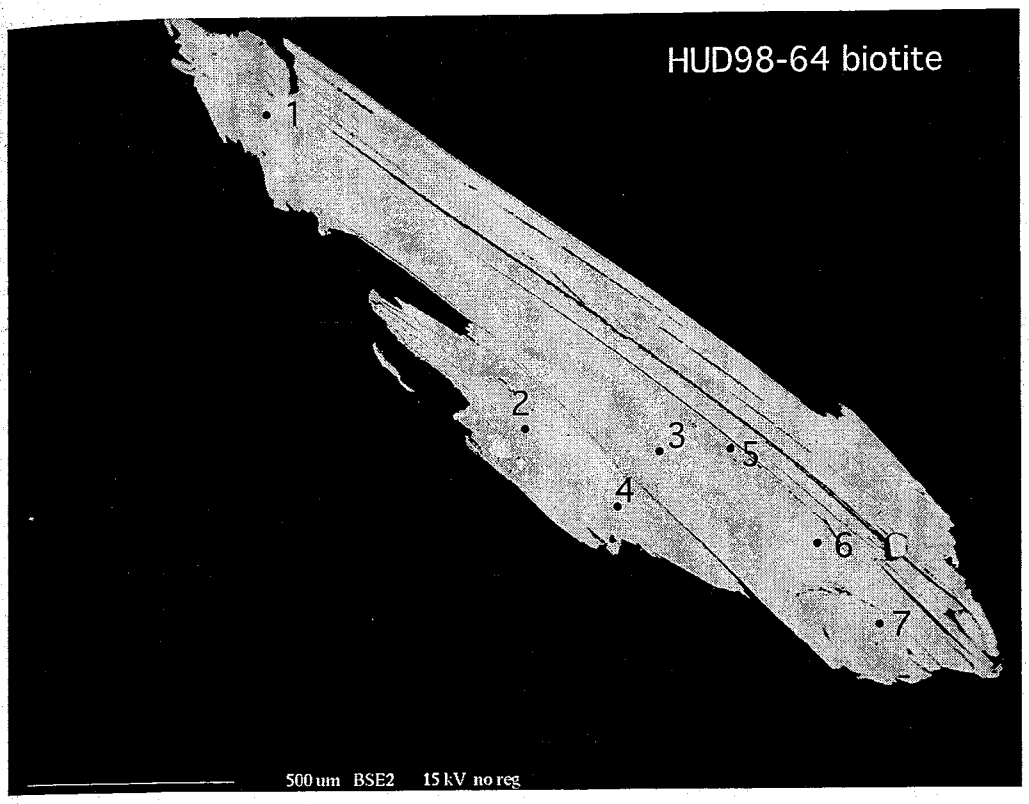
HUD98-64 biotite
1
2
3
4
5
6
7
500 um BSE2 15 kV no reg

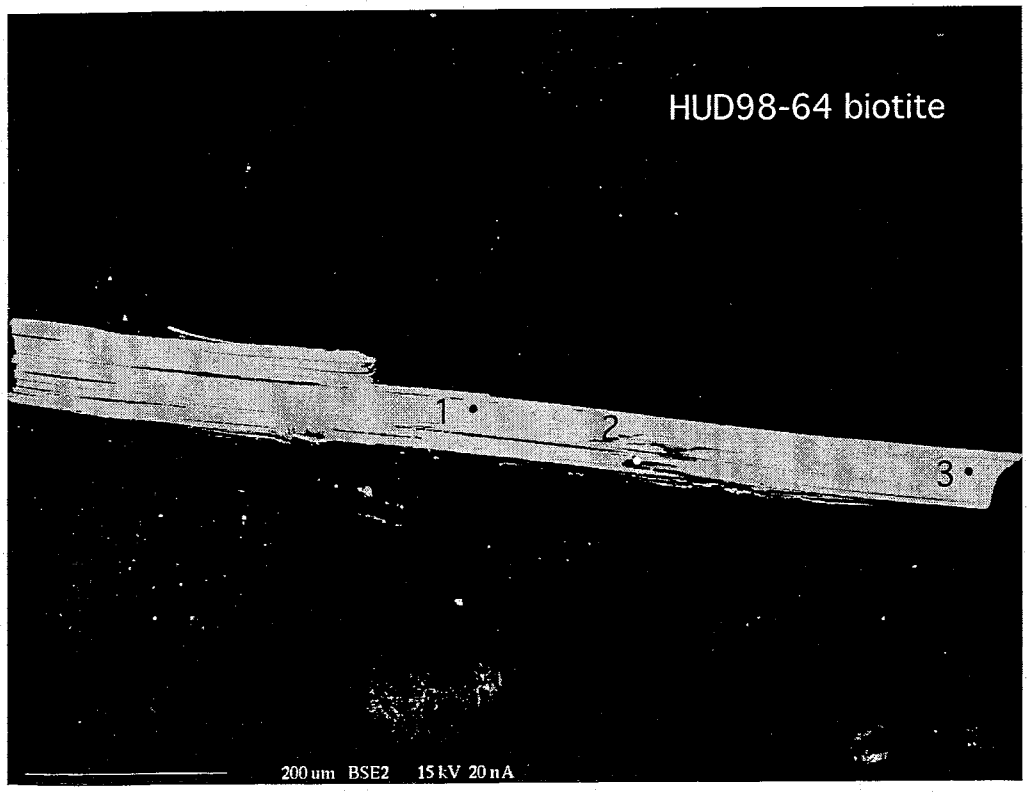
HUD98-64 biotite
1
2
3
200 um BSE2 15 kV 20 nA


10
9
8
7
2
3
1
5
6
500 um BSE2 15 kV 20 nA
HUD98-72 biotite

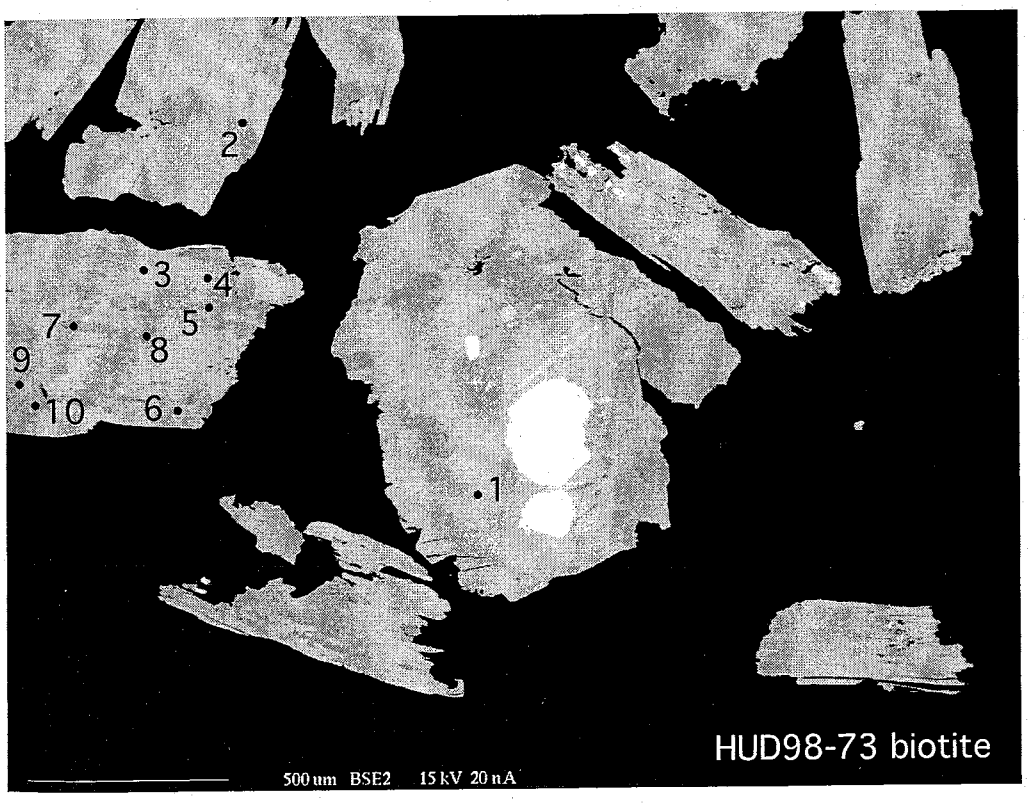
2
3
4
7
5
8
9
10
6
1
500 um BSE2 15 kV 20 nA
HUD98-73 biotite

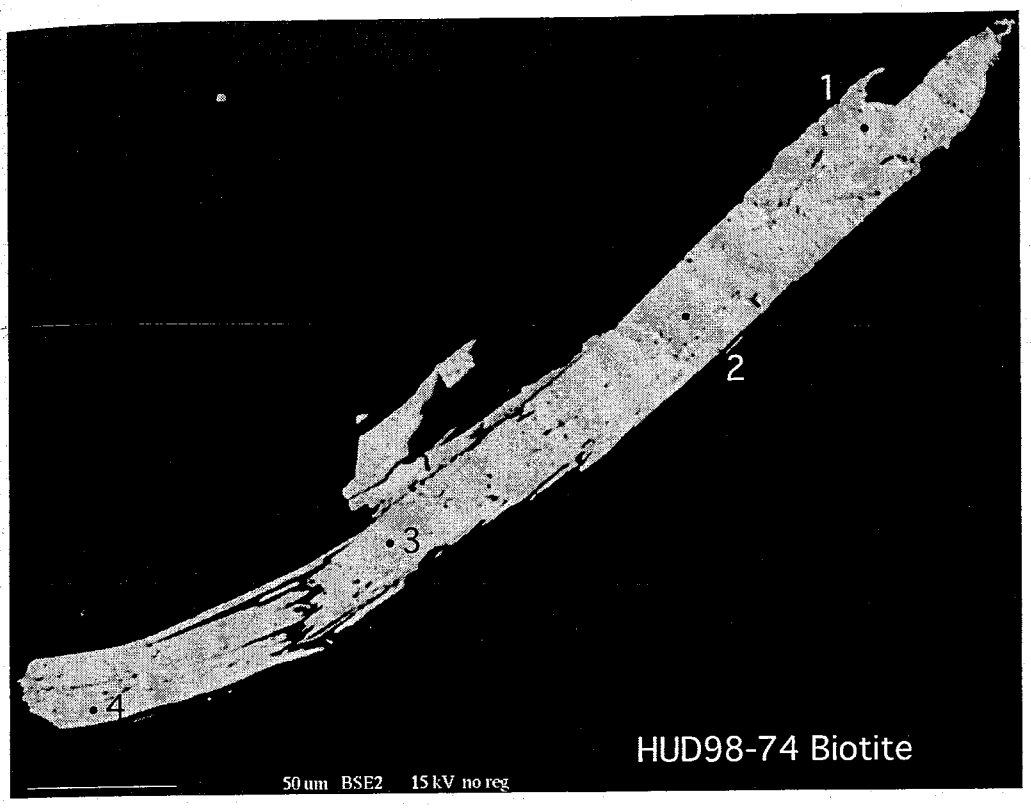
1
2
3
4
HUD98-74 Biotite
50 um BSE2 15 kV no reg

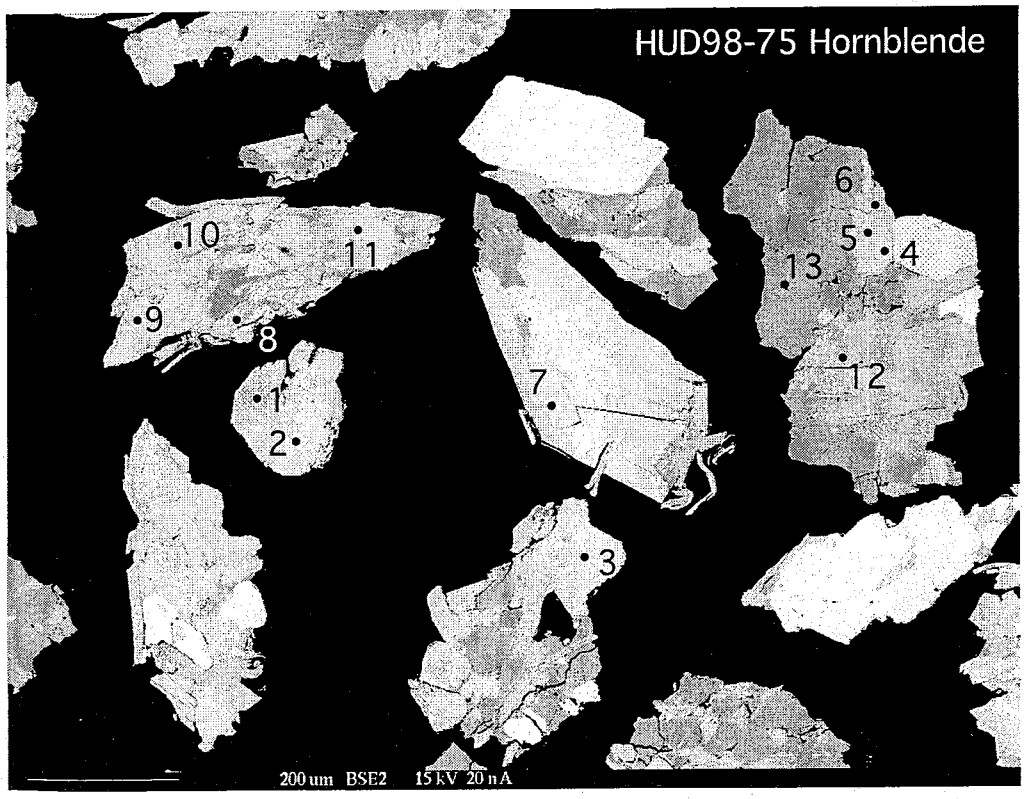
HUD98-75 Hornblende
1
2
3
4
5
6
7
8
9
10
11
12
13
200 um BSE2 15 kV 20 nA

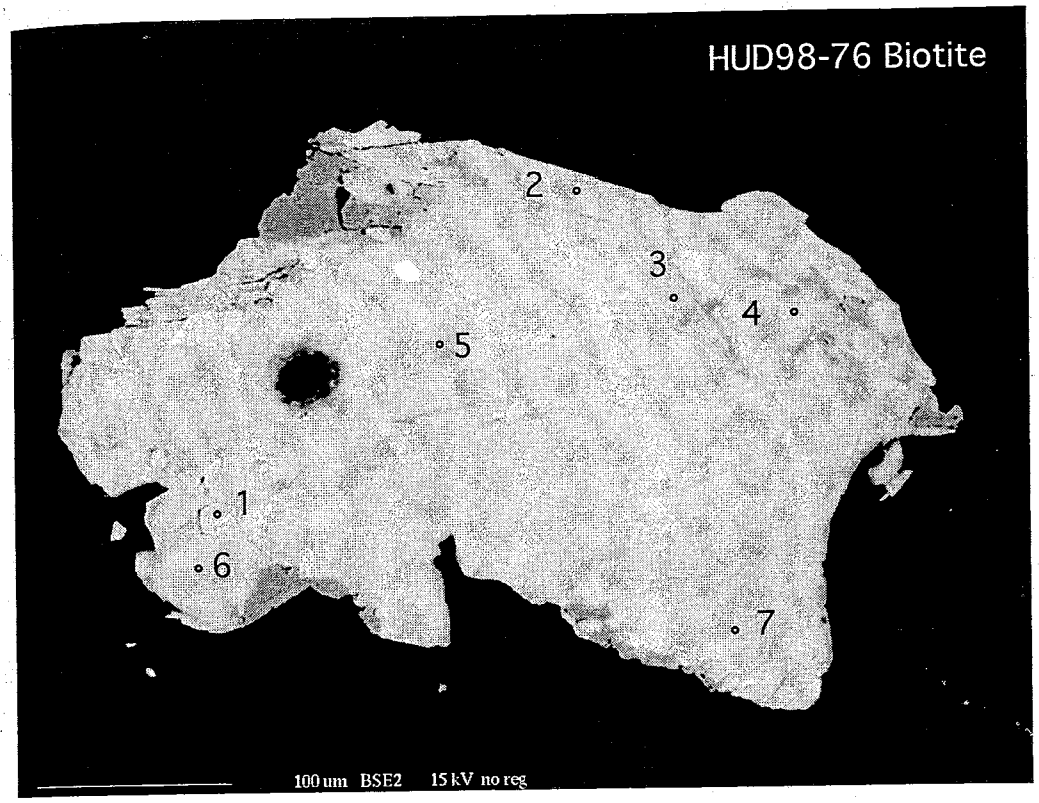
HUD98-76 Biotite
1
2
3
4
5
6
7
100 um BSE2 15 kV no reg


HUD98-77 Biotite
1
2
3
4
5
6
7
100 um BSE2 15 kV no reg

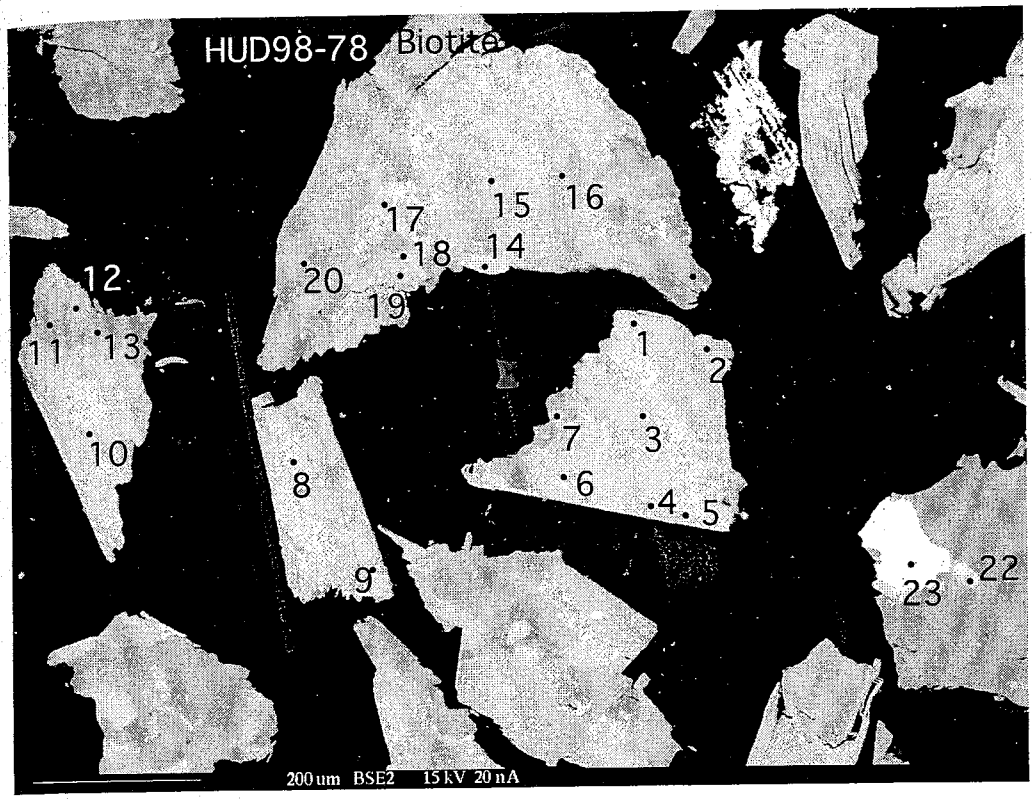
HUD98-78 Biotite
17
15
16
18
14
12
20
19
11
13
1
2
7
3
10
8
6
4
5
9
23
22
200 um BSE2 15 kV 20 nA

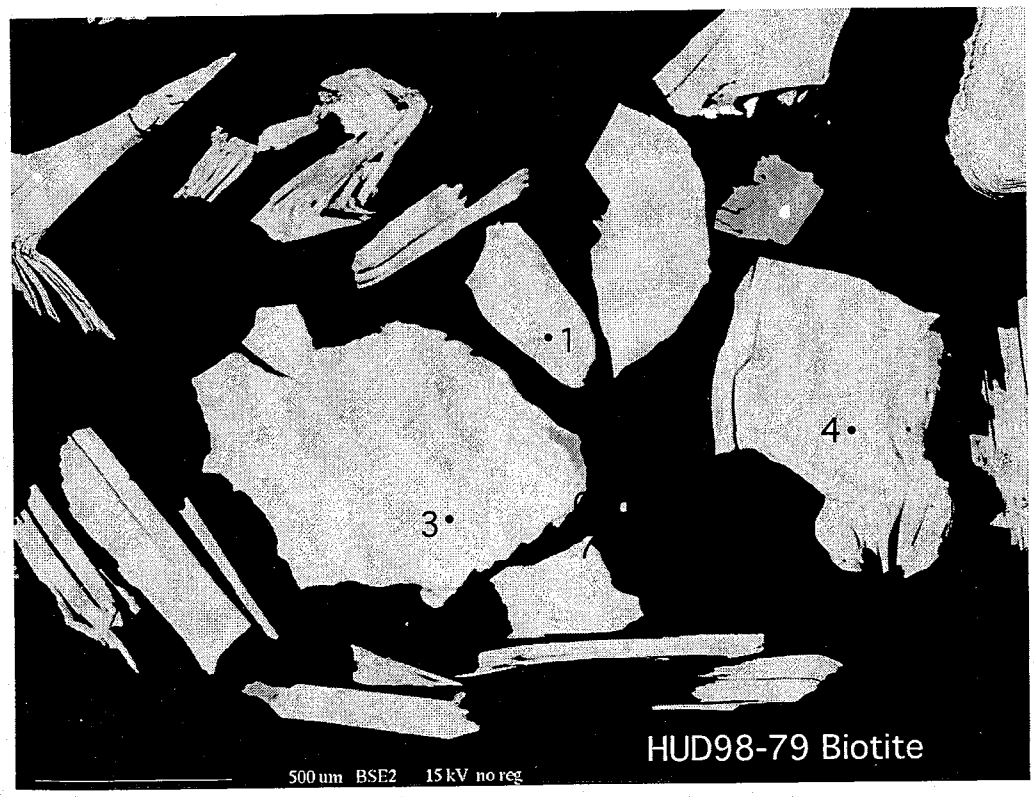
1
4
3
500 um BSE2 15 kV no reg
HUD98-79 Biotite

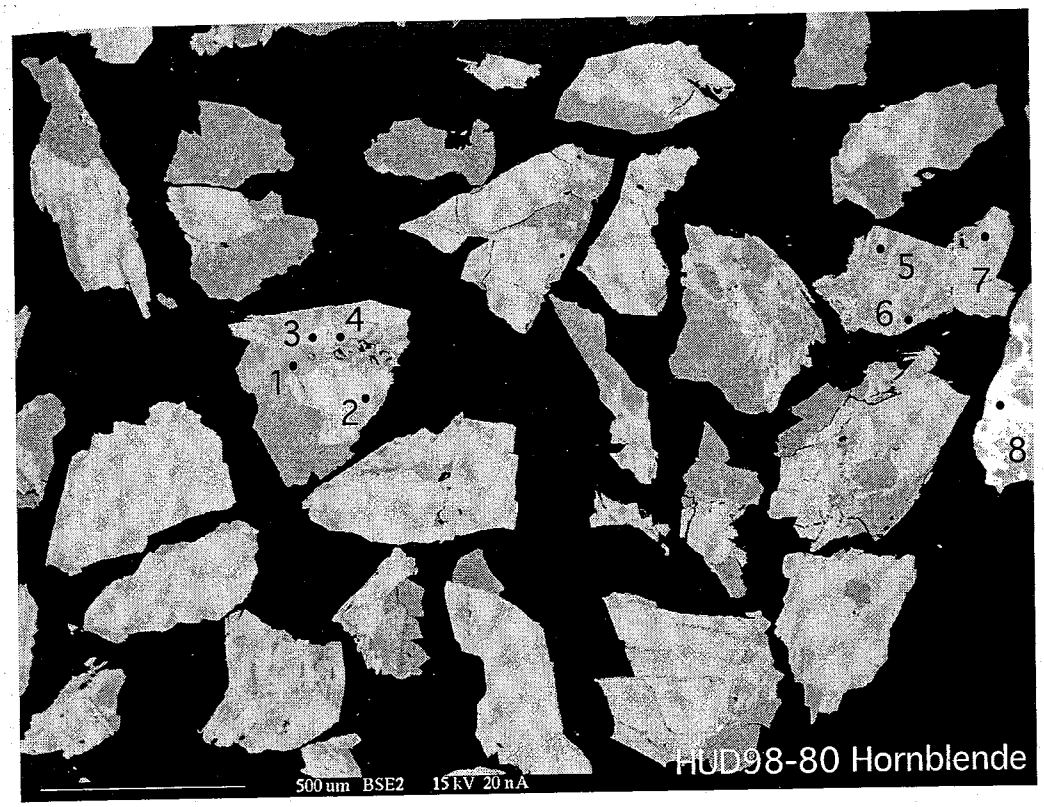
1
2
3
4
5
6
7
8
500 um BSE2 15 kV 20 nA
HUD98-80 Hornblende


1
3
4
5
7
8
9
500 um BSE2 15 kV 20 nA
HUD98-80 Biotite

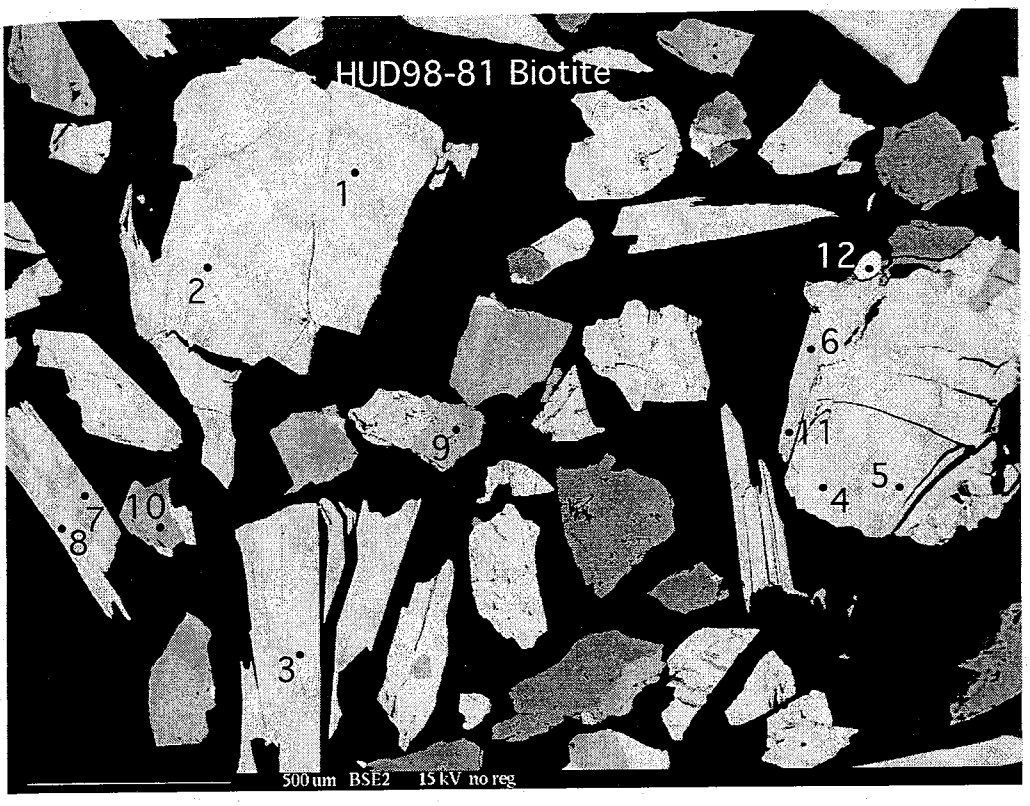
HUD98-81 Biotite
1
2
3
4
5
6
7
8
9
10
11
12
500um BSE2 15kV no reg

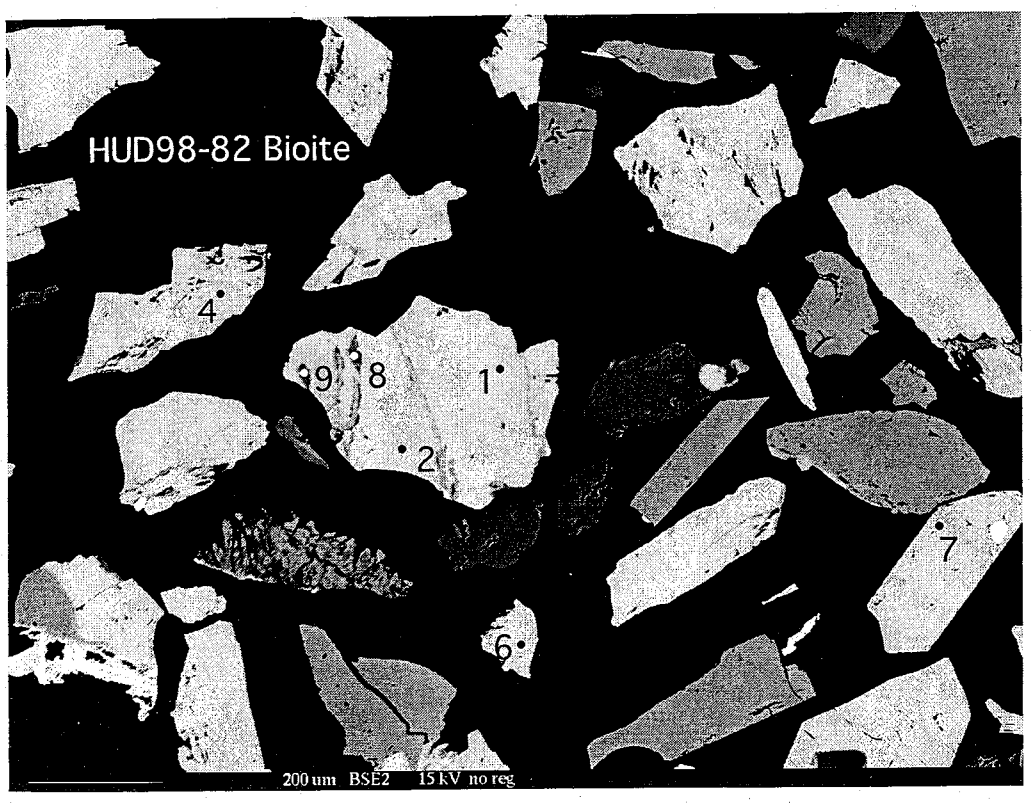
HUD98-82 Bioite
1
2
3
4
6
7
8
9
200um BSE2 15kV no reg

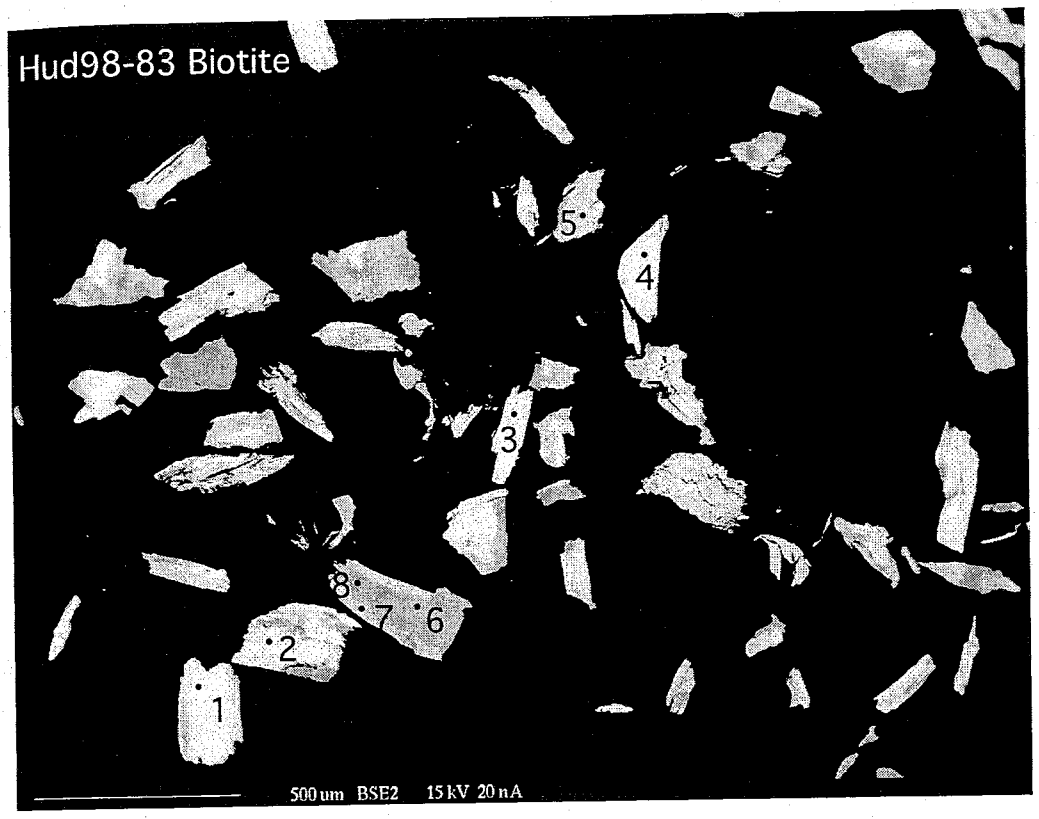
Hud98-83 Biotite
1
2
3
4
5
6
7
8
500 um BSE2 15 kV 20 nA

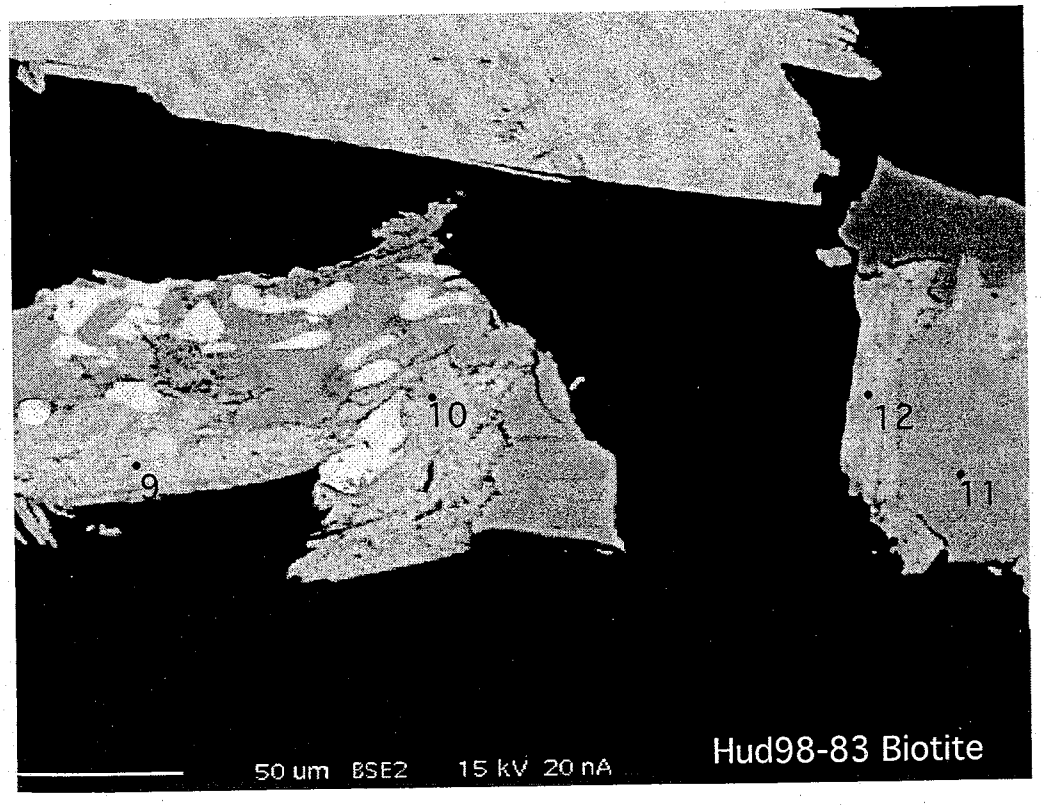
9
10
11
12
50 um BSE2 15 kV 20 nA
Hud98-83 Biotite


HUD98-84 Biotite
11
9
10
12
2
5
3
6
8
4
7
500 um BSE2 15 kV no reg


4
5
6
2
1
7
9
8
3
500 um BSE2 15 kV no reg
HUD98-85 Biotite

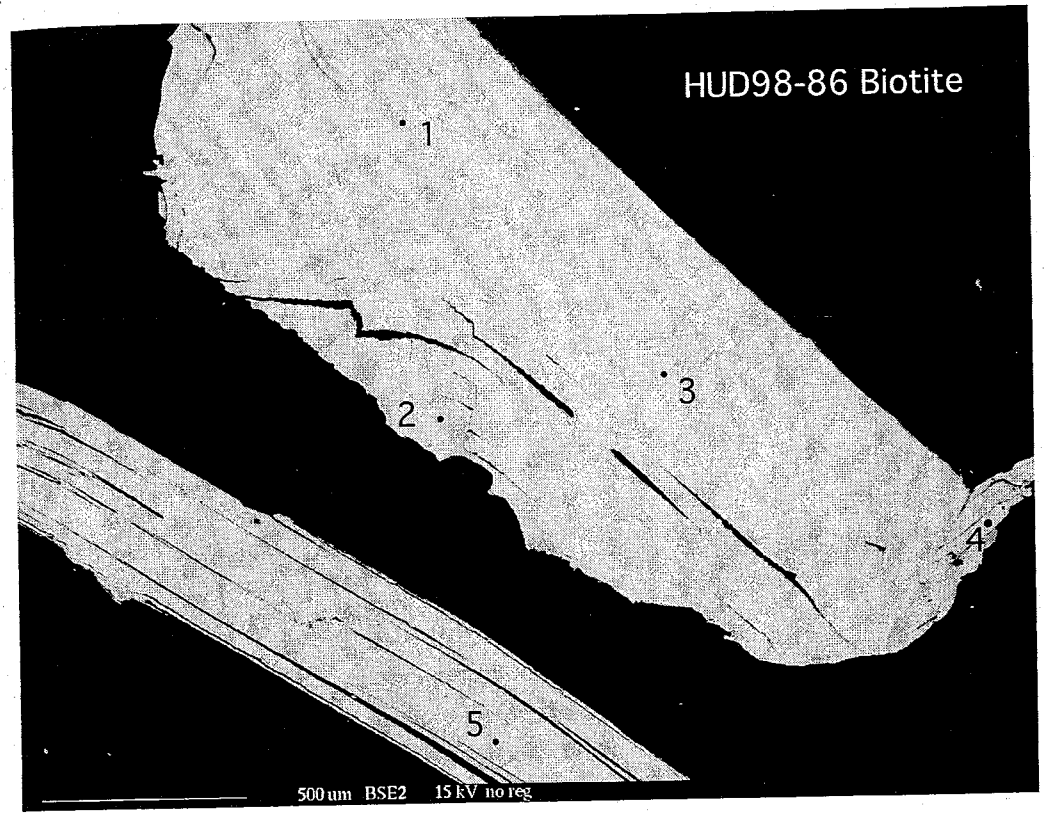
HUD98-86 Biotite
1
2
3
4
5
500 um BSE2 15 kV no reg

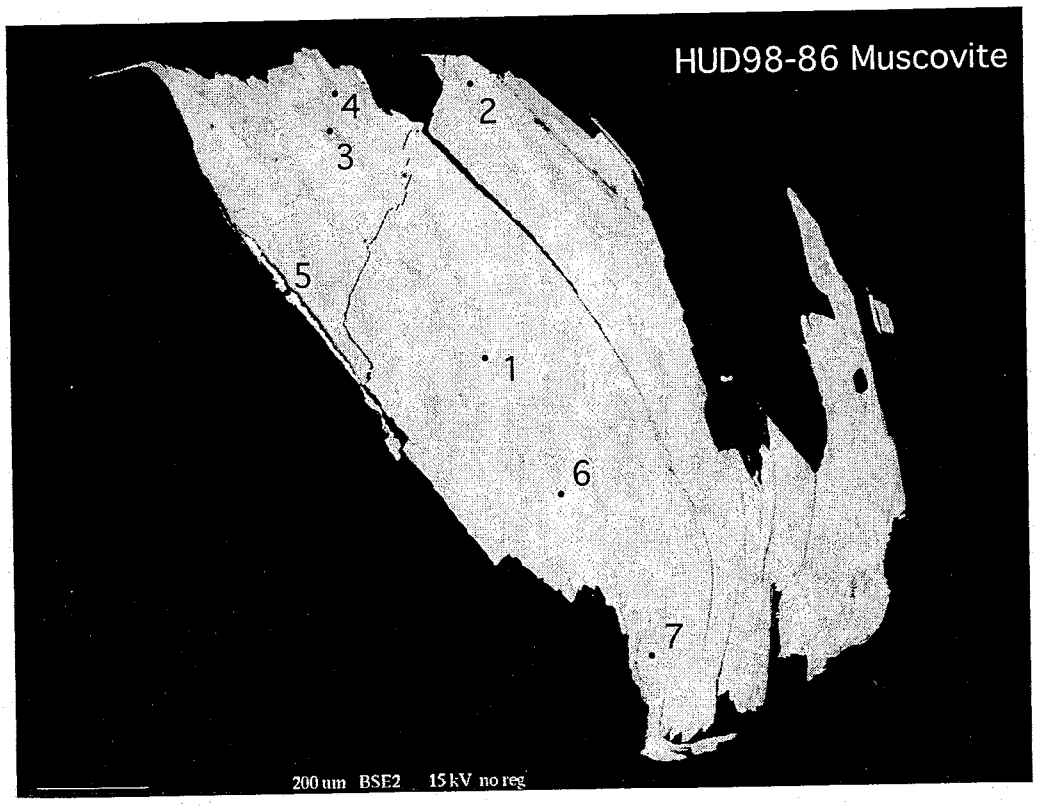
HUD98-86 Muscovite
1
2
3
4
5
6
7
200 um BSE2 15 kV no reg

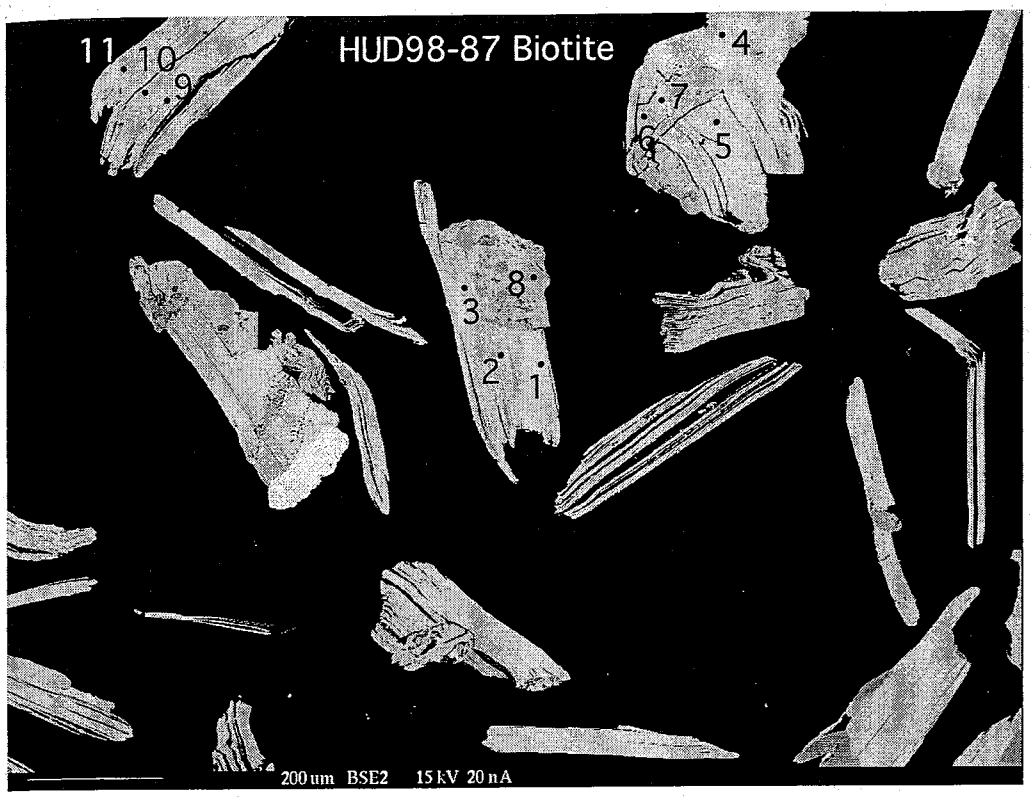
HUD98-87 Biotite
11
10
9
4
7
6
5
8
3
2
1
200um BSE2 15kV 20nA

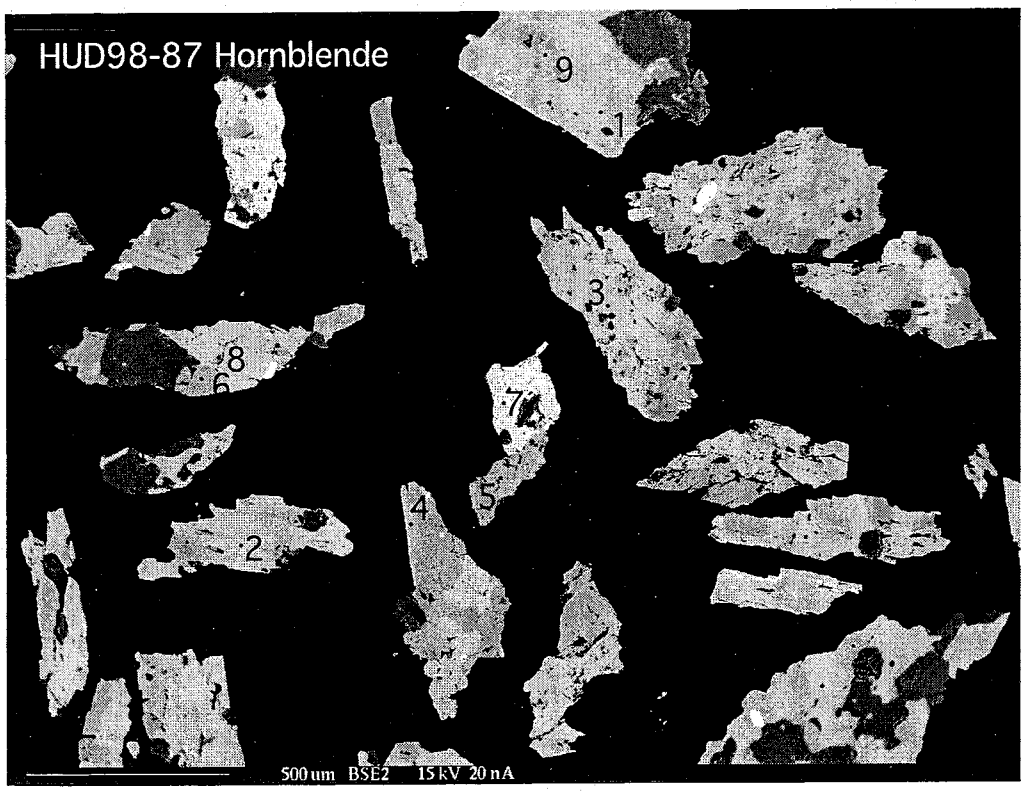
HUD98-87 Hornblende
9
1
3
8
6
7
5
4
2
500um BSE2 15kV 20nA

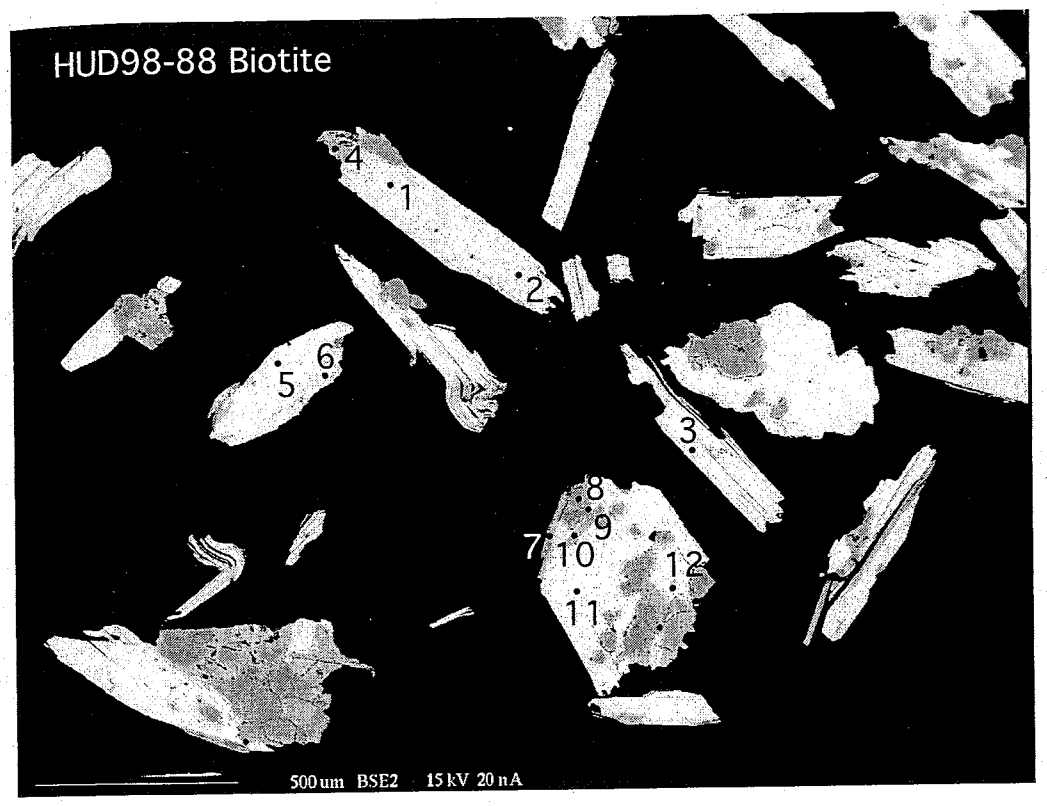
HUD98-88 Biotite
4
1
2
5
6
3
8
9
7
10
12
11
500 um BSE2 15 kV 20 nA

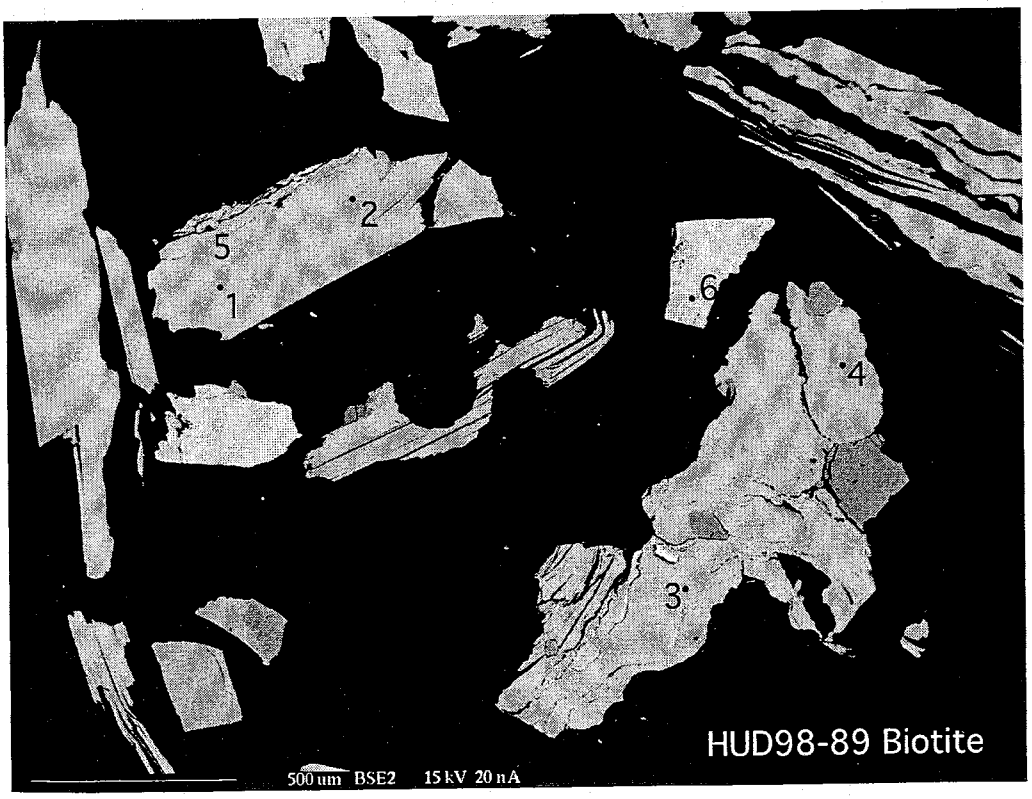
2
5
1
6
4
3
HUD98-89 Biotite
500 um BSE2 15 kV 20 nA


HUD98-88 Muscovite
3
1
5
6
8
500 um BSE2 15 kV no reg

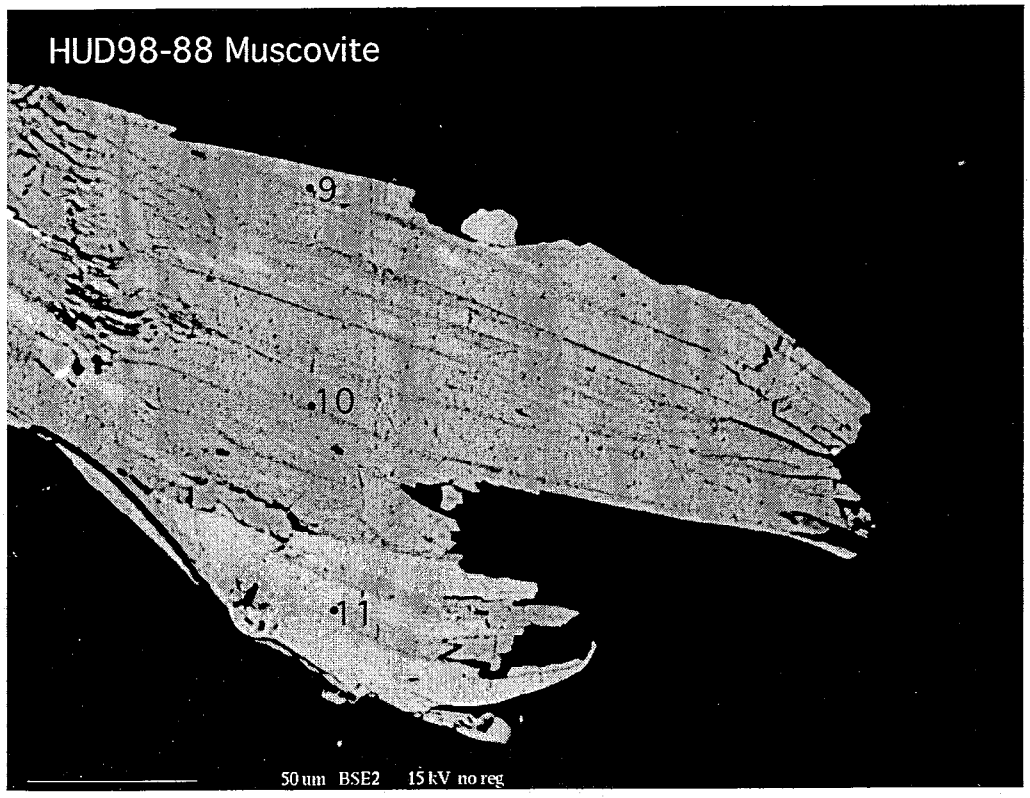
HUD98-88 Muscovite
9
10
11
50 um BSE2 15 kV no reg

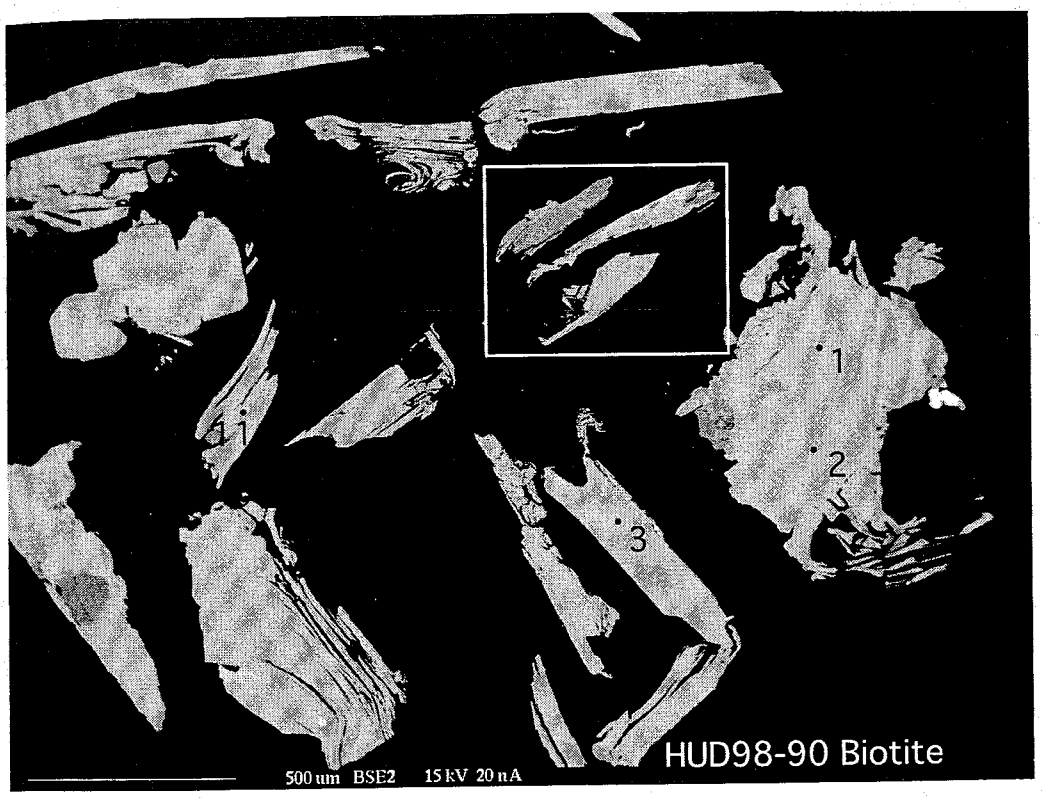
1
2
3
4
500 um BSE2 15 kV 20 nA
HUD98-90 Biotite

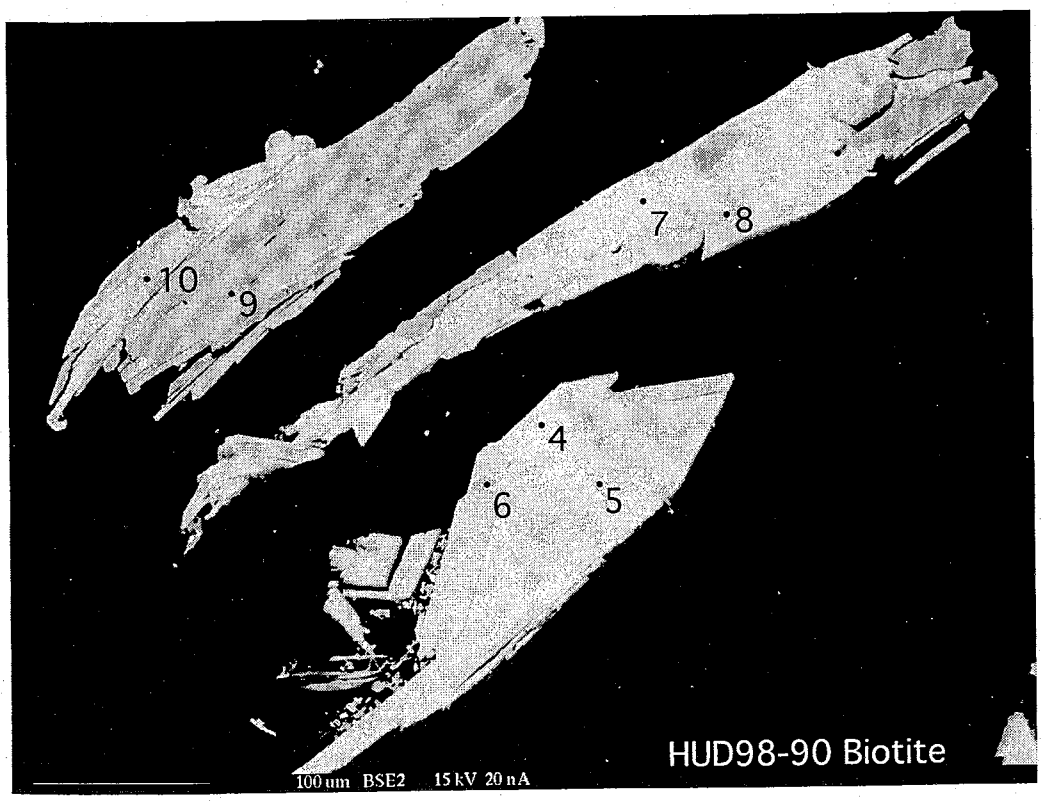
7
8
10
9
4
6
5
100 um BSE2 15 kV 20 nA
HUD98-90 Biotite

Appendix E

Explanation of Appendix E

The following section contains all of the analytical data for the 6 K-feldspars analyzed in this study. Information for the individual samples includes sample number, lab ID number, J-value, and irradiation ID number. Irradiation ID numbers can be correlated to Table A to determine nuclear interference correction factors. All errors are at the 1σ level and propagate errors in j-values, mass discrimination and system blank measurements.

ID	Temp (°C)	$^{40}Ar/^{39}Ar$	$^{37}Ar/^{39}Ar$	$^{36}Ar/^{39}Ar$ (x 10^{-3})	$^{39}Ar_K$ (x 10^{-16} mol)	K/Ca	$^{40}Ar^*$ (%)	^{39}Ar (%)	Age (Ma)	±1σ (Ma)	Time (min)
HUD-98-69, K-feldspar, 1.64 mg, J=0.0163017, NM-107, Lab#=50326-01											
A	450	115.6	0.0084	10.50	8.49	61.1	97.3	0.7	1878.5	3.3	14.8
B	450	36.10	0.0102	0.9531	6.72	50.2	99.1	1.2	829.3	3.5	24.6
C	500	40.00	0.0117	0.4542	17.2	43.8	99.6	2.5	902.8	1.9	14.3
D	500	39.58	0.0138	0.2084	13.9	37.0	99.8	3.6	896.6	2.2	24.4
E	550	51.96	0.0144	0.4981	20.6	35.5	99.7	5.2	1104.2	1.9	14.8
F	550	42.38	0.0096	0.3955	14.9	53.4	99.7	6.4	945.1	2.0	24.8
G	600	52.56	0.0046	0.5966	19.7	110.9	99.6	7.9	1113.3	1.8	14.7
H	600	43.95	0.0023	0.1347	14.4	217.1	99.8	9.0	973.6	2.0	24.8
I	650	55.71	0.0018	0.7451	19.3	285.4	99.6	10.5	1161.9	1.8	15.1
J	650	44.13	0.0020	0.1159	15.4	257.7	99.9	11.7	976.6	2.0	25.2
K	700	47.52	0.0020	0.4201	19.4	261.6	99.7	13.2	1032.3	1.8	14.9
L	700	44.09	0.0020	0.2067	16.9	250.6	99.8	14.5	975.6	2.1	25.0
M	750	45.74	0.0019	0.1926	19.8	263.5	99.8	16.1	1003.6	1.7	15.5
N	750	43.95	0.0028	0.2694	17.2	183.7	99.8	17.4	972.8	1.9	25.5
O	800	46.12	0.0023	0.1230	7.98	223.5	99.9	18.0	1010.4	2.8	3.4
P	850	51.30	0.0028	0.7075	18.8	185.2	99.5	19.5	1092.6	1.8	3.8
Q	900	48.69	0.0028	0.2593	25.1	180.5	99.8	21.4	1052.3	1.5	4.1
R	950	47.92	0.0038	0.2510	27.2	135.0	99.8	23.5	1039.8	1.4	3.6
S	1000	49.07	0.0032	0.3083	27.7	160.1	99.8	25.7	1058.5	1.7	3.8
T	1050	52.63	0.0034	0.2640	29.8	149.3	99.8	28.0	1115.9	1.8	3.9
U	1100	56.67	0.0022	0.5037	22.1	235.4	99.7	29.7	1177.7	1.7	3.4
V	1100	62.82	0.0036	0.5392	43.9	143.1	99.7	33.2	1269.4	1.7	25.4
W	1100	69.78	0.0026	0.7274	43.9	197.6	99.7	36.6	1367.2	3.9	54.7
X	1100	73.70	0.0028	1.110	50.3	183.5	99.5	40.5	1418.9	3.0	114.7
Y	1100	75.36	0.0028	1.220	62.9	180.0	99.5	45.4	1440.5	2.3	234.7
Z	1100	75.84	0.0030	1.448	52.4	171.3	99.4	49.4	1446.0	2.0	255.8
ZA	1250	74.09	0.0035	1.139	161.1	147.3	99.5	62.0	1423.9	3.0	4.0
ZB	1300	81.37	0.0042	1.031	220.1	122.2	99.6	79.1	1519.1	2.0	3.7

ID	Temp (°C)	$^{40}Ar/^{39}Ar$	$^{37}Ar/^{39}Ar$	$^{36}Ar/^{39}Ar$ (x 10^{-3})	$^{39}Ar_K$ (x 10^{-16} mol)	K/Ca	$^{40}Ar^*$ (%)	^{39}Ar (%)	Age (Ma)	±1σ (Ma)	Time (min)
ZC	1400	87.85	0.0040	1.094	209.3	126.7	99.6	95.4	1599.1	3.9	4.0
ZD	1700	86.92	0.0041	1.259	59.7	123.0	99.5	100.0	1587.2	2.2	3.4
total gas age			n=30		1286.0	149.8			1361.8	2.3	
HUD-98-78, K-feldspar, 1.57 mg, J=0.0163083, NM-107, Lab#=50327-01											
A	450	71.01	0.0254	24.37	2.39	20.1	89.8	0.2	1286.5	8.5	14.7
B	450	48.08	0.0148	6.266	0.985	34.5	96.1	0.3	1013.2	20.0	24.7
C	500	45.24	0.0281	4.478	2.11	18.2	97.0	0.5	974.1	9.8	14.2
D	500	42.70	0.0286	1.982	1.90	17.9	98.6	0.7	942.8	10.8	24.4
E	550	46.20	0.0538	1.446	4.41	9.5	99.0	1.1	1005.6	4.6	14.9
F	550	47.65	0.0690	1.628	4.34	7.4	98.9	1.5	1028.9	4.8	25.0
G	600	52.30	0.0717	0.6568	9.14	7.1	99.6	2.4	1109.3	2.9	14.7
H	600	54.97	0.0641	0.4556	9.52	8.0	99.7	3.3	1152.2	2.6	24.8
I	650	59.56	0.0414	0.4330	17.6	12.3	99.7	5.0	1222.2	2.2	15.1
J	650	63.36	0.0186	0.3449	17.3	27.4	99.8	6.6	1278.5	2.1	25.2
K	700	68.13	0.0110	0.3653	26.1	46.6	99.8	9.1	1346.1	1.8	15.0
L	700	70.89	0.0094	0.2350	24.5	54.4	99.9	11.5	1384.8	2.2	24.9
M	750	75.02	0.0089	0.2720	31.2	57.5	99.9	14.4	1440.1	2.1	15.5
N	750	78.02	0.0045	0.2280	28.3	112.2	99.9	17.1	1479.6	2.3	25.5
O	800	79.67	0.0055	0.2160	17.4	92.4	99.9	18.8	1501.0	2.4	3.4
P	850	81.98	0.0058	0.0690	28.4	88.2	99.9	21.5	1530.8	2.1	3.6
Q	900	85.40	0.0086	0.3036	35.2	59.7	99.9	24.9	1572.5	2.0	4.0
R	950	88.80	0.0123	0.3203	34.3	41.6	99.9	28.1	1613.8	1.9	3.6
S	1000	90.48	0.0104	0.3817	37.8	49.2	99.8	31.7	1633.7	2.1	3.8
T	1050	90.56	0.0090	0.3500	41.7	56.6	99.9	35.7	1634.7	2.5	3.5
U	1100	87.49	0.0086	0.3017	51.9	59.3	99.9	40.6	1598.1	3.8	3.3
V	1100	86.64	0.0061	0.3174	103.8	84.1	99.9	50.5	1587.6	2.4	25.3
W	1100	88.24	0.0050	0.2849	77.0	102.3	99.9	57.9	1607.1	3.2	54.7

ID	Temp (°C)	$^{40}Ar/^{39}Ar$	$^{37}Ar/^{39}Ar$	$^{36}Ar/^{39}Ar$ (x 10^{-3})	$^{39}Ar_K$ (x 10^{-16} mol)	K/Ca	$^{40}Ar^*$ (%)	^{39}Ar (%)	Age (Ma)	±1σ (Ma)	Time (min)
X	1100	88.70	0.0036	0.4871	71.3	141.8	99.8	64.7	1612.0	2.9	114.7
Y	1100	88.88	0.0033	0.6385	79.8	154.5	99.8	72.3	1613.6	2.9	234.7
Z	1100	90.10	0.0020	0.8315	62.0	260.0	99.7	78.2	1627.5	3.7	354.8
ZA	1250	86.35	0.0029	0.3156	48.2	174.5	99.9	82.8	1584.2	2.7	3.4
ZB	1300	87.69	0.0034	0.4511	89.9	148.7	99.8	91.3	1599.9	2.3	4.3
ZC	1400	88.45	0.0035	0.6006	48.1	144.7	99.8	95.9	1608.6	3.0	4.0
ZD	1700	89.03	0.0031	0.8118	42.7	167.0	99.7	100.0	1614.9	2.6	4.0
total gas age			n=30		1049.5	109.2			1553.7	2.5	
HUD-98-80, K-feldspar, 1.27 mg, J=0.0162749, NM-107, Lab#=50328-01											
A	450	187.5	0.1001	129.7	1.37	5.1	79.6	0.3	2222.8	15.1	14.4
B	450	53.91	0.0713	9.675	1.36	7.2	94.7	0.5	1090.7	13.9	25.6
C	500	55.27	0.1889	7.692	2.45	2.7	95.9	1.0	1122.0	7.7	14.2
D	500	49.50	0.4859	1.906	2.12	1.1	98.9	1.4	1057.3	8.8	24.3
E	550	60.83	0.6983	5.137	4.56	0.73	97.6	2.3	1219.8	4.2	14.9
F	550	59.21	0.5357	1.234	4.95	0.95	99.4	3.3	1212.5	4.1	25.0
G	600	68.89	0.4692	4.068	9.78	1.1	98.3	5.2	1340.3	2.5	14.7
H	600	68.36	0.3655	0.7435	9.21	1.4	99.7	6.9	1346.4	2.8	24.9
I	650	74.12	0.2233	1.939	16.2	2.3	99.2	10.1	1420.0	2.2	15.2
J	650	75.15	0.0892	0.5139	15.3	5.7	99.8	13.0	1439.1	2.5	25.2
K	700	79.10	0.0758	0.7116	19.9	6.7	99.7	16.9	1489.7	2.3	15.0
L	700	81.33	0.0613	0.4259	19.3	8.3	99.8	20.7	1519.2	2.1	25.1
M	750	84.31	0.0731	0.3647	23.6	7.0	99.8	25.2	1556.8	2.1	15.5
N	750	86.24	0.0641	0.2870	20.6	8.0	99.9	29.2	1580.9	2.0	25.5
O	800	87.77	0.0845	0.5926	15.6	6.0	99.8	32.3	1598.4	2.4	7.5
P	850	88.47	0.1082	1.053	23.9	4.7	99.6	36.9	1605.2	3.7	7.6
Q	900	89.12	0.1154	1.041	28.9	4.4	99.6	42.5	1613.2	1.9	7.5
R	950	88.71	0.1009	0.6118	28.7	5.1	99.8	48.1	1609.6	3.5	7.4

ID	Temp (°C)	$^{40}Ar/^{39}Ar$	$^{37}Ar/^{39}Ar$	$^{36}Ar/^{39}Ar$ (x 10^{-3})	$^{39}Ar_K$ (x 10^{-16} mol)	K/Ca	$^{40}Ar^*$ (%)	^{39}Ar (%)	Age (Ma)	±1σ (Ma)	Time (min)
S	1000	86.34	0.0864	1.211	28.0	5.9	99.6	53.5	1578.7	2.4	7.3
T	1050	84.80	0.0875	1.914	29.3	5.8	99.3	59.2	1557.2	2.0	7.4
U	1100	85.85	0.1087	3.314	21.0	4.7	98.8	63.3	1565.2	2.6	7.4
V	1100	87.97	0.1179	3.684	26.2	4.3	98.7	68.3	1589.8	2.2	25.4
W	1100	89.45	0.1331	4.034	30.6	3.8	98.6	74.3	1606.4	1.9	55.3
X	1100	91.17	0.1193	3.311	39.4	4.3	98.9	81.9	1629.6	5.4	115.3
Y	1100	92.84	0.1070	2.908	40.9	4.8	99.1	89.9	1650.7	3.1	235.2
Z	1100	95.39	0.1220	3.499	22.0	4.2	98.9	94.1	1678.5	3.3	285.2
ZA	1250	97.88	0.0855	1.310	19.8	6.0	99.6	98.0	1714.4	2.1	7.0
ZB	1300	97.94	0.2534	2.182	3.19	2.0	99.3	98.6	1712.4	5.5	7.7
ZC	1400	98.85	0.3542	3.054	4.82	1.4	99.1	99.5	1720.0	4.5	7.9
ZD	1700	99.90	0.1167	20.41	2.42	4.4	93.9	100.0	1672.8	7.5	7.5
total gas age			n=30		515.6	4.9			1571.3	2.6	
HUD-98-83, K-feldspar, 1.14 mg, J=0.0162438, NM-107, Lab#=50329-01											
A	450	75.36	0.0049	34.78	0.692	104.8	86.3	0.1	1301.0	25.6	14.7
B	450	42.32	0.0014	10.85	0.284	361.8	92.4	0.1	886.9	65.8	24.6
C	500	51.46	0.0064	4.650	0.746	79.2	97.3	0.3	1073.6	23.8	14.3
D	500	39.20	0.0000	1.253	0.685	-	99.0	0.4	881.8	27.1	24.5
E	550	49.73	0.0133	4.835	1.91	38.3	97.1	0.6	1044.5	10.0	14.9
F	550	44.28	0.0166	2.437	1.94	30.7	98.3	0.9	964.9	9.9	25.0
G	600	54.10	0.0099	2.896	5.53	51.6	98.4	1.7	1123.9	3.7	14.6
H	600	50.76	0.0070	0.7116	5.58	72.7	99.5	2.5	1081.1	3.6	24.8
I	650	55.67	0.0062	0.7055	10.1	81.7	99.6	4.0	1158.3	2.3	15.1
J	650	57.89	0.0066	0.5792	8.52	77.7	99.7	5.2	1192.9	2.5	25.2
K	700	61.08	0.0061	0.7016	10.1	84.3	99.6	6.7	1239.9	2.5	15.0
L	700	64.25	0.0066	1.130	7.52	77.7	99.4	7.8	1284.4	2.9	25.1
M	750	65.76	0.0086	0.7448	7.14	59.6	99.6	8.8	1307.4	3.3	15.5
N	750	68.78	0.0064	0.8394	5.21	80.2	99.6	9.6	1349.5	3.9	25.6

ID	Temp (°C)	$^{40}Ar/^{39}Ar$	$^{37}Ar/^{39}Ar$	$^{36}Ar/^{39}Ar$ (x 10^{-3})	$^{39}Ar_K$ (x 10^{-16} mol)	K/Ca	$^{40}Ar^*$ (%)	^{39}Ar (%)	Age (Ma)	±1σ (Ma)	Time (min)
O	800	71.77	0.0128	0.1588	3.63	39.7	99.9	10.1	1393.3	5.2	7.4
P	850	75.12	0.0149	0.8286	6.39	34.3	99.6	11.0	1435.4	3.2	7.6
Q	900	82.24	0.0128	1.841	9.62	40.0	99.3	12.4	1523.4	2.9	7.5
R	950	87.89	0.0134	1.502	13.4	38.0	99.5	14.4	1594.4	2.6	7.4
S	1000	92.34	0.0113	1.114	16.0	45.2	99.6	16.7	1648.8	2.2	7.3
T	1050	90.82	0.0106	1.352	21.5	48.1	99.5	19.9	1630.1	2.2	7.5
U	1100	85.37	0.0113	1.922	39.3	45.1	99.3	25.6	1562.1	2.2	7.4
V	1100	87.52	0.0113	1.211	49.2	45.0	99.6	32.7	1591.0	3.2	25.3
W	1100	89.83	0.0097	0.9103	43.6	52.9	99.7	39.1	1619.8	2.8	54.8
X	1100	90.71	0.0086	0.9501	39.3	59.1	99.7	44.8	1630.2	3.8	114.7
Y	1100	90.66	0.0095	1.393	35.1	53.7	99.5	49.9	1628.0	2.1	234.7
Z	1100	91.41	0.0082	2.558	22.1	62.5	99.1	53.1	1632.9	2.0	354.7
ZA	1200	88.32	0.0092	1.314	6.89	55.7	99.5	54.1	1600.3	3.3	3.0
ZB	1300	89.36	0.0087	1.175	184.3	58.9	99.6	80.9	1613.3	3.6	3.8
ZC	1400	90.97	0.0107	1.084	49.9	47.7	99.6	88.2	1632.8	2.0	3.9
ZD	1700	94.85	0.0112	0.8061	81.2	45.7	99.7	100.0	1679.1	3.9	3.8
total gas age			n=30		687.4	54.0			1577.8	2.9	
HUD-98-84, K-feldspar, 1.72 mg, J=0.0154412, NM-102, Lab#=50015-01											
A	500	301.2	0.0317	16.42	47.5	16.1	98.4	0.8	3100.2	4.8	23.0
B	500	60.50	0.0150	11.51	28.8	34.0	94.3	1.3	1140.1	3.1	34.3
C	500	58.64	0.0155	9.678	4.59	32.9	95.1	1.4	1120.5	8.9	12.6
D	500	59.93	0.0151	12.36	9.52	33.7	93.9	1.5	1127.9	5.9	24.0
E	550	55.42	0.0140	3.194	28.9	36.3	98.2	2.0	1100.8	2.6	13.9
F	550	53.76	0.0128	3.968	34.6	39.8	97.8	2.6	1072.0	2.4	24.1
G	600	116.4	0.0172	2.082	97.0	29.7	99.4	4.3	1849.1	2.6	14.5

ID	Temp (°C)	$^{40}Ar/^{39}Ar$	$^{37}Ar/^{39}Ar$	$^{36}Ar/^{39}Ar$ (x 10^{-3})	$^{39}Ar_K$ (x 10^{-16} mol)	K/Ca	$^{40}Ar^*$ (%)	^{39}Ar (%)	Age (Ma)	±1σ (Ma)	Time (min)
H	600	61.95	0.0249	3.499	57.5	20.5	98.3	5.3	1195.8	2.2	24.2
I	650	101.1	0.0203	2.648	130.1	25.2	99.2	7.5	1687.9	2.5	14.2
J	650	61.57	0.0224	2.523	67.7	22.8	98.7	8.7	1194.5	2.1	24.5
K	700	89.81	0.0249	1.892	118.2	20.5	99.3	10.7	1562.7	2.4	14.6
L	700	60.81	0.0300	3.304	72.2	17.0	98.4	11.9	1180.1	2.3	24.7
M	750	69.91	0.0451	1.767	50.6	11.3	99.2	12.8	1313.5	2.5	4.5
N	800	75.72	0.0503	1.255	122.9	10.1	99.5	14.9	1392.0	2.2	5.1
O	850	68.40	0.0487	0.8231	174.5	10.5	99.6	17.9	1296.9	2.2	5.1
P	900	64.80	0.0548	0.4946	199.8	9.3	99.7	21.3	1248.7	2.1	5.2
Q	950	65.28	0.0673	0.4240	219.3	7.6	99.8	25.1	1255.6	2.0	5.2
R	1000	66.63	0.0839	0.6795	238.3	6.1	99.7	29.1	1273.4	2.1	5.2
S	1050	66.78	0.0533	0.7236	264.5	9.6	99.6	33.7	1275.1	1.9	5.1
T	1100	69.05	0.0320	0.6914	464.9	16.0	99.7	41.6	1306.1	2.1	5.2
U	1130	73.40	0.0299	0.9567	840.0	17.0	99.6	56.0	1363.0	2.1	24.7
V	1130	84.36	0.0428	1.511	362.4	11.9	99.4	62.2	1499.0	2.1	54.8
W	1130	91.91	0.0432	1.945	457.8	11.8	99.3	70.1	1586.9	3.0	114.7
X	1130	97.16	0.0445	3.730	376.2	11.5	98.8	76.5	1640.6	2.9	234.7
Y	1130	98.08	0.0452	4.869	412.0	11.3	98.5	83.6	1647.3	3.1	474.7
Z	1230	95.75	0.0392	0.2356	222.3	13.0	99.9	87.4	1636.5	2.5	5.0
ZA	1280	96.38	0.0602	0.4345	318.2	8.5	99.8	92.8	1642.8	2.6	5.4
ZB	1330	93.78	0.1362	0.7919	157.5	3.7	99.7	95.5	1612.4	2.4	5.5
ZC	1430	92.89	0.3355	2.377	62.2	1.5	99.2	96.6	1597.2	3.0	5.7
ZD	1530	95.73	0.1020	1.711	160.4	5.0	99.4	99.3	1631.4	2.8	5.7
ZE	1650	81.92	0.1387	13.61	39.8	3.7	95.1	100.0	1424.7	3.1	5.4
total gas age			n=31		5840.3	13.0			1470.6	2.2	

ID	Temp (°C)	$^{40}Ar/^{39}Ar$	$^{37}Ar/^{39}Ar$	$^{36}Ar/^{39}Ar$ (x 10^{-3})	$^{39}Ar_K$ (x 10^{-16} mol)	K/Ca	$^{40}Ar^*$ (%)	^{39}Ar (%)	Age (Ma)	±1σ (Ma)	Time (min)
HUD-98-86, K-feldspar, 1.45 mg, J=0.0154392, NM-102, Lab#=50016-01											
A	450	380.4	0.0061	93.25	6.03	83.8	92.7	0.1	3362.0	16.0	23.9
B	450	72.28	0.0000	71.59	2.07	-	70.7	0.2	1049.2	32.2	33.3
C	500	87.13	0.0144	10.17	11.6	35.5	96.5	0.4	1501.4	6.2	13.5
D	500	56.92	0.0000	21.79	7.27	-	88.6	0.5	1039.2	8.1	24.1
E	550	89.51	0.0053	7.061	30.2	95.4	97.6	1.1	1540.9	3.8	15.1
F	550	76.95	0.0048	8.276	25.7	105.8	96.8	1.6	1380.8	4.1	23.9
G	600	90.34	0.0053	3.593	56.9	97.0	98.8	2.8	1562.8	3.1	14.5
H	600	82.31	0.0065	3.464	49.6	78.1	98.7	3.7	1466.7	3.1	24.7
I	650	86.48	0.0055	1.846	73.8	92.0	99.3	5.2	1523.2	2.9	14.4
J	650	86.47	0.0029	2.133	65.7	175.9	99.2	6.5	1522.0	2.6	24.2
K	700	89.14	0.0019	1.304	85.1	267.4	99.5	8.2	1556.7	2.3	14.9
L	700	89.05	0.0028	2.312	69.6	184.1	99.2	9.6	1552.1	2.9	24.9
M	750	90.52	0.0038	1.785	41.9	134.7	99.4	10.4	1571.1	3.2	4.6
N	800	90.66	0.0034	0.8753	67.3	150.8	99.7	11.7	1575.8	2.9	5.3
O	850	91.75	0.0035	2.061	97.6	146.8	99.3	13.7	1584.5	2.4	5.2
P	900	88.31	0.0038	2.588	87.1	133.8	99.1	15.4	1542.4	2.7	5.4
Q	950	88.22	0.0031	1.574	108.1	166.6	99.4	17.5	1544.8	2.7	5.3
R	1000	86.27	0.0032	1.261	115.7	159.0	99.5	19.8	1522.8	2.3	5.0
S	1050	85.07	0.0036	0.8739	147.5	141.1	99.7	22.7	1509.7	2.9	4.9
T	1100	85.51	0.0041	0.6857	212.6	125.2	99.7	26.9	1515.7	2.3	5.0
U	1100	86.57	0.0044	1.098	303.9	116.5	99.6	32.9	1526.9	2.3	24.8
V	1100	87.85	0.0033	1.833	332.6	153.7	99.4	39.5	1539.6	2.4	54.8
W	1100	90.02	0.0031	2.384	326.8	162.0	99.2	46.0	1563.2	4.2	114.8
X	1100	91.36	0.0032	3.541	315.7	161.4	98.8	52.2	1574.9	2.9	234.8
Y	1100	93.35	0.0027	6.328	244.5	188.1	98.0	57.1	1588.4	2.5	311.4
Z	1230	90.23	0.0048	1.074	67.7	106.0	99.6	58.4	1570.2	2.9	5.3

ID	Temp (°C)	$^{40}Ar/^{39}Ar$	$^{37}Ar/^{39}Ar$	$^{36}Ar/^{39}Ar$ (x 10^{-3})	$^{39}Ar_K$ (x 10^{-16} mol)	K/Ca	$^{40}Ar^*$ (%)	^{39}Ar (%)	Age (Ma)	±1σ (Ma)	Time (min)
ZA	1280	89.59	0.0034	0.6010	277.3	148.8	99.8	63.9	1564.4	3.0	5.4
ZB	1330	92.39	0.0046	0.5599	1206.2	110.6	99.8	87.7	1597.0	3.9	5.5
ZC	1430	94.86	0.0046	0.5669	548.3	109.7	99.8	98.6	1625.1	3.5	5.5
ZD	1530	96.18	0.0068	2.369	71.8	74.5	99.2	100.0	1634.0	3.2	5.5
total gas age			n=30		5056.3	134.6			1570.4	3.0	

Appendix F

Explanation of Appendix F

The following section contains plots that graphically display the data for the step-heated K-feldspar. Each spectra consists of the age of the individual heating steps plotted against the total $\%^{39}Ar$ released. Each plot is also accompanied by the K/Ca for the individual heating steps.

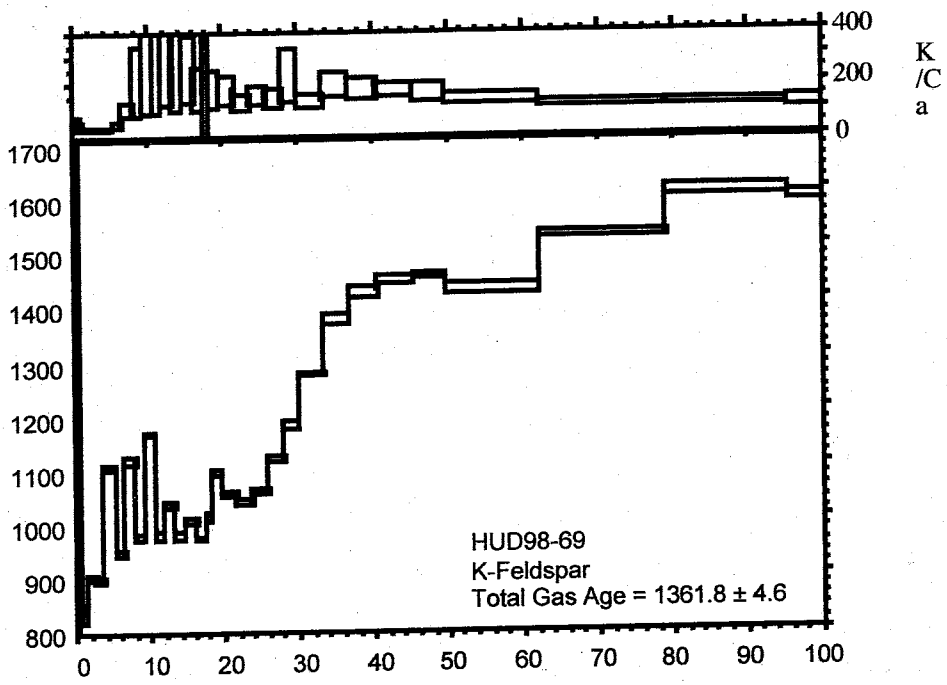
400
200
0
K
/C
a
1700
1600
1500
1400
1300
1200
1100
1000
900
800
0
10
20
30
40
50
60
70
80
90
100
HUD98-69
K-Feldspar
Total Gas Age = 1361.8 ± 4.6

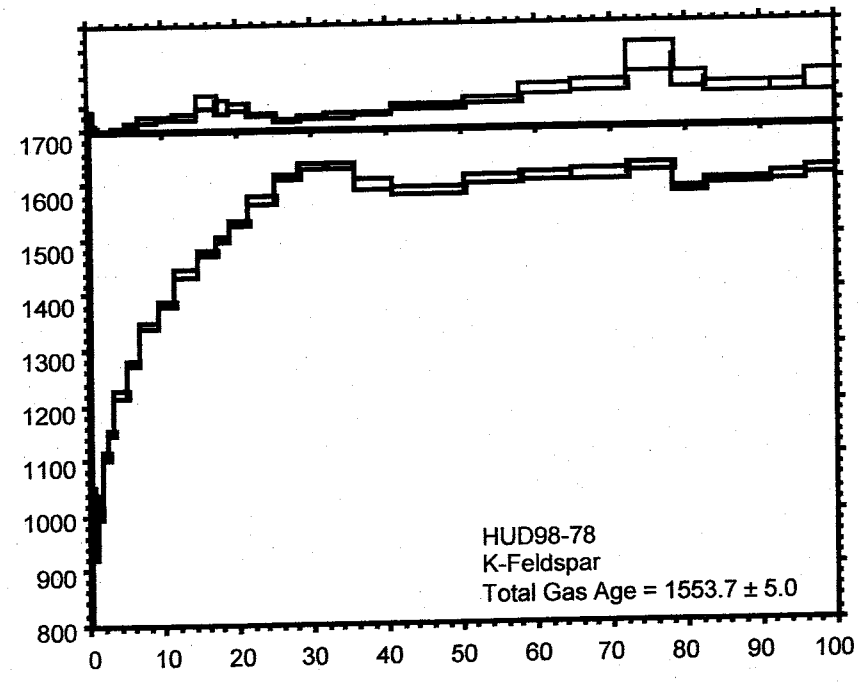
1700
1600
1500
1400
1300
1200
1100
1000
900
800
0
10
20
30
40
50
60
70
80
90
100
HUD98-78
K-Feldspar
Total Gas Age = 1553.7 ± 5.0

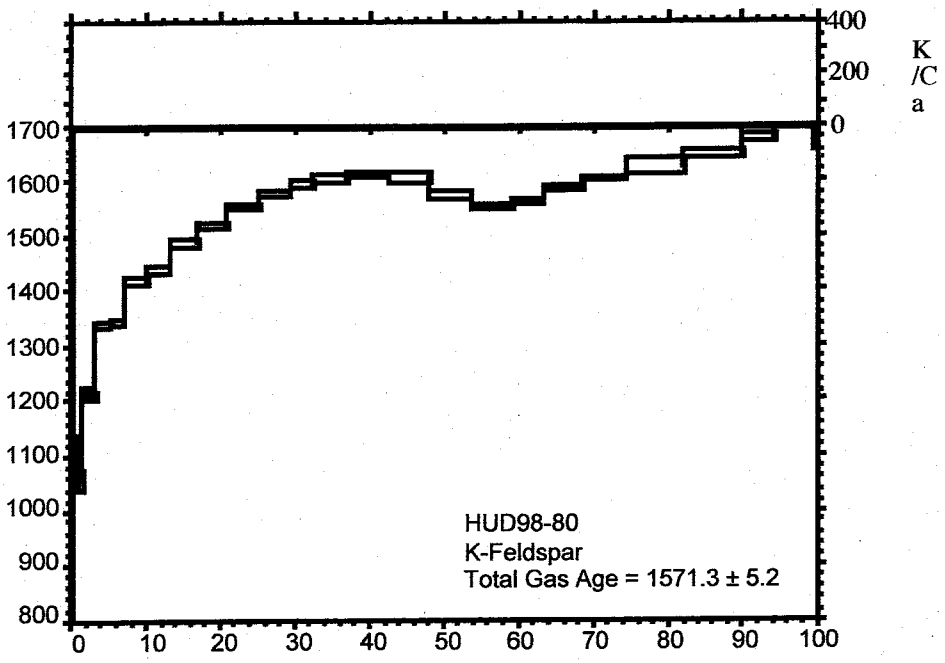
400
200
0
K/Ca
1700
1600
1500
1400
1300
1200
1100
1000
900
800
0
10
20
30
40
50
60
70
80
90
100
HUD98-80
K-Feldspar
Total Gas Age = 1571.3 ± 5.2

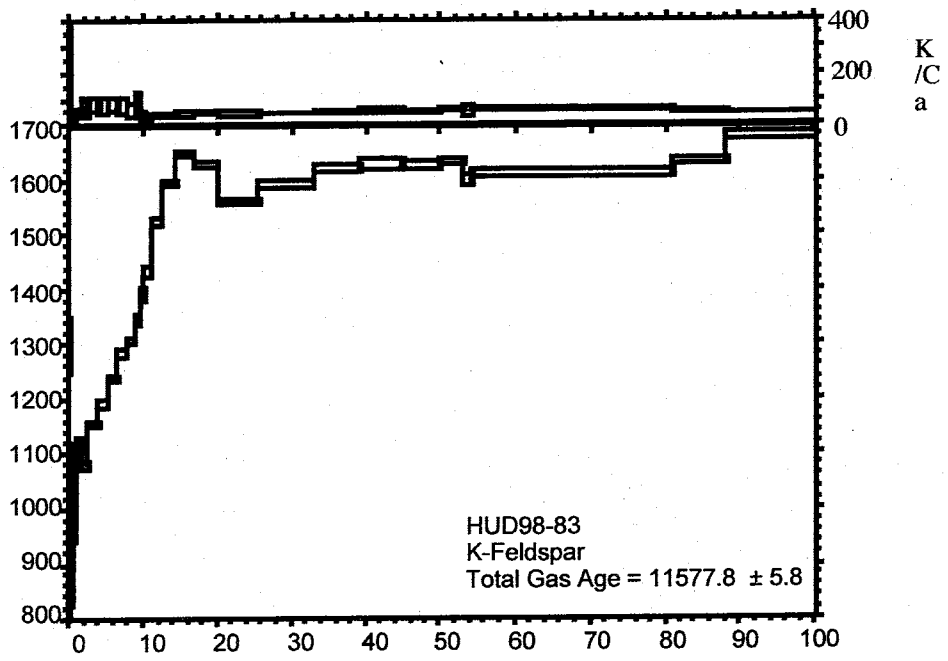
400
200
0
K/Ca
1700
1600
1500
1400
1300
1200
1100
1000
900
800
0
10
20
30
40
50
60
70
80
90
100
HUD98-83
K-Feldspar
Total Gas Age = 11577.8 ± 5.8

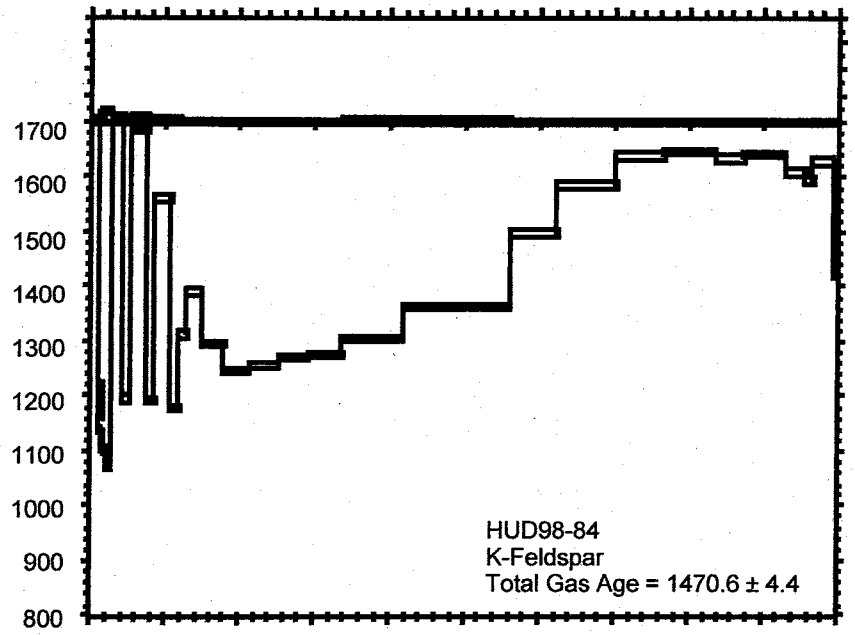
1700
1600
1500
1400
1300
1200
1100
1000
900
800
HUD98-84
K-Feldspar
Total Gas Age = 1470.6 ± 4.4

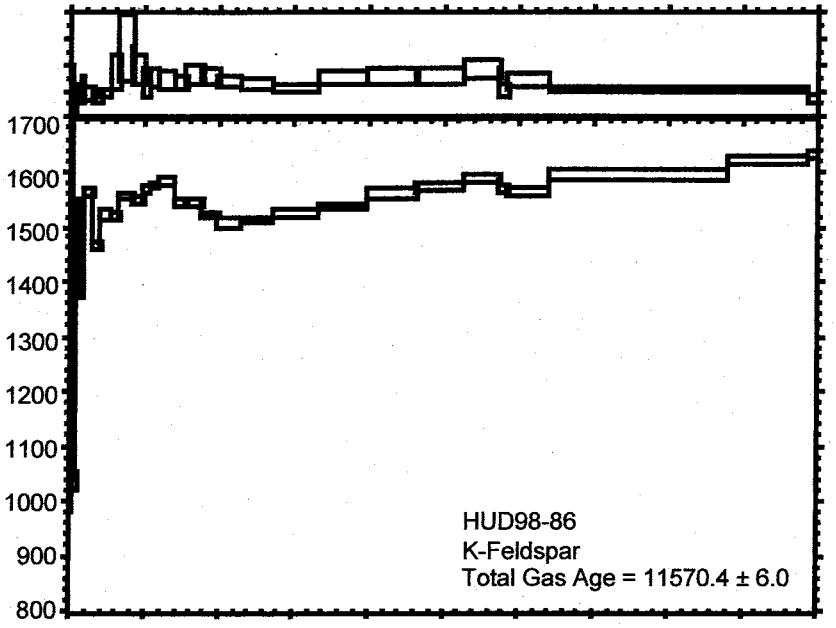
1700
1600
1500
1400
1300
1200
1100
1000
900
800
HUD98-86
K-Feldspar
Total Gas Age = 11570.4 ± 6.0

Appendix G

Explanation of Appendix G

The following section contains plots that graphically display the results of K-feldspar modeling programs. Four plots are displayed for each sample. The measured age and modeled spectrum are plotted as apparent age vs. cumulative $\%^{39}Ar$ released. The measured and modeled Arrhenious plots are shown as $\log(D/r^2)s\text{-}1$ vs. 10000/T(K), Also plotted are the measured and modeled $\log(r/r_0)$ in the lower left corner. The calculated model histories are shown in the lower right as temperature vs. time (Ma).

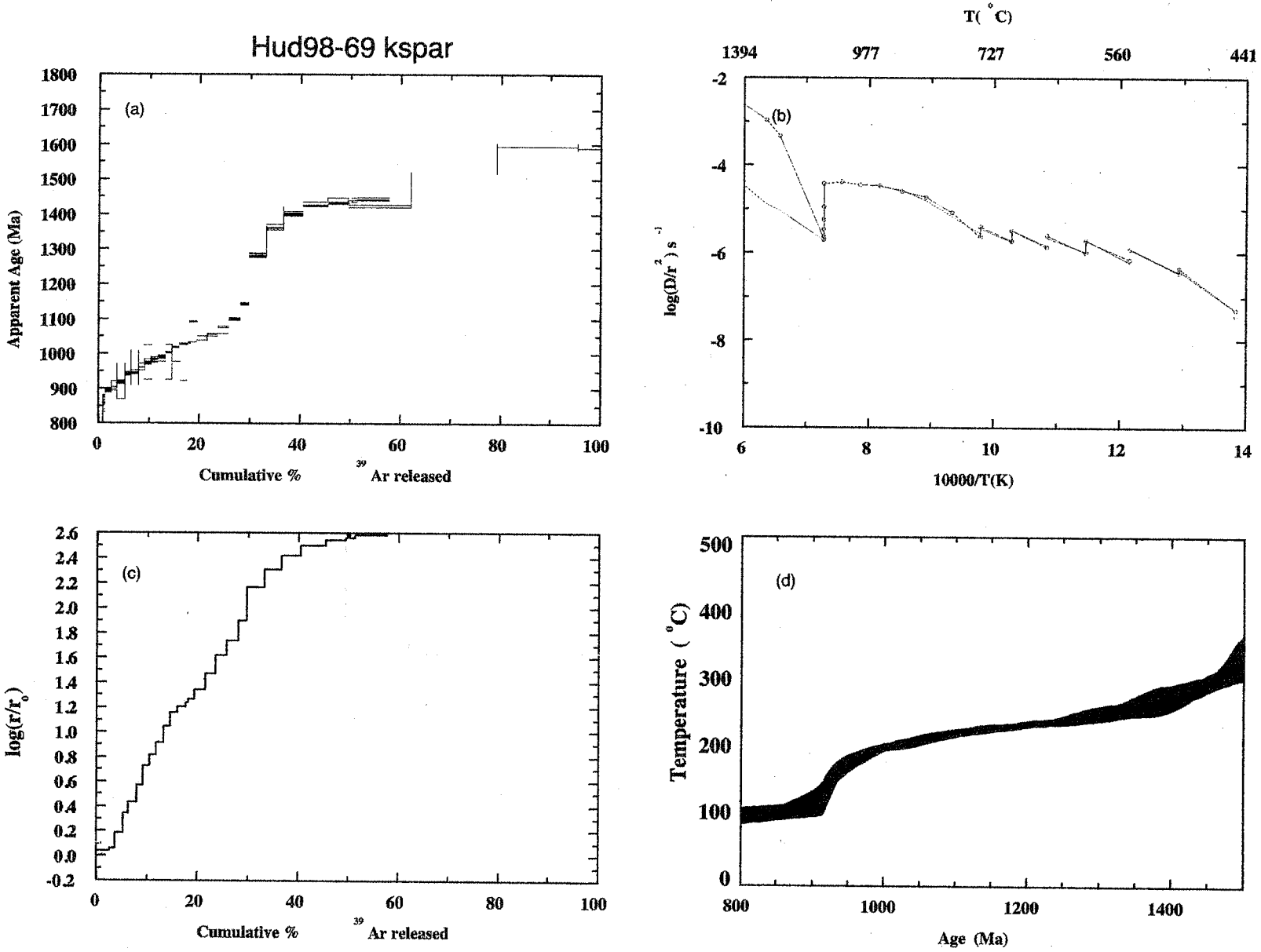
Hud98-69 kspar
(a)
Apparent Age (Ma)
Cumulative % ^{39}Ar released
(b)
T(°C)
1394
977
727
560
441
log(D/r^2) s^{-1}
10000/T(K)
(c)
log(r/r$_o$)
Cumulative % ^{39}Ar released
(d)
Temperature (°C)
Age (Ma)

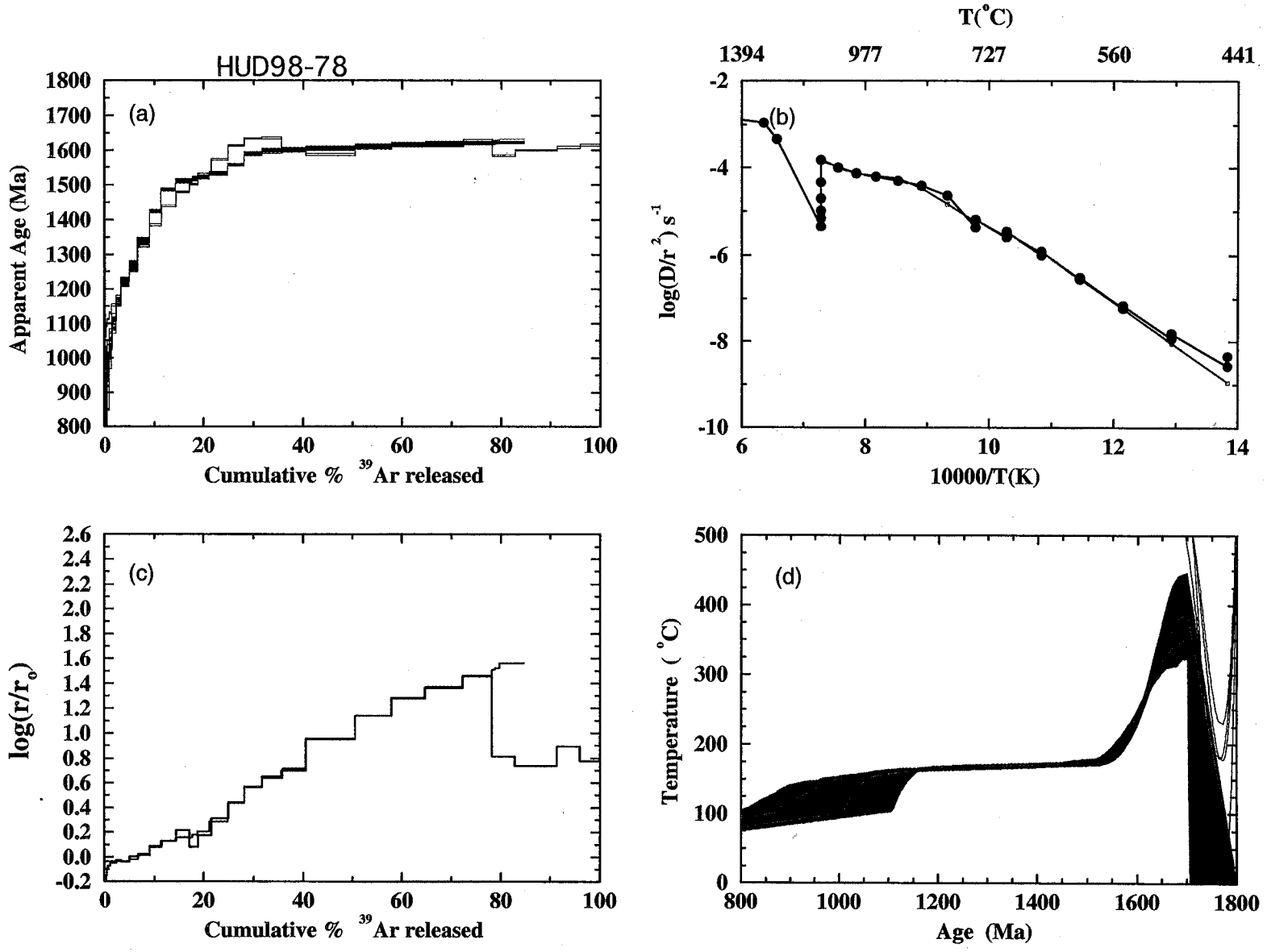
HUD98-78
(a)
Apparent Age (Ma)
Cumulative % 39Ar released
(b)
T(°C)
1394
977
727
560
441
log(D/r2) s-1
10000/T(K)
(c)
log(r/ro)
Cumulative % 39Ar released
(d)
Temperature (°C)
Age (Ma)

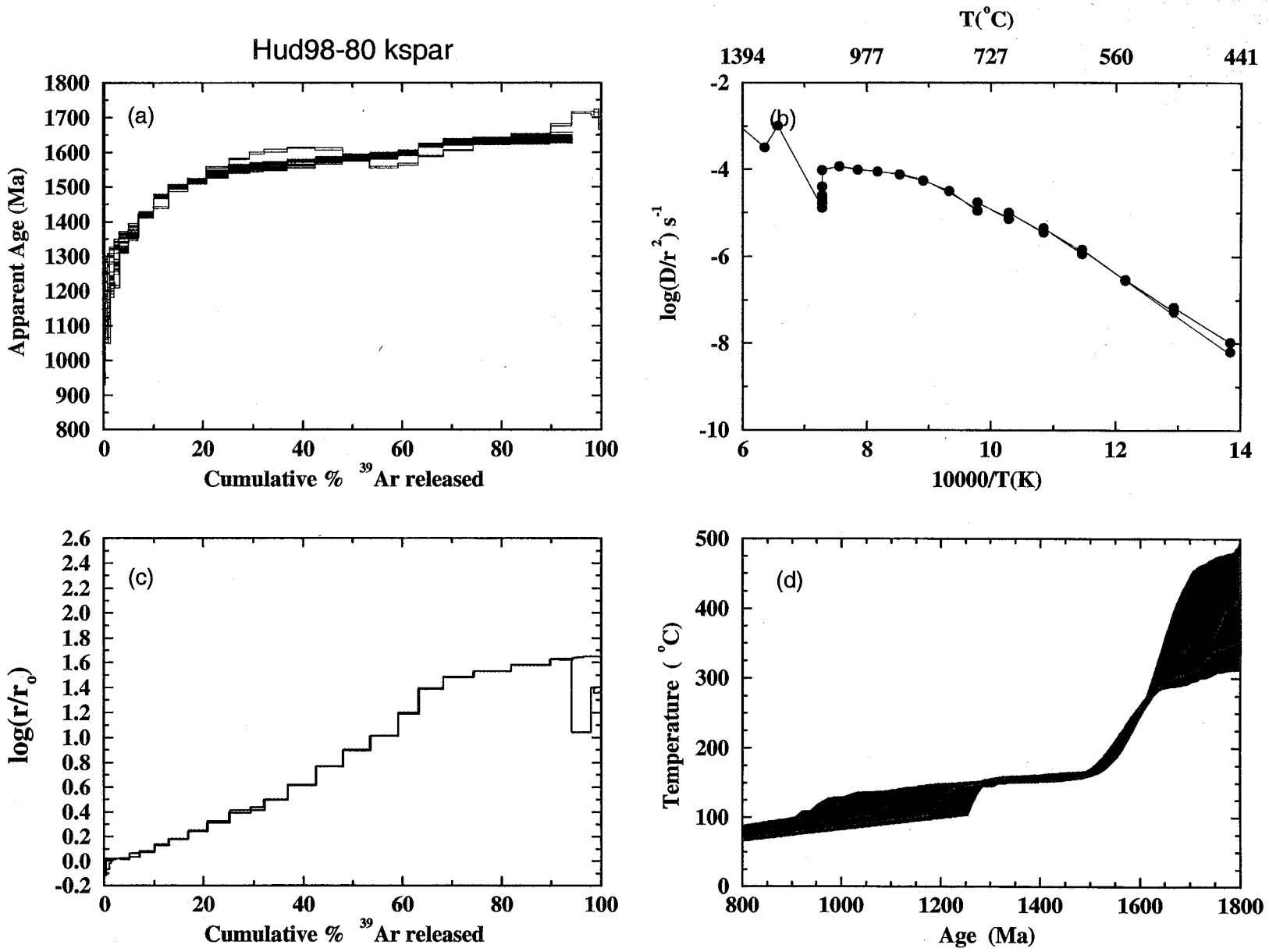
Hud98-80 kspar
(a)
Apparent Age (Ma)
Cumulative % 39Ar released
(b)
T(°C)
1394
977
727
560
441
log(D/r2) s-1
10000/T(K)
(c)
log(r/r0)
Cumulative % 39Ar released
(d)
Temperature (°C)
Age (Ma)

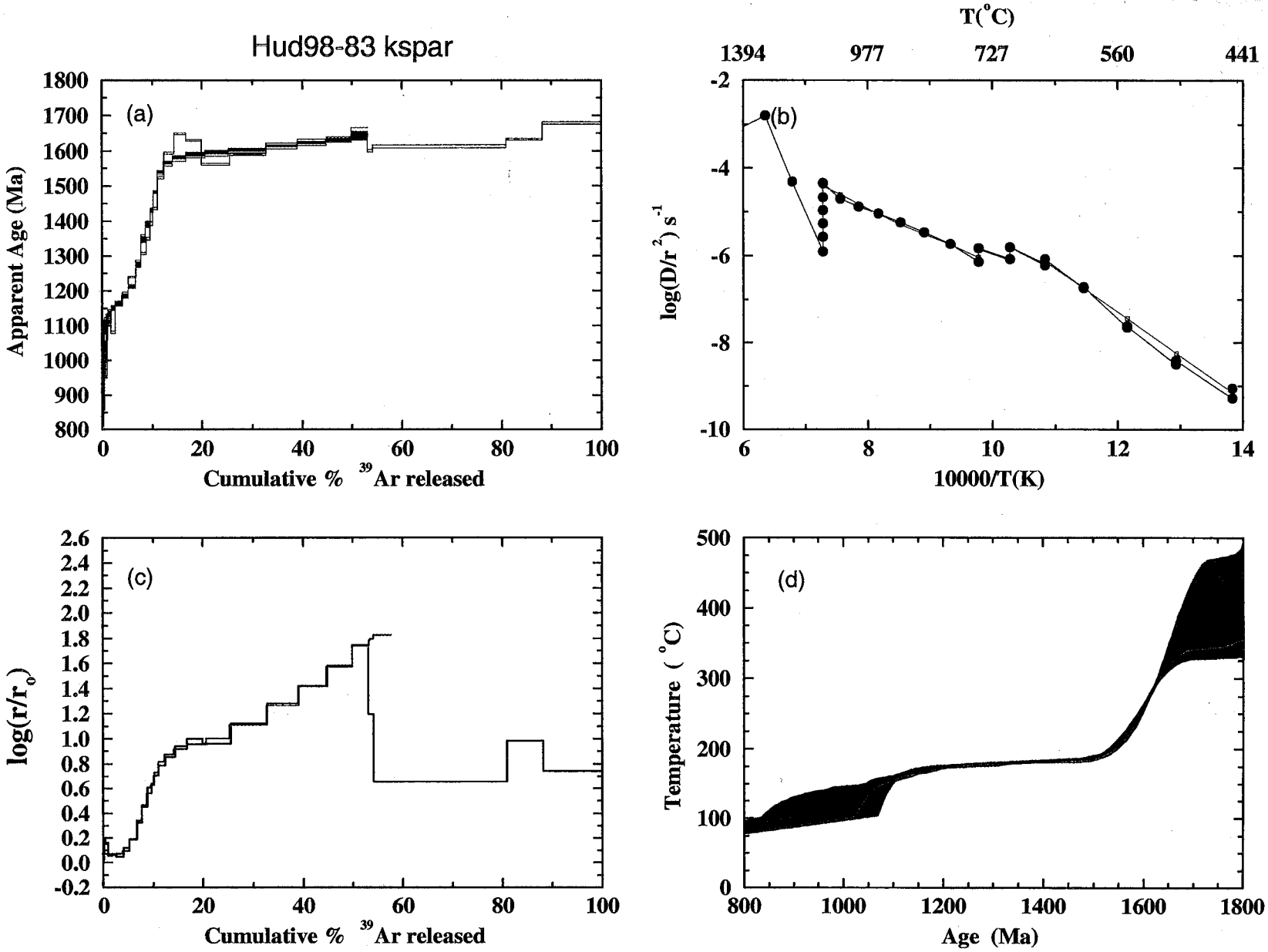
Hud98-83 kspar
(a)
Apparent Age (Ma)
Cumulative % 39Ar released
(b)
T(°C)
1394
977
727
560
441
log(D/r2) s-1
10000/T(K)
(c)
log(r/r0)
Cumulative % 39Ar released
(d)
Temperature (°C)
Age (Ma)

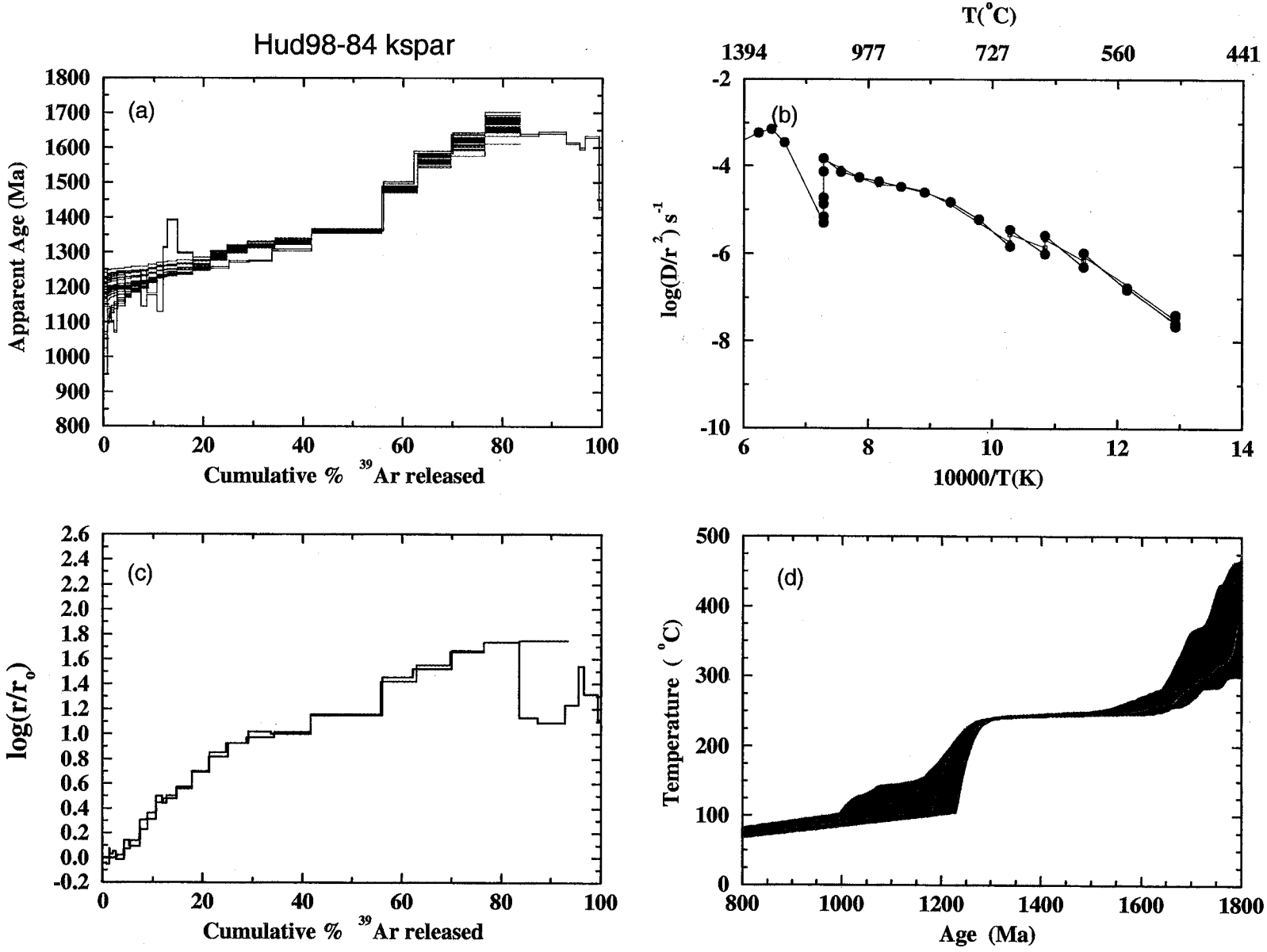
Hud98-84 kspar
(a)
Apparent Age (Ma)
Cumulative % 39Ar released
(b)
T(°C)
1394
977
727
560
441
log(D/r2) s-1
10000/T(K)
(c)
log(r/ro)
Cumulative % 39Ar released
(d)
Temperature (°C)
Age (Ma)

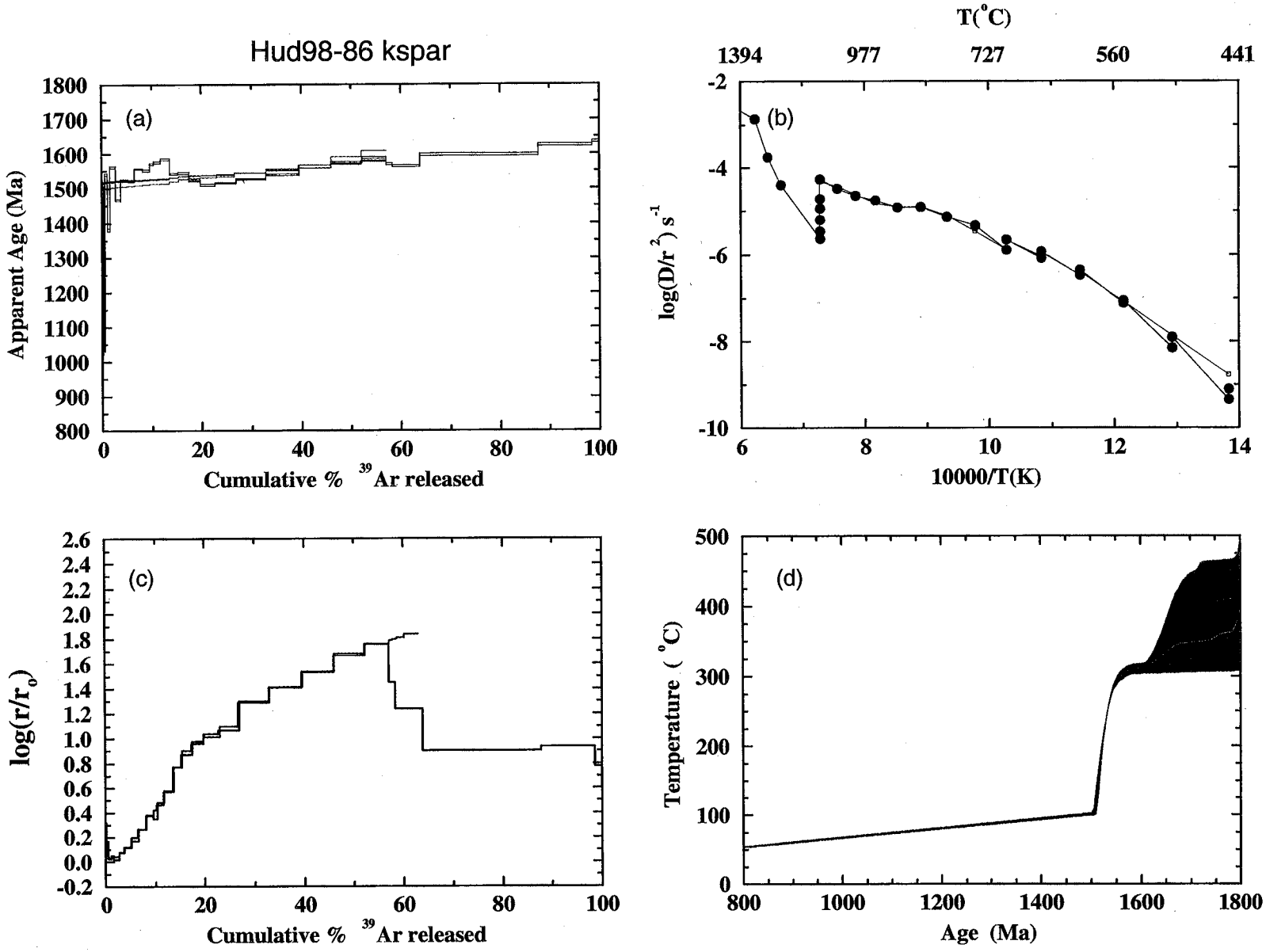
Hud98-86 kspar
(a)
Apparent Age (Ma)
Cumulative % 39Ar released
(b)
T(°C)
1394
977
727
560
441
log(D/r2) s-1
10000/T(K)
(c)
log(r/ro)
Cumulative % 39Ar released
(d)
Temperature (°C)
Age (Ma)

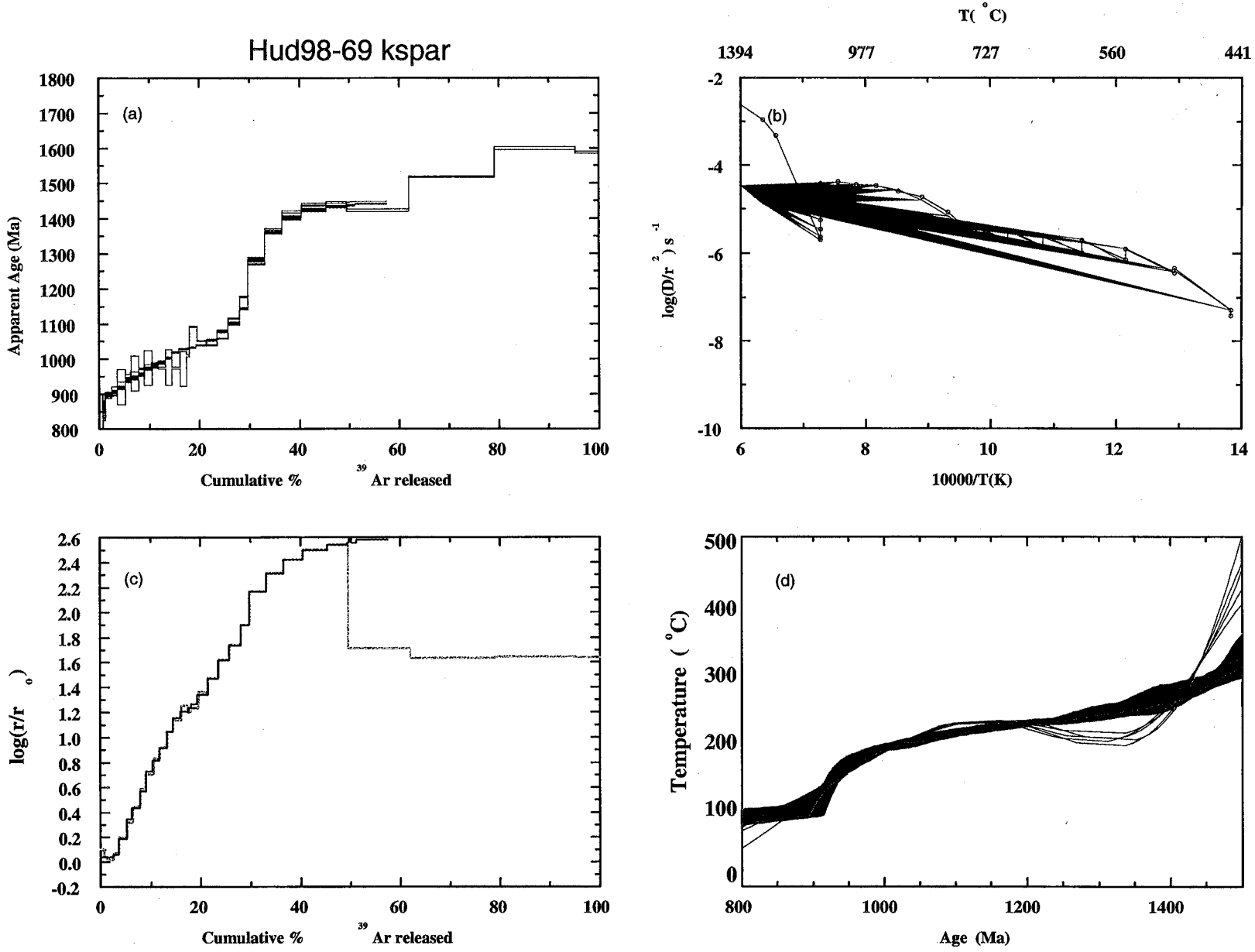
Hud98-69 kspar
(a)
Apparent Age (Ma)
Cumulative % 39Ar released
(b)
T(°C)
1394
977
727
560
441
log(D/r2) s-1
10000/T(K)
(c)
log(r/ro)
Cumulative % 39Ar released
(d)
Temperature (°C)
Age (Ma)

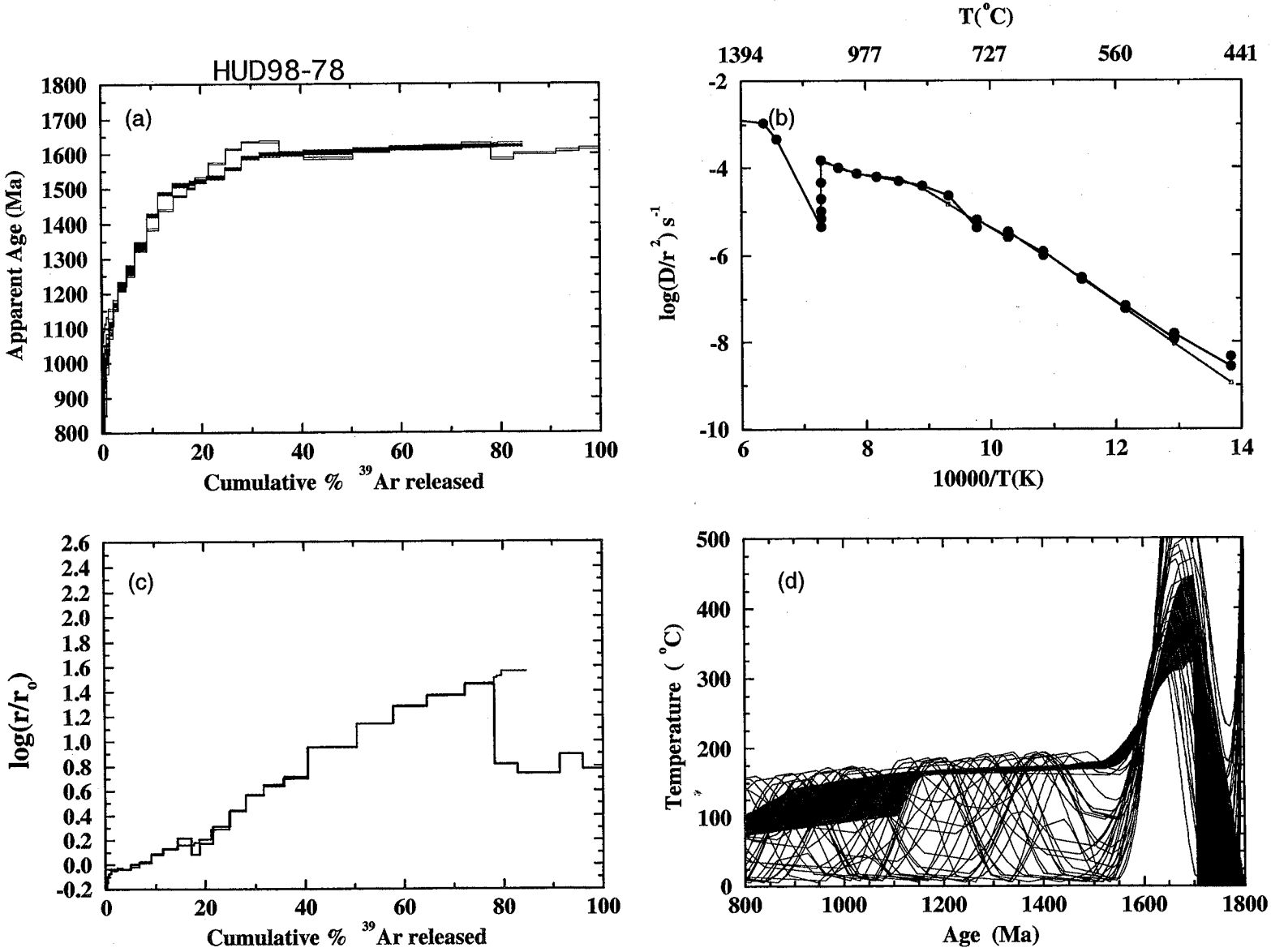
HUD98-78
(a)
Apparent Age (Ma)
Cumulative % 39Ar released
(b)
T(°C)
1394
977
727
560
441
log(D/r2) s-1
10000/T(K)
(c)
log(r/ro)
Cumulative % 39Ar released
(d)
Temperature (°C)
Age (Ma)

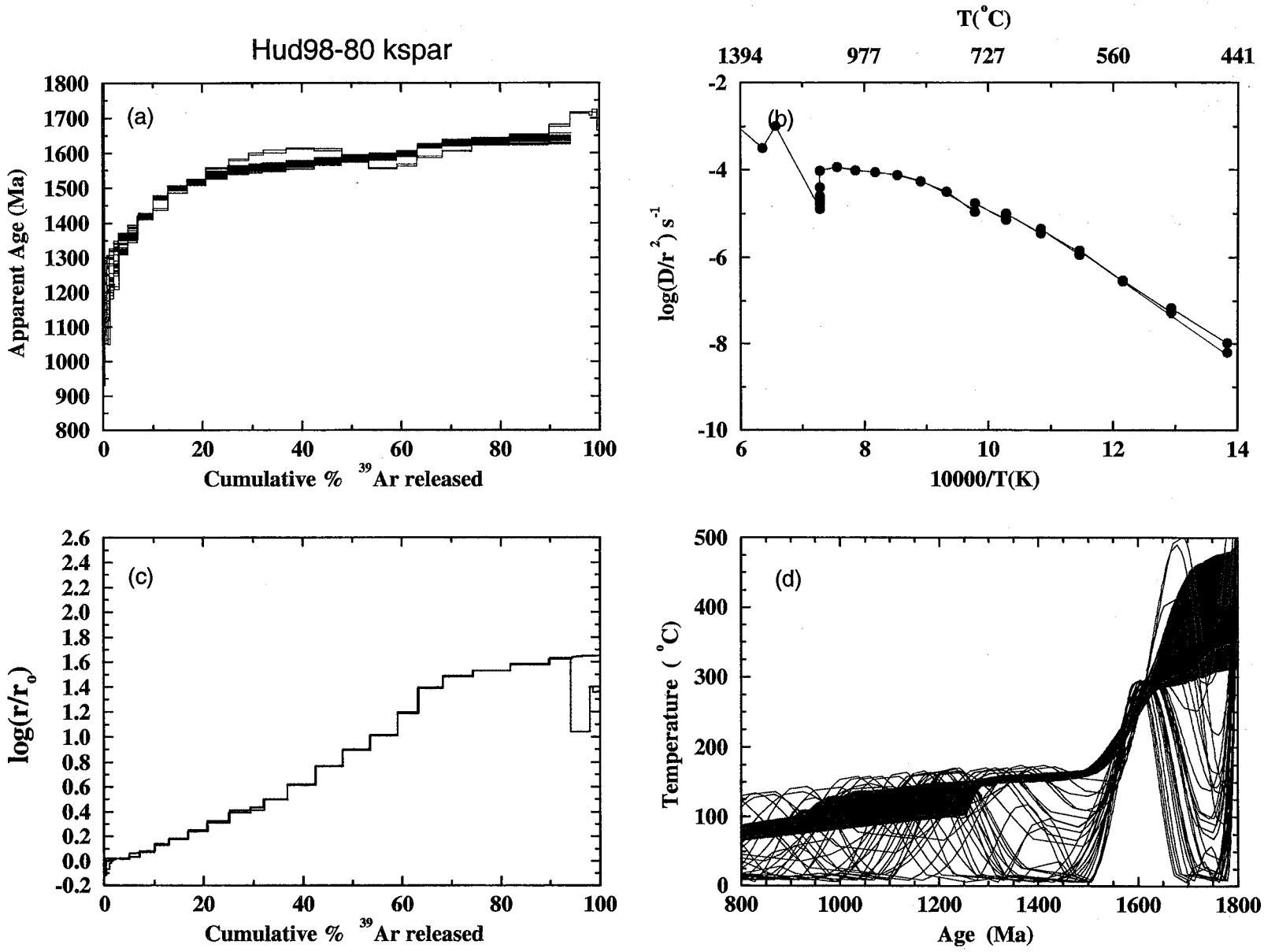
Hud98-80 kspar
(a)
Apparent Age (Ma)
Cumulative % ^{39}Ar released
(b)
T(°C)
1394
977
727
560
441
log(D/r^2) s^{-1}
10000/T(K)
(c)
log(r/r$_o$)
Cumulative % ^{39}Ar released
(d)
Temperature (°C)
Age (Ma)

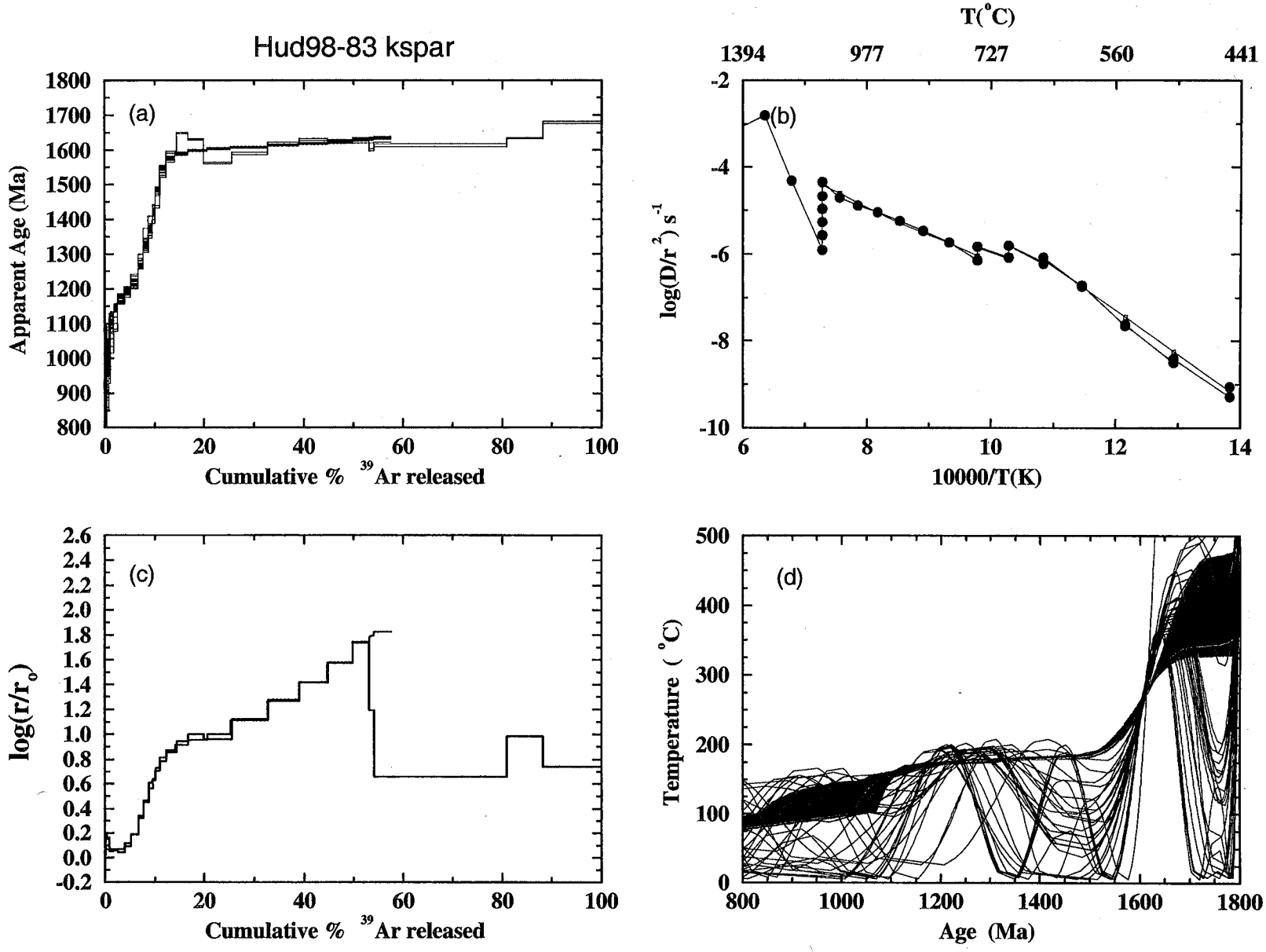
Hud98-83 kspar
(a)
Apparent Age (Ma)
Cumulative % 39Ar released
(b)
T(°C)
1394
977
727
560
441
log(D/r2) s-1
10000/T(K)
(c)
log(r/ro)
Cumulative % 39Ar released
(d)
Temperature (°C)
Age (Ma)

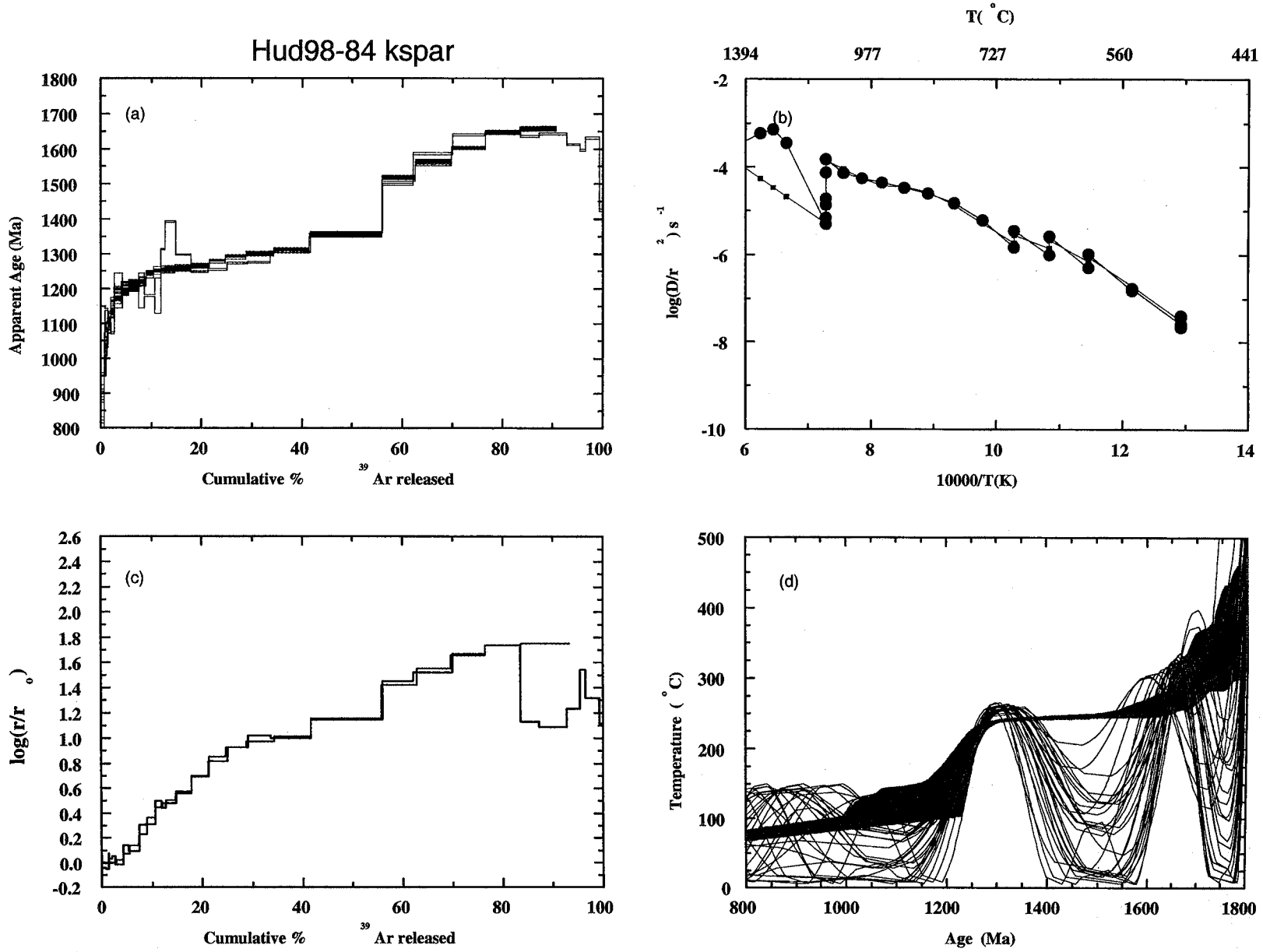
Hud98-84 kspar
(a)
Apparent Age (Ma)
Cumulative % 39Ar released
(b)
T(°C)
log(D/r2) s-1
10000/T(K)
(c)
log(r/ro)
Cumulative % 39Ar released
(d)
Temperature (°C)
Age (Ma)

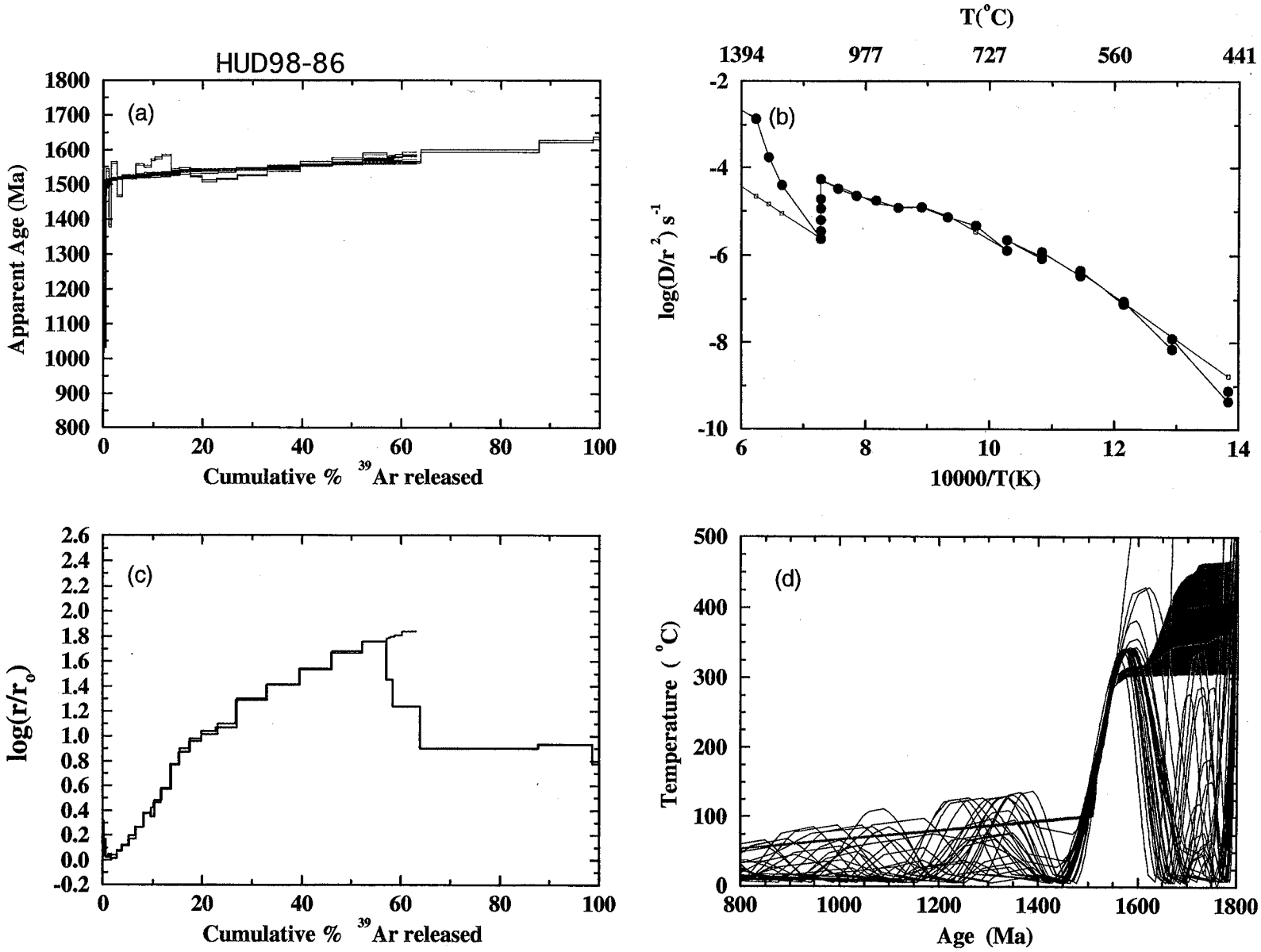
HUD98-86
(a)
Apparent Age (Ma)
Cumulative % 39Ar released
(b)
T(°C)
1394
977
727
560
441
log(D/r2) s-1
10000/T(K)
(c)
log(r/r0)
Cumulative % 39Ar released
(d)
Temperature (°C)
Age (Ma)

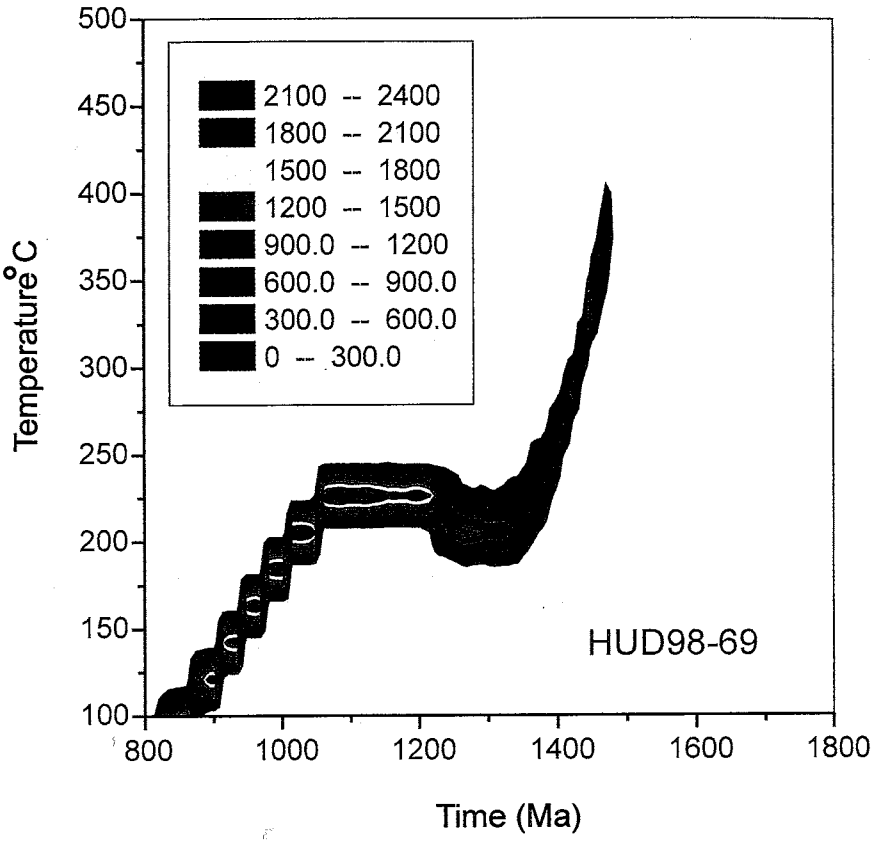
2100 -- 2400
1800 -- 2100
1500 -- 1800
1200 -- 1500
900.0 -- 1200
600.0 -- 900.0
300.0 -- 600.0
0 -- 300.0
HUD98-69
Temperature °C
Time (Ma)
500
450
400
350
300
250
200
150
100
800
1000
1200
1400
1600
1800

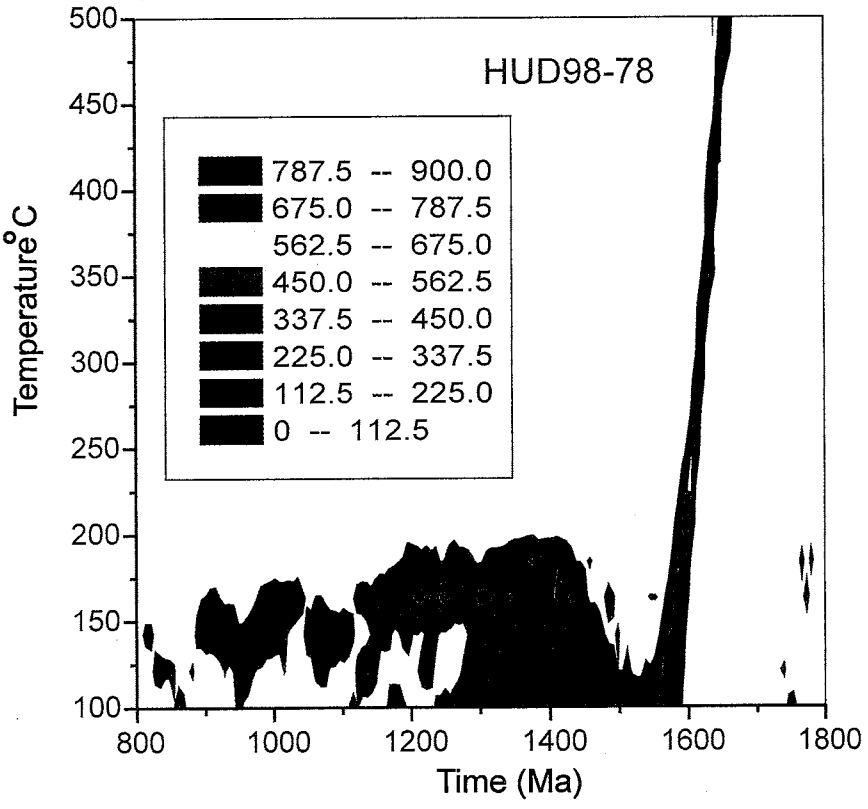
HUD98-78
787.5 -- 900.0
675.0 -- 787.5
562.5 -- 675.0
450.0 -- 562.5
337.5 -- 450.0
225.0 -- 337.5
112.5 -- 225.0
0 -- 112.5
Temperature °C
Time (Ma)
500
450
400
350
300
250
200
150
100
800
1000
1200
1400
1600
1800

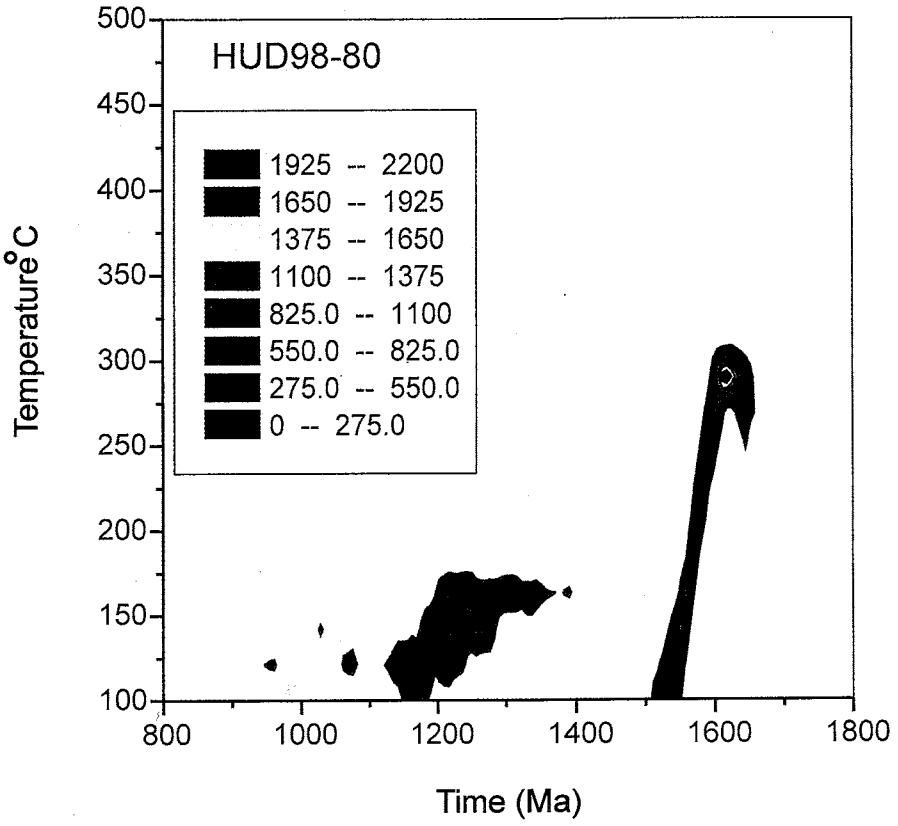
HUD98-80
1925 -- 2200
1650 -- 1925
1375 -- 1650
1100 -- 1375
825.0 -- 1100
550.0 -- 825.0
275.0 -- 550.0
0 -- 275.0
Temperature °C
Time (Ma)
500
450
400
350
300
250
200
150
100
800
1000
1200
1400
1600
1800

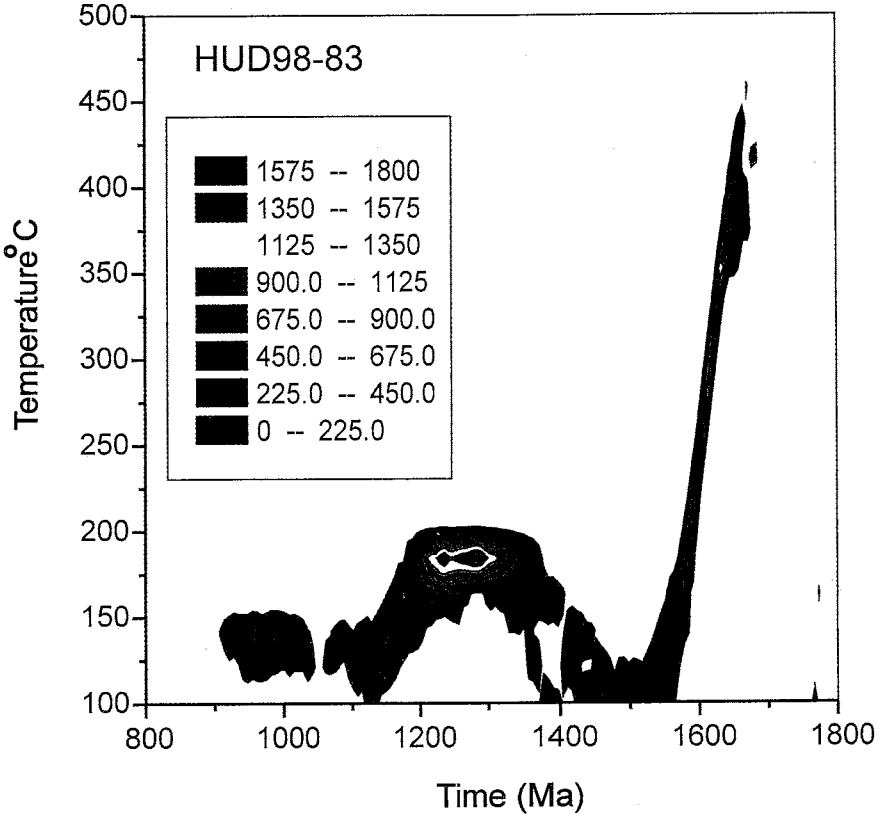
HUD98-83
1575 -- 1800
1350 -- 1575
1125 -- 1350
900.0 -- 1125
675.0 -- 900.0
450.0 -- 675.0
225.0 -- 450.0
0 -- 225.0
Temperature °C
Time (Ma)
500
450
400
350
300
250
200
150
100
800
1000
1200
1400
1600
1800

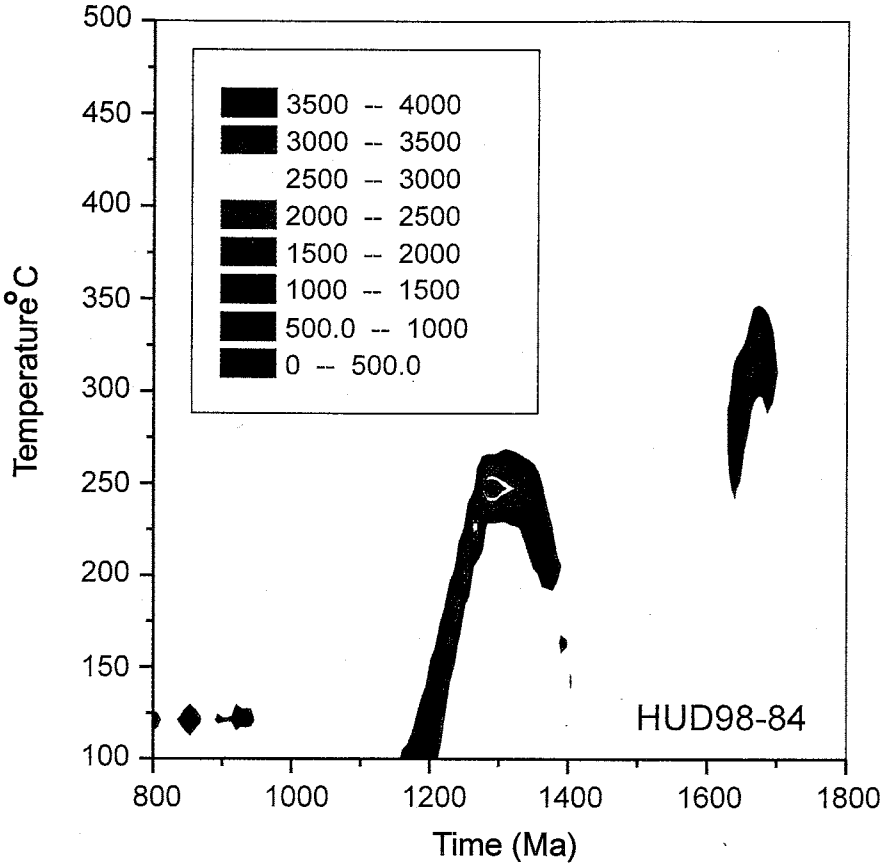
3500 -- 4000
3000 -- 3500
2500 -- 3000
2000 -- 2500
1500 -- 2000
1000 -- 1500
500.0 -- 1000
0 -- 500.0
HUD98-84
Temperature °C
Time (Ma)
500
450
400
350
300
250
200
150
100
800
1000
1200
1400
1600
1800

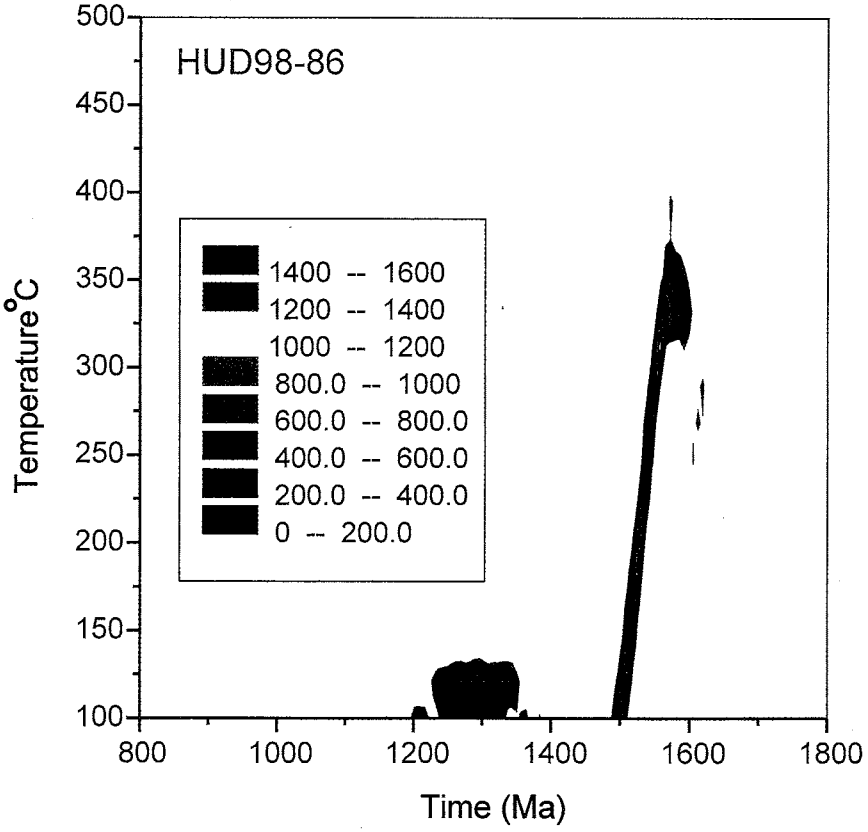
HUD98-86
1400 -- 1600
1200 -- 1400
1000 -- 1200
800.0 -- 1000
600.0 -- 800.0
400.0 -- 600.0
200.0 -- 400.0
0 -- 200.0
Temperature °C
Time (Ma)
500
450
400
350
300
250
200
150
100
800
1000
1200
1400
1600
1800

Appendix H

Explanation of AppendixH

The following section contains apatite fission track age data for each sample. Sample numbers are listed in the upper left of each table. The number of spontaneous (Ns) and induced (Ni) fission tracks are listed per individual grain. Area counted for each grain is also given. Age and standard deviation in millions of years are listed for each grain. The mean age is determined my averaging the individual grain ages.

	Ns	Ni	area	Ps	Pi	Ps/Pi	Age (Ma)
HUD86-9 Apatite							
1	103	89	1.00E-04	1.03E+06	8.90E+05	1.16	310.53
2	123	104	1.00E-04	1.23E+06	1.04E+06	1.18	317.18
3	77	63	1.00E-04	7.70E+05	6.30E+05	1.22	327.52
4	59	59	1.00E-04	5.90E+05	5.90E+05	1.00	269.16
5	86	56	1.00E-04	8.60E+05	5.60E+05	1.54	409.00
6	50	40	1.00E-04	5.00E+05	4.00E+05	1.25	334.78
7	148	118	1.00E-04	1.48E+06	1.18E+06	1.25	335.89
8	78	49	2.00E-04	3.90E+05	2.45E+05	1.59	423.48
9	102	51	2.00E-04	5.10E+05	2.55E+05	2.00	527.87
10	71	44	2.00E-04	3.55E+05	2.20E+05	1.61	429.10
11	34	28	2.00E-04	1.70E+05	1.40E+05	1.21	325.45
12	110	84	1.00E-04	1.10E+06	8.40E+05	1.31	350.31
13	67	35	2.00E-04	3.35E+05	1.75E+05	1.91	506.08
14	59	44	2.00E-04	2.95E+05	2.20E+05	1.34	358.49
15	34	23	2.00E-04	1.70E+05	1.15E+05	1.48	394.14
16	28	19	2.00E-04	1.40E+05	9.50E+04	1.47	392.96
17	78	40	1.00E-04	7.80E+05	4.00E+05	1.95	515.17
Total	1307	946	2.50E-03				

Apparent Age ± 2sigma= 383.95 ± 35.7

	Ns	Ni	area	Ps	Pi	Ps/Pi	Age (Ma)
HUD86-23 Apatite							
1	325	124	1.00E-04	3.25E+06	1.24E+06	2.62	685.80
2	196	89	1.00E-04	1.96E+06	8.90E+05	2.20	580.86
3	184	87	1.00E-04	1.84E+06	8.70E+05	2.11	558.77
4	202	106	1.00E-04	2.02E+06	1.06E+06	1.91	505.52
5	310	152	1.00E-04	3.10E+06	1.52E+06	2.04	539.62
6	309	134	1.00E-04	3.09E+06	1.34E+06	2.31	607.01
7	401	191	1.00E-04	4.01E+06	1.91E+06	2.10	554.85
8	262	128	2.00E-04	1.31E+06	6.40E+05	2.05	541.50
9	164	73	2.00E-04	8.20E+05	3.65E+05	2.25	592.05
10	262	144	2.00E-04	1.31E+06	7.20E+05	1.82	483.46
11	218	115	2.00E-04	1.09E+06	5.75E+05	1.90	502.96
12	299	158	1.00E-04	2.99E+06	1.58E+06	1.89	502.13
13	86	41	2.00E-04	4.30E+05	2.05E+05	2.10	554.36
14	102	51	2.00E-04	5.10E+05	2.55E+05	2.00	529.58
15	99	69	2.00E-04	4.95E+05	3.45E+05	1.43	384.13
16	156	82	2.00E-04	7.80E+05	4.10E+05	1.90	504.70
17	234	113	1.00E-04	2.34E+06	1.13E+06	2.07	547.57
18	146	63	2.00E-04	7.30E+05	3.15E+05	2.32	609.90
19	161	73	1.00E-04	1.61E+06	7.30E+05	2.21	581.68
20	51	32	1.00E-04	5.10E+05	3.20E+05	1.59	425.36
Totals	4167	2025	2.90E-03				

Apparent Age ± 2 sigma 539.59 ±35.6

	Ns	Ni	area	Ps	Pi	Ps/Pi	Age (Ma)
HUD86-26 Apatite							
1	72	36	1.00E-04	7.20E+05	3.60E+05	2.00	531.28
2	110	68	1.00E-04	1.10E+06	6.80E+05	1.62	432.94
3	112	53	1.00E-04	1.12E+06	5.30E+05	2.11	560.13
4	191	107	1.00E-04	1.91E+06	1.07E+06	1.79	476.17
5	76	39	1.00E-04	7.60E+05	3.90E+05	1.95	518.18
6	108	47	1.00E-04	1.08E+06	4.70E+05	2.30	606.91
7	172	82	1.00E-04	1.72E+06	8.20E+05	2.10	556.15
8	61	27	2.00E-04	3.05E+05	1.35E+05	2.26	597.16
9	35	18	2.00E-04	1.75E+05	9.00E+04	1.94	517.08
10	109	64	2.00E-04	5.45E+05	3.20E+05	1.70	455.05
11	92	42	2.00E-04	4.60E+05	2.10E+05	2.19	579.74
12	75	33	1.00E-04	7.50E+05	3.30E+05	2.27	600.56
13	55	40	2.00E-04	2.75E+05	2.00E+05	1.38	369.76
14	76	38	2.00E-04	3.80E+05	1.90E+05	2.00	531.28
15	158	108	2.00E-04	7.90E+05	5.40E+05	1.46	392.73
16	62	29	2.00E-04	3.10E+05	1.45E+05	2.14	566.41
17	84	50	1.00E-04	8.40E+05	5.00E+05	1.68	449.07
18	118	63	2.00E-04	5.90E+05	3.15E+05	1.87	498.78
19	47	21	2.00E-04	2.35E+05	1.05E+05	2.24	591.80
Totals	1813	965	2.90E-03				

Apparent Age ± 2sigma= 531.29 ± 46.7

	Ns	Ni	area	Ps	Pi	Ps/Pi	Age (Ma)
HUD98-58 Apatite							
1	64	33	1.00E-04	6.40E+05	3.30E+05	1.94	427.97
2	114	59	2.00E-04	5.70E+05	2.95E+05	1.93	426.43
3	54	30	2.00E-04	2.70E+05	1.50E+05	1.80	398.11
4	47	27	2.00E-04	2.35E+05	1.35E+05	1.74	385.37
5	205	118	1.00E-04	2.05E+06	1.18E+06	1.74	384.63
6	137	90	2.00E-04	6.85E+05	4.50E+05	1.52	338.20
7	266	125	2.00E-04	1.33E+06	6.25E+05	2.13	468.16
8	154	66	2.00E-04	7.70E+05	3.30E+05	2.33	511.64
9	50	26	2.00E-04	2.50E+05	1.30E+05	1.92	424.48
10	342	153	1.00E-04	3.42E+06	1.53E+06	2.24	490.92
11	81	58	1.00E-04	8.10E+05	5.80E+05	1.40	310.92
12	188	97	1.00E-04	1.88E+06	9.70E+05	1.94	427.70
13	254	144	2.00E-04	1.27E+06	7.20E+05	1.76	390.35
14	109	65	2.00E-04	5.45E+05	3.25E+05	1.68	371.63
15	72	36	2.00E-04	3.60E+05	1.80E+05	2.00	440.91
16	137	88	1.00E-04	1.37E+06	8.80E+05	1.56	345.69
17	40	26	2.00E-04	2.00E+05	1.30E+05	1.54	341.72
18	166	83	3.00E-04	5.53E+05	2.77E+05	2.00	440.91
19	99	66	2.00E-04	4.95E+05	3.30E+05	1.50	333.39
Totals	2579	1390	3.30E-03				

Apparent Age ± 2 sigma: 403.11 ± 25.8

	Ns	Ni	area	Ps	Pi	Ps/Pi	Age (Ma)
HUD98-59 Apatite							
1	540	376	2.00E-04	2.70E+06	1.88E+06	1.44	319.53
2	117	53	2.00E-04	5.85E+05	2.65E+05	2.21	485.04
3	206	119	2.00E-04	1.03E+06	5.95E+05	1.73	383.30
4	141	77	2.00E-04	7.05E+05	3.85E+05	1.83	404.80
5	501	329	1.00E-04	5.01E+06	3.29E+06	1.52	338.33
6	117	65	2.00E-04	5.85E+05	3.25E+05	1.80	398.11
7	295	194	2.00E-04	1.48E+06	9.70E+05	1.52	337.85
8	345	181	2.00E-04	1.73E+06	9.05E+05	1.91	420.84
9	231	162	2.00E-04	1.16E+06	8.10E+05	1.43	317.31
10	312	177	2.00E-04	1.56E+06	8.85E+05	1.76	390.10
11	401	250	1.00E-04	4.01E+06	2.50E+06	1.60	355.89
12	450	261	1.00E-04	4.50E+06	2.61E+06	1.72	381.80
13	128	68	1.00E-04	1.28E+06	6.80E+05	1.88	415.77
14	86	44	1.00E-04	8.60E+05	4.40E+05	1.95	431.21
15	128	56	2.00E-04	6.40E+05	2.80E+05	2.29	501.58
16	440	224	2.00E-04	2.20E+06	1.12E+06	1.96	433.29
17	143	89	2.00E-04	7.15E+05	4.45E+05	1.61	356.49
18	183	129	2.00E-04	9.15E+05	6.45E+05	1.42	315.72
19	223	156	2.00E-04	1.12E+06	7.80E+05	1.43	318.08
20	86	57	2.00E-04	4.30E+05	2.85E+05	1.51	335.29
21	143	107	2.00E-04	7.15E+05	5.35E+05	1.34	297.84
22	79	43	2.00E-04	3.95E+05	2.15E+05	1.84	406.09
23	221	145	2.00E-04	1.11E+06	7.25E+05	1.52	338.62
Totals	5516	3362	4.10E-03				

Apparent Age ± 2 sigma 378 ± 23.8

	Ns	Ni	area	Ps	Pi	Ps/Pi	Age (Ma)
HUD98-60 Apatite							
1	227	148	2.00E-04	1.14E+06	7.40E+05	1.53	340.71
2	284	180	2.00E-04	1.42E+06	9.00E+05	1.58	350.23
3	203	109	2.00E-04	1.02E+06	5.45E+05	1.86	411.49
4	334	162	2.00E-04	1.67E+06	8.10E+05	2.06	454.07
5	367	187	1.00E-04	3.67E+06	1.87E+06	1.96	432.92
6	391	254	2.00E-04	1.96E+06	1.27E+06	1.54	341.92
7	243	157	2.00E-04	1.22E+06	7.85E+05	1.55	343.73
8	302	162	2.00E-04	1.51E+06	8.10E+05	1.86	411.88
9	411	268	2.00E-04	2.06E+06	1.34E+06	1.53	340.66
10	430	286	2.00E-04	2.15E+06	1.43E+06	1.50	334.14
11	179	85	1.00E-04	1.79E+06	8.50E+05	2.11	463.46
12	174	76	1.00E-04	1.74E+06	7.60E+05	2.29	502.38
13	132	78	1.00E-04	1.32E+06	7.80E+05	1.69	374.95
14	500	323	1.00E-04	5.00E+06	3.23E+06	1.55	343.78
15	293	175	1.00E-04	2.93E+06	1.75E+06	1.67	371.06
16	402	260	1.00E-04	4.02E+06	2.60E+06	1.55	343.38
17	267	147	1.00E-04	2.67E+06	1.47E+06	1.82	401.61
18	211	106	1.00E-04	2.11E+06	1.06E+06	1.99	438.90
19	498	244	1.00E-04	4.98E+06	2.44E+06	2.04	449.65
Totals	5848	3407	2.80E-03				

Apparent Age ± 2 sigma: 392.15 ± 22.4

	Ns	Ni	area	Ps	Pi	Ps/Pi	Age (Ma)	
HUD98-63 Apatite								
	1	307	174	1.00E-04	3.07E+06	1.74E+06	1.76	467.60
	2	311	190	1.00E-04	3.11E+06	1.90E+06	1.64	434.88
	3	87	52	1.00E-04	8.70E+05	5.20E+05	1.67	444.19
	4	363	171	1.00E-04	3.63E+06	1.71E+06	2.12	558.71
	5	331	204	1.00E-04	3.31E+06	2.04E+06	1.62	431.20
	6	346	201	1.00E-04	3.46E+06	2.01E+06	1.72	456.59
	7	193	80	1.00E-04	1.93E+06	8.00E+05	2.41	631.45
	8	684	405	2.00E-04	3.42E+06	2.03E+06	1.69	448.25
	9	298	172	2.00E-04	1.49E+06	8.60E+05	1.73	459.45
	10	587	348	2.00E-04	2.94E+06	1.74E+06	1.69	447.71
	11	475	251	2.00E-04	2.38E+06	1.26E+06	1.89	500.29
	12	163	92	1.00E-04	1.63E+06	9.20E+05	1.77	469.48
	13	513	284	2.00E-04	2.57E+06	1.42E+06	1.81	478.33
	14	395	226	2.00E-04	1.98E+06	1.13E+06	1.75	463.35
	15	321	178	2.00E-04	1.61E+06	8.90E+05	1.80	477.57
	16	550	336	2.00E-04	2.75E+06	1.68E+06	1.64	434.89
	17	103	52	1.00E-04	1.03E+06	5.20E+05	1.98	522.75
	18	585	301	2.00E-04	2.93E+06	1.51E+06	1.94	513.29
	19	106	68	1.00E-04	1.06E+06	6.80E+05	1.56	414.78
	20	305	168	1.00E-04	3.05E+06	1.68E+06	1.82	480.66
Totals		7023	3953	2.90E-03				

Apparent Age ± 2 sigma 476.77 ± 25.9

	Ns	Ni	area	Ps	Pi	Ps/Pi	Age (Ma)
HUD98-72 Apatite							
1	79	43	2.00E-04	3.95E+05	2.15E+05	1.84	478.53
2	358	182	1.00E-04	3.58E+06	1.82E+06	1.97	509.40
3	260	148	2.00E-04	1.30E+06	7.40E+05	1.76	456.76
4	119	79	2.00E-04	5.95E+05	3.95E+05	1.51	393.53
5	96	55	2.00E-04	4.80E+05	2.75E+05	1.75	453.92
6	371	205	1.00E-04	3.71E+06	2.05E+06	1.81	470.07
7	183	92	2.00E-04	9.15E+05	4.60E+05	1.99	514.90
8	172	86	2.00E-04	8.60E+05	4.30E+05	2.00	517.61
9	109	61	1.00E-04	1.09E+06	6.10E+05	1.79	464.33
10	234	142	2.00E-04	1.17E+06	7.10E+05	1.65	429.35
11	98	56	2.00E-04	4.90E+05	2.80E+05	1.75	455.06
12	214	145	2.00E-04	1.07E+06	7.25E+05	1.48	385.80
13	129	74	2.00E-04	6.45E+05	3.70E+05	1.74	453.37
14	274	156	2.00E-04	1.37E+06	7.80E+05	1.76	456.68
15	196	121	2.00E-04	9.80E+05	6.05E+05	1.62	422.27
16	185	118	1.00E-04	1.85E+06	1.18E+06	1.57	409.11
17	249	156	1.00E-04	2.49E+06	1.56E+06	1.60	416.28
18	219	108	1.00E-04	2.19E+06	1.08E+06	2.03	524.52
19	154	85	2.00E-04	7.70E+05	4.25E+05	1.81	470.57
20	153	81	1.00E-04	1.53E+06	8.10E+05	1.89	489.88
Totals	3852	2193	3.30E-03				

Apparent Age ± 2sigma=456.95 ± 29.9

	Ns	Ni	area	Ps	Pi	Ps/Pi	Age (Ma)
HUD98-77 Apatite							
1	388	225	2.00E-04	1.94E+06	1.13E+06	1.72	448.64
2	201	114	1.00E-04	2.01E+06	1.14E+06	1.76	458.37
3	256	150	2.00E-04	1.28E+06	7.50E+05	1.71	444.16
4	209	116	2.00E-04	1.05E+06	5.80E+05	1.80	468.05
5	224	110	2.00E-04	1.12E+06	5.50E+05	2.04	526.66
6	388	203	1.00E-04	3.88E+06	2.03E+06	1.91	495.49
7	244	133	2.00E-04	1.22E+06	6.65E+05	1.83	476.29
8	122	79	2.00E-04	6.10E+05	3.95E+05	1.54	403.16
9	170	77	1.00E-04	1.70E+06	7.70E+05	2.21	569.15
10	85	53	2.00E-04	4.25E+05	2.65E+05	1.60	418.21
11	403	206	2.00E-04	2.02E+06	1.03E+06	1.96	506.72
12	197	123	2.00E-04	9.85E+05	6.15E+05	1.60	417.66
13	200	110	2.00E-04	1.00E+06	5.50E+05	1.82	472.18
14	241	126	2.00E-04	1.21E+06	6.30E+05	1.91	495.84
15	148	71	2.00E-04	7.40E+05	3.55E+05	2.08	538.62
16	338	182	1.00E-04	3.38E+06	1.82E+06	1.86	481.94
17	94	55	1.00E-04	9.40E+05	5.50E+05	1.71	444.77
18	194	106	1.00E-04	1.94E+06	1.06E+06	1.83	475.19
19	441	294	1.00E-04	4.41E+06	2.94E+06	1.50	391.93
20	101	68	2.00E-04	5.05E+05	3.40E+05	1.49	388.19
Totals	4644	2601	3.30E-03				

Apparent Age ± 2 sigma: 466.06 ± 28.8

	Ns	Ni	area	Ps	Pi	Ps/Pi	Age (Ma)
HUD98-78 Apatite							
1	335	218	2.00E-04	1.68E+06	1.09E+06	1.54	402.57
2	78	42	1.00E-04	7.80E+05	4.20E+05	1.86	481.94
3	133	69	2.00E-04	6.65E+05	3.45E+05	1.93	499.54
4	126	73	2.00E-04	6.30E+05	3.65E+05	1.73	449.04
5	98	56	2.00E-04	4.90E+05	2.80E+05	1.75	455.06
6	87	49	1.00E-04	8.70E+05	4.90E+05	1.78	461.47
7	82	42	2.00E-04	4.10E+05	2.10E+05	1.95	505.74
8	80	38	2.00E-04	4.00E+05	1.90E+05	2.11	543.77
9	95	53	1.00E-04	9.50E+05	5.30E+05	1.79	465.73
10	108	66	2.00E-04	5.40E+05	3.30E+05	1.64	426.44
11	150	100	2.00E-04	7.50E+05	5.00E+05	1.50	391.93
12	53	34	2.00E-04	2.65E+05	1.70E+05	1.56	406.84
13	42	28	2.00E-04	2.10E+05	1.40E+05	1.50	391.93
14	90	53	2.00E-04	4.50E+05	2.65E+05	1.70	442.01
15	101	51	2.00E-04	5.05E+05	2.55E+05	1.98	512.73
16	264	147	1.00E-04	2.64E+06	1.47E+06	1.80	466.60
17	121	71	1.00E-04	1.21E+06	7.10E+05	1.70	443.55
18	90	50	1.00E-04	9.00E+05	5.00E+05	1.80	467.62
19	56	37	2.00E-04	2.80E+05	1.85E+05	1.51	395.35
20	168	87	1.00E-04	1.68E+06	8.70E+05	1.93	500.42
Totals	2357	1364	3.30E-03				

Apparent Age ± 2 sigma: 453.15 ± 35.2

	Ns	Ni	area	Ps	Pi	Ps/Pi	Age (Ma)
HUD98-79 Apatite							
1	690	407	2.00E-04	3.45E+06	2.04E+06	1.70	449.90
2	475	317	2.00E-04	2.38E+06	1.59E+06	1.50	399.18
3	454	295	2.00E-04	2.27E+06	1.48E+06	1.54	409.66
4	350	209	2.00E-04	1.75E+06	1.05E+06	1.67	444.59
5	526	270	2.00E-04	2.63E+06	1.35E+06	1.95	514.47
6	119	65	1.00E-04	1.19E+06	6.50E+05	1.83	484.57
7	495	328	2.00E-04	2.48E+06	1.64E+06	1.51	401.95
8	482	278	2.00E-04	2.41E+06	1.39E+06	1.73	459.77
9	491	297	1.00E-04	4.91E+06	2.97E+06	1.65	439.08
10	255	173	2.00E-04	1.28E+06	8.65E+05	1.47	392.86
11	417	227	2.00E-04	2.09E+06	1.14E+06	1.84	486.16
12	225	152	1.00E-04	2.25E+06	1.52E+06	1.48	394.48
13	570	323	2.00E-04	2.85E+06	1.62E+06	1.76	467.68
14	203	99	1.00E-04	2.03E+06	9.90E+05	2.05	540.43
15	394	199	2.00E-04	1.97E+06	9.95E+05	1.98	522.53
16	404	242	2.00E-04	2.02E+06	1.21E+06	1.67	443.25
17	264	161	1.50E-04	1.76E+06	1.07E+06	1.64	435.62
18	152	93	1.50E-04	1.01E+06	6.20E+05	1.63	434.25
19	96	65	1.00E-04	9.60E+05	6.50E+05	1.48	393.62
20	173	108	1.00E-04	1.73E+06	1.08E+06	1.60	425.87
Totals	7235	4308	3.30E-03				
		1.31E+06					

Apparent Age ± 2 sigma: 447±23.8

	Ns	Ni	area	Ps	Pi	Ps/Pi	Age (Ma)
HUD98-80 Apatite							
1	105	70	2.00E-04	5.25E+05	3.50E+05	1.50	399.59
2	266	201	2.00E-04	1.33E+06	1.01E+06	1.32	353.76
3	226	127	2.00E-04	1.13E+06	6.35E+05	1.78	471.47
4	61	46	2.00E-04	3.05E+05	2.30E+05	1.33	354.47
5	90	61	2.00E-04	4.50E+05	3.05E+05	1.48	393.23
6	85	64	1.00E-04	8.50E+05	6.40E+05	1.33	355.00
7	119	66	2.00E-04	5.95E+05	3.30E+05	1.80	477.48
Totals	952	635	1.30E-03				

Apparent Age ± 2 sigma: 400.71 ± 43.6

	Ns	Ni	area	Ps	Pi	Ps/Pi	Age (Ma)
HUD98-81, Apatite							
1	514	327	2.00E-04	2.57E+06	1.64E+06	1.57	410.14
2	410	297	1.00E-04	4.10E+06	2.97E+06	1.38	361.53
3	304	225	2.00E-04	1.52E+06	1.13E+06	1.35	354.04
4	291	146	2.00E-04	1.46E+06	7.30E+05	1.99	515.90
5	180	86	2.00E-04	9.00E+05	4.30E+05	2.09	540.73
Totals	1699	1081	9.00E-04				

Apparent Age ± 2 sigma: 436.47 ±37.7

	Ns	Ni	area	Ps	Pi	Ps/Pi	Age (Ma)
HUD98-82 Apatite							
1	516	281	2.00E-04	2.58E+06	1.41E+06	1.84	476.72
2	187	115	1.00E-04	1.87E+06	1.15E+06	1.63	423.84
3	638	387	2.00E-04	3.19E+06	1.94E+06	1.65	429.52
4	379	242	2.00E-04	1.90E+06	1.21E+06	1.57	408.68
5	446	267	2.00E-04	2.23E+06	1.34E+06	1.67	435.03
6	192	112	1.00E-04	1.92E+06	1.12E+06	1.71	446.08
7	695	479	2.00E-04	3.48E+06	2.40E+06	1.45	379.47
8	232	139	2.00E-04	1.16E+06	6.95E+05	1.67	434.69
9	252	126	1.00E-04	2.52E+06	1.26E+06	2.00	517.61
10	374	215	2.00E-04	1.87E+06	1.08E+06	1.74	452.43
11	460	270	2.00E-04	2.30E+06	1.35E+06	1.70	443.42
12	637	397	2.00E-04	3.19E+06	1.99E+06	1.60	418.40
13	534	371	2.00E-04	2.67E+06	1.86E+06	1.44	376.52
14	641	421	2.00E-04	3.21E+06	2.11E+06	1.52	397.65
15	631	419	2.00E-04	3.16E+06	2.10E+06	1.51	393.44
16	614	378	1.00E-04	6.14E+06	3.78E+06	1.62	423.40
17	205	136	1.00E-04	2.05E+06	1.36E+06	1.51	393.79
18	114	67	1.00E-04	1.14E+06	6.70E+05	1.70	442.86
19	283	188	1.00E-04	2.83E+06	1.88E+06	1.51	393.28
20	549	311	2.00E-04	2.75E+06	1.56E+06	1.77	458.90
Totals	8579	5321	3.30E-03				

Apparent Age ± 2 sigma: 427.29 ± 21.9

	Ns	Ni	area	Ps	Pi	Ps/Pi	Age (Ma)
HUD98-83 Apatite							
1	539	293	2.00E-04	2.70E+06	1.47E+06	1.84	479.13
2	266	131	1.00E-04	2.66E+06	1.31E+06	2.03	525.21
3	399	248	2.00E-04	2.00E+06	1.24E+06	1.61	419.50
4	215	120	2.00E-04	1.08E+06	6.00E+05	1.79	465.53
5	336	197	2.00E-04	1.68E+06	9.85E+05	1.71	443.89
6	275	151	1.00E-04	2.75E+06	1.51E+06	1.82	472.94
7	117	67	2.00E-04	5.85E+05	3.35E+05	1.75	454.13
8	436	236	2.00E-04	2.18E+06	1.18E+06	1.85	479.52
9	263	161	1.00E-04	2.63E+06	1.61E+06	1.63	425.73
10	120	79	2.00E-04	6.00E+05	3.95E+05	1.52	396.74
11	309	200	2.00E-04	1.55E+06	1.00E+06	1.55	403.34
12	126	63	2.00E-04	6.30E+05	3.15E+05	2.00	517.61
13	97	53	2.00E-04	4.85E+05	2.65E+05	1.83	475.19
14	141	82	2.00E-04	7.05E+05	4.10E+05	1.72	447.40
15	103	61	2.00E-04	5.15E+05	3.05E+05	1.69	439.59
16	336	185	1.00E-04	3.36E+06	1.85E+06	1.82	471.69
17	255	106	1.00E-04	2.55E+06	1.06E+06	2.41	617.87
18	146	109	1.00E-04	1.46E+06	1.09E+06	1.34	351.06
19	119	68	2.00E-04	5.95E+05	3.40E+05	1.75	455.06
Totals	4598	2610	3.20E-03				

Apparent Age ± 2 sigma: 460.06 ± 28.4

	Ns	Ni	area	Ps	Pi	Ps/Pi	Age (Ma)
HUD98-91 Apatite							
1	555	376	2.00E-04	2.78E+06	1.88E+06	1.48	385.85
2	386	272	1.00E-04	3.86E+06	2.72E+06	1.42	371.37
3	475	323	2.00E-04	2.38E+06	1.62E+06	1.47	384.46
4	333	191	2.00E-04	1.67E+06	9.55E+05	1.74	453.42
5	206	104	2.00E-04	1.03E+06	5.20E+05	1.98	512.82
6	477	334	1.00E-04	4.77E+06	3.34E+06	1.43	373.67
7	465	285	2.00E-04	2.33E+06	1.43E+06	1.63	425.23
8	209	131	2.00E-04	1.05E+06	6.55E+05	1.60	416.10
9	167	93	1.00E-04	1.67E+06	9.30E+05	1.80	466.54
10	189	106	2.00E-04	9.45E+05	5.30E+05	1.78	463.36
11	219	158	2.00E-04	1.10E+06	7.90E+05	1.39	362.96
12	388	227	2.00E-04	1.94E+06	1.14E+06	1.71	444.81
13	153	94	2.00E-04	7.65E+05	4.70E+05	1.63	424.24
14	281	181	2.00E-04	1.41E+06	9.05E+05	1.55	405.23
15	229	118	2.00E-04	1.15E+06	5.90E+05	1.94	502.82
16	127	83	1.00E-04	1.27E+06	8.30E+05	1.53	399.57
17	124	71	1.00E-04	1.24E+06	7.10E+05	1.75	454.18
18	323	158	1.00E-04	3.23E+06	1.58E+06	2.04	528.63
19	114	77	1.00E-04	1.14E+06	7.70E+05	1.48	386.98
20	549	311	2.00E-04	2.75E+06	1.56E+06	1.77	458.90
Totals	5969	3693	3.30E-03				

Apparent Age ± 2 sigma: 431.06 ± 24.2